

The Interpretation of Remote Sensing,
a feasibility study

CENTRALE LANDBOUWCATALOGUS



0000 0325 5482

40951

Promotor: dr. ir. C.T. de Wit,
buitengewoon hoogleraar in de theoretische teeltkunde

Co-promotor: dr. ir. J. Goudriaan
universitair hoofddocent, vakgroep theoretische produktie-ecologie

NN08201, 1265

Jan Arie den Dulk

The Interpretation of Remote Sensing,
a feasibility study

Proefschrift
ter verkrijging van de graad van
doctor in de landbouwwetenschappen,
op gezag van de rector magnificus,
dr. H.C. van der Plas,
in het openbaar te verdedigen
op woensdag 12 april 1989
des namiddags te vier uur in de aula
van de Landbouwuniversiteit te Wageningen

BIBLIOTHEEK
LANDBOUWUNIVERSITEIT
WAGENINGEN

NN 2 118456

CIP-GEGEVENS KONINKLIJKE BIBLIOTHEEK, DEN HAAG

Dulk, Jan Arie den

The interpretation of remote sensing, a feasibility study

/ Jan Arie den Dulk. - [S.l. : s.n.]. - Ill., fig., tab.

Proefschrift Wageningen. - Met lit. opg. - Met
samenvatting in het Nederlands.

ISBN 90-9002707-6

SISO 630.4 UDC 528.88:631(043.3)

Trefw.: remote sensing ; landbouw.

This thesis is the reflection of a research project that was initiated and financed by the Dutch Ministry of Agriculture and Fisheries in the framework of the Science Management Fund. The actual research work was carried out between november 1981 and september 1985 at the Centre for Agrobiological Research (CABO) in Wageningen (The Netherlands) in close cooperation with the Department of Theoretical Production Ecology of the Wageningen Agricultural University.

STELLINGEN

1. Wegens een vereenvoudigde representatie van de verstrooide straling in modellen voor de absorptie van straling door gewassen zijn deze modellen ongeschikt voor het berekenen van de reflectie in teledetectie-toepassingen.

Dit proefschrift

2. Het modelleren van de bodem als een horizontaal, isotroop reflecterend oppervlak is een acceptabele vereenvoudiging in modellen voor gewasreflectie.

Dit proefschrift

3. De invloed van azimuthale componenten in de bladhoekverdeling op de richtingsafhankelijke reflectie is zodanig groot dat met deze componenten rekening gehouden zou moeten worden bij de interpretatie van teledetectie-waarnemingen.

Dit proefschrift

4. Het corrigeren van gescande beelden voor helderheidsverschillen die samenhangen met de geometrie van de waarneming geeft alleen verbetering onder condities die niet aan de hand van die zelfde beelden te verifiëren zijn.

Dit proefschrift

5. Het mag verwacht worden dat een reflectiemodel waarin de structuur van gewassen op fractals is gebaseerd, meer inzicht geeft in de invloed van de gewasstructuur op de waargenomen helderheden en met name op de spreiding in die helderheden.

MANDELBROT, B., The fractal geometry of nature; W.H. Freeman & Co., San Fransisco (1982).

6. Het systeem voor de verkiezing van student-leden in de clusterbesturen van de Landbouwniversiteit is voor wat betreft het bestaan van de eis tot registratie negatief discriminerend voor de studenten, en voor wat betreft de registratie-eisen in strijd met de bedoeling van de wetgever.

Kiesreglement Clusterbesturen Rijkslandbouwniversiteit 1988.

7. De garantieregeling voor boventallige leerkrachten in het basisonderwijs verlaagt de kwaliteit van dat onderwijs, ondanks het feit dat door deze regeling ook de leerling/docent-verhouding verkleind wordt. Deze kwaliteitsverlaging is groter naarmate meer scholen onder hetzelfde bestuur vallen.

Diverse circulaire Ministerie van Onderwijs en Wetenschappen.

8. De implementatie van een *priority-queue* als *ternaire heap* is in veel gevallen efficiënter dan een implementatie als *binaire heap*.

KNUTH, D.E., The art of computer programming, Vol. 3 / Sorting & searching; Addison-Wesley Publishing Company, Reading, Massachusetts (1973).

9. Vanwege de verkeersveiligheid zou de looprichting in de Veluwe loop omgedraaid moeten worden.
10. Het in veel computertalen gebruikte begrip *real* als type-aanduiding voor niet-geheeltallige numerieke entiteiten in discrete machines is verwarrend en principiële onjuist; een juistere aanduiding zou zijn *approx-real*.
11. Onderzoek met gebruik van computers is als pianospelen: je moet aan de presentatie niet kunnen merken hoe moeilijk de techniek is.

Jan Arie den Dulk

The Interpretation of Remote Sensing, a feasibility study

Wageningen, 12 april 1989

Voor mijn moeder

Acknowledgements

First of all, I want to express my great gratitude to prof.dr.ir. C.T. de Wit and to dr.ir. J. Goudriaan for their inspiration and, in a later phase, for their unremitting pressure to finish this manuscript. Without them, this thesis should never have been completed.

Several institutions in Wageningen contributed substantially to this research project. I am especially grateful to the staff of the Centre for Agrobiological Research (CABO) for offering me hospitality at their institute for several years in the direct neighbourhood of ir. Th.A. de Boer and ir. H.W.J. van Kasteren. They taught me a lot about remote sensing. My thanks are also due to the staff of the Wageningen Agricultural University (LUW), to prof.dr.ir. R. Rabbinge and all other members of the Department of Theoretical Production Ecology (TPE), and to the members of the Department of Computer Science of the University, who all offered me indispensable facilities in the preparation of this thesis.

With great pleasure I recall the fruitful discussions I had with dr.ir. N.J.J. Bunnik (National Aerospace Laboratory (NLR), now at the Netherlands' Remote Sensing Board (BCRS)), ing. W. Verhoef (NLR), dr.ir. P.A. Leffelaar (TPE), prof.dr.ir. H. van Keulen (CABO), dr.ir. C.J.T. Spitters (TPE, now in CABO), drs. B.R. Damsté and drs. M.H. Hendriks (both LUW, Department of Mathematics). They all acted many times as conversation partners, and their suggestions were of great help.

An enormous support I got from my present colleagues at the Department of Computer Science of the LUW. Their considerations and technical assistance during the last three years were invaluable. Among them, I will mention explicitly prof.ir. M.S. Elzas, drs. E.W. van Ammers and ir. D.L. Kettenis. I am also indebted to Dominique van Eick, Hans Cox and Alfred Boom (students of this department) for their assistance in the implementation of the models on the VAX¹ computer system of the LUW after the installation of a new computer system.

I owe very special words of thanks to my wife Greet, who did all the typing and typesetting. To do this job, she also spent many hours in studying the document preparation program \LaTeX ².

I also want to express my thanks to mrs. H.H. van Laar (TPE) and ir. H.J.W. van Roermund, who assisted in various aspects of the preparation of this manuscript, to mrs. J. Burroughs-Boenisch who reviewed and corrected my 'pitcoal-English' and to mr. J. Engelsman (CABO), who prepared all manually drawn figures. The plotted figures, including the cover figure, were generated in cooperation with the personnel of

¹VAX is a trademark of Digital Equipment Corporation, Maynard, Massachusetts, USA

² \LaTeX is a document preparation system, based on \TeX . \TeX is a typesetting system developed by Donald E. Knuth at Stanford University.

the Computer Centre of the LUW. All figures were photographically reduced to their definite size by P.R. Stadt (CABO).

A substantial financial contribution to the printing-expenses of this thesis was received from the Foundation "*Fonds Landbouw Export Bureau 1916/1918*". Also the Wageningen Agricultural University and the Centre for Agrobiological Research contributed to these.

Finally, I want to thank my family for their patience and understanding during several years. Because of the limited knowledge of the English language of one of my children, I will do that in Dutch. *Greet, Jasper, Lieneke, hartelijk bedankt. Ik zal proberen in de toekomst meer echtgenoot en vader voor jullie te zijn dan in de afgelopen jaren het geval is geweest.*

Contents

1	The interpretation of remote sensing data	13
2	Reflection models	17
2.1	Crop reflection models	17
2.1.1	Primary and secondary reflection	17
2.1.2	A simple model for the directional distribution of the reflected radiation	21
2.2	Existing models	28
2.2.1	De Wit's photosynthesis model	28
2.2.2	Crop reflection according to Suits	29
2.2.3	Goudriaan's model	29
2.2.4	Chen's reflection model	30
2.3	Conclusions	30
2.4	List of symbols used in Chapter 2	31
3	TURTLE, HARE and SOIL model	33
3.1	The TURTLE model	33
3.1.1	General description of the TURTLE model	34
3.1.2	Distribution of the reference directions	35
3.1.3	Optical properties of the leaves	36
3.1.4	Geometrical structure of a crop layer	39
3.1.5	Optical properties of a crop layer	39
3.1.6	A simple soil reflection model	44
3.1.7	Crop properties ignored	45
3.1.8	Combining layers to form a canopy	45
3.1.9	The division of the canopy into layers	49
3.1.10	Model verification and validation	50
3.2	The HARE model	57

3.2.1	Principles of the HARE model	58
3.2.2	One step in the algorithm	58
3.2.3	Calculations for a homogeneous crop layer	59
3.2.4	Calculations for a non-homogeneous crop layer	61
3.2.5	Application and use	61
3.3	The SOIL model	62
3.3.1	General description of the SOIL model	64
3.3.2	One cylinder in the model	65
3.3.3	Horizontal elements	66
3.3.4	Vertical elements, the cylinder wall	67
3.3.5	Combination of horizontal and vertical elements	68
3.3.6	The spatial density of the cylinders π/E	69
3.3.7	Calibration	71
3.3.8	Model calculations and conclusions	71
3.4	List of symbols used in Chapter 3	73
4	Calculations on hypothetical crops	79
4.1	The crop and radiation parameters used	80
4.1.1	Crop geometry	80
4.1.2	Leaf reflection and transmission	84
4.1.3	Leaf surface	87
4.1.4	Soil reflection coefficient	91
4.1.5	Incoming radiation, sky irradiance	92
4.1.6	Summary	94
4.2	Presentation of the calculation results	94
4.2.1	Radiative properties	95
4.2.2	Crop properties	96
4.3	Calculations on the reflection in single spectral bands	97
4.3.1	Crop geometry	98
4.3.2	Optical properties of the leaves	99
4.3.3	Soil reflection	101
4.3.4	Incoming radiation	103
4.3.5	Observation direction	104
4.3.6	Conclusions	105
4.4	Combination of the reflection in different spectral bands	109

4.4.1	Crop geometry	111
4.4.2	Optical properties of the leaves	111
4.4.3	Reflection and transmission coefficients of the leaves	112
4.4.4	Soil reflection	113
4.4.5	Incident radiation and observation direction	114
4.4.6	Conclusions	114
4.5	Improvement of the estimation of the crop parameters by a correction on the measured radiation	116
4.5.1	LAI=1 for the whole area	118
4.5.2	A uniform LAI distribution	120
4.5.3	Non-uniform LAI distributions	120
4.5.4	Conclusions	123
4.6	List of symbols used in Chapter 4	125
5	Calculations with actual crop data	127
5.1	Winter wheat	127
5.1.1	Individual spectral bands	132
5.1.2	Combinations of two bands	135
5.2	Drooping of leaves by sugarbeet	139
A	Kubelka-Munk equations	143
B	Orientations of Model Directions	149
C	Arbitrary directions	151
D	The associative property of the adding algorithm	153
D.1	The proof for three layers	153
D.2	The proof for an arbitrary number of layers	157
	Summary	161
	Samenvatting	165
	References	169
	Curriculum Vitae	173

Chapter 1

The interpretation of remote sensing data

The interpretation of remote sensing data is a very difficult and complicated process. Especially in case of passive techniques (techniques in which the already present radiation is used, and the observer does not use his own radiative source), the measured radiation coming from a crop is a function of a great number of factors. These are the directional distribution of the downward radiation that is reflected by the crop, the reflective properties of the crop and the underlying soil, the optical properties of the atmosphere, the observation direction and the properties of the sensor.

Even if it is assumed that the atmosphere is absolutely transparent for the reflected radiation (which is surely an oversimplification if the sensor is located at some distance from the crop) and assumed at the same time the sensor is fully calibrated, the number of factors that govern the intensity of the radiation, measured when the sensor is pointed to the earth surface is still large. Of these factors only the observation direction is known accurately. The directional distribution of the downward radiation can generally only be estimated, because it is a function of the direction of the sun and the transmissive properties of the atmosphere which may change continuously, due to changes in humidity or other factors.

Focussing on the observed crop itself, it will be clear that also here a number of factors play a role in its reflective properties. To mention some of them:

- The total surface of the reflecting organs.
- The relative position of these organs.
- Their orientation.
- The optical properties (reflecting and transmission coefficients) of these organs.
- The reflective properties of the soil underneath.

Knowledge about some of these properties is in fact the ultimate target which legitimates the efforts that must be provided when remote sensing data are interpreted, but most of the mentioned properties can be considered to be also sources of noise in this interpretation process.

For instance, as long as a crop is not closed, the soil reflection is a factor that influences directly the measured reflection of that crop. The reflection coefficient of the soil is very sensitive to the moisture content of the upper layer, so the measured radiation depends on a factor that is generally not only of very limited importance, but also hardly known, because it can vary very rapidly. Also changes in the orientations of the leaves of a crop may cause serious differences in the reflected radiation in one direction, and the cause of these changes may be wind, a factor that is generally of little importance and not known.

Of course, in spite of the problems that are mentioned, remote sensing may be of great value in many situations. For instance, in the visible part of the spectrum, the differences between the reflection of a bare soil and of a closed crop are so large that they can be distinguished under all conditions. Remote sensing has also been proved to be a good tool for recognition of crops and even varieties within one species can be distinguished under some conditions. But, if one tries to use remote sensing for the determination of quantitative properties of crops serious problems arise, because of the number of unknown factors that influence the radiation that comes from the crop.

A more formal way to describe a reflecting crop is to consider it as a system that interacts with an input (the incoming radiation). The result of this interaction is an output (the reflected radiation). The reflection process is of a deterministic nature, which means that the output completely depends on the properties of the input and on the properties of the system itself. So, if the input should be known with an acceptable level of accuracy and the reflective properties of the crop are also known, the output of the system (e.g. the reflected radiation) could be predicted. However, the interpretation of remote sensing data is a process that goes completely the other way around: a part of the output is measured and the optical properties of the system are to be calculated. Only a part of the output is measured, because the output does not only consist of the upward flux, leaving the crop after being reflected, but also its spatial distribution and the measurements of the reflected radiation only concern one direction. On the other hand in modern remote sensing techniques, this is done for several wavelength bands simultaneously.

Also the input can only be estimated with a limited accuracy, due to the knowledge of the atmospheric properties. This is because the incoming radiation is measured near the sensor, at some distance of the reflecting crop.

To make things even more complex, the interest of the interpreter does generally not concern the optical properties of the crop themselves, but some other properties that are known to influence the reflective behaviour, like biomass or development stage. Figure 1.1 shows the components of the reflecting system in a very schematic way. At the upper lefthand side we see an arrow, marked I . This arrow stands for the input of the system, being the incoming radiation near the crop. The box R in the centre of the figure depicts the reflective behaviour of the crop, and the arrow O that leaves the box at the upper righthand side symbolizes the output of the system. The two circles beside the box indicate the crop properties that influence the reflective behaviour of the crop. One of them (P_1) stands for the properties that are of interest, the other (P_2) depicts those crop properties that influence the reflection too, but which are not of interest.

The interpretation of remote sensing is basically a reconstruction process: from the measured elements of the output and an estimation of the input, the interpreter must

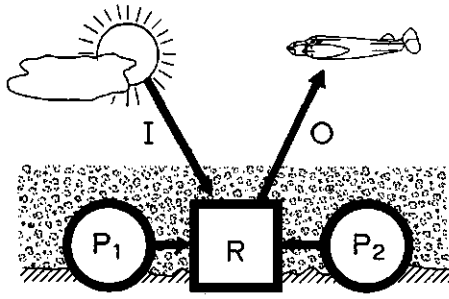


Figure 1.1: A schematic view of a reflecting crop. See text for meaning of symbols.

reconstruct the reflective behaviour R of the crop and from that, the values of the parameters that are symbolized with P_1 . The problem in this reconstruction process is that the number of unknown factors in P_1 , P_2 and, to some extent, I exceeds generally the number of measured elements of O . This makes the reconstruction process only unambiguous, if so many elements of P_1 , P_2 and I or relations between these elements are known, that the number of independent entities is as small as the number of measured outputs. Only on a very limited scale, like under trial field conditions the number of known elements of P and I may be so great that the inversion or reconstruction can be performed. On a large scale base this is generally not the actual situation.

In this study it will be shown that under the usual circumstances the reconstruction can yield only approximate quantitative values for the elements of P_1 . This is done by defining a model of a reflecting crop, where several factors of P can be given a value independently. Also the input I can be varied over a range of possible values, after which the variations in O are compared to the variations in elements of P and I .

The result of the study is a set of estimations of possible errors that may occur when remote sensing data are used for quantitative crop analysis.

Chapter 2

Reflection models

Because several reflection models already exist, it makes sense to compare the properties of these models with the features that a reflection model that can be applied in crop yield prediction should have. To do so, it is important to discuss at first these desired features. This is done in Section 2.1. In Section 2.2 some existing models are discussed. Finally, in Section 2.3 it is concluded that, for different reasons, the existing models are not suitable to evaluate the applicability of remote sensing methods. So in the next chapter a new model is developed.

2.1 Crop reflection models

To be able to model the reflective behaviour of a crop, it is absolutely necessary to know which crop properties influence the reflection and what is their quantitative influence on the reflection of the intercepted radiation.

In recent decades, various authors have published models that describe the behaviour of plants as radiation interceptors. These models have generally been developed to explain or to take account of the photosynthetic activity of the plant, and hence the accent is on an accurate description of the absorption of the intercepted radiative energy in relation to the total incoming flux. From this point of view, reflection is merely a loss. Because in the photosynthetically active part of the spectrum, plants absorb almost all of the incoming radiation, photosynthetic activity is almost completely governed by the primary radiation, i.e. by the radiation that comes directly from the sky and that has not previously been reflected or transmitted by plant organs. The influence of the so-called secondary radiation is small, so for the calculation of the photosynthetic activity the directional distribution of this radiation may be simplified strongly, with only a few consequences. A simple example may illustrate that an absorption model need not deal very precisely with the reflected fraction of the intercepted radiation.

2.1.1 Primary and secondary reflection

Assume a crop with a very high leaf area index or LAI. The LAI of a crop is defined as the ratio of the total one-side leaf surface and the (horizontal) soil surface below the crop. Its dimension is m^2/m^2 . The reflection coefficient of the individual leaves is ρ ,

the transmission coefficient is τ and the absorption coefficient is α . Of course the sum of these is equal to 1, so

$$\rho + \tau + \alpha = 1 \quad (2.1)$$

All leaves are horizontally oriented and ρ , τ and α are assumed to be independent of the angle of incidence. The LAI is so high that the influence of the soil may be neglected. So, because all incoming radiative energy D_0 is intercepted by a leaf at some depth in the crop, the total primary absorption A_p is:

$$A_p = \alpha \cdot D_0 \quad (2.2)$$

Kubelka & Munk (1931) derived and solved a set of differential equations (the so-called KM-equations), that describe the total downward flux $D_{t,d}$ and the total upward flux $U_{t,d}$ at some depth in the crop as functions of the incident flux D_0 , the leaf reflection and transmission coefficients ρ and τ and the depth in the crop d (d is expressed in LAI units). This set is:

$$\begin{pmatrix} dD_{t,d}/dd \\ dU_{t,d}/dd \end{pmatrix} = \begin{pmatrix} \tau - 1 & \rho \\ -\rho & -(\tau - 1) \end{pmatrix} \begin{pmatrix} D_{t,d} \\ U_{t,d} \end{pmatrix} \quad (2.3)$$

(The minus signs in the lower line signify that the upward flux is concerned). The boundary conditions under the given assumptions are:

$$\begin{aligned} \text{for } d = 0 \text{ (top)} & : D_{t,0} = D_0 \\ \text{for } d \rightarrow \infty & : D_{t,\infty} = 0 \\ & \text{and } U_{t,\infty} = 0 \end{aligned} \quad (2.4)$$

The solution of these equations as given by Kubelka & Munk is presented in Appendix A. For the total upward flux at the top of the crop $U_{t,0}$ it holds that:

$$U_{t,0} = \frac{D_0}{\rho} \cdot \left(1 - \tau - \sqrt{(1 - \tau)^2 - \rho^2} \right) \quad (2.5)$$

The total crop absorption A_t is:

$$A_t = D_0 - U_{t,0} = D_0 \cdot \left\{ 1 - \frac{1}{\rho} \cdot \left(1 - \tau - \sqrt{(1 - \tau)^2 - \rho^2} \right) \right\} \quad (2.6)$$

The primary absorption A_p is:

$$A_p = \alpha \cdot D_0 = (1 - \rho - \tau) \cdot D_0 \quad (2.7)$$

The secondary and higher order absorption A_s is equal to the difference between A_t and A_p :

$$A_s = A_t - A_p \quad (2.8)$$

$$\begin{aligned} &= D_0 \cdot \left\{ 1 - \frac{1}{\rho} \cdot \left(1 - \tau - \sqrt{(1 - \tau)^2 - \rho^2} \right) \right\} - D_0 \cdot (1 - \rho - \tau) \\ &= D_0 \cdot \left\{ \rho + \tau - \frac{1}{\rho} \cdot \left(1 - \tau - \sqrt{(1 - \tau)^2 - \rho^2} \right) \right\} \end{aligned} \quad (2.9)$$

In the photosynthetically active range of the spectrum (300 - 700 nm), the values for ρ and τ are much smaller than one. This permits the following simplifying approximations:

$$A_s = D_0 \cdot \left\{ \rho + \tau - \frac{1-\tau}{\rho} \cdot \left(1 - \sqrt{1 - \left(\frac{\rho}{1-\tau} \right)^2} \right) \right\} \quad (2.10)$$

$$\approx D_0 \cdot \left\{ \rho + \tau - \frac{1-\tau}{\rho} \cdot \left(1 - \left[1 - \frac{1}{2} \cdot \left(\frac{\rho}{1-\tau} \right)^2 \right] \right) \right\}$$

$$= D_0 \cdot \left\{ \rho + \tau - \frac{1}{2} \cdot \left(\frac{\rho}{1-\tau} \right) \right\}$$

$$\approx D_0 \cdot \left\{ \rho + \tau - \frac{1}{2} \cdot \rho \cdot (1 + \tau) \right\}$$

$$A_s \approx D_0 \cdot (\tau + \rho/2) \quad (2.11)$$

An approximation with $\rho = 0.08$ and $\tau = 0.04$ is:

$$A_t = 0.96 \cdot D_0 \quad (2.12)$$

$$A_p = 0.88 \cdot D_0 \approx 0.92 \cdot A_t \quad (2.13)$$

$$A_s = 0.08 \cdot D_0 \approx 0.08 \cdot A_t \quad (2.14)$$

Hence over 90% of the total absorption by the crop is absorption of primary radiation. The influence of the directional distribution of the non-primary radiation in the crop on the absorption and hence on the photosynthetic activity is therefore negligible. This property justifies a very simple implementation of the secondary fluxes, including the reflected radiation, in absorption models.

The situation is completely different for the reflected radiation. This can be shown by comparison of the total reflected flux $U_{t,0}$ and the primary reflected flux at the top of the crop $U_{p,0}$. These are:

$$U_{t,0} = \frac{D_0}{\rho} \cdot \left(1 - \tau - \sqrt{(1-\tau)^2 - \rho^2} \right) \quad (2.15)$$

$$U_{p,0} = D_0 \cdot \int_0^\infty \rho \cdot (e^{-d})^2 \cdot dd$$

$$U_{p,0} = D_0 \cdot \rho/2 \quad (2.16)$$

Figure 2.1 shows the relations between the incoming flux D_0 and the different upward and downward fluxes inside the crop. Two diagrams have been drawn: one for the visible part of the spectrum and one with characteristic values for infrared radiation.

It is illustrative to examine the ratio between $U_{p,0}$ and $U_{t,0}$ as a function of the optical parameters of the leaf. In Figure 2.2 this ratio is drawn as a function of the scatter coefficient σ and the ratio reflection coefficient/scatter coefficient r . σ and r replace ρ and τ . Their mutual relation is:

$$\sigma = \rho + \tau \quad (2.17)$$

$$r = \rho/\sigma \quad (2.18)$$

Figure 2.2 shows that for all combinations of ρ and τ that occur in practice, the primary upward flux $U_{p,0}$ plays an important role in the total upward flux, where in case of

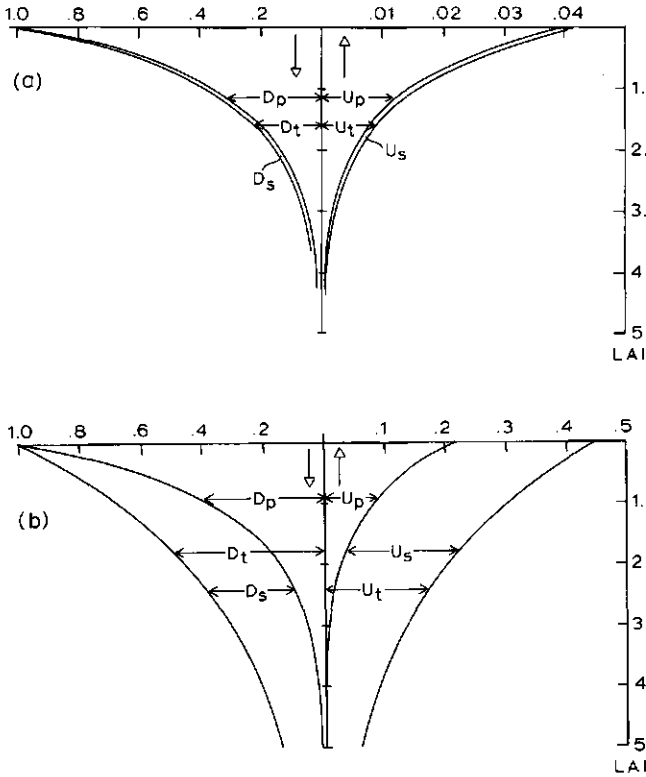


Figure 2.1: Flux profile in a crop with horizontal leaves. Figures show downward fluxes in the left halves, upwards fluxes in the right halves of the figures. The downward flux D_t is split up in the direct incident flux D_p and the flux that has already been intercepted and remitted flux D_s . The total upward flux U_t is split up in the direct reflected flux U_p and the multiple scattered flux U_s .

a): Visible radiation, $\rho = 0.08, \tau = 0.04$.

b): Near-infrared radiation, $\rho = 0.45, \tau = 0.40$.

The vertical axis gives depth in LAI-units, the horizontal axis the flux. ($D_t = 1$ at the surface.) The horizontal axes of the left and right halves are drawn with different scales.

visible radiation the ratio $U_{p,0}/U_{t,0}$ exceeds 90%. It can therefore be expected that the directional distribution of the reflected radiation depends for an important part on the directional distribution of the primary upward flux $U_{p,0}$.

The interpretation of remote sensing images is always based on the measured reflection in one single direction for each pixel in the image. A second simple model will show that the directional reflection of a crop not only depends on the total reflection of the crop, but also on the reflective properties of the crop components, on their solid distribution and, in particular on the directional distribution of the incident radiation.

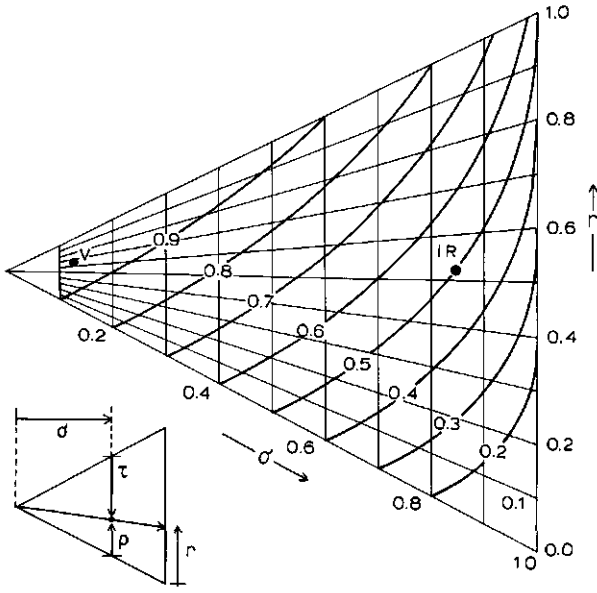


Figure 2.2: Ratio between $U_{p,0}$ and $U_{t,0}$ of a canopy with infinite LAI and horizontal leaves. The figure shows values for all combinations of $\sigma = \rho + \tau$ and $r = \rho/\sigma$ (for further explanation see text). The figure has to be read as shown in the small triangle. The dots indicate the applied values for visible (V) and near-infrared (IR) radiation in the other figures in this chapter.

2.1.2 A simple model for the directional distribution of the reflected radiation

This model is based on a crop with infinite depth and a spherical leaf angle distribution. This means that all possible leaf orientations occur with equal density. The calculations concern the visible part of the spectrum, and therefore the leaf reflection and transmission coefficients ρ and τ are small. As computed in the previous subsection this causes the major part of the upward flux to be the result of reflection of primary incident radiation. The calculation of the directional distribution of this primary crop reflection proceeds as follows.

Assume all incoming radiation incidents from one source direction i (the sun), with inclination θ . The observer looks at the crop in direction b with inclination v . The azimuthal angle between directions i and b is γ (see Figure 2.3). For every depth d in the crop (d expressed in LAI-units) the direct incident radiation can be calculated as a fraction of the incoming flux above the crop. Exponential radiation extinction is assumed. Only the primary reflected radiation is taken into account, so the extinction

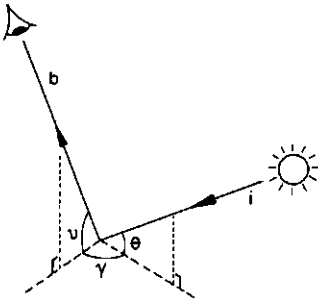


Figure 2.3: Nomenclature of angles and directions as used in the model in Subsection 2.1.2.

is equal to the interception. The interception coefficient K is the product of the relative pathlength $1/\sin \theta$ and the ratio between the projected leaf surface perpendicular to the direction of incidence and the total leaf surface. Because of the spherical leaf angle distribution this value is 0.5, regardless of the direction of incidence, so for K it holds that:

$$K = 0.5/\sin \theta \quad (2.19)$$

The remaining radiation intensity $P_{i,d}$ (expressed as a fraction of the incident radiation and assuming exponential extinction) at depth d is now:

$$P_{i,d} = e^{-(0.5/\sin \theta) \cdot d} \quad (2.20)$$

An equivalent expression can be used to express the radiation that leaves the crop from depth d in upward direction with an inclination v as a fraction $P_{u,d}$ of the total radiation in that direction generated at depth d . The remaining fraction of this radiation is:

$$P_{u,d} = e^{-(0.5/\sin v) \cdot d} \quad (2.21)$$

It also holds that the reflection from direction i to direction b is proportional to a factor F , which depends on ρ , τ , θ , v and γ and to the interception at depth d . This interception I is the product of K and layer thickness dd :

$$I_{dd} = (0.5/\sin \theta) \cdot dd \quad (2.22)$$

The total reflection $R_{d,dd}$ that is caused by a thin crop layer with thickness dd at depth d now becomes:

$$R_{d,dd} = P_{i,d} \cdot P_{u,d} \cdot F(\rho, \tau, \theta, v, \gamma) \cdot I_{dd} \quad (2.23)$$

Integration of $R_{d,dd}$ over $0 \leq d < \infty$ yields the total reflection R . F does not depend on d , and can therefore be removed from the integral part of the function:

$$R = F(\rho, \tau, \theta, v, \gamma) \cdot \int_0^\infty P_{i,d} \cdot P_{u,d} \cdot I_{dd} \quad (2.24)$$

Substitution of Equations (2.20), (2.21) and (2.22) yields:

$$R = F(\rho, \tau, \theta, v, \gamma) \cdot \int_0^\infty \left(e^{-\left(\frac{0.5}{\sin \theta} + \frac{0.5}{\sin v}\right) \cdot d} \right) \cdot \frac{0.5}{\sin \theta} \cdot dd \quad (2.25)$$

Integration of Equation (2.23) results in:

$$R = \frac{\sin v}{\sin v + \sin \theta} \cdot F(\rho, \tau, \theta, v, \gamma) \quad (2.26)$$

The radiance H_b in some direction b is proportional to the flux in that direction divided by the sine of the inclination. Hence, the radiance in direction b with inclination v is (ignoring a proportional factor):

$$\begin{aligned} H_b &= R/\sin v \\ &= F(\rho, \tau, \theta, v, \gamma) / (\sin v + \sin \theta) \end{aligned} \quad (2.27)$$

The next step to take is the calculation of $F(\rho, \tau, \theta, v, \gamma)$. F can be computed as the sum of the contributions of the leaf surface elements with all possible orientations. Because

of the continuous distribution of these orientations, F can be computed as an integral of the product of the contribution W of leaves with one orientation c and the relative density of these leaves.

Leaves are considered to be Lambertian reflectors and transmitters. For the radiation W remitted in direction b , the combination of the direction of incidence i , the direction of remission b and the normal direction c of an arbitrary leaf element (again ignoring a proportional factor), is now:

$$W = |\cos \mu_{i,c} \cdot \cos \mu_{c,b}| \cdot [\rho \vee \tau] \quad (2.28)$$

In Equation (2.28), $\mu_{p,q}$ depicts the angle between arbitrary directions p and q . If the product of the cosines in Equation (2.28) is positive, the reflection situation exists and ρ must be applied; if the product is negative we are dealing with transmission and τ must be used. Equation (2.27) already takes account of the interception caused by an increasing pathlength with decreasing θ . So, for the calculation of F only the relative orientations of directions i , b and c are of interest. The leaf angle distribution is spherical. This means that the relative density of the leaves in a given orientation is equal for all orientations, and hence, that we are free to choose any other orientation for a coordinate system without additional problems with the interception coefficient or with the leaf density distribution function. The formula to calculate the angle $\mu_{1,2}$ between two arbitrary directions (ϕ_1, χ_1) and (ϕ_2, χ_2) is known from spherical trigonometry:

$$\cos \mu_{1,2} = \sin \chi_1 \cdot \sin \chi_2 + \cos \chi_1 \cdot \cos \chi_2 \cdot \cos (\phi_2 - \phi_1) \quad (2.29)$$

An adapted form of Equation (2.29) must be applied twice in Equation (2.28). But, because the coordinate system may be oriented freely, the orientation of a new system with ϕ and χ as the pseudo azimuth and pseudo inclination respectively can be chosen in such way that both i and b are vectors in the equator plane (the plane where $\chi = 0$). In this (ϕ, χ) -coordinate system it holds for both cosines from Equation (2.28) that when they are substituted by Equation (2.29), one of the sines of the first term becomes 0 and one of the cosines becomes 1, yielding a serious simplification. The azimuthal orientation of this coordinate system is chosen in such way that i coincides with $\phi = \pi/2$ (see Figures 2.4a and 2.4b). These figures also show that only a quarter of the complete sphere has to be considered: each line through the centre of the sphere intersects the sphere in two opposite points, where the sphere surfaces, which in fact are representatives of leaf elements, are parallel. So we can limit ourselves to the points on the upper hemisphere. It is also true that if $\phi' = \phi + \pi$ and $\chi' = \chi$, then it holds that $\cos \mu_{c',b} = \cos \mu_{c,b}$ and $\cos \mu_{i,c'} = \cos \mu_{i,c}$. So the calculations can be limited to that part of the hemisphere with $0 \leq \phi < \pi$ and $0 < \chi < \pi/2$. The total reflection factor $F(\rho, \tau, \theta, v, \gamma)$ can now be computed as the integral of W (from Equation (2.28)) over this part of the sphere. A factor $\cos \chi$ must be included in the integral because the integration concerns a spherical surface:

$$F = \int_0^\pi \int_0^{\pi/2} W(\rho, \tau, i, c, b) \cdot \cos \chi \cdot d\chi \cdot d\phi \quad (2.30)$$

Figure 2.4 shows that if $0 < \phi < \pi - \mu_{i,b}$, reflection occurs, whereas if $\pi - \mu_{i,b} < \phi < \pi$ we are dealing with transmission. (At the boundaries 0, $\pi - \mu_{i,b}$ and π the value of W is 0.) Application of Equation (2.29), but with angles $\mu_{i,c}$ and $\mu_{c,b}$ instead of (ϕ, χ) at the spherical surface yields:

$$\cos \mu_{i,c} = \cos \chi \cdot \cos (\pi/2 - \phi) = \cos \chi \cdot \sin \phi \quad (2.31)$$

$$\cos \mu_{b,c} = \cos \chi \cdot \cos (\pi/2 - \mu_{i,b} - \phi) = \cos \chi \cdot \sin (\mu_{i,b} + \phi) \quad (2.32)$$

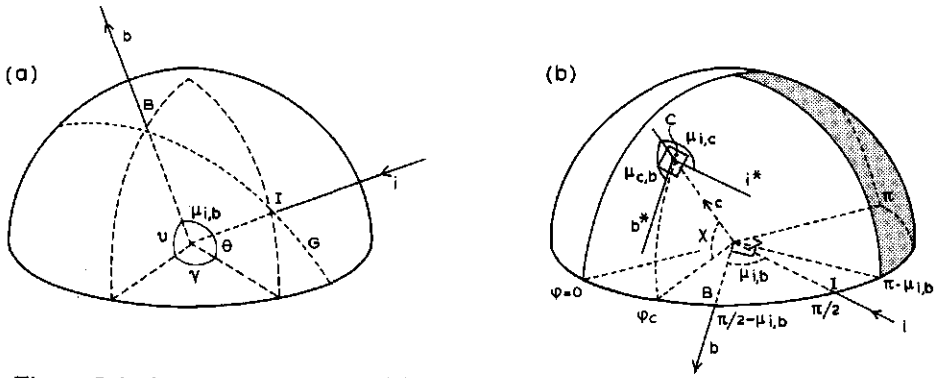


Figure 2.4: Orientations in the model of Subsection 2.1.2.

a): The directions and their mutual relations in the original orientation.

b): The sphere of Figure 2.4a is rotated in such way that the great circle G is in the equator plane. Orientation of ϕ and the situation with respect to a surface element C perpendicular to direction c are drawn. It can be seen that, if C should be in the grey region of the sphere, remittance from i^* to b^* is the result of the transmission by leaf element C .

(Notice that in the (ϕ, χ) coordinate system the inclinations of b and i are both equal to 0.)

Substitution of Equations (2.31) and (2.32) in (2.30) and addition of a minus sign for the transmission results in:

$$F = \rho \int_0^{\pi - \mu_{i,b}} \int_0^{\pi/2} \cos^3 \chi \cdot \sin(\mu_{i,b} + \phi) \cdot \sin \phi \cdot d\chi \cdot d\phi \dots$$

$$\dots - \tau \int_{\pi - \mu_{i,b}}^{\pi} \int_0^{\pi/2} \cos^3 \chi \cdot \sin(\mu_{i,b} + \phi) \cdot \sin \phi \cdot d\chi \cdot d\phi \quad (2.33)$$

Because there are no combined factors of ϕ and χ , this integral may be rewritten as:

$$F = \left\{ \rho \int_0^{\pi - \mu_{i,b}} f(\phi) \cdot d\phi - \tau \cdot \int_{\pi - \mu_{i,b}}^{\pi} f(\phi) \cdot d\phi \right\} \cdot \int_0^{\pi/2} g(\chi) \cdot d\chi \quad (2.34)$$

With:

$$f(\phi) = \sin(\phi + \mu_{i,b}) \cdot \sin \phi \quad (2.35)$$

$$g(\chi) = \cos^3 \chi \quad (2.36)$$

After some conversion and reduction, integration of these functions yields:

$$\int f(\phi) \cdot d\phi = \int \sin(\phi + \mu_{i,b}) \cdot \sin \phi \cdot d\phi \quad (2.37)$$

$$= \left(\frac{\phi}{2} - \frac{\sin 2\phi}{4} \right) \cdot \cos \mu_{i,b} + \frac{\sin^2 \phi \cdot \sin \mu_{i,b}}{2} \quad (2.38)$$

$$\int g(\chi) \cdot d\chi = \int \cos^3 \chi \cdot d\chi \quad (2.39)$$

$$= \sin \chi - \frac{\sin^3 \chi}{3} \quad (2.40)$$

Substitution of Equations (2.38) and (2.40) in (2.34) and substitution of the values for the integration boundaries gives:

$$F = \frac{1}{3} \{(\rho + \tau)(\pi - \mu_{i,b}) + \cos \mu_{i,b} + \sin \mu_{i,b} - \pi \cdot \tau \cdot \cos \mu_{i,b}\} \quad (2.41)$$

As in the previous subsection, ρ and τ are replaced by the scatter coefficient σ and the ratio reflection coefficient/scatter coefficient r . Equation (2.41) can now be reduced to:

$$F = \frac{1}{3} [\sigma \{(\pi - \mu_{i,b}) \cos \mu_{i,b} + \sin \mu_{i,b}\} - (1 - r \cdot \sigma) \cdot \pi \cdot \cos \mu_{i,b}] \quad (2.42)$$

$$= \frac{1}{3} \sigma \{ \sin \mu_{i,b} - \mu_{i,b} \cdot \cos \mu_{i,b} + r \cdot \pi \cdot \cos \mu_{i,b} \} \quad (2.43)$$

As done before in Equations (2.24) and (2.26), the constant $1/3$ is ignored. Regrouping yields:

$$F = \sigma \{ \sin \mu_{i,b} + (\pi \cdot r - \mu_{i,b}) \cdot \cos \mu_{i,b} \} \quad (2.44)$$

According to Equation (2.27), the relative radiance $H(\sigma, r, i, b)$ in direction b is now given by the equation:

$$H(\sigma, r, i, b) = \frac{\sigma}{\sin \theta + \sin \nu} \cdot \{ \sin \mu_{i,b} + (\pi \cdot r - \mu_{i,b}) \cdot \cos \mu_{i,b} \} \quad (2.45)$$

Where for $\mu_{i,b}$ it holds that (Equation (2.29)):

$$\mu_{i,b} = \arccos(\sin \theta \cdot \sin \nu + \cos \theta \cdot \cos \nu \cdot \cos \gamma) \quad (2.46)$$

Some calculations were carried out with this model for two values of r (0.5 ($\rho = \tau$) and 1.0 (reflection only)) and for two values of θ (30° and 60°). Diagrams of the ratio $H(\sigma, r, i, b) / H(\sigma, r, i, \text{zenith})$ are presented in Figures 2.5 and 2.6.

If an aeroplane is used for the collection of remote sensing data, the directions in which the radiation is measured may deviate up to 45° from the nadir direction. The result is that, depending on the relative position of the observed spot with respect to the position of the plane, the radiation coming from this spot is measured in one single direction somewhere in a cone with a half top angle of 45° and with the zenith direction as the central axis. By examination of Figures 2.5 and 2.6 it can be concluded that differences of up to a factor 2 can occur between the directional radiances within this cone. Even if it is taken into account that up to 50% of the reflected radiation may be completely diffuse because of the different distribution of the sky irradiation and of the more diffuse character of the second-order reflection of the crop (for instance for infrared radiation), differences of up to 50% within the observed cone will occur. It is possible that other differences in radiance must be superimposed on these, because of other factors such as variations in leaf-angle distributions and non-Lambertian behaviour of leaves.

A similar calculation was done for a crop with vertical leaves only. The results are presented in Figures 2.7 and 2.8. Because of the fact that $H(\sigma, r, i, \text{zenith})$ is equal to 0 in this case, the radiances are divided by the radiance in direction i instead of by the radiance in the zenith direction.

The previous calculations prove that the radiation that is reflected by a crop cover shows large differences in the directional radiance, even if the crop itself has very simple optical

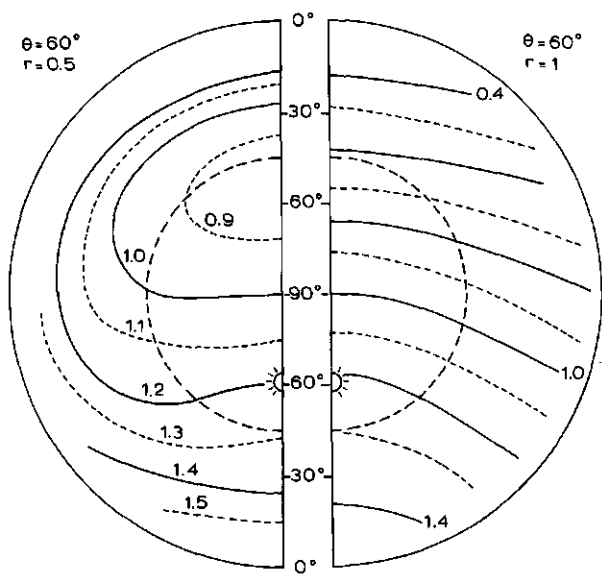


Figure 2.5: Relative radiance differences in the direct reflected flux by a canopy of infinite depth with a spherical leaf angle distribution for two values of the ratio r . The zenith radiance is set to 1.

a): $r=0.5 \rightarrow \rho = \tau = \sigma/2$.

b): $r=1.0 \rightarrow \rho = \sigma, \tau = 0$.

Sun's inclination is 60° . The dashed circle indicates an inclination ν of 45° .

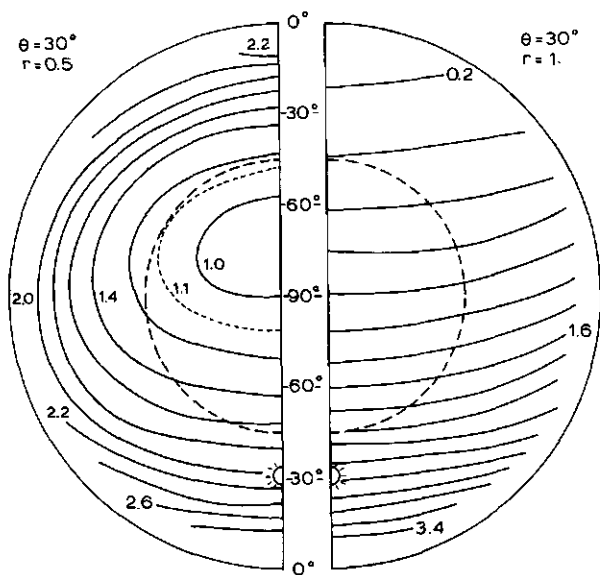


Figure 2.6: As Figure 2.5, sun's inclination is 30° .

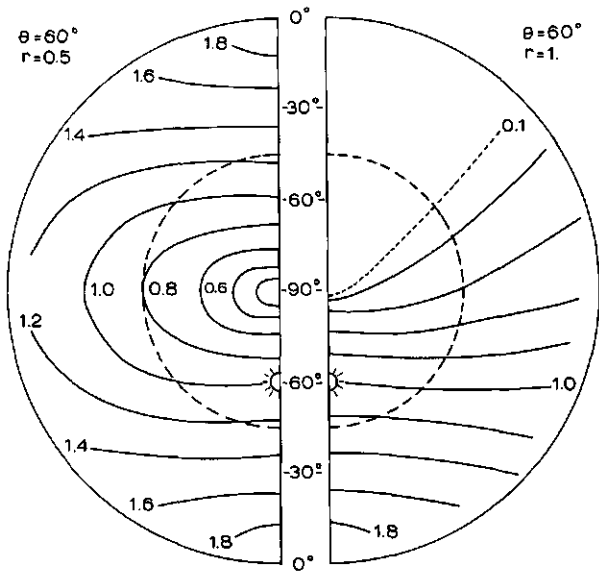


Figure 2.7: Relative radiance differences in the direct reflected flux by a canopy of infinite depth with vertical leaves without azimuthal preference for two values of ratio r . The backward radiance in direction of incidence is set to 1.

a): $r=0.5 \rightarrow \rho = \tau = \sigma/2$.

b): $r=1.0 \rightarrow \rho = \sigma, \tau = 0$.

Sun's inclination is 60° . The dashed circle indicates an inclination ν of 45° .

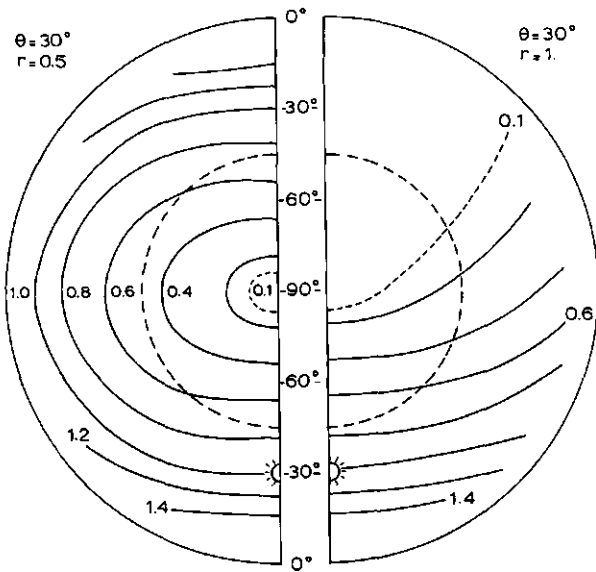


Figure 2.8: As Figure 2.7, sun's inclination is 30° .

and geometrical properties. The interpretation of remote sensing images is always based on the (differences in) radiance in different pixels, generally in several wavelength bands.

So, for a good interpretation it must at least be possible to estimate what differences between observed radiances are caused by variations in crop properties and what differences are caused by different viewing directions. Moreover, one must take account of the fact that, if some time elapses between consecutive observations, the distribution of the sky irradiation and the direction of major incidence change because the sun moves across the sky.

For more complex situations (a layered crop, wind disturbance, soil influences) it is not possible to calculate the differences in radiance with a simple analytical method from the properties of crop and soil. To do this requires a numerical crop reflection model that has enough possibilities for incorporating those properties that really affect the crop reflection. However, before developing such a model, the merits and demerits of some existing models with respect to the target of this study, (viz. a good approximation of the reflected fraction of the incident radiation and of its spatial distribution) are examined in the next section.

2.2 Existing models

In this section four existing models are briefly described and their properties are compared with the requirements of a model that can be applied in this study. The models that are discussed are De Wit's photosynthesis model (Subsection 2.2.1), Suits' reflection model (Subsection 2.2.2), Goudriaan's model (Subsection 2.2.3) and Chen's model (Subsection 2.2.4).

2.2.1 De Wit's photosynthesis model

In the 1960s, De Wit (1965) published a method for calculating photosynthesis. One of the major components of his method is the calculation of the interception of the incoming radiation. To do this, he applied a numerical model based on two principles:

- The crop is divided into thin layers, each layer having an LAI of 0.1. Within individual layers, mutual shading and multiple reflection and transmission are ignored.
- Except for the gaps in each layer, both the reflected and transmitted radiation are assumed to be isotropically scattered in a Lambertian way. The leaf angle distribution is only used to calculate the interception in each layer, not to calculate the directional pattern of the remitted radiation.

De Wit distinguished nine inclination classes, both for radiative fluxes and for the leaf inclination orientations. Each class covers a range of 10° . Each possible leaf angle distribution can be modelled, as can every possible distribution of the incoming radiation. Azimuthal non-uniformity is ignored, all orientations with equal azimuths are lumped to one inclination class. Finally, the soil reflection coefficient is set at 0.10.

De Wit's model shows very good results for the calculation of the interception of the incoming radiation and with that, for the calculation of photosynthesis. Also, the total crop reflection, expressed as the ratio between the total upward flux above the crop and the incoming flux, is approximated fairly well. The directional distribution of the upward flux is, however, not computed but, as mentioned earlier, is fixed to a Lambertian distribution. Because of these simplifications, the model is not suitable for the interpretation of remote sensing observations.

2.2.2 Crop reflection according to Suits

In 1972, Suits published a model that in its original form is mainly usable in developing theories. This model is based on the Duntley equations (Duntley, 1942), similar to the model developed two years earlier by Allen *et al.* (1970). In Suits' model, all leaves and other crop elements are replaced by their projections to three mutually perpendicular planes (one horizontal and two vertical planes). The Duntley equations are used to calculate the forward and backward scatter coefficients in the crop, and, based on those coefficients, the complete radiation profile. A relaxation method is used to calculate the complete diffuse radiation profile, based on the assumption of ideal Lambertian properties of the projection of the leaves. Because of the high absorption, and with that, the low scatter in the visible part of the spectrum, this relaxation process works so fast that after one iteration step fairly accurate results are generally obtained. Because of the extreme simplification in the modelling of the leaf angle distributions (only horizontal leaves and vertical leaves in two perpendicular directions), this model is, like De Wit's model, not suitable for the calculation of the azimuthal distribution of the reflected radiation.

2.2.3 Goudriaan's model

In 1977, Goudriaan presented a layered crop model. This model is developed, starting with a crop with only horizontal leaves and equal reflection and transmission coefficients. In some steps he introduces a model with the possibility to model a crop with an arbitrary leaf angle distribution and unequal reflection and transmission coefficients for the leaves. Other crop properties are similar to those in the De Wit's model: Lambertian scattering by the leaves and absence of azimuthal preference. The calculations are based on a relaxation method. Like De Wit, Goudriaan uses nine inclination classes for leaf angles and for upward and downward radiation. Unlike De Wit, the optical behaviour of a layer is not assumed to be Lambertian, but calculated as a function of the leaf angle distribution. Because the model was primarily developed to calculate light absorption, azimuthal uniformity of the crop is assumed and no azimuthal classes for the radiation are distinguished. All possible directions within one inclination class are lumped together. The result is that also this model is too rough to calculate the directional crop reflection.

2.2.4 Chen's reflection model

In 1984, Chen published a model that deals with most of the properties relevant to this study. He distinguishes 9 inclination classes and 36 azimuthal classes for radiation and for leaf orientation, i.e. in all $9 * 36 = 324$ direction classes. Leaf orientations are defined as planes perpendicular to the 324 reference vectors. Chen makes use of the Kubelka-Munk equations. To do so, he redefines them for application to matrices and vectors. In his model, fluxes are represented by vectors with 324 elements, and the reflection and transmission coefficients from the KM-equations are written as $324 * 324$ matrices, in a similar way as will be described in Section 3.1. The KM-equations permit the calculation of the reflective and transmissive properties of a layer of arbitrary thickness, so Chen's model also allows this.

If the model is to be used for the calculation of the reflection of a non-homogeneous crop, this crop is defined as a stack of internally homogeneous layers. These layers can be combined by means of the adding algorithm, which will be presented in Subsection 3.1.8. Non-Lambertian leaf properties do not cause problems. The model is used in combination with nine inclination classes in the generalized KM-equations (for the incoming radiation). The azimuthal distribution within each class is set to be equal to the distribution that is found after the remission at the first intercepting layer. If the model is applied to crops that show no azimuthal preference in their leaf orientation distribution, the computing time can be considerably reduced.

From a theoretical point of view, Chen's model could be applicable for the research on the directional reflectance of crops. In the infrared region of the spectrum, however, the scatter is so great that the approximation of the directional distribution of the total radiation by the distribution of the primary scattered radiation is not sufficient, so a complete calculation is needed. In the case of a non-uniform azimuthal distribution of the leaves, this causes repeated inversion and multiplication of matrices with $324 * 324 = 104976$ elements, which is practically impossible.

2.3 Conclusions

The models presented in Section 2.2 all have their merits and demerits. The models of De Wit, Suits and Goudriaan are inadequate for the calculation of the directional reflectance because they lack aspects that, as shown by the results presented in Figures 2.5 to 2.8, should be incorporated in the model required. Chen's model should be applicable, but in the infrared region the computing time becomes unacceptably long, so this model becomes unwieldy. But by using many aspects of these models as building blocks, a new model can be developed. This TURTLE model is presented in the next chapter.

2.4 List of symbols used in Chapter 2

		Eqn.	Fig.
A_p	primary absorption	2.2	
A_s	secondary absorption by the crop	2.8	
A_t	total absorption by the crop	2.6	
b	observation direction		2.3
b^*	direction b in the rotated coordinate system		2.4
c	normal direction to a leaf surface element	2.28	
C	leaf element perpendicular to direction c		2.4
d	depth in the crop (LAI units, top=0)	2.3	
dd	layer thickness	2.22	
D_0	downward radiation above the crop	2.2	
D_p	primary downward flux		2.1
D_s	secondary downward flux		2.1
D_t	total downward flux		2.1
$D_{t,d}$	total downward radiation at depth d	2.3	
f, g	arbitrary function names	2.34	
F	distribution function for reflection	2.23	
H_b	radiance in direction b	2.27	
i	source direction		2.3
i^*	direction i in the rotated coordinate system		2.4
I_{dd}	interception by a layer with thickness dd at depth d	2.22	
K	interception coefficient	2.19	
$P_{i,d}$	ratio downward radiation intensity at depth d / downward radiation intensity at the surface	2.20	
$P_{u,d}$	ratio upward radiation intensity at the surface / upward radiation intensity at depth d	2.21	
r	ratio reflection coefficient/scatter coefficient	2.18	
R	total reflection in direction b	2.24	
$R_{d,dd}$	upward radiation intensity caused by reflection by a layer thickness dd at depth d	2.23	
U_p	direct reflected upward flux		2.1
$U_{p,d}$	primary upward flux at depth d	2.16	
U_s	secondary upward flux		2.1
U_t	total upward flux		2.1
$U_{t,d}$	total upward radiation at depth d	2.3	
W	radiation remitted by one leaf element	2.28	
α	absorption coefficient	2.1	
γ	azimuthal angle between source and observation direction		2.3
θ	inclination of the sun	2.19	
$\mu_{p,q}$	angle between directions p and q	2.28	

		Eqn.	Fig.
ρ	reflection coefficient	2.1	
σ	scatter coefficient	2.17	
τ	transmission coefficient	2.1	
v	inclination of the observation	2.21	
ϕ_p	azimuth of direction p in the rotated coordinate system	2.29	
χ_p	inclination of direction p in the rotated coordinate system	2.29	

Chapter 3

TURTLE, HARE and SOIL model

In Chapter 2 it was proved that for the interpretation of remote sensing observations a detailed crop reflection model is needed, and that such a model is not available. Therefore model TURTLE (an acronym for *The Universal Reflection and Transmission model for Layered crop Experiments*) was developed. It is presented in Section 3.1. With the TURTLE model it is possible to calculate the complete flux profile inside a crop. This can be an advantage in some cases, especially if it is used for calculations on photosynthetic activity or if one is interested in the available radiation at some depth in the crop. A disadvantage of the model is the amount of computing time required. Because in remote sensing one is in general only interested in the reflective behaviour of a crop as a whole, an adaption of the formulas used in the TURTLE model could be made to decrease the number of calculations considerably. This is done in the model that is described in Section 3.2, the model HARE (= *Handy and Accurate Reflection model for crop Experiments*). Because the reflective behaviour of a crop is not only determined by the crop itself, but also by the soil, also a separate SOIL submodel is developed. This model is described in Section 3.3.

3.1 The TURTLE model

The TURTLE model is a discrete mathematical description of a continuous physical process. The physical process that is modelled is the reflective behaviour of a crop. It was proved in Chapter 2 that a crop is a very complex reflector, which results almost automatically in a complex model. The description of the TURTLE model in this section is therefore divided in several parts that are discussed separately. The general aspects of the model (Subsection 3.1.1), the definition of reference directions (Subsection 3.1.2), the optical properties of leaves and their modelling (Subsection 3.1.3) and the description of the geometry of a layer (Subsection 3.1.4) are discussed in turn. In Subsection 3.1.5 the optical properties of the leaves and the geometrical structure of a layer are used to derive the optical behaviour of that layer as a whole. A simple soil model is presented in Subsection 3.1.6. In Subsection 3.1.7 a short review of the ignored crop properties is presented. Layers are combined to a crop in Subsection 3.1.8, after which in Subsection 3.1.9 the consequences of this partitioning of a crop in layers is discussed. Finally in Subsection 3.1.10, the model is verified and validated by comparing the results it yielded with the results found by analytical methods and those found by Goudriaan (1977).

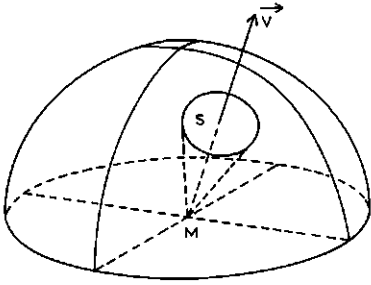


Figure 3.1: Discretisation of the continuity of all possible solid directions. Vector V represents all directions originating in M that intersect the sphere's surface somewhere in region S .

3.1.1 General description of the TURTLE model

As in other numerical models of crop reflection, the continuity of all possible directions is replaced by a number of reference directions. Each reference direction represents all directions in a cone around it (Figure 3.1). Leaf directions are defined by the normal direction on the leaf-plane. In the TURTLE model, 46 directions are distinguished. Similar to Chen's model these directions are used as ray directions for radiation and as normal vectors of leaf orientations. The total canopy is divided into layers. For each layer the optical and geometrical parameters of the canopy elements (leaves) may be defined separately. For these input data, a set of matrices that defines the optical behaviour (reflection, transmission and absorption) of that layer is computed for each layer. All matrices have $46 * 46$ elements. Each matrix element (j, i) or (k, i) depicts the fraction of an incident flux from the direction that is indicated by index i and that leaves the latter in direction j or that is absorbed by leaves with normal direction k . All calculated matrices can be considered as sets of coefficients of linear equations. These equations denote the relations between the vector that represents the radiation that hits a layer and the vectors for the reflected, transmitted and absorbed radiation.

In the computations with the model two soil models are used. Where the TURTLE model is verified by comparison with other models, a flat soil with Lambertian properties is assumed. The calculations on hypothetical and real crops in Chapters 4 and 5 are done with a more sophisticated soil model, in which the soil is modelled as a rough plane. That model is presented and validated in Section 3.3.

Because all relations between fluxes are given as coefficients of linear equations, the reflective behaviour of the crop can be written as a large set of linear equations and solved in that way. A complicating factor in the calculations is the mutual dependence between the input and output vectors, which makes double inversion of a large coefficient matrix necessary. (The downward output of one layer is the input from above for the next layer, whereas one of the output vectors of the latter is an input for the former one.) The number of equations is $46 + 92 * (\text{total LAI/LAI per layer})$. For a crop with an LAI of 5 and an LAI per model-layer of 0.1, this means a set of 4646 equations with the same number of unknowns. Of these, only 46 are of interest for the description of the canopy reflection.

Fortunately, there is a method to solve this type of problem as a series of smaller sets of linear equations. This so-called 'adding method' was described by Van der Hulst (1980) and was applied by Cooper *et al.* (1982). An advantage of this method is that the matrices that represent the influence of the canopy on the incoming radiation are

computed independently of this radiation, so the results of the calculations can be used as a set of linear transformation matrices. These matrices can be applied to the input vector that describes an arbitrary incoming radiation to compute the flux distribution throughout the canopy, and the upward reflection of the radiation above the canopy.

3.1.2 Distribution of the reference directions

A commonly used method to distribute all directions in a hemisphere over a set of representative vectors, is to divide a spherical surface into regions. All radiant vectors to points in one region are represented by the radiant vector of the centre of that region (Figure 3.1).

Models that are based on this concept are generally based on a partitioning according to meridians and parallels on a globe. All intersections of a predefined selection of meridians and parallels are used as reference directions. This method has a disadvantage: with equidistant values $d\kappa$ between the parallels, the represented solid angles per vector decrease with increasing inclination κ and the angles between azimuthally adjacent directions decrease too. When one tries to keep the represented solid angles unchanged, the 'cones' toward the zenith become narrow rectangles or even triangles.

A good partitioning of the spherical surface should fulfil the following principles:

- The angles between the representative vectors of adjacent regions are equal.
- The shape of the regions is circular, to minimize the maximum angle between represented and representative vectors.
- All regions are of equal size.

The best way to fulfil the three given conditions should be a partitioning into hexagons like a honeycomb. But from solid geometry it is known that in a polyhedron the sum of the angular deficiency over all vertices is 4π . (The angular deficiency is the difference between 2π and the sum of the face angles that meet in one vertex.) This property of convex polyhedrons is called Descartes' formula (Williams, 1972). The face angle of a hexagon is $2\pi/3$, and because three faces meet in each vertex, the sum of the face angles in each vertex is 2π . Therefore the angular deficiency is 0 for one vertex, and this can never sum to 4π . This means that a solution with only hexagons must be rejected. (In fact, if a vertex is the intersecting of three faces, and the angular deficiency in that vertex is 0, that means that these faces are in one plane.)

To close a surface that consists of polygons to a polyhedron some polygons with fewer than six edges are needed. To meet the second condition as well as possible, pentagons are a good alternative. The face angle of a pentagon is $3\pi/5$. If in all vertices three faces meet, this angle must be subtracted from $2\pi/3$ to obtain the individual contribution for one angle of one pentagon to the total angular deficiency. This contribution is $2\pi/3 - 3\pi/5 = \pi/15$. The contribution of one pentagon is $5\pi/15 = \pi/3$, so the number of pentagons needed to close the sphere is $(4\pi)/(\pi/3) = 12$. (Notice that hexagons do not contribute to the angular deficiency, so their number is unlimited with respect to the angular deficiency.)

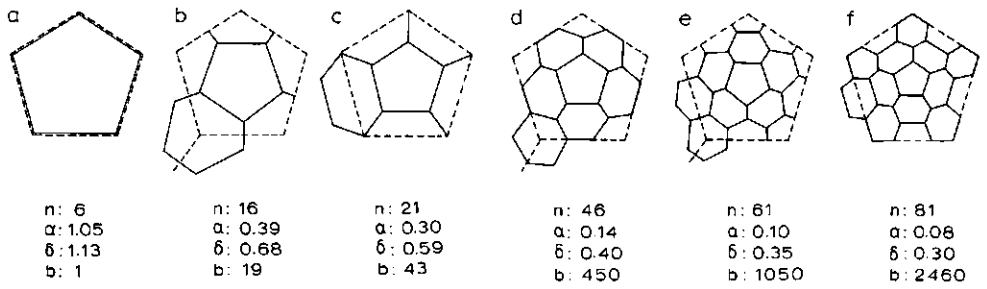


Figure 3.2: Possible partitionings of one face of a pentadodecaeder that result in a partitioning of the surface of a sphere in hexagons and pentagons. With each figure are given:

n : The number of polygons on a hemisphere.

α : The represented solid angle per direction.

δ : An estimation for the mean angle between adjacent vectors.

b : An approximation of the relative number of basic calculation steps (compared to the simplest one) for a model based on that specific partitioning.

The pentagonal face is drawn with a dotted line, the partitionings with solid lines.

The possible numbers of hexagons can be derived from a distribution drawn on a dodecahedron (a regular polyhedron with 12 pentagonal faces). It suffices to draw one pentagon with its possible partitionings. All parts of the face except for the central one, must be a hexagon itself, or it must be possible to complete such part to a hexagon with corresponding parts of adjacent faces. In Figure 3.2 some of these partitionings are drawn. The possibility chosen must necessarily be a compromise between the need for a good representation of the continuity of the spherical surface by a discrete number of points on it on one hand, and on the other hand the need for a so limited number of points that the computing process is technically executable. The computing time needed for matrix multiplications and inversions is roughly proportional to the third power of the number of vectors, and the angle between them is proportional to the square root of this number; so, halving the mean angle between adjacent vector leads to the computing time increasing by a factor of 64. As the result of the need to reach a balance between these conflicting demands, the TURTLE model is based on partitioning according to Figure 3.2d. This means that the chosen number of directions in the hemisphere is 46 with a mean angular distance of about $24^\circ = 0.42$ rad. The calculation of the directions is carried out with a computer program. The directions that coincide with face-centres and vertices on a dodecahedron are computed by use of the geometrical properties of a dodecahedron, the directions of the remaining vectors are computed in such way that the differences between adjacent directions are minimized. A view of the upper hemisphere with the 46 faces is shown in Figure 3.3. The data about the vectors are listed in Appendix B.

3.1.3 Optical properties of the leaves

When a leaf intercepts a light beam, the result of this process can be divided into three separate fractions: a reflected fraction R , a transmitted fraction T and an absorbed

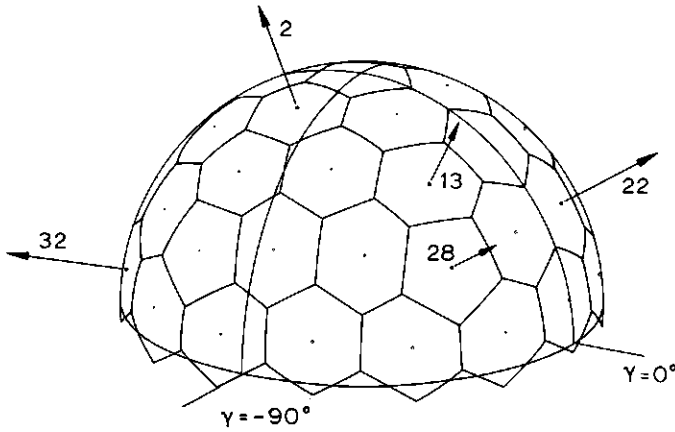


Figure 3.3: The distribution of hexagons and pentagons and reference directions on the upper hemisphere. For some directions the vectors are also presented.

fraction A . These fractions sum to 1:

$$R + T + A = 1 \quad (3.1)$$

The total reflected fraction is the sum of two reflection processes: a fraction R_o is reflected at the leaf surface, and a fraction R_i is caused by multiple scattering by the leaf tissue:

$$R_o + R_i = R \quad (3.2)$$

Another way to divide the reflected fraction is to split it into a diffuse fraction R_d and a specular reflected fraction R_s :

$$R_d + R_s = R \quad (3.3)$$

In the case of very thin leaves, it is possible that a fraction of the light that impinges a leaf will pass through that leaf tissue unaffected. So, the transmitted fraction T can also be split up into two separate fractions: the 'transparently' transmitted fraction T_t and a fraction that leaves the leaf after multiple scattering T_d :

$$T_t + T_d = T \quad (3.4)$$

Although for most crop species T_t for individual leaves is so small compared with the other fractions that it could be neglected, it has been incorporated into the model. It can also be applied to describe gaps in clusters of leaves, like the spaces between the needles of conifers.

R_o (and also T_t) depends on the angle of incidence, so the other parameters do also. Therefore, R_o , R_i , T_d , T_t and A cannot simply be introduced as model parameters. For each combination of the incident direction i and the leaf orientation k , these coefficients have to be computed from the angle of incidence α_i , k and other parameters. α is the angle between the incident direction and the leaf's normal direction.

Specular reflection only occurs at the leaf's surface. For a dielectric boundary its magnitude can be computed with Fresnel's law, as a function of the refraction index n of the leaves, the angle of incidence α and the angle of refraction β (the refraction index of the air is so close to 1 that it is omitted from the formulas). β is computed with Snell's law:

$$\beta = \arcsin \left(\frac{\sin \alpha}{n} \right) \quad (3.5)$$

The surface reflection R_o is computed with Fresnel's law with $\alpha_{i,k}$, $\beta_{i,k}$ and n as parameters, and ignoring polarization. Fresnel's law is:

$$R_o(\alpha, n) = \frac{1}{2} \left\{ \left(\frac{\sin(\alpha - \beta)}{\sin(\alpha + \beta)} \right)^2 + \left(\frac{\tan(\alpha - \beta)}{\tan(\alpha + \beta)} \right)^2 \right\} \quad (3.6)$$

It is possible that the leaf's surface is so curled that the basically specular reflected fraction R_o seems to be scattered diffusely, at least partly. For this purpose a roughness index r is introduced. The specular (R_s) and diffuse (R_{od}) reflected fractions of R_o are now:

$$R_s = (1 - r) * R_o \quad (3.7)$$

$$R_{od} = r * R_o \quad (3.8)$$

The remaining fraction of the intercepted radiation P penetrates the leaf:

$$P = 1 - R_o \quad (3.9)$$

On its way through the leaf, the fraction P will loose energy by internal scattering and absorption. Some of it will reach the opposite side of the leaf. The fraction that does so depends on the transparency of the leaf and the pathlength through the leaf. The transparency is indicated by a transparency index t , which gives the unaffected fraction of P for perpendicular traversal. The relative pathlength is equal to the reciprocal of $\cos \beta$. Because the surface-crossing process also occurs on the underside of the leaf, the fraction P has to be applied again as a multiplication factor to describe the transparent transmission, T_t :

$$T_t = P.t^{1/\cos \beta}.P = P^2.t^{1/\cos \beta} \quad (3.10)$$

All radiation that is not reflected at the surface and not transmitted transparently is assumed to be scattered diffusely or absorbed:

$$D = 1 - R_o - T_t \quad (3.11)$$

Equation (3.11) is equivalent to:

$$D = P - T_t \quad (3.12)$$

The distribution of D over absorption and scattering will be assumed to be independent of the angle of incidence α . Two indices are used to describe this distribution: an absorption index a , to compute the absorbed fraction A :

$$A = a.D \quad (3.13)$$

and a diffuse reflection index d to compute the fraction that is reflected by internal scattering R_i :

$$R_i = d.(D - A) \quad (3.14)$$

$$= D.(1 - a).d \quad (3.15)$$

Now, the total diffusely reflected fraction R_d is:

$$R_d = R_i + R_{od} \quad (3.16)$$

and the remaining fraction of D is the diffusely transmitted fraction, T_d :

$$T_d = D - A - R_i \quad (3.17)$$

$$= D.(1 - a).(1 - d) \quad (3.18)$$

A scheme of the interaction between leaf and radiation is presented in Figure 3.4.

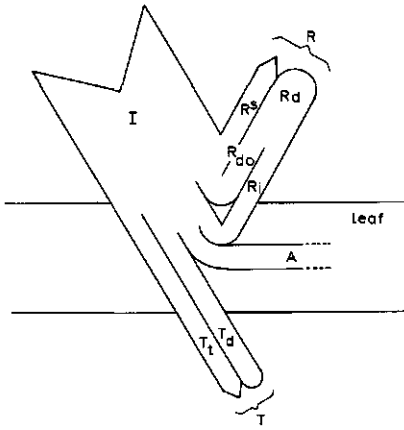


Figure 3.4: Scheme of the distribution of the radiation I that incidents on a leaf over the five possible output destinations. R_s (specular reflection), R_d (diffuse reflection), A (absorption), T_d (diffuse transmission) and T_t (transparent transmission). For further explanation see Subsection 3.1.3.

3.1.4 Geometrical structure of a crop layer

The geometrical distribution of the canopy elements is an important factor in the calculation of the directional dependence of the reflection. One of the major constraints in existing models is the representation of the geometrical distribution of the canopy elements. In most models, the influence of azimuthal variation cannot be modelled at all, and the modelling of inclination density distributions is sometimes limited to a small number of very smooth or hypothetical distributions.

The TURTLE model does not have the mentioned defects. All conceivable leaf-orientation distributions can be defined merely by setting the relative densities for all reference directions to the appropriate values. According to this principle, special leaf-orientation distributions can be defined very simply: to model a hypothetical crop with only horizontal leaves, the element of the vector that belongs to the vertical (normal) direction is set to 1, and all others to 0. For a spherical distribution with an equal density in all directions, all 46 elements of this vector are given the value $1/46$. A distribution of only vertical leaves can be presented by distributing unity over the 15 near-horizontal normal-directions. This is an approximation, because exactly horizontal vectors (and hence vertical planes) do not occur in the model. The LAI of a layer can also be taken into account. To do this, all vector elements must be multiplied with the desired LAI. Because they initially summed up to 1, their sum will now be this LAI. For instance, if a layer with a spherical leaf angle distribution with a total LAI of 0.1 has to be modelled, all vector elements must be set equal to $0.1/46 = 0.002174$.

3.1.5 Optical properties of a crop layer

The optical properties of a layer are a function of the optical properties of the leaves in that layer and their orientational distribution. The effect of leaves on incident radiation can be summed for all leaf directions to obtain the properties of a layer. This statement holds only if the LAI per layer is so low that mutual covering of leaves and multiple

scattering can be ignored.

Interception — A fraction of all the radiation from direction i that penetrates in layer l is intercepted by leaves in direction k . This fraction $I_{k,i}$ depends on:

- The LAI of the leaves in the considered direction (LAI_k).
- The projection of the leaf surface on a plane perpendicular to direction k ($|\cos \phi_{i,k}|$, $\phi_{i,k}$ can be computed from the orientations of i and k with Equation (2.29)).
- The relative pathlength of the beam through the layer ($1/\sin v_i$).

In equation:

$$I_{k,i} = LAI_k \cdot |\cos \phi_{i,k}| / \sin v_i \quad (3.19)$$

(Because in this subsection all equations concern only one model layer, all layer indices l are deleted from the symbols used in this subsection.)

This intercepted fraction $I_{k,i}$ must be distributed over five output destinations, proportional to the distribution factors from Subsection 3.1.3 (here presented in parentheses, following the corresponding output destination):

- A diffusely reflected fraction (R_d)
- A diffusely transmitted fraction (T_d)
- A specularly reflected fraction (R_s)
- A transparently transmitted fraction (T_i)
- An absorbed fraction (A)

The values of the distribution factors depend on the appropriate value of $\phi_{i,k}$

Diffuse reflection and transmission — The diffusely scattered fractions $I_{k,i} \cdot R_d$ (reflection) and $I_{k,i} \cdot T_d$ (transmission) are distributed over all output directions. The distribution is proportional to the cosines of the reflection angles $\phi_{k,j}$ between the normal vector on the leaf plane k and the output direction j . Because all vectors j represent an equal part of the space, these cosines can be used without additional weight factors. Notice that for a part of the combinations (incident direction i - leaf direction k - output direction j) leaf transmission leads to layer reflection and vice versa (see Figure 3.5). The total effect can be written as $R_{d,j,k,i}$ (for layer reflection) and $T_{d,j,k,i}$ (for layer transmission):

$$R_{d,j,k,i} = I_{k,i} \cdot \frac{|\cos \phi_{k,j}|}{\sum_{m=1}^{46} |\cos \phi_{k,m}|} \cdot [R_d \vee T_d] \quad (3.20)$$

and

$$T_{d,j,k,i} = I_{k,i} \cdot \frac{|\cos \phi_{k,j}|}{\sum_{m=1}^{46} |\cos \phi_{k,m}|} \cdot [T_d \vee R_d] \quad (3.21)$$

The choice between the first and the second element from the factors $[R_d \vee T_d]$ and $[T_d \vee R_d]$ depends on the value of $\cos \phi_{i,k} \cdot \cos \phi_{k,j}$: if this value is positive, the former

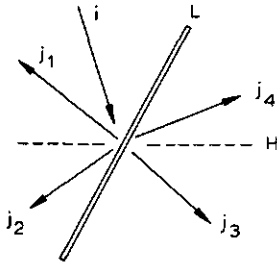


Figure 3.5: Possibilities for remittance of intercepted radiation by a leaf L . The (horizontal) layer direction is indicated with an H . Leaf reflection of incident radiation i can result in layer reflection (j_1) or layer transmission (j_2). Leaf transmission can result in layer transmission (j_3) or layer reflection (j_4).

must be chosen; if it is negative, the latter one.

Specular reflection — The specularly reflected fraction of $I_{i,k}$ is equal to $I_{k,i} \cdot R_s$. The output direction $d_{i,k}$ of this fraction is determined by the direction of the incoming radiation i and the direction of the leaf plane k . In general, $d_{i,k}$ does not coincide with one of the 46 reference directions, so the fraction $I_{k,i} \cdot R_s$ should be distributed over the two or three directions around the output direction $d_{i,k}$. Dealing with the specular reflection in this way introduces unacceptable discontinuities, caused by the divergence of specularly reflected radiation by a non-flat surface. Therefore, another method is used to deal with the specular reflection.

The product $I_{k,i} \cdot R_s$ describes the specularly reflected fraction of the incoming radiation from direction i that is intercepted by leaves with orientation k . Summation over k yields the total specularly reflected fraction S_i of the incoming radiation from direction i :

$$S_i = \sum_{k=1}^{46} I_{k,i} \cdot (1 - r) \cdot R_s(\phi_{k,i}, n) \quad (3.22)$$

S_i must be distributed among all 92 outgoing directions. To do so, the mutual ratios of all fluxes in these 92 directions are calculated, after which S_i is distributed proportionally to these ratios over 92 elements $R_{s,j,i}$ ($j = 1 \dots 92$). These must be used in the calculation of the reflection matrix and the transmission matrix of the layer.

The derivation of the equation that describes the 92 fractions of the specularly reflected radiation is done in two steps. First, it is shown that a simple equation can be used for a crop that exists of perfectly specularly reflecting leaves in a spherical arrangement. In the second step, this equation is adapted to an arbitrary leaf angle distribution and to a coefficient for specular reflection that depends on the angle of incidence.

1. Spherical distribution with perfectly specularly reflecting leaves — The spherical distribution of the leaves permits the replacement of the leaf mass by a sphere with an ideal mirroring surface. Because only the relative flux densities have to be calculated, the size of this sphere is of no importance. It is assumed to be very small, with radius x . It is located in the centre of a large sphere with radius X . The ratio X/x is so large, that all radiation that reaches the inside surface of the large sphere may be considered to originate in the centre of this sphere if it originates somewhere at the surface of the small sphere. The small sphere is hit by a monodirectional beam with a circular cross-section of light with radius d and flux density f , of which the centre points to the centre of the small sphere. This beam is completely intercepted by this sphere (so $d \leq x$). The sphere has an ideal mirroring surface, so all radiation is remitted specularly to the

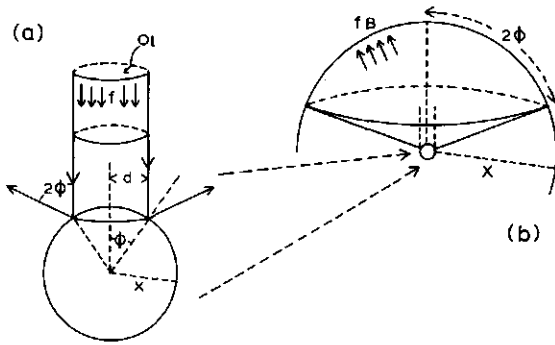


Figure 3.6: Scheme for the calculation of the distribution of specularly reflected radiation by a little glossy sphere.

a): The little sphere with the reflection at the surface.
 b): The upper half of the large sphere with the irradiated section.
 See text for more explanation.

inside surface of the large sphere (see Figure 3.6). For the size of the cross-section O_1 of this beam it holds that:

$$O_1 = \pi \cdot d^2 \quad (3.23)$$

The fraction of the large sphere that is illuminated by means of reflection by the small sphere is the fraction of that sphere within a cone with half top-angle 2ψ . The surface of that fraction is O_b :

$$O_b = 2\pi \cdot (1 - \cos 2\psi) \cdot X^2 \quad (3.24)$$

Substitution of $\cos(2\psi)$ by $1 - 2 \cdot \sin^2 \psi$ in Equation (3.24) yields:

$$O_b = 4\pi \cdot \sin^2 \psi \cdot X^2 \quad (3.25)$$

The relation between ψ , d and x is given by

$$\sin \psi = d/x \quad (3.26)$$

The total incoming flux F_i is equal to $f \cdot O_1$:

$$F_i = f \cdot O_1 = f \cdot \pi \cdot d^2 \quad (3.27)$$

The average flux density \bar{f}_b at the illuminated part of the inner surface of the large sphere is equal to the ratio of the total flux F_i , divided by the surface of that part O_b :

$$\bar{f}_b = \frac{f \cdot \pi \cdot d^2}{4 \cdot \pi \cdot \sin^2 \psi \cdot X^2} \quad (3.28)$$

Substitution of Equation (3.26) in (3.28) and simplification yields:

$$\bar{f}_b = f \cdot \left(\frac{x}{X}\right)^2 / 4 \quad (3.29)$$

So the average flux density at the illuminated fraction of the large sphere is independent of the size of that fraction and of the diameter of the incoming beam of light. This is only possible if the flux densities in all points of the illuminated part of the large sphere are equal. In the case of a specularly reflecting sphere as reflector, the incoming flux is distributed isotropically over all possible directions. The result will be a uniform distribution of S_i over all 92 outgoing directions.

2. *The adaptation to an arbitrary leaf angle distribution and to a specular reflection coefficient depending on the angle of incidence* — A model crop may differ from the simple crop described in the previous paragraph in two aspects:

- The leaf angle distribution needs not be spherical. This influences the interception.
- The specular reflection coefficient depends on the angle of incidence for each combination of leaf orientation and direction of incidence.

So, the uniform distribution as computed before for the extremely simple crop, must be replaced by an equation for the distribution of the remitted radiation that incidents form direction i over the 92 outgoing directions j that takes into account the mentioned aspects. To do so, for each combination of directions (j, i) the bisectrix $k'_{j,i}$ is defined. The angle between directions i and $k'_{j,i}$ is equal to $\phi_{j,i}/2$. Now both aspects (interception and specular reflection coefficient) can be related to this direction:

- The interception $I_{k'_{j,i}}$ is proportional to the relative LAI in direction $k'_{j,i}$ and the cosine of the angle of incidence:

$$I_{k'_{j,i}} \propto LAI_{k'_{j,i}} \cdot \cos(\phi_{j,i}/2) \quad (3.30)$$

- The specular reflection coefficient is computed by the Fresnel function (see Equations (3.5) and (3.6) with α substituted by $\phi_{j,i}/2$):

$$R_{k'_{j,i}} \propto R_o(\phi_{j,i}/2, n) \quad (3.31)$$

Generally, k' does not coincide with one of the reference directions in the model. If this does happen, the leaf density in direction k' is not necessarily known; only if the leaf angle distribution is defined as a continuous function, it should be possible to calculate the relative density in direction k' . For reasons of uniformity the leaf density with reference (=normal) direction $k'_{j,j}$ is always composed as a weighted average over three adjacent directions, according to the algorithm that is presented in Appendix C.

A special case is the situation where the outgoing direction is in a direct line with the incoming direction. In that case, the bisectrixal direction cannot be determined uniquely, but all directions in the normal plane to the incoming direction are bisectrixal directions. In that case, the leaf density is computed as the mean density, calculated over 15 directions that are distributed uniformly in that normal plane. Instead of $\pi/2$, $\arcsin(0.99725) = 1.49662$ rad is used as an estimate of the average value of $\phi_{j,i}/2$. This value is calculated by averaging 150 combinations of directions within the cone that is represented by one direction vector. (Use of $\pi/2$ should lead to another problem, viz. that the projection is set to 0 and that therefore no radiation is intercepted at all.)

Summarizing all statements and equations in the previous paragraphs, for the specularly reflected flux $R_{s,j,i}$ in outgoing directions j ($j = 1 \dots 46$ for reflection, $j = 47 \dots 92$ for transmission) resulting from the incident radiation in direction i it holds that:

$$R_{s,j,i} = S_i \cdot \frac{R_o(\phi_{j,i}/2, n) \cdot LAI_{k'_{j,i}} \cdot \cos(\phi_{j,i}/2)}{\sum_{m=1}^{46} \{R_o(\phi_{m,i}/2, n) \cdot LAI_{k'_{m,i}} \cdot \cos(\phi_{m,i}/2)\}} \quad (3.32)$$

Transparent transmission — The transparent transmission $T_{t,k,i}$ can be computed

as $I_{k,i} \cdot T_t$. This fraction of $I_{k,i}$ can simply be used in the calculation of the layer transmission. It is written here as:

$$T_{t,k,i} = I_{k,i} \cdot T_t \quad (3.33)$$

Absorption — The absorbed fraction of the incident radiation $I_{k,i} \cdot A$ is stored as element $AL_{k,i}$ of the matrix AL :

$$AL_{k,i} = I_{k,i} \cdot A \quad (3.34)$$

Each column sum of AL gives the absorbed fraction of input direction i , summed over all leaf directions k .

Combination to layer matrices — In the preceding paragraphs all partial outputs were computed. They can be combined to the reflection matrix RL and the transmission matrix TL by adding the appropriate results of the former calculations. For the element $TL_{i,i}$ both the transparent transmission T_t through the leaves and the transparency caused by the gaps between the leaves U_i must be taken into account. The latter concerns the non-intercepted fraction, and is equal to the complement of the sum of all intercepted fractions. For incoming direction i :

$$U_i = 1 - \sum_{k=1}^{46} I_{k,i} \quad (3.35)$$

Summarizing for the reflection matrix of the layer RL :

$$RL_{j,i} = \sum_{k=1}^{46} R_{d,j,k,i} + R_{s,j,i} \quad (3.36)$$

and for the transmission matrix TL :

$$TL_{j,i} = \sum_{k=1}^{46} T_{d,j,k,i} + R_{s,j+46,i} \quad (j \neq i) \quad (3.37)$$

and

$$TL_{i,i} = \sum_{k=1}^{46} (T_{d,i,k,i} + T_{t,k,i}) + R_{s,i+46,i} + U_i \quad (3.38)$$

To avoid exceeding the storage capacity of the computer, all summations are done during the computing process, and not as its last step, so the temporary storage of about 185,000 individual values of $R_{d,j,k,i}$ and $T_{d,j,k,i}$ for all combinations of i , j and k is not required.

3.1.6 A simple soil reflection model

The soil is a reflecting rough surface. Therefore a reflection model in which the soil is represented as a flat Lambertian reflector is probably an oversimplification. On the other hand, other crop models use this approximation. Therefore, all verification tests of the TURTLE model were done with the soil modelled as a flat, horizontal reflecting

surface with ideal Lambertian properties. The mathematical aspects of this model are presented here. A more sophisticated soil model is described in Section 3.3.

If the soil is represented as a flat surface, the reflection matrix for the soil, RS , is rather simple. The reflected fraction of the incoming radiation is equal to the soil reflection coefficient ω for every incoming direction i . This reflected fraction must be distributed over all possible output directions j proportional to the cosines of the angles between the output direction and the soils normal vector. For the soil reflection matrix RS this means (v is the complement of the mentioned angle):

$$RS_{j,i} = \frac{\omega \cdot \sin v_j}{\sum_{m=1}^{46} \sin v_m} \quad (3.39)$$

and for the soil absorption matrix AS (notice that the soil is assumed to be flat and horizontal, so for soil direction $k = 0$):

$$AS_{1,i} = 1 - \omega \quad (1 \leq i \leq 46) \quad (3.40)$$

$$AS_{k,i} = 0 \quad (1 \leq i \leq 46, 2 \leq k \leq 46) \quad (3.41)$$

3.1.7 Crop properties ignored

In the model for the leaf-radiation interactions one phenomenon is completely ignored: for some crops there is a noticeable difference between the upper- and underside of the leaves. This can be taken into account, but then some extensions to the model are needed:

- The functions that define the spatial distribution of the leaves must be made suitable for the definition of leaves that are turned upside-down (this sometimes happens and is caused by wind).
- The definition of the optical properties must be extended with the data for the leaf undersides.
- All computations as mentioned in this paragraph double, as do the number of matrices that define the optical properties of one layer.

This not implemented extension of the model has no effect on the computations as described in the next section.

3.1.8 Combining layers to form a canopy

In Subsection 3.1.5 three matrices are computed for each layer: a reflection matrix RL , a transmission matrix TL , and an absorption matrix AL , (if the model is extended as described in Subsection 3.1.7, six matrices are computed). These matrices are referred

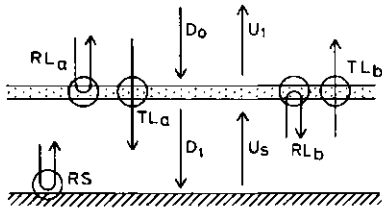


Figure 3.7: Nomenclature in a system with one canopy layer and the soil (see text). D_0 , D_1 , U_s and U_1 are vectors with 46 elements, RL_a , TL_a , RS , RL_b , and TL_b are 46×46 matrices.

to in this paragraph by (as far as possible, layer indices l are deleted):

RL_a	reflection of radiation from above
RL_b	reflection of radiation from below
RS	soil reflection
TL_a	transmission of radiation from above
TL_b	transmission of radiation from below
AL_a	absorption of radiation from above
AL_b	absorption of radiation from below
AS	soil absorption

In the equations also some vectors are used. These are:

D_l	downward flux below layer l
U_l	upward flux above layer l
D_0	downward flux above the canopy
U_s	upward flux above the soil

Finally some matrices are computed that relate the fluxes and absorption at any depth in the crop to the flux vector above the crop D_0 :

DN_l	downward flux below layer l
UP_l	upward flux above layer l
AU_l	absorption from above by layer l
AD_l	absorption from below by layer l

Considering a system that consists of one layer and the soil the following relations can be determined (see Figure 3.7, layer indices are deleted):

$$U_1 = TL_b \cdot U_s + RL_a \cdot D_0 \quad (3.42)$$

$$D_1 = TL_a \cdot D_0 + RL_b \cdot U_s \quad (3.43)$$

$$U_s = RS \cdot D_1 \quad (3.44)$$

Substitution of Equation (3.44) in (3.43) and rewriting leads to Equation (3.48):

$$D_1 = TL_a \cdot D_0 + RL_b \cdot RS \cdot D_1 \quad (3.45)$$

$$D_1 - RL_b \cdot RS \cdot D_1 = TL_a \cdot D_0 \quad (3.46)$$

$$(E - RL_b \cdot RS) \cdot D_1 = TL_a \cdot D_0 \quad (3.47)$$

(E =unitary matrix)

$$D_1 = (E - RL_b \cdot RS)^{-1} \cdot TL_a \cdot D_0 = X \cdot D_0 \quad (3.48)$$

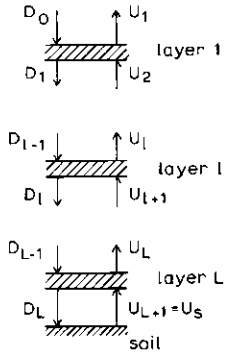


Figure 3.8: Nomenclature in a system with L canopy layers and the soil (see text). All D 's and U 's are vectors with 46 elements.

The matrix $(E - RL_b.RS)^{-1}.TL_a$ is called the compound transmission matrix X for the layer directly above the soil. As can be seen, X depends not only on this crop layer, but also on the soil properties. The explanation of this phenomenon is that X denotes the relation between the downward radiation above this layer and the downward radiation below it. The influence of the soil is caused by the repeated reflection between the soil and the underside of the crop layer. To compute the reflection of the complete system Equation (3.48) must be substituted in (3.44) and then Equation (3.44) in (3.42):

$$U_s = RS.X.D_0 \quad (3.49)$$

$$U_1 = (RL_a + TL_b.RS.X).D_0 = S.D_0 \quad (3.50)$$

The matrix $(RL_a + TL_b.RS.X)$ is called the compound reflection matrix S for the one-layer-and-soil system. This matrix S describes the reflection of this one-layer-and-soil system.

The calculations as presented above suit for a crop and soil system with one single crop layer. If we have to deal with a crop that consists of two layers, we must repeat the procedure as described in Equations (3.42) to (3.50). First, these equations are applied to the lower layer and the soil. The resulting matrix S represents the reflective behaviour of this one layer and soil system. With respect to the upper layer, the combination of the lower layer and the soil can be considered to be a reflecting 'soil' with S as the reflection matrix. Hence, in the second step of the calculations, we use the RL , TL and AL matrices of the upper layer and the S matrix instead of the soil reflection matrix RS . The result is another S matrix which represents the reflective behaviour of the complete two-layers-and-soil system, the newly yielded X -matrix represents the compound transmission of the upper layer (in combination with the underlying system). When more layers are needed to describe the canopy, the calculation process can be repeated for all subsequent layers, computing upwardly.

The total distribution of radiation in a canopy with L layers can now be calculated easily (see Figure 3.8):

$$D_1 = X_1.D_0 \quad (3.51)$$

$$D_l = X_l.D_{l-1} \quad (2 \leq l \leq L) \quad (3.52)$$

$$U_1 = S_1.D_0 \quad (3.53)$$

$$U_l = S_l.D_{l-1} \quad (2 \leq l \leq L) \quad (3.54)$$

$$U_s = RS.D_L \quad (3.55)$$

Using the following notations:

$$s = L + 1 \quad (3.56)$$

$$RS = S_{L+1} \quad (3.57)$$

$$AS = AL_{a,L+1} \quad (3.58)$$

and

$$\prod_{m=0}^1 X_m = E \quad (E : \text{unitary matrix}) \quad (3.59)$$

$$\prod_{m=l}^1 X_m = X_l \cdot X_{l-1} \cdot X_{l-2} \cdots X_1 \quad (3.60)$$

the Equations (3.51), (3.52), (3.53), (3.54) and (3.55) can be written as:

$$D_l = \left(\prod_{m=l}^1 X_m \right) \cdot D_0 \quad (1 \leq l \leq L) \quad (3.61)$$

and

$$U_l = S_l \cdot \left(\prod_{m=l-1}^1 X_m \right) \cdot D_0 \quad (1 \leq l \leq L + 1) \quad (3.62)$$

The absorption in one layer can be expressed in a similar way. Let the absorbed radiation incidenting on the upperside of layer l be CA_l and the absorbed radiation incidenting on the underside of that layer CB_l . Hence:

$$CA_l = AL_{a,l} \cdot D_{l-1} \quad (3.63)$$

$$CB_l = AL_{b,l} \cdot U_{l+1} \quad (3.64)$$

Substitution of Equations (3.61) and (3.62) in (3.63) and (3.64) yields:

$$CA_l = AL_{a,l} \cdot \left(\prod_{m=l-1}^1 X_m \right) \cdot D_0 \quad (3.65)$$

$$CB_l = AL_{b,l} \cdot S_{l+1} \cdot \left(\prod_{m=l}^1 X_m \right) \cdot D_0 \quad (3.66)$$

The Equations (3.61), (3.62), (3.65) and (3.66) enable all relevant information on the distribution of the incident radiation to be computed without knowing the input vector D_0 . The matrices:

$$DN_l = \prod_{m=l}^1 X_m \quad (1 \leq l \leq L) \quad (3.67)$$

$$UP_l = S_l \cdot \prod_{m=l-1}^1 X_m \quad (1 \leq l \leq L + 1) \quad (3.68)$$

$$AU_l = AL_{a,l} \cdot \prod_{m=l-1}^1 X_m \quad (1 \leq l \leq L + 1) \quad (3.69)$$

$$AD_l = AL_{b,l} \cdot S_{l+1} \cdot \prod_{m=l}^1 X_m \quad (1 \leq l \leq L) \quad (3.70)$$

can be used as linear transformation matrices. Premultiplication of the input vector D_0 with one of these matrices results in the calculation of the desired flux or absorption (e.g. the downward flux below layer 4 D_4 can be computed as $DN_4 \cdot D_0$).

3.1.9 The division of the canopy into layers

As mentioned in Subsection 3.1.1, the modelled canopy is split up into horizontal layers. Each layer is assumed to be homogeneous, and different layers can have different properties. Within one layer, leaves are assumed to be arranged in such way that they do not cover each other. There is no relation between the position of the leaves in subsequent layers. All calculations that result in the optical properties are based on the principle that multiple effects in one layer such as mutual covering of leaves and multiple reflection are so small that they can be ignored. This means that the leaf area index per layer LAI_l has an upper limit. De Wit (1965) and Goudriaan (1977) state that a value of 0.1 is acceptable as the LAI per sublayer.

A method to compute an upper limit for the LAI per sublayer is presented here. This method is based on the fact that for each possible leaf distribution the interception of radiation coming from one direction may not exceed 1. Equation (3.19) can be used to derive the intercepted fraction of the radiation in one incident direction I_i :

$$I_i = \sum_{k=1}^{46} (LAI_k \cdot \cos \phi_{i,k} / \sin v_i) \quad (3.71)$$

The worst case occurs for perpendicular incidence, so for $\cos \phi_{i,k} = 1$. This is equivalent to $i = k$. If the total leaf surface within one model layer is oriented in direction k , then:

$$LAI_k = LAI_l \quad (3.72)$$

and

$$LAI_m = 0 \quad \text{for } m \neq k \quad (3.73)$$

Equation (3.71) becomes:

$$I_i = LAI_l / \sin v_i \quad (3.74)$$

For the most oblique directions in the model, it holds that $v = 0.1512$ rad, so $\sin v = 0.1605$. I_i must not exceed 1, so:

$$\frac{LAI_l}{0.1605} < 1 \quad (3.75)$$

this is equivalent to:

$$LAI_l < 0.1605 \quad (3.76)$$

The choice of 0.1 for the LAI per sublayer does not violate this condition.

A second approach for a choice of a LAI per sublayer is to compare the results obtained with different numbers of layers in the same canopy. For relatively simple properties of the canopy an analytical solution can be used for comparison. Here the comparisons are done using a canopy with horizontal leaves and ideal scattering properties. The analytical solutions are obtained with the Kubelka-Munk equations as described in Appendix A.

Numerical solutions for the situation that the canopy is divided in sublayers can be derived easily:

The LAI per layer LAI_l can be found as the quotient of the total LAI LAI_t and the number of layers L :

$$LAI_l = LAI_t / L \quad (3.77)$$

The reflection of a sublayer r_l can be derived from LAI_l and the leaf reflection ρ :

$$r_l = \rho \cdot LAI_l \quad (3.78)$$

The sublayer transmission t_l is the sum of the fraction of gaps in the layer ($1 - LAI_l$) and the product of the leaf transmission τ and the leaf surface LAI_l (notice that the LAI per sublayer cannot exceed 1, because then the area of the gaps would be negative):

$$t_l = (1 - LAI_l) + \tau \cdot LAI_l \quad (3.79)$$

The algorithm that is applied to combine the sublayers to the crop with LAI_l , is very similar to the adding algorithm as described in Subsection 3.1.8. The adaptations to the situation here are:

- Instead of inverted matrices, the reciprocals of scalars are applied.
- For calculations without a soil, the soil reflection is set to 0 (boundary condition II in the KM-equations, see Appendix A).
- A downward flux below the underside is introduced. (This is equivalent to the extension of the adding algorithm, as will be derived in the Section 3.2).

The comparison of some cases is presented in Figure 3.9. As illustrated in this figure, the choice of 0.1 for LAI_l gives satisfactory results again, both for calculations on separate layers as for calculations on crops with a soil underneath.

3.1.10 Model verification and validation

Besides a check on the syntax and the semantics of a program with respect to the programming language, the verification of a computer model always contains at least two other components: an internal consistency check and a comparison between the results and the expected values and an evaluation of the differences between them. These expected values can be results obtained by others and proved to be correct or observations on the modelled system. Sometimes analytical solutions of the equations used in the numerical model are available and can be used also.

Consistency checks — The consistency checks of the TURTLE model are done on four levels:

- Output destinations for a beam intercepted by a leaf (as described in Subsection 3.1.3).
- Total output-flux for one layer as induced by one incident beam.
- All fluxes that deal with one layer.
- All output destinations for the canopy as a whole (e.g. the sum of absorption by leaves and soil and the upward flux above the canopy).

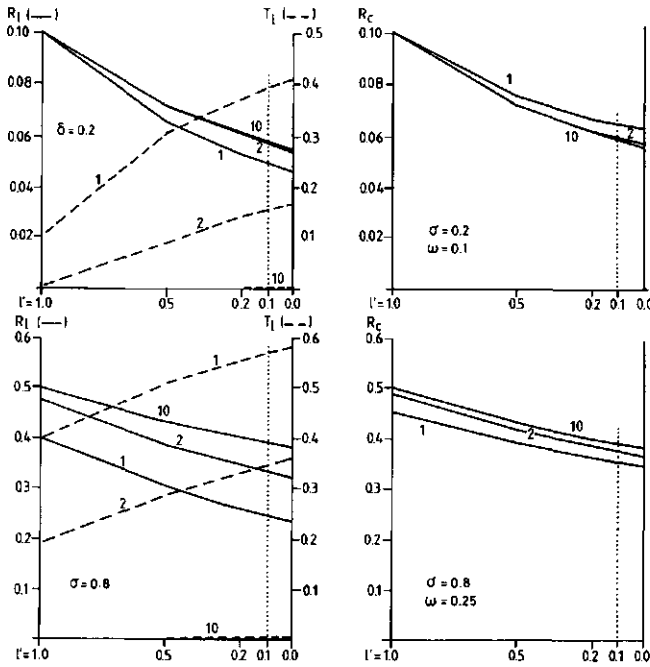


Figure 3.9: Layer reflection R_l , layer transmission T_l and canopy reflection R_c as functions of the leaf area index per sublayer l' for a canopy with horizontal leaves for two values of the leaf scattering σ . Leaf reflection and transmission are assumed to be equal to $\sigma/2$. Left figures represent layer data without, right figures with a soil. Numbers in the figures indicate total canopy LAI. $l' = 0$ represents the analytical solution. The vertical dotted line at $l' = 0.1$ indicates the value for l' that is used in most other calculations.

If the incoming radiation is considered to be a source and the remitted radiation and the absorption together as a sink, then the model can be considered at each of these levels as a manipulator that distributes the radiation from one or more sources over one or more sinks. This means that on all levels the total radiation from all sources must be equal to the total of the radiation that is assigned to all sinks. Then the bookkeeping nature of the model is correct. The following checks were done:

One beam incidenting on one leaf — For many combinations of the optical input parameters for individual leaves the relation between these parameters and the output destinations was carefully examined. The angular dependency of the relation was also considered. No values were found beyond the possible range, and the outputs always summed to 1.

One beam incidenting on a layer — A beam from direction i that finds a canopy layer in its way is distributed over many output destinations. These are 46 reflecting directions, 46 transmission directions and absorbing leaves in 46 orientations. These 138 destinations are the matrix elements $RL(j, i)$ (with $j = 1 \dots 46$), $TL(j, i)$ (with $j = 1 \dots 46$) and $AL(k, i)$ (with $k = 1 \dots 46$), respectively. Because the sum of the outputs must be

equal to the input, the following equation must hold:

$$\sum_{j=1}^{46} RL_{j,i} + \sum_{j=1}^{46} TL_{j,i} + \sum_{k=1}^{46} AL_{k,i} = 1 \quad (1 \leq i \leq 46) \quad (3.80)$$

The easiest way to verify this is to define a one-layer canopy on a non-reflecting soil, and then illuminate it with light from one direction. No invalidation of Equation (3.80) could be found in about 200 cases that have been examined.

All radiation incidenting on one layer — The third check concerns all radiation that deals with one layer. For that case the bookkeeping concerns the incoming and outgoing fluxes for that layer. When absorption is seen as an output, input and output must be equal. The total flux F in upward and downward direction is the sum of all elements of the vector that describe the appropriate flux; for instance:

$$F(D_i) = \sum_{i=1}^{46} D_{i,i} \quad (3.81)$$

In a similar way, the absorbed flux can be written as:

$$F(CA_i) = \sum_{i=1}^{46} CA_{i,i} \quad (3.82)$$

Now the bookkeeping equation is:

$$F(D_{i-1}) + F(U_{i+1}) = F(D_i) + F(U_i) + F(CA_i) + F(CB_i) \quad (3.83)$$

Even in extreme situations (e.g. no absorption, only specular reflection) this equation could not be invalidated.

All radiation incidenting on a total canopy — The last check concerns the total canopy. It says that the total incoming flux $F(D_0)$ is equal to all absorbed fluxes ($F(AU_l, D_0)$, $F(AD_l, D_0)$ and $F(AU_s, D_0)$) and the flux reflected to the sky $F(U_1)$:

$$F(D_0) = \sum_{l=1}^L (F(AU_l, D_0) + F(AD_l, D_0)) + F(AU_s, D_0) + F(U_1) \quad (3.84)$$

The condition given in Equation (3.84) was also satisfied in all tests.

Verification — To verify the complete model, some of the results of the calculations with the model were compared with the results of analytical solutions. These are:

- The downward and upward fluxes for canopies with only horizontal leaves for several combinations of leaf reflection, leaf transmission and soil reflection.
- The downward flux for a canopy with black leaves in a spherical distribution for several inclination directions of the incident radiation.

As a first verification test, a crop with only horizontal leaves was modelled and the results were compared with the analytical results as calculated with the KM-equations (see Appendix A). The results of this comparison are presented in Figures 3.10 and 3.11. In Figure 3.10 average values for leaf reflection and transmission for visible

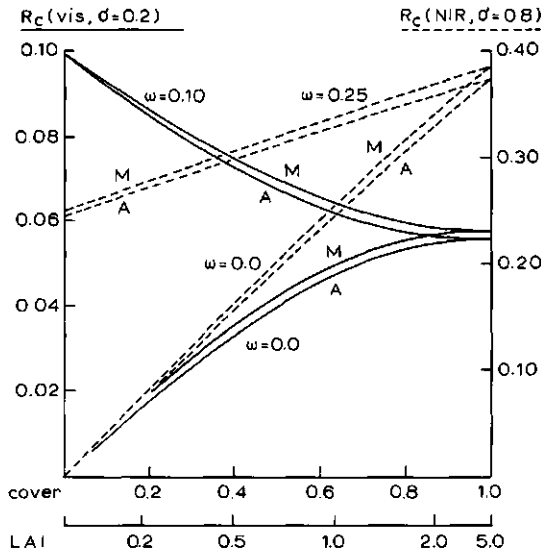


Figure 3.10: Canopy reflection R_c as a function of the total canopy LAI for a canopy with horizontal leaves. Comparison for visible (solid lines, left ordinate) and near infrared radiation (dotted lines, right ordinate). Both the model results with $l' = 0.1$ (M) and the analytical solution (A) are presented. The horizontal axes show both LAI and coverage $1 - e^{-LAI}$, the second of them drawn linearly.

($\sigma = \tau = 0.1$) and near infrared radiation ($\rho = \tau = 0.4$) and for soil reflection ($\omega = 0.1$ for visible, $\omega = 0.25$ for near infrared) are applied. Also the curves for $\omega = 0$ are given. As can be seen, the TURTLE model gives good results. In Figure 3.11 some more hypothetical cases are examined. For five combinations of ρ and τ that satisfy the condition $\rho + \tau = 1$, and a soil reflection ω of 0.5 the model results are compared with the analytical solution. Here too there is good agreement between the corresponding values.

The second verification of the model is done by computing the downward flux in a canopy with black leaves in a spherical density distribution. For six directions of direct radiation and for uniformly distributed diffuse radiation (e.g. a sky with an equal radiance in all

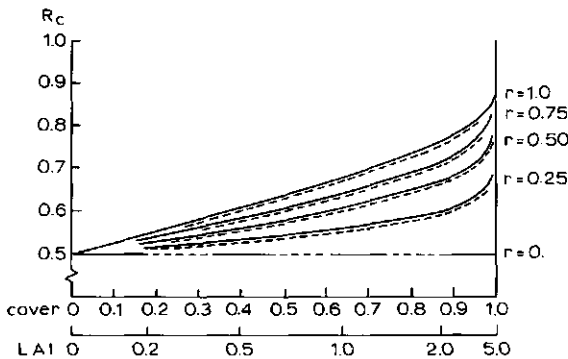


Figure 3.11: Canopy reflection R_c as a function of total canopy LAI for a canopy with horizontal leaves. Comparison for five values of relative reflection r in absence of absorption ($\sigma = 1$). Soil reflection ω is 0.5 in all cases. Both the model results (solid lines) and the analytical solution (dotted lines) are presented. Horizontal axes are like Figure 3.10.

directions) the model results are compared with the analytical solutions for the same situations. For direct radiation the flux is exponentially extinguishing according to:

$$D_d = D_0 \cdot e^{-K \cdot d} \quad (3.85)$$

In this equation, the depth in the crop d is expressed in leaf area units. K is equal to the product of the ratio between the projection of the leaves seen in the incident direction and the surface of the leaves themselves, and the pathlength. For a spherical leaf angle distribution the projection is, independently of the view direction, equal to 0.5. The pathlength is proportional to the reciprocal of the sine of the inclination θ , so:

$$K_\theta = 0.5 / \sin \theta \quad (3.86)$$

When the incident radiation does not come from one direction but is uniformly distributed over the sky the value of D must be computed as the integral over all values of θ , with respect to their contribution to the total incident flux:

$$D_d = \frac{\int_0^{\pi/2} f(\theta) \cdot e^{(-0.5/\sin\theta) \cdot d} \cdot d\theta}{\int_0^{\pi/2} f(\theta) \cdot d\theta} \quad (3.87)$$

The denominator of this fraction is for scaling, whereas $f(\theta)$ is the product of the relative density of the flux of radiation with the considered inclination and its contribution to the downward flux. The relative density is $\cos \theta$. The contribution equals $\sin \theta$.

$$f(\theta) = \sin \theta \cdot \cos \theta \quad (3.88)$$

Transfer of the integrand to $x = \sin \theta$ and corresponding adaptation of the interval gives:

$$D_d = \frac{\int_0^1 x \cdot e^{(-0.5/x) \cdot d} \cdot dx}{0.5} \quad (3.89)$$

For the integral in Equation (3.89) no analytical solution is known. A numerical solution is found with a Gaussian integration with 7 points. To distinguish it from the model results, it is nevertheless called an analytical solution.

From Figure 3.12, it can be seen that in most cases the differences between the model results and the analytical solution are small. They have two sources: partitioning of the canopy in layers and the discretizing of the continuous leaf distribution over 46 discrete directions. To examine which of these two is responsible for the differences, an intermediate solution was computed too. In this solution the real leaf density is maintained, so the relative projection is left unchanged, but instead of the exponential extinction of the flux, the computations are done with assumption of a stack of $L = LAI_i/0.1$ independent layers with an LAI_i of 0.1, so with the same total LAI. As can be derived, the functions for D_d become: for direct radiation with inclination:

$$D_d = \left(1 - \frac{0.05}{\sin \theta}\right)^L \quad (3.90)$$

and for a uniform overcast situation:

$$D_d = \frac{\int_0^1 x \cdot \left(1 - \frac{0.05}{x}\right)^L \cdot dx}{0.5} \quad (3.91)$$

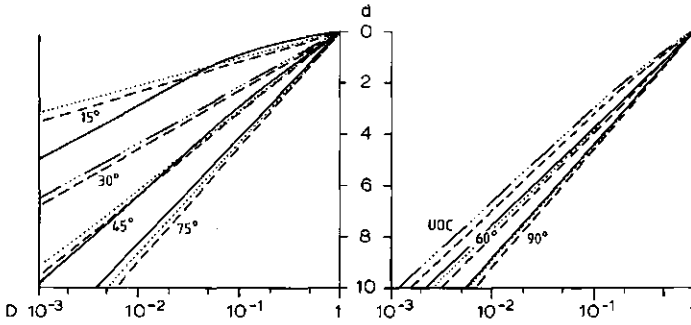


Figure 3.12: Downward flux D as a function of depth d for 6 direct radiation directions and a uniform overcast sky (UOC) on a crop with black leaves in a spherical distribution. Three computation methods are compared: the analytical solution (broken lines), a model with layers with $L' = 0.1$ and an exact direction of incidence (dotted lines), and the computations with the TURTLE model (solid lines). D_0 is 1, d is expressed in LAI-units. For reasons of clearness, the lines are given in two separate figures.

As for Equation (3.89), this integration is also done with a 7-point Gaussian integration.

Now we see that except in one case (for $\theta = 15^\circ$) the differences are mainly caused by the partitioning in layers. The partitioning of the continuity of all directions over 46 fixed ones hardly contributes to the deviations found. In the case of $\theta = 15^\circ$, below $LAI=1.5$, the extinction computed with the model is much lower than the value computed with the Equation (3.90). The explanation for this is that the incoming flux is partitioned into three fluxes according to the partitioning algorithm from Appendix C. The computed fractions are 0.80 at an incident angle of 10.8° , and twice 0.10 at angles of 31.1° . This means that the function that describes the extinction is approximated by:

$$D_d = 0.2.e^{-0.5d/\sin 31.1^\circ} + 0.8.e^{-0.5d/\sin 10.8^\circ} \quad (3.92)$$

At $d = 1.5$ the ratio between the two terms is 3.2 and this value increases rapidly with increasing d , hence the second term does not contribute much at higher LAI-values. This means that for this situation the curve for $\theta = 15^\circ$ is similar to the curve for $\theta = 30^\circ$, but with a flux of 20% of that curve at the same depth.

In addition to the comparisons with analytical solutions the results of some runs with the model are compared with the results presented by Goudriaan (1977). These runs concern:

- Downward and upward fluxes for canopies with a high LAI and a spherical leaf angle distribution.
- Reflection coefficients for several combinations of incident flux and leaf angle distributions.

The first comparison concerns nine cases: three values for the leaf scatter coefficient σ and three types of incident flux are compared. The results are presented in Figure 3.13. The differences between the results obtained by Goudriaan and those obtained with the

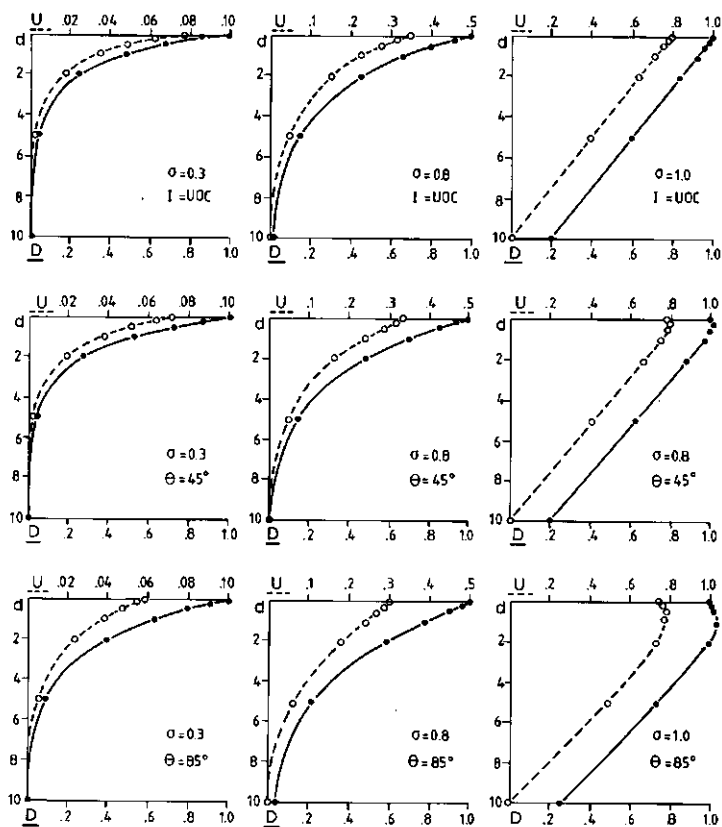


Figure 3.13: Fluxes inside a canopy with a spherical leaf angle distribution and a total LAI=10. Three different values of the scattering coefficient σ and three types of incident radiation are compared with the result of Goudriaan (1977). Leaves show equal reflection and transmission, soil reflection is set to 0. Both downward flux D (solid lines, lower abscissa) and upward flux U (broken lines, upper abscissa) are presented. Vertical axis: depth in LAI-units. Values given by Goudriaan are indicated by small circles.

TURTLE model are so small that they can hardly be seen in the figures. Notice that for direct radiation both computing methods produce at some depth a downward flux that exceeds the incident flux above the canopy.

The second comparison is presented in Table 3.1. Here, the deviations between the results of the two methods are greater, especially in the case of vertical leaves. The differences found in this case may be attributed to the impossibility of exactly modelling vertical leaves in the TURTLE model.

Generally spoken, the results obtained with the TURTLE model give enough confidence to use the model for studies on the spatial distribution of reflected radiation as a function of the optical and geometrical properties of the crop and the properties of the incident radiation.

Table 3.1: Canopy reflection depending on scattering coefficient σ , leaf orientation and angle of incidence of the incoming flux. Leaf reflection and transmission are both equal to $\sigma/2$. Soil reflection is 0. Results are presented in pairs: left value is found by Goudriaan, right value with the TURTLE-model. Differences that exceed 10% are marked with an asterisk, differences between 5% and 10% with a plus.

σ	inclination angle of incoming flux					
	only direct				only diffuse	
	25°	45°	65°	85°	UOC	SOC
horizontal leaves						
.3	(all leaf inclination angles)					.093 .093
.5						.178 .178
.8						.387 .387
leaf inclination 45°						
.3	.091 .096 +	.074 .078 +	.074 .074	.074 .074	.079 .084 +	
.5	.175 .183 +	.145 .153 +	.145 .146	.145 .146	.155 .163 +	
.8	.386 .406 +	.332 .351 +	.332 .340	.332 .339	.350 .366	
vertical leaves						
.3	.090 .096 +	.062 .064	.038 .043 *	.014 .030 *	.059 .069 *	
.5	.174 .185 +	.124 .128	.078 .088 *	.029 .063 *	.117 .135 *	
.8	.388 .405	.297 .308	.199 .228 *	.076 .171 *	.275 .316 *	
spherical leaf angle distribution						
.3	.092 .098 +	.072 .075	.063 .066 +	.059 .062 +	.078 .080	.074 .077
.8	.396 .407	.334 .341	.302 .310	.290 .297	.350 .355	.333 .343

3.2 The HARE model

The TURTLE model described in Section 3.1 has a serious disadvantage. The calculations of the reflective behaviour of a crop as a function of the optical properties of the crop elements and the mutual spatial orientation of the leaves are carried out by adding crop layers one by one (Subsection 3.1.8). This number of layers can be rather large. The adding algorithm must be completely carried out once for each model layer. If, besides that, the premultiplication matrices that define the complete flux profile inside the crop are computed also, the number of matrix multiplications and inversions per layer increases up to eight. Even if the flux profile is not calculated, five calculations of this type still have to be made. The order of the matrices involved is 46, so it will be obvious that the calculations carried out with the TURTLE model are very time-consuming. Therefore, a second model, the HARE model has been derived. This model gives exactly the same results as the TURTLE model for the reflection matrix of the complete crop, generally using only a fraction of the computing time needed for the equivalent calculations with the TURTLE model. The HARE model does not compute the flux profile inside the canopy, but in remote sensing, one is generally interested in the reflective properties of the complete crop and not in the fluxes inside it.

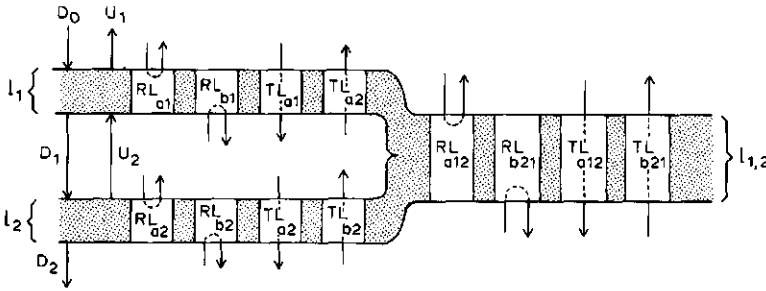


Figure 3.14: Nomenclature of canopy layers (l), interaction matrices (RL and TL) and flux vectors (D and U) as used in the HARE model.

3.2.1 Principles of the HARE model

In the TURTLE model, the matrices that describe the reflection and transmission of one model layer are calculated from the optical and geometrical properties of the crop (Subsections 3.1.3 to 3.1.5). These RL and TL matrices can also be used in an adaptation of the adding algorithm to compute the properties of a layer that consists of two of these layers. In turn, this doubling algorithm can be applied again to the resulting matrices $RL_{1,2}$ and $TL_{1,2}$ to calculate $RL_{1...4}$ and $TL_{1...4}$, describing the properties of a stack of four of the initial layers. To calculate the properties of an even thicker stack, this doubling can be repeated as many times as desired, so matrices for a thick layer can be computed in relatively few steps. Another advantage of this method is that it is relatively easy to calculate the soil influence on the crop reflection. Where in the TURTLE model the soil is one of the first elements to be included in the calculations, in the HARE model it is possible to calculate the matrices for the crop first and then add the soil to the crop in the last adding step. Changing the soil reflection matrix means that only the last step must be carried out again.

3.2.2 One step in the algorithm

The calculation of one step in the doubling algorithm is similar to a step of the original adding algorithm as described in Subsection 3.1.8 (see Figure 3.14 for the meaning of the symbols in this section). At first, only the flux vector incidenting from above (D_0) is considered:

$$D_1 = TL_{a,1} \cdot D_0 + RL_{b,1} \cdot U_2 \quad (3.93)$$

$$U_2 = RL_{a,2} \cdot D_1 \quad (3.94)$$

U_1 and D_2 are the output vectors on the upper and the lower side of the stack, respectively.

$$U_1 = RL_{a,1} \cdot D_0 + TL_{b,1} \cdot U_2 \quad (3.95)$$

$$D_2 = TL_{a,2} \cdot D_1 \quad (3.96)$$

For the combined layers we define $RL_{a,1,2}$ and $TL_{a,1,2}$ as:

$$U_1 = RL_{a,1,2} \cdot D_0 \quad (3.97)$$

$$D_2 = TL_{a,1,2} \cdot D_0 \quad (3.98)$$

In exactly the same way as is done with Equations (3.45) to (3.48), D_1 is computed by means of substitution and inversion. The result is:

$$D_1 = (E - RL_{b,1} \cdot RL_{a,2})^{-1} \cdot TL_{a,1} \cdot D_0 \quad (3.99)$$

$TL_{a,1,2}$ is computed by substitution of Equation (3.99) in (3.98). The calculation of U_1 and $RL_{a,1,2}$ is similar to the calculation of U_1 and S_1 in Equations (3.49) and (3.50):

$$D_2 = TL_{a,2} \cdot (E - RL_{b,1} \cdot RL_{a,2})^{-1} \cdot TL_{a,1} \cdot D_0 \quad (3.100)$$

$$TL_{a,1,2} = TL_{a,2} \cdot (E - RL_{b,1} \cdot RL_{a,2})^{-1} \cdot TL_{a,1} \quad (3.101)$$

$$U_2 = RL_{a,2} \cdot (E - RL_{b,1} \cdot RL_{a,2})^{-1} \cdot TL_{a,1} \cdot D_0 \quad (3.102)$$

$$U_1 = RL_{a,1} + \dots \\ \dots \cdot TL_{b,1} \cdot RL_{a,2} \cdot (E - RL_{b,1} \cdot RL_{a,2})^{-1} \cdot TL_{a,1} \cdot D_0 \quad (3.103)$$

$$RL_{a,1,2} = RL_{a,1} + \dots \\ \dots \cdot TL_{b,1} \cdot RL_{a,2} \cdot (E - RL_{b,1} \cdot RL_{a,2})^{-1} \cdot TL_{a,1} \quad (3.104)$$

The matrices that describe the reflection and transmission of radiation that incidents at the combined layer from below are derived in an analogous way from the single layer matrices. To do this all indices for upper and lower layer 1 and 2 and for 'above' and 'below' a and b are interchanged:

$$RL_{b,2,1} = RL_{b,2} + \dots \\ \dots \cdot TL_{a,2} \cdot RL_{b,1} \cdot (E - RL_{a,2} \cdot RL_{b,1})^{-1} \cdot TL_{b,2} \quad (3.105)$$

$$TL_{b,2,1} = TL_{b,1} \cdot (E - RL_{a,2} \cdot RL_{b,1})^{-1} \cdot TL_{b,2} \quad (3.106)$$

3.2.3 Calculations for a homogeneous crop layer

In the model the upper and lower sides of the leaves are assumed to be identical. This causes the matrices of the upper and lower sides of a model layer to be identical too, so $RL_{a,i} = RL_{b,i}$ and $TL_{a,i} = TL_{b,i}$ for every layer i . But if model layers 1 and 2 are identical, then it is also true that $RL_{a,1} = RL_{b,1} = RL_{a,2} = RL_{b,2}$ and $TL_{a,1} = TL_{b,1} = TL_{a,2} = TL_{b,2}$. This means that Equations (3.104) and (3.105) are equivalent, just like Equations (3.101) and (3.106), so $RL_{b,2,1}$ and $TL_{b,2,1}$ need not be calculated separately, but are equal to $RL_{a,1,2}$ and $TL_{a,1,2}$ respectively. The matrices $RL_{a,1,2}$, $RL_{b,2,1}$, $TL_{a,1,2}$ and $TL_{b,2,1}$ as computed so far, can be used again as matrices belonging to an upper and a lower layer. Of course the statements about equality of matrices in the previous subsection also hold for these matrices. After application of the algorithm in Equations (3.99) to (3.104) the matrices belonging to a stack of four layers are known. These doubling steps may be repeated, so after n steps, the properties of a stack of 2^n layers are obtained. For a homogeneous crop with LAI = 3.2 and a model layer thickness of LAI = 0.1, this means a reduction of the number of adding steps from 32 to 6 (five doubling steps and the addition of the soil).

Table 3.2: Review of the calculation steps needed to obtain the RL - and TL -matrices of a stack of 50 model-layers. DOUBLE stands for doubling, ADDING for adding two layers.

step 1:	DOUBLE	$(RL, TL)_1$:	$(RL, TL)_2$
step 2:	DOUBLE	$(RL, TL)_2$:	$(RL, TL)_4$
step 3:	DOUBLE	$(RL, TL)_4$:	$(RL, TL)_8$
step 4:	DOUBLE	$(RL, TL)_8$:	$(RL, TL)_{16}$
step 5:	DOUBLE	$(RL, TL)_{16}$:	$(RL, TL)_{32}$
step 6:	ADDING	$(RL, TL)_2$ & $(RL, TL)_{16}$:	$(RL, TL)_{18}$
step 7:	ADDING	$(RL, TL)_{18}$ & $(RL, TL)_{32}$:	$(RL, TL)_{50}$

If it is undesirable to construct a homogeneous layer as a stack in which the number of layers is a power of 2 (so 2, 4, 8, ...), the RL and TL matrix cannot be computed by means of doubling only. In that case the calculations deviate slightly from those described in the previous section. At first, the same doubling algorithm is carried out as far as possible. The intermediate results (the RL and TL matrices for 2, 4, 8, ... layers respectively) are stored. The adding algorithm (Equations (3.101) and (3.104) to (3.106)) allows layers with unequal properties to be combined. This means that the properties of a stack of an arbitrary number of layers may be computed in an arbitrary order of adding steps. So, the intermediate results already computed can be mutually combined to obtain the matrices of a stack with the desired number of layers. For instance, if a stack of 50 layers is desired, the doubling algorithm is applied five times, with combinations of 2, 4, 8, 16 and 32 layers as intermediate results. Then the matrices for 50 layers can be calculated as $(2+16)+32$ layers. The steps are shown in Table 3.2. The total number of steps is 7. The last two steps of the calculations above show a special feature. For these layers the property that $RL_{a,1} = RL_{b,2}$, $RL_{a,1} = RL_{b,2}$, $TL_{a,1} = TL_{b,2}$ and $TL_{a,1} = TL_{b,2}$ does not hold. Nevertheless, it is not necessary to repeat the calculations for the underside of the combined layers. It will be clear that for reasons of symmetry $RL_{a,1,2} = RL_{b,2,1}$ and $TL_{a,1,2} = TL_{b,2,1}$. These two equations can be accepted for a more general case. Although it has not been proved, it will be clear that for every stack of layers, independent of its composition of identical or non-identical layers, it holds that $RL_{a,1,2} = RL_{b,2,1}$ and $TL_{a,1,2} = TL_{b,2,1}$ if the stack is symmetrical with respect to its central plane. Because a stack of L identical layers is obviously symmetrical with respect to its central plane, this property holds indefinitely for a stack of identical layers. The formal proof for this can be derived easily from the proof in Appendix D, that concerns the associative property of the adding algorithm.

A second remark can be made on the order of the calculation of a stack of an arbitrary number of identical layers: there is no general solution to find the fastest way to compute the combined matrices for such a stack. Although the method that was applied (doubling as far as possible, followed by the adding of previous results) generally does not require too many calculations, examples can be given that another order of combinations results in a faster calculation (Knuth, 1969). A simple example of this is a stack of 15 layers: with the chosen method the calculation takes 6 steps (with as intermediate calculations $1 + 1 = 2$, $2 + 2 = 4$, $4 + 4 = 8$, $1 + 2 = 3$, $3 + 4 = 7$ and, finally, $7 + 8 = 15$ layers), whereas a faster path can be found that needs only 5 steps (e.g. $1 + 1 = 2$, $1 + 2 = 3$, $3 + 3 = 6$, $6 + 6 = 12$, $12 + 3 = 15$ layers).

3.2.4 Calculations for a non-homogeneous crop layer

If a crop consists of layers with different properties, then the HARE model can be used both for the calculation of the matrices per homogeneous crop layer (by means of the process described in Subsection 3.2.3) and for the combination of these crop layers to form the complete crop (combination of different layers). In these calculations generally $RL_{a,1} \neq RL_{a,2}$, $RL_{a,2} \neq RL_{b,1}$, $TL_{a,1} \neq TL_{b,2}$ and $TL_{a,2} \neq TL_{b,1}$. Therefore, explicit application of Equations (3.105) and (3.106) is needed for the calculation of $RL_{b,2,1}$ and $TL_{b,2,1}$ in the successive steps of the calculation for the crop.

$RL_{b,2,1}$ and $TL_{b,2,1}$ are not calculated if the lower layer includes a soil underneath. Because $TL_{a,2}$ is a zero matrix (the soil is not transparent), $TL_{a,1,2}$ need not be calculated either. In that case only the steps that are involved in the calculation of $RL_{a,1,2}$ are carried out.

As shown before, there are many possible orderings in which the calculations can be carried out if many layers are involved. It may be expected however, that the final result (the optical properties of the complete stack in terms of RL and TL matrices), is not influenced by the computational order. In other words, the extended adding formula's show the associative property. The proof for this is given in Appendix D.

3.2.5 Application and use

As could be expected, practical use has shown that the calculations with the HARE model are 5 to 10 times faster than the equivalent calculations with the TURTLE model. No differences between the results have been found. However, although the calculation speed is faster, the internal radiation regime is no longer calculated. If the model is used in a remote sensing application this will hardly be a disadvantage, because in these applications of this type only the reflection of the complete crop including the soil is to be considered. To enable some statements to be made about the internal fluxes in the crop, the matrices that relate D_l and U_{l+1} to D_0 for the last step in the adding algorithm (the step that couples the combined layers $[1 \dots l]$ to the combination of layers $[(l+1) \dots L, \text{soil}]$) are saved after their calculations. So, if the radiation at a certain depth in the crop has to be calculated, the last step in the algorithm must be the combination of the crop layers above and below this depth (the latter one must include the already appended soil or be the soil itself).

Furthermore, the HARE and TURTLE model share the property that the calculation results are the matrices that are needed to calculate the spatial distribution of the reflected radiation above the crop and of the radiation at some depth in the crop. This means that the vector that represents the spatial distribution of the incoming radiation is not involved in the model, only the crop matrices themselves are computed. So, changes in the distribution of the reflected radiation that are caused by changes in the radiance distribution of the incoming radiation can be investigated without a recalculation of the matrices for the crop themselves.

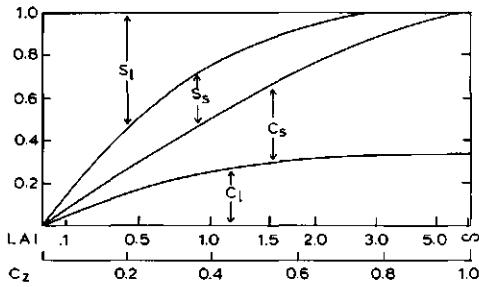


Figure 3.15: Distribution of the observers view when looking at a crop canopy with spherical leaf angle distribution over the fractions sunlit (C_l) and shaded (C_s) crop elements and sunlit (S_l) soil surface. Horizontal axis gives both LAI and vertically measured coverage C_z . Sun's and observer's inclination angle are 45° , the azimuthal difference between the direction of the sun and of the observer is 90° .

3.3 The SOIL model

The techniques that are applied to determine crop properties from reflectional data are mainly based on the observation and interpretation of the differences in radiance between reflecting crops and a reflecting soil. If the effects of multiple scattering could be ignored or eliminated, under certain circumstances there should be a fairly linear relation between coverage and reflection (Bunnik, 1978; Clevers, 1986). A crop, however, is a transparent medium, so multiple effects may not be ignored. The soil under the crop participates in the scattering process even if the crop is completely closed and the soil is invisible from above the crop. The relative importance of the participation of the soil in this process depends on the difference between the scatter coefficients of crop and soil and of the transparency of the crop. This transparency has two independent sources:

- The presence of gaps in the crop. In other words, the fraction of the soil that can be seen directly from the observation direction. The calculations show that an even more important quantity than the directly visible fraction of the soil is the fraction of the soil that is both irradiated by the sun directly and that can be seen by the observer or his equipment.
- Leaves and other crop components are not optically black. This means that even if the soil is completely hidden by the crop above, it still participates in the reflection process. In the infrared spectral band, where the absorption of the crop is low ($< 15\%$), this multiple effect causes the soil to have an especially important contribution to the crop reflection.

The influence of the soil on the total reflection has also two aspects: a quantitative aspect, being the influence on the reflected flux and a qualitative aspect, the influence on the spatial distribution of the reflected radiation. In all cases where crop reflection also depends on the soil reflection, the reflection coefficient of the soil ω plays a role. The influence on the spatial distribution of the reflected radiation is nearly only perceptible if the direct observation of the directly irradiated soil is a noticeable fraction of the complete observed area. To examine these influences closely, at first some calculations were done for a crop with a spherical leaf angle distribution. These calculations concerned the fractions in the observation of directly irradiated leaves, shaded leaves, and directly irradiated and shaded soil. Figure 3.15 shows the results of these calculations for an inclination of sun and observer of 45° and an azimuthal difference of 90° between

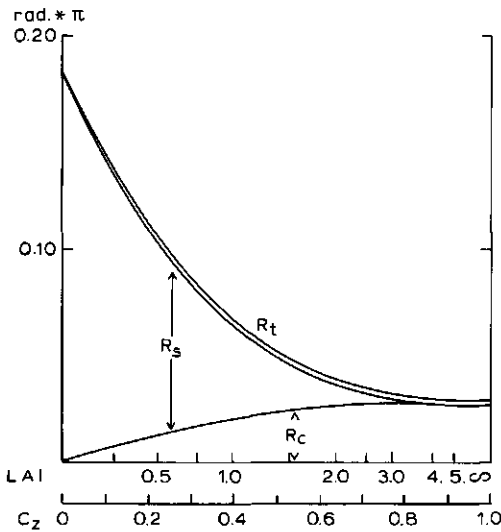


Figure 3.16: Calculated vertical upward radiance of a spherical crop in the red spectral band. Incoming radiation is 80% direct (sun's inclination = 60°), 20% diffuse (SOC-distribution). The total radiance R_t is distributed over the influence of the sole crop (R_c), the primary soil reflection (R_s) and the combination of these (R_b). On the abscissa both LAI and coverage are presented. π is introduced to show numerical values that can be compared to values of upward flux.

these. This figure shows that for an LAI=1.75, over 10% of the observation concerns the directly irradiated soil. If LAI exceeds 2, the fraction of directly irradiated leaves does not change appreciably.

The HARE model (Section 3.2) was used to calculate the influence of the soil reflection coefficient on the total reflection. The parameters in these calculations were leaf reflection $\rho = 0.08$, leaf transmission $\tau = 0.04$ and soil reflection $\gamma = 0.19$, all for red light ($\lambda = 670\text{nm}$). For infrared ($\lambda = 880\text{nm}$) these values were 0.45, 0.40 and 0.30, respectively. The calculations concerned the direct influence of the soil (i.e. a crop with optically black leaves), the influence of the crop itself (with an optically black soil), both compared with the reflection of a 'normal' crop and soil combination. The results are presented in Figures 3.16 (red) and 3.17 (infrared radiation). Figure 3.16 shows that in the red part of the spectrum the interaction between soil and crop can be ignored, because of the high absorption by the leaves. The visible soil plays an important role, but it must be noted that almost the complete contribution of the soil to the reflected flux comes from the directly irradiated soil. The infrared part of the spectrum shows (Figure 3.17) completely different contributions of crop and soil to the reflection. Because of the relatively small difference between the reflection coefficients of crop and soil (0.40 and 0.30, respectively) the influence of the primary soil reflection on the level of the total reflection is small compared with Figure 3.16. On the other hand, because of the high transparency of the crop in this part of the spectrum, the influence of leaf transmission and, concomitantly, that of multiple scatter, increases and therefore the influence of the mutual crop-soil effects increase. So the soil is also important in the infrared wavelength band. In Figures 3.16 and 3.17 it was shown that the soil contributes considerably to the reflective behaviour of a crop if the LAI of the crop is less than 3, and that in the case of red radiation, the soil contribution concerns both the reflected flux and the spatial distribution of the reflected radiation, whereas for infrared radiation this is only the case if the LAI is less than 2.

The existing models generally approximate the soil by a reflecting flat horizontal plane with ideal Lambertian properties. However, a soil is an irregular surface, and if the

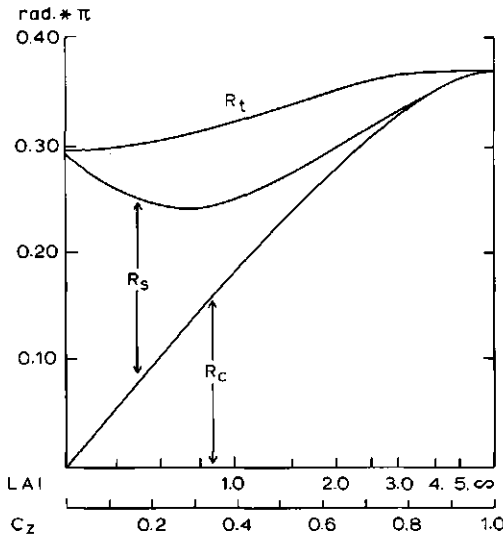


Figure 3.17: As Figure 3.16, for infrared radiation.

sun is not in the zenith, a considerable fraction of the soil can be shaded (Figure 3.18). Even if the surface elements of the soil may be modelled as Lambertian reflectors, the soil as a whole shows a non-Lambertian behaviour.

Although the development of a soil model was not a major topic in this study, a soil model that is somewhat more sophisticated than a flat horizontal surface is developed, mainly to get an impression of the need for such model. This model is described in Subsections 3.3.1 to 3.3.6. In Subsection 3.3.7 some comparative calculations are presented.

3.3.1 General description of the SOIL model

In the SOIL model the soil surface is represented by a flat plane which is partly covered by roughnesses. To simplify the calculations done with this model, the shape of these roughnesses must not be too complex. For this reason it was decided to represent these roughnesses by vertical cylinders with radius 1 and with a flat, horizontal topside. The height of the cylinders is equal to the diameter, so the cylinder height is 2. The spatial density of the cylinders in the base plane is π/E with $E > \pi$. E represents the area of the base plane on which one cylinder is assumed (Figure 3.19), π is the horizontal area that is covered by one cylinder. All surfaces, i.e. the uncovered base plane, and

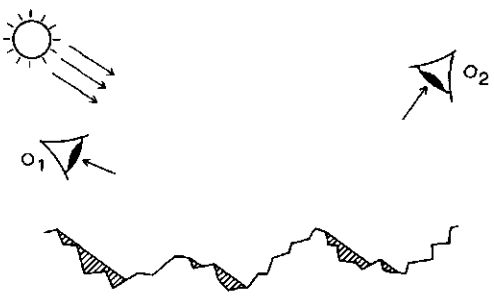


Figure 3.18: Schematic view of a sunlit soil. Shaded regions are dashed. Observer O_1 sees almost only sunlit soil-elements, observer O_2 sees almost only shaded soil-elements.



Figure 3.19: An impression of the soil geometry as used in the SOIL model.

the walls and top of the cylinders are assumed to be Lambertian reflectors. Multiple reflection and mutual shading are disregarded in the calculations. Starting with this, it is possible to calculate the directional scattering for every incoming direction, and with that, the soil reflection matrix RS related to this model can be computed. This matrix replaces the soil reflection matrix RS as given in Subsection 3.1.6.

3.3.2 One cylinder in the model

The influence of one cylinder can be thought of as being the sum of three influences (see Figure 3.20):

- The cylinder hides a part of the base plane. This part has two fractions that partly overlap: the fraction that is hidden from the source (called A in Figure 3.20) and the fraction that is hidden from the observer (B). The total area of this part is therefore the sum of A and B , minus the overlap (AB). Because this part with surface $(A + B - AB)$ does not participate in the reflection of radiation from source to observer, it is a negative component in the equation for the directional reflection.

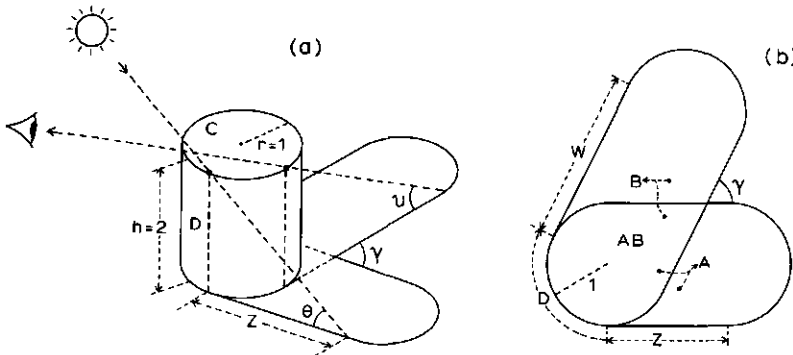


Figure 3.20: Symbols concerning one cylinder in the SOIL model.

θ : sun's inclination; ν : observer's inclination; γ : azimuthal angle between these. h , r : cylinder height and radius; z , w : length of rectangular parts of hidden area's. A , B : part of the base plane hidden for observer or sun; AB : overlap of A and B . C , D : cylinder top and wall.

a): View on one cylinder.

b): Base plane.

- The top of the cylinder (*C*) takes part in the reflection process, so this is a positive component in the equation for the directional reflection.
- A part of the cylinder wall (*D*) is irradiated by the source and also seen by the observer. The remaining part of the cylinder is hidden to the source or to the observer or to both.

In the further calculations in this section the following symbols are used:

- θ : source inclination
- ν : observer's inclination
- λ : azimuthal difference between source and observer
- ω : soil reflection coefficient

The calculations are divided in four parts:

- The influence of the horizontal elements (Subsection 3.3.3)
- The influence of the vertical elements (Subsection 3.3.4)
- The combination of these (Subsection 3.3.5)
- The estimation of E (Subsection 3.3.6)

3.3.3 Horizontal elements

For the visible horizontal elements, it holds that the upward flux F_h from a certain point and in a certain direction is proportional to the product of the sines of θ and ν and the reflection coefficient ω (the incoming flux from direction θ is set to 1).

$$F_h = \omega \cdot \sin \theta \cdot \sin \nu \quad (3.107)$$

If for a combination of θ , ν and ω the radiance R_f of a horizontal surface has to be computed, the related value of F_h must be divided by $\pi \cdot \sin \nu$. Because in the incoming direction the flux is the reference, F_h must also be divided by $\sin \theta$:

$$R_f = F_h / (\sin \nu \cdot \sin \theta \cdot \pi) \quad (3.108)$$

Substitution of Equation (3.107) in (3.108) gives:

$$R_f = \omega / \pi \quad (3.109)$$

Except for the factor $1/\pi$ this equation does indeed give the Lambertian reflection for a flat plane. R_f is independent of ν and θ . This means that the radiance observed does not depend on the direction in which the soil is observed, or on the direction of the incoming radiation. Only the total incoming flux perpendicular to the plane and the reflection coefficient determine the observed radiance.

Because a part of the base is covered or hidden, a correction must be applied to this. The spatial density of the cylinders is $1/E$. Each cylinder withdraws S_1 and adds S_2 to the reflecting horizontal surface, so:

$$R_h = (1 - S_1/E + S_2/E) \cdot \omega / \pi \quad (3.110)$$

The further calculations of the net hidden surface $S_H = S_1 - S_2$ depend on the magnitude of the three parameters: θ , v and γ . Because these calculations are based on simple geometrical formula's, only the final results of these calculations are presented. The cylinder height h is set to 2, the cylinder radius to 1.

$$\left. \begin{aligned} z &= 2/\tan \theta \\ w &= 2/\tan v \end{aligned} \right\} \Rightarrow \left\{ \begin{aligned} k &= \min(w, z) \\ l &= \max(w, z) \end{aligned} \right. \quad (3.111)$$

$$\begin{aligned} x &= k \cdot \cos \gamma + \sin \gamma \\ y &= k \cdot \sin \gamma - \cos \gamma \\ t &= \sqrt{(1 - k \cdot \cos \gamma)^2 + (k \cdot \sin \gamma - 1)^2} \end{aligned} \quad (3.112)$$

For $y \geq 1$ or $x \leq 0$:

$$S_H = 2 \cdot (k + l) + \frac{\pi - \gamma}{2} - \frac{1}{\tan(\gamma/2)} \quad (3.113)$$

For $y < 1$ and $x > 0$ and $t \geq 1$:

$$S_H = 2l + \frac{\pi}{4} + k \cdot (1 - \cos \gamma) + \frac{k^2 \cdot \sin \gamma \cdot \cos \gamma + g \cdot \sqrt{1 - g^2} + \arcsin g}{2} \quad (3.114)$$

with $g = k \cdot \sin \gamma - 1$

For $y < 1$ and $x > 0$ and $t < 1$:

$$S_H = k + l + \frac{k \cdot l \cdot \sin \gamma}{2} + \frac{\pi}{2} - \arccos d + d \cdot \sqrt{1 - d^2} \quad (3.115)$$

with $d = \frac{1}{2} \cdot \sqrt{k^2 + l^2 - 2 \cdot k \cdot l \cdot \cos \gamma}$

3.3.4 Vertical elements, the cylinder wall

To calculate the influence of the cylinder wall on the upward flux F_P at an arbitrary point P at the wall, it holds that (similar to Equation (3.108)):

$$F_P = \omega \cdot \sin i \cdot \sin u \quad (3.116)$$

In this equation i and u represent the angles between the cylinder wall in P and the incoming (i) and outgoing (u) directions. For the radiance at that point it holds that (compare Equation (3.108)):

$$R_P = \frac{\omega \cdot \sin i \cdot \sin u}{\sin \theta \cdot \sin v \cdot \pi} \quad (3.117)$$

For i and u it holds that (see Figure 3.21):

$$\sin i = \cos \theta \cdot \cos(\mu - \gamma) \quad (3.118)$$

$$\sin u = \cos v \cdot \cos \mu \quad (3.119)$$

R_P must be integrated over the fraction of the cylinder wall between $\mu = \gamma - \pi/2$ and $\mu = \pi/2$. The height of the cylinder is 2. A factor $1/E$ must be applied to take account of the relative coverage of the base with cylinders:

$$R_w = \frac{1}{E} \cdot \int_0^2 \int_{\gamma - \pi/2}^{\pi/2} \frac{\omega \cdot \sin i \cdot \sin u}{\sin \theta \cdot \sin v \cdot \pi} \cdot d\mu \cdot dh \quad (3.120)$$

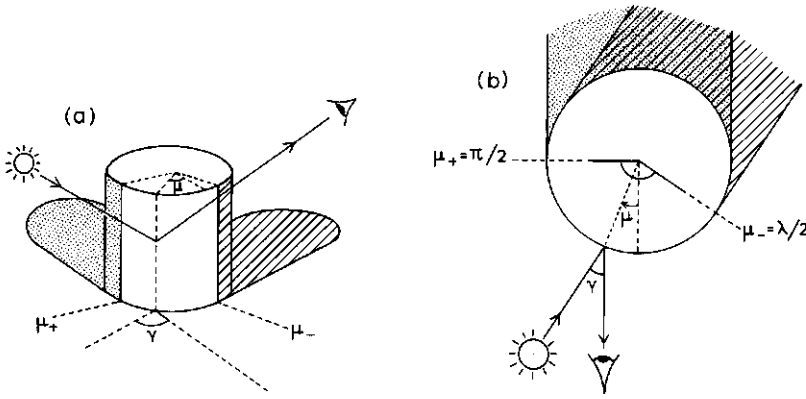


Figure 3.21: Reflection of the cylinder-wall.

a): Perspective view, only the not-dashed and not-speckled part of the wall contributes to the reflection.

b): Vertical projection indicating the used nomenclature.

For further explanation see text.

Substitution of Equations (3.118) and (3.119) gives for the radiance R_v :

$$R_v = \frac{1}{E} \frac{2 \cdot \omega / \pi}{\tan \theta \cdot \tan v} \int_{\gamma - \pi/2}^{\pi/2} \cos \mu \cdot \cos(\mu - \gamma) \cdot d\mu \quad (3.121)$$

$$R_v = \frac{\omega / \pi}{E \cdot \tan \theta \cdot \tan v} \{(\pi - \gamma) \cdot \cos \gamma + \sin \gamma\} \quad (3.122)$$

3.3.5 Combination of horizontal and vertical elements

The radiance R_c of the total system of base and cylinders can be written as the sum R_c of R_h (Equation (3.110)) and R_v (Equation (3.122)):

$$R_c = R_h + R_v \quad (3.123)$$

The radiance of a flat soil R_f is given in Equation (3.109), so the ratio R_c/R_f can now be computed:

$$\frac{R_c}{R_f} = \frac{R_h + R_v}{\omega / \pi} = \left(1 - \frac{S_H}{E}\right) + \frac{(\pi - \gamma) \cdot \cos \gamma + \sin \gamma}{E \cdot \tan \theta \cdot \tan v} \quad (3.124)$$

or

$$\frac{R_c}{R_f} = 1 + \frac{-S_H + \{(\pi - \gamma) \cdot \cos \gamma + \sin \gamma\} / (\tan \theta \cdot \tan v)}{E} \quad (3.125)$$

In this equation the net hidden horizontal surface S_H is computed with one of the Equations (3.113), (3.114) or (3.115), depending on the values of x , y and t (Equations (3.112)).

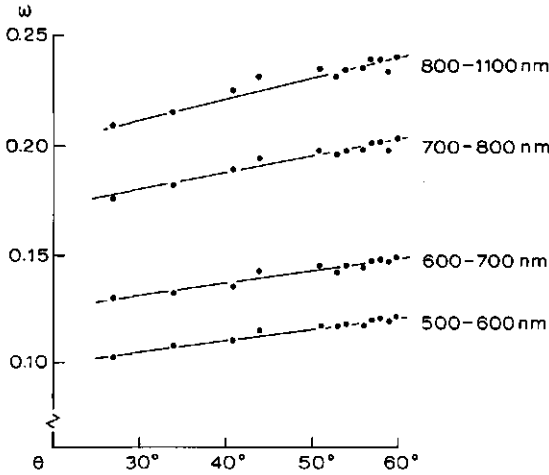


Figure 3.22: Reflection ω of a bare soil measured with an EXOTECH-100 radiometer. Reflection is defined as the ratio between total upward and total downward flux. Ordinate: the reflection in different wavelength bands λ depending on the sun's inclination (abscissa). Data from Ranson *et al.* (1984).

3.3.6 The spatial density of the cylinders π/E

Ranson *et al.* (1984) have done many reflection observations on a field of soja. These observations include some observations on bare soil. These are presented in Figure 3.22. This figure shows that if the inclination of the sun increases from 30° to 60°, the reflection in all four spectral bands examined increases by 13%. The remarkable resemblance between the optical behaviour in the four bands justifies the conclusion that the relation between the reflection and the inclination of the sun is caused solely by the soil geometry. This resemblance is indeed very remarkable; even the small deviations from a smooth curve that represents the overall relation between the inclination and the reflection are identical in the four bands. By means of the 46 reference directions in the HARE model it is possible to determine a value for E in Equation (3.125) in such a way that the reflection in the model increases also by 13%.

This gives the equation:

$$1.13 \cdot \left(1 + \frac{S(30^\circ)}{E}\right) = \left(1 + \frac{S(60^\circ)}{E}\right) \quad (3.126)$$

$S(\theta)$ represents the numerator of the right term of the righthand side of Equation (3.125) for source inclination θ , summed over all HARE directions with weighting factors for the relative contribution of each direction to the upward flux. The values for $S(30^\circ)$ and $S(60^\circ)$ with this function were determined to be -8.92 and -6.83, respectively. Substitution of these values gives:

$$1.13 \cdot \left(1 + \frac{-8.92}{E}\right) = \left(1 + \frac{-6.83}{E}\right) \quad (3.127)$$

Transformation gives:

$$1.13 \cdot (E - 8.92) = E - 6.83 \quad (3.128)$$

$$0.13 \cdot E = 3.25$$

$$E = 25.0 \quad (3.129)$$

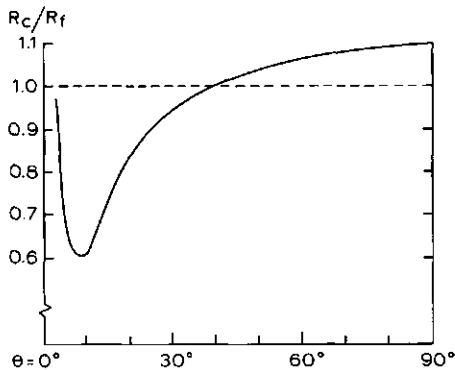


Figure 3.23: Ratio between soil reflection computed with the cylinder-model ω_c and with a flat soil ω_f as a function of the inclination of the sun θ . The sharp increase of the ratio for $\theta \rightarrow 0$ is caused by the important contribution of the cylinder-wall. See text for more explanation.

Figure 3.24: Polar diagrams of the ratio between the total soil reflection coefficients computed with the SOIL model and with a flat soil as a function of the incoming radiation.
 a): Sun's inclination 60° , 20% diffuse radiation (SOC).
 b): Sun's inclination 30° , 40% diffuse radiation (SOC).

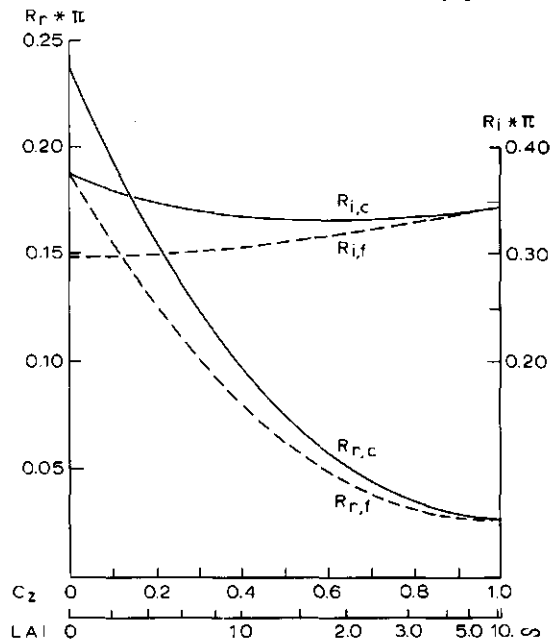
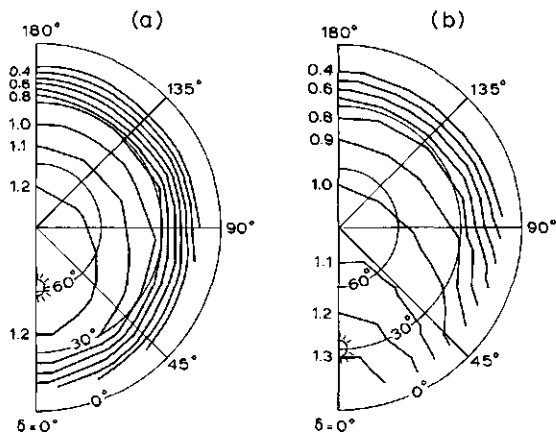


Figure 3.25: Computed reflection of a spherical crop for red (R_r) and near-infrared (R_i) radiation as a function of the LAI. The left ordinate gives the zenith radiance for red (R), the right ordinate for infrared radiation (IR). Broken lines: flat soil; solid lines: SOIL model. Incoming radiation: sun's inclination: 60° , 20% diffuse (SOC).

This means that if a physical model of this soil was made, and the cylinders were placed in a regular triangular pattern, the distance between the centres of the cylinders would be about 5 times the diameter of the cylinders. The ratio between vertical and horizontal elements in the model is $4\pi/25 \approx 1/2$. It must be noticed that the value found for E , although applied in all calculations in the next chapters, in fact is a parameter of the soil. Its relation to the soil roughness is of a reciprocal nature: a larger value of E is related to a flatter soil.

3.3.7 Calibration

In the calculations in Section 3.3, the mutual shading or hiding of cylinders is disregarded. This causes the shaded and hidden base-fraction of the cylinders to be overestimated, because of the division by $(\tan v \cdot \tan \theta)$ for low values of v or θ (see Equation (3.111)). This results in negative values for R_c/R_f . In the model this is prevented by assuming an arbitrary minimum value of $\pi/25$ for R_c/R_f for each individual combination of v , θ and γ ($\pi/25$ denotes the surface of the top faces of the cylinders).

The calculated soil reflection in the model generally has a lower value than the value of ω . To enable the model results to be compared with field trials, where the measured value of ω is generally the measured ratio between incoming and reflected fluxes F , and with calculations using the model with a flat soil, a correction factor was introduced. To calculate this factor, an SOC sky is assumed (SOC = *Standard Overcast*). It is a sky with a radiance distribution proposed by Moon & Spencer (1942). This distribution is proportional to:

$$R(\theta) = (1 + 2 \cdot \sin \theta) / 3 \quad (3.130)$$

$R(\theta)$ gives the radiance of the sky in one point in a direction with inclination θ .

For these calculations, the ratio F_c/ω was calculated. F_c denotes the total upward flux computed with the SOIL model, ω is the soil reflection coefficient. For a flat soil it holds for the total upward flux F_f that $F_f = \omega$, so the ratio F_c/F_f can be used to calculate the reflection of the model soil surface ω' . The value found for F_c/F_f was 0.6921, so ω' can be calculated as:

$$\omega' = \omega / 0.6921 \quad (3.131)$$

Application of ω' in the SOIL model instead of ω gives for the total upward flux the same result as the application of ω with a flat soil. Figure 3.23 shows the reflection as computed with the SOIL model as a function of the inclination of the sun. Figure 3.24 shows the radiative distribution of the reflected radiation (for a Lambertian flat soil, this value is 1 for all directions).

3.3.8 Model calculations and conclusions

To ascertain the influence of the soil model (flat or rough) on the reflection of a crop with a soil, the HARE model was used for a number of calculations. Figure 3.25 represents the zenith radiance for both red and infrared radiance, R_r and R_i respectively. It appears that the cylinder model results in higher values for the calculated radiance for all LAI values. As can be seen in Figure 3.26, the quotient R_i/R_r and the vegetation

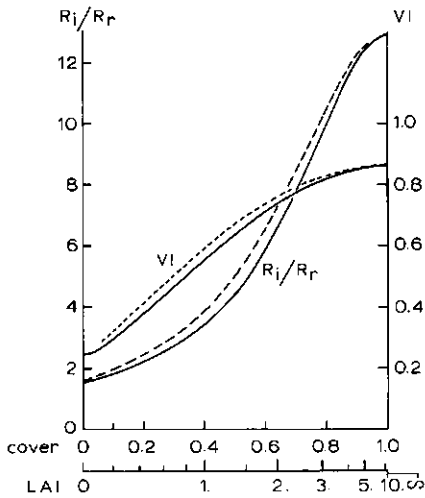


Figure 3.26: Infrared - red reflection ratio R_i/R_r (left ordinate) and vegetation index VI (right ordinate), computed with the same data as Figure 3.25. Broken lines: flat soil; solid lines: SOIL model. Abcissa as Figure 3.25.

index VI are hardly influenced by the choice of the soil model. The vegetation index is computed as the normalized difference of the quotient R_i/R_r , that is computed follows:

$$VI = \frac{R_i/R_r - 1}{R_i/R_r + 1} = \frac{R_i - R_r}{R_i + R_r} \quad (3.132)$$

The use of the vegetation index VI will be explained further in Section 4.4.

For low values of the LAI, where the reflection of the soil itself is an important factor, this can be explained by the fact that the soil model itself has an identical proportional effect on the calculated radiance in both spectral bands. So, functions that are based on the ratio infrared/red are not influenced. For the higher values of the LAI it holds that, if a soil influence is present, it is always indirect, so the incoming radiation is scattered thoroughly. This means that the directional effects are small, compared with the effects on the total flux near the soil. Within the whole range between bare soil and complete coverage, it appears that if the vegetation index is used to estimate the coverage, and the soil type were the only unknown factor in this process, an error of at most 5% is made. It may be concluded that only the soil reflection coefficient ω is of importance, and that the role of the spatial variation in the radiance of the reflecting soil is small. So, if a reflection model is used to estimate crop properties from reflection data, and this estimation is based on ratios between the reflected radiation in different wavelength bands, it is sufficient to know the soil reflection coefficient. The spatial distribution of the reflected radiation near the soil is of little importance.

3.4 List of symbols used in Chapter 3

		Eqn.	Fig.
a	absorption index	3.13	
A	leaf absorption, fraction of incident radiation	3.1	
A	parameter in SOIL model		3.20
AB	parameter in SOIL model		3.20
AD_l	matrix for the calculation of the absorption from below in layer l	3.70	
AL_a	absorption matrix for radiation from above	3.63	3.7
AL_b	absorption matrix for radiation from below	3.64	3.7
$AL_{k,i}$	fraction of radiation incidenting from direction i that is absorbed by leaves with orientation k	3.34	
AS	soil absorption matrix	3.58	3.7
$AS_{k,i}$	fraction of radiation incidenting from direction i that is absorbed by soil elements with orientation k	3.40	
AU_l	matrix for the calculation of the absorption from above in layer l	3.69	
b	relative number of calculation steps		3.2
B	parameter in SOIL model		3.20
C	parameter in SOIL model		3.20
CA_l	absorbed radiation vector from above for layer l	3.63	
CB_l	absorbed radiation vector from below for layer l	3.64	
d	diffuse reflection index	3.14	
d	depth in the crop in LAI units	3.85	
d	radius of light beam (parameter in the calculation of the specular reflection)	3.23	
d	parameter in SOIL model	3.115	
$d_{i,k}$	output direction for specular reflection for radiation incidenting in direction i on a leaf with orientation k	Subject.	3.1.5
D	fraction that is internally influenced by a leaf	3.11	
D	parameter in SOIL model		3.20
D_0	downward radiation vector above the crop	3.42	3.7
D_d	flux intensity at depth d	3.85	
D_l	downward radiation vector below layer l	3.51	3.7
DN_l	matrix for calculation of downward flux below layer l	3.67	
E	parameter in SOIL model	3.124	
f	flux density (parameter in the calculation of specular reflection)	3.27	
\bar{f}_b	average flux density (parameter in the calculation of the specular reflection)	3.28	
F	flux function	3.81	
F_c	total upward flux computed with SOIL model	Subject.	3.3.7

		Eqn.	Fig.
F_f	total upward flux computed with a horizontal soil	Subject.	3.3.7
F_h	unidirectional upward flux caused by reflection of a horizontal soil	3.107	
F_i	incoming flux (parameter in the calculation of the specular reflection)	3.27	
F_P	parameter in SOIL model	3.116	
g	parameter in SOIL model	3.114	
h	height of cylinder in SOIL model		3.20
i	index for incoming radiation		
i	parameter in SOIL model	3.116	
$I_{k,i}$	fraction of radiation from direction i that is intercepted by leaves with orientation k	3.19	
j	index for remitted radiation		
k	index for leaf orientation		
k	parameter in SOIL model	3.111	
$k'_{j,i}$	bisectrix direction between directions j and i	3.30	
K	interception coefficient	3.85	
l	layer index (top layer =1)	3.52	
l	parameter in SOIL model	3.111	
l'	LAI per model layer		3.9
L	number of layers	3.56	
LAI_k	LAI of leaves with orientation k	3.19	
$LAI_{k'_{j,i}}$	LAI of leaves with orientation $k'_{j,i}$	3.30	
LAI_l	total LAI of layer l	3.72	
LAI_m	LAI of leaves with orientation m	3.73	
LAI_t	total crop LAI	3.77	
n	index of refraction	3.5	
n	possible number of polygons on a sphere		3.2
O_b	illuminated surface of small sphere (parameter in the calculation of the specular reflection)	3.24	
O_t	cross section of a beam of light (parameter in the calculation of specular reflection)	3.23	
P	leaf penetration fraction of incident radiation	3.9	
P	reference index in SOIL model	Subject.	3.3.4
r	roughness index	3.7	
r	radius of cylinder in SOIL model		3.20
r_l	sublayer reflection	3.78	
R	leaf reflection, fraction of incident radiation	3.1	
$R(\theta)$	sky irradiance from direction with inclination θ	3.130	
R_b	upward radiance by interaction of crop and soil		3.16
R_c	crop reflection		3.9

		Eqn.	Fig.
R_c	parameter in SOIL model	3.123	
R_c	upward radiance by crop reflection		3.16
R_d	diffuse leaf reflection	3.3	
$R_{d,j,k,i}$	fraction of radiation incidenting from direction i that is remitted backward to direction j by leaves with orientation k as a part of the diffuse reflection process	3.20	
R_f	upward radiance caused by reflection of a horizontal soil	3.108	
R_h	parameter in SOIL model	3.110	
R_i	internal leaf reflection	3.2	
R_i	radiance for $\lambda=870$ nm (infrared)	3.132	
$R_{k'_{j,i}}$	specular reflection coefficient for incidence from direction i on leaves with orientation $k'_{j,i}$	3.31	
R_l	layer reflection		3.9
R_o	leaf surface reflection	3.2	
$R_o(\phi, n)$	Fresnel function for angle of incidence ϕ and index of refraction n	3.31	
R_{od}	diffuse surface reflection	3.8	
R_p	parameter in SOIL model	3.117	
R_r	radiance for $\lambda=550$ nm (red)	3.132	
R_s	specular leaf reflection	3.3	
R_s	upward radiance by soil reflection		3.16
$R_{s,j,i}$	fraction of radiation incidenting from direction i that is specularly reflected to direction j	3.32	
R_t	total upward radiance above the crop		3.16
R_v	parameter in SOIL model	3.120	
RL_a	reflection matrix for radiation from above	3.42	3.7
RL_b	reflection matrix for radiation from below	3.43	3.7
$RL_{j,i}$	fraction of radiation incidenting from direction i that is reflected by a layer to direction j	3.36	
RS	soil reflection matrix	3.44	3.7
$RS_{j,i}$	fraction of radiation incidenting from direction i that is reflected by the soil to direction j	3.39	
s	index representing SOIL ($s = L + 1$)	3.56	
S	compound reflection matrix for one layer and soil	3.50	
S_1	parameter in SOIL model	3.110	
S_2	parameter in SOIL model	3.110	
S_i	total specularly reflected fraction of radiation incidenting from direction i	3.22	
S_l	compound reflection matrix for layer l	3.53	
S_H	parameter in SOIL model	3.113	
t	transparency index	3.10	

		Eqn.	Fig.
t	parameter in SOIL model	3.112	
t_l	sublayer transmission	3.79	
T	leaf transmission, fraction of incident radiation	3.1	
T_d	diffuse leaf transmission	3.4	
T_l	layer transmission		3.9
$T_{d,j,k,i}$	fraction of radiation incidenting from direction i that is remitted forward to direction j by leaves with orientation k as a part of the diffuse reflection process	3.21	
T_t	transparent leaf transmission	3.4	
$T_{t,k,i}$	fraction of radiation incidenting from direction i that is transparently transmitted through leaves with orientation k	3.33	
TL_a	transmission matrix for radiation from above	3.43	3.7
TL_b	transmission matrix for radiation from below	3.42	3.7
$TL_{j,i}$	fraction of radiation incidenting from direction i that is transmitted through a layer to direction j	3.37	
u	parameter in SOIL model	3.116	
U_i	not intercepted fraction of radiation incidenting from direction i	3.35	
U_l	upward radiation vector above layer l	3.53	3.7
U_s	upward radiation vector above the soil	3.55	3.7
UP_l	matrix for calculation of upward flux above layer l	3.68	
VI	vegetation index	3.132	
w	parameter in SOIL model	3.111	
X	radius of large sphere (parameter in the calculation of the specular reflection)	3.24	
x	radius of small sphere (parameter in the calculation of the specular reflection)	3.26	
x	auxiliary variable for integration	3.89	
x	parameter in SOIL model	3.112	
X	compound transmission matrix for one layer and soil	3.48	
X_l	compound transmission matrix for layer l	3.51	
y	parameter in SOIL model	3.112	
z	parameter in SOIL model	3.111	
α	angle of incidence (Snell's law)	3.5	
α	solid angle represented by one vector		3.2
β	angle of refraction (Snell's law)	3.5	
γ	azimuthal difference angle		3.20
δ	mean angle between adjacent vectors		3.2
θ	inclination of the incident radiation	3.86	
θ	sun's inclination		3.20
λ	wavelength	Sect.3.3	

		Eqn.	Fig.
μ	parameter in SOIL model	3.118	
ρ	leaf reflection coefficient	3.78	
σ	scatter coefficient		3.9
τ	leaf transmission coefficient	3.79	
v	observer's inclination		3.20
v_i	inclination of direction i	3.71	
v_i	inclination of direction of incidence i	3.19	
ϕ	angle of incidence	3.19	
$\phi_{i,j}$	angle between directions i and j	3.30	
ψ	half top angle of illuminated sphere sector (parameter in the calculation of the specular reflection)	3.24	
ω	soil reflection coefficient		
ω'	reflection coefficient of a soil surface element	3.131	

Chapter 4

Calculations on hypothetical crops

The models from Chapter 3 have been used to determine some relations between crop properties and the reflection that would be measured if a crop with that properties was subjected to a remote sensing observation. Of course, the ultimate goal of such observation is the estimation or the calculation of crop properties that are relevant for agricultural purposes. It may be expected, however, that the reflective behaviour of a crop is not only determined by its agriculturally relevant properties (e.g. biomass, LAI, development stage and parasitical damages), but also by factors that have only a very limited effect on the growth and development of the crop (for instance the instantaneous moisture content of the top of the soil and leaf orientation disturbances caused by wind). Moreover, the direction of irradiation on the crop changes permanently, due to the daily course of the sun and the changes in the atmosphere, and these changes will also have an effect on the measured reflected radiation. This combination of factors makes the reconstruction of the crop properties from the reflection data very difficult, and it may be expected that this reconstruction is influenced by the mentioned factors.

In this chapter, a great number of calculations for a number of model crops under various sky irradiation distributions will be presented. With these crops as inputs in the HARE model it was possible to investigate the influence of sole properties and combinations of properties on the measured radiation. The properties of those crops were derived from literature data. The crop properties thus defined were translated into parameter values for the HARE model. This part of the calculations is described in Section 4.1. The definition of a set of model crops enabled the investigation of the influence of variation in the values of the parameters on the reflection of the crop and the derived quantities such as vegetation index to be calculated. This was done by varying either one factor (e.g. soil reflection) or combinations of factors (e.g. leaf angle distribution and solar inclination). The calculations were used to derive the expected inaccuracies in the estimation of agriculturally relevant crop properties such as LAI or biomass from remote sensing. In practice, an important moment in the development of a crop is the moment that it becomes closed. If a crop is closed, no photosynthetically active radiation penetrates directly through the crop to the soil. The result of the high absorption in the photosynthetically active part of the spectrum (> 80%) is that the secondary (and higher order) radiation (radiation that has previously been intercepted and remitted) is only of little importance. As soon as the crop is closed, the assimilation rate reaches its maximum level, as far as this rate is related to the intercepted radiation. For this last reason the calculations in this chapter are limited to LAI values in the range

[0...5]. LAI=5 corresponds to a vertically measured coverage of 86 to 97%, depending on the leaf angle distribution. For this maximum LAI value, the sun's inclinations that are used in the model (45° and 60°) gave a penetration of the direct radiation to the soil of 2 to 10%. The calculations were done with optical parameters in three wavelength bands: $\lambda = 550$ nm (green), $\lambda = 670$ nm (red) and $\lambda = 870$ nm (near infrared). The choice of these bands was inspired by Bunnik (1978), who indicates that the simultaneously measured reflections in these bands give the most information about the crop. The various parameters that define the crop and the incoming radiation are presented in Section 4.1. A number of calculations is carried out. Section 4.2 deals with the method of the presentation of these calculations. The calculations themselves are presented in Sections 4.3 (single bands) and 4.4 (combination of wavelength bands). Section 4.5 finally deals with a generally applied method for the correction of measured radiations in order to achieve a better estimation of relevant crop properties.

4.1 The crop and radiation parameters used

The crop properties and the sky irradiation distributions as used in the succeeding sections of this chapter were all derived from literature data. First the crop geometry is discussed (Subsection 4.1.1), followed by the reflection and transmission coefficients of the leaves (Subsection 4.1.2) and the optical properties of the leaves (Subsection 4.1.3). The soil reflection coefficient is defined in Subsection 4.1.4, the sky irradiation in Subsection 4.1.5. Finally a review on all calculations that were done with the HARE model is given in Subsection 4.1.6.

4.1.1 Crop geometry

Leaves are generally the major organs in the process of interception and remission of light, especially in young plants. Therefore, in the TURTLE and HARE models crops are modelled as a set of flat elements with a certain density and orientation distribution between the soil and the top of the crop. The orientations of the leaves are the planes normal to the 46 model directions. In the calculations four different leaf orientation distributions were used. Three of them are idealized, in other words, they can be described as simple continuous density functions on a hemisphere. The fourth one is a distribution that was measured on a real crop.

Idealized distributions

The three idealized or hypothetical distributions show no azimuthal preference, so they can be compared easily to the distribution as classified by De Wit (1965) erectophile, uniform, planophile or spherical (the latter being a special form of an erectophile distribution). In Table 4.1 the functions that determine the distributions as used in this study and the major distributions as defined by Bunnik (1978) are presented. In this table three values are given for each distribution:

- The relative density B_{κ} for all leaves with an inclination of the leaf normal κ .

Table 4.1: Properties of several leaf angle distributions.

Leaf angle distributions:	Symbols:			
P : planophile (Bunnik, 1978)	B_κ : relative density for all leaves with normal's inclination κ			
F : planophile, this study	P_κ : relative unidirectional density for leaves with normal's orientation (γ, κ)			
U : uniform (De Wit, 1965)	F_κ : integral of B_κ ($0 \leq k \leq \kappa$)			
S : spherical (De Wit, 1965) and used in this study	K : interception coefficient for vertical incidence			
E : erectophile, (Bunnik, 1978) and used in this study				
	B_κ	P_κ	F_κ	K
P	$(4 \cdot \sin^2 \kappa) / \pi$	$2 \cdot (1 / \cos \kappa - \cos \kappa) / \pi^2$	$(2 \cdot \kappa - \sin 2\kappa) / \pi$	0.849
F	$\sin 2\kappa$	$(\sin \kappa) / \pi$	$(1 - \cos 2\kappa) / 2$	0.667
U	$2 / \pi$	$1 / (\pi \cdot \cos \kappa)$	$2 \cdot \kappa / \pi$	0.637
S	$\cos \kappa$	$1 / (2 \cdot \pi)$	$\sin \kappa$	0.500
E	$(4 \cdot \cos^2 \kappa) / \pi$	$(2 \cdot \cos \kappa) / \pi^2$	$(2 \cdot \kappa / \pi + \sin 2\kappa) / \pi$	0.424

- The relative density P_κ for the leaves with an orientation of the leaf normal given by γ (azimuth) and κ (inclination). The relation between B_κ and P_κ is given by

$$P_\kappa = \frac{B_\kappa}{2 \cdot \pi \cdot \cos \kappa} \quad (4.1)$$

- The integral F_κ of B_κ : The value of F_κ is equal to the fraction of all leaves that have an inclination of the leaf's normal between 0 and κ . The relation between B_κ and F_κ is given by

$$F_\kappa = \int_0^\kappa B_\kappa \cdot d\kappa \quad (4.2)$$

Of course, B_κ must be calculated in such way that $F_{\pi/2} = 1$.

- The vertical interception coefficient K , calculated as

$$K = \int_0^{\pi/2} B_\kappa \cdot \sin \kappa \cdot d\kappa \quad (4.3)$$

As can be seen in Table 4.1, the distribution P and U will cause problems if the unidirectional density P_κ is used to determine the parameters for use in the HARE and TURTLE models, because for $\kappa = 90^\circ$ (horizontal leaves) for these distributions $P_\kappa \rightarrow \infty$. For this reason instead of the planophile distribution another distribution is defined that does not show this property. This distribution is indicated with F in Table 4.1.

The distributions that are used in the further calculations in this chapter are:

Spherical distribution — Referring to Ross (1981, Table 1.6.1), this distribution was found in practice for maize by Ross & Nilson (1967a,b), Ross & Vlasova (1967), Ross & Ross (1969), Nichiporovich (1963), for rye grass by De Wit (1965), for wheat and timothy grass by Nichiporovich (1961). In the Anglosaxon world this density distribution is sometimes called 'uniform'. However it should not be confused with the distribution that is called uniform by De Wit (1965).

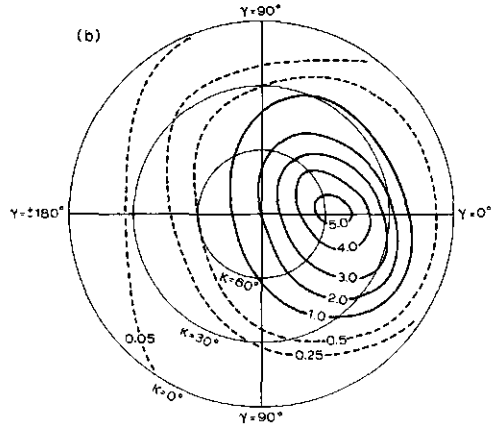
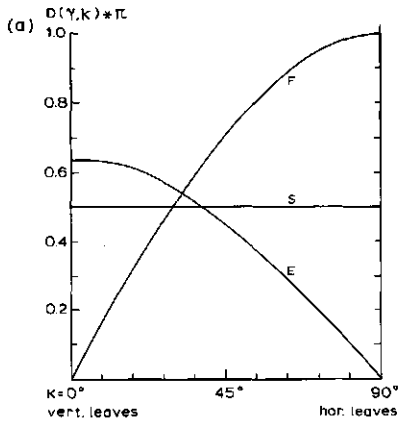


Figure 4.1: Relative uni-directional leaf density for four model crops.

a): Distributions without azimuthal preference. Vertical axis: uni-directional density. Horizontal axis: inclination of the leaf's normal, (S) spherical, (E) erectophile, (F) planophile leaf angle distribution.

b): Leaf angle distribution of a crop with azimuthal preference (Lang, 1973). For comparison: a spherical distribution should have a value 1 over the whole diagram.

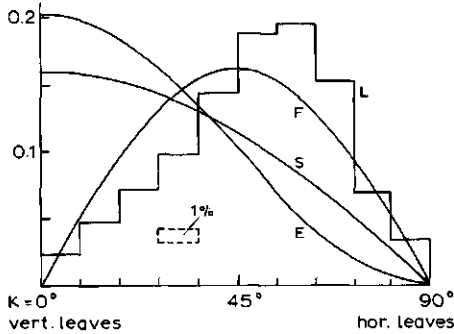
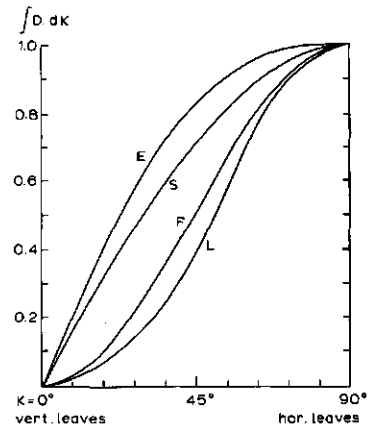


Figure 4.2: Leaf density B_{κ} as a function of the inclination of the leaf's normal κ for four model crops. Horizontal axis: Total leaf mass for all leaves with indicated inclination per inclination class of 9° . Curves are given for spherical (S), erectophile (E), planophile (F) leaf angle distribution and for the distribution according to Lang (L) (1973).

Figure 4.3: Cumulative leaf density F_{κ} as a function of the inclination of the leaf's normal κ . Horizontal axis and symbols as in Figure 4.1a.



Erectophile distribution — In the previously mentioned table Ross gives comparable values for young rye grass (De Wit, 1965).

Planophile distribution — Density distributions comparable to the planophile distribution were reported by Ross as to be found for maize by Ross & Vlasova (1967) and De Wit (1965), for potatoes by Ross & Ross (1969) and Nichiporovich (1961), for lucerne by Warren Wilson (1965) and for rye grass by De Wit (1965).

Distribution with azimuthal preference

In practice, measuring the leaf orientation distribution is very time-consuming, especially if not only the inclination itself but also its combination with azimuths is required. This is probably the reason why so few measured complete orientation distributions have been published. In most models for the interaction between crops and incident radiation, the azimuthal distribution is assumed to be uniform. The few more detailed measurements that have been presented, generally only concern the azimuth of the major vein or of the sprout orientation. Lang (1973) determined the spatial coordinates of several points on the surfaces of a great number of leaves of a cotton plant. He considered these to be the vertices of triangles. From the coordinates of these vertices he calculated the orientation and size of each triangle. The results of his measurements and calculations show very clearly that cotton plants are heliotropic: the leaves orientate perpendicular to the sun, which results in maximum light interception. Lang presented his measurements in a table, in which he distinguished 10 azimuthal and 10 inclination classes. The tripartition formulas (see Appendix C) were used to transform the values reported by Lang to the 46 model directions of the HARE model. An azimuthal rotation was applied in such a way that the mass centre of the distribution was orientated to the direction with azimuth $\gamma = 0^\circ$.

The properties of the four density distributions discussed and mentioned for further use are presented graphically in Figures 4.1 to 4.4. Figure 4.1a shows the uni-directional density of the three hypothetical distributions, Figure 4.1b the density distribution of the Lang distribution in a polar diagram. Figure 4.2 shows the densities summed over the various inclination classes. Figure 4.3 shows the cumulative densities of the four distributions. Finally, Figure 4.4 shows the relation between the interception coefficients and the inclination of the incoming direction, in Figure 4.4a for the distribution without azimuthal preference and in Figure 4.4b for the distributions with azimuthal preference. The values in Figure 4.4 are divided by the corresponding value for the spherical distribution. The function to compute the interception coefficient K for the penetrating fraction D_d of light at a depth d in the crop (d is measured in LAI units) is:

$$D_d = e^{-K \cdot d} \quad (4.4)$$

For a crop with a spherical leaf angle distribution, the ratios between the projection of the leaves perpendicular to any arbitrary direction and the leaf surface itself is equal to 0.5. The length of the path is $1/\sin \theta$ and must be taken in the equation. So, for a spherical distribution, D_d at depth d is given by:

$$D_d = e^{-0.5 \cdot d / \sin \theta} \quad (4.5)$$

Figure 4.4a shows that for larger inclinations of the sun ($\theta > 35^\circ$) the primary radiation penetrates deeper in an erectophile crop than in a planophile crop, whereas for lower sun inclinations, the opposite is true. Figure 4.4b shows that the distribution according

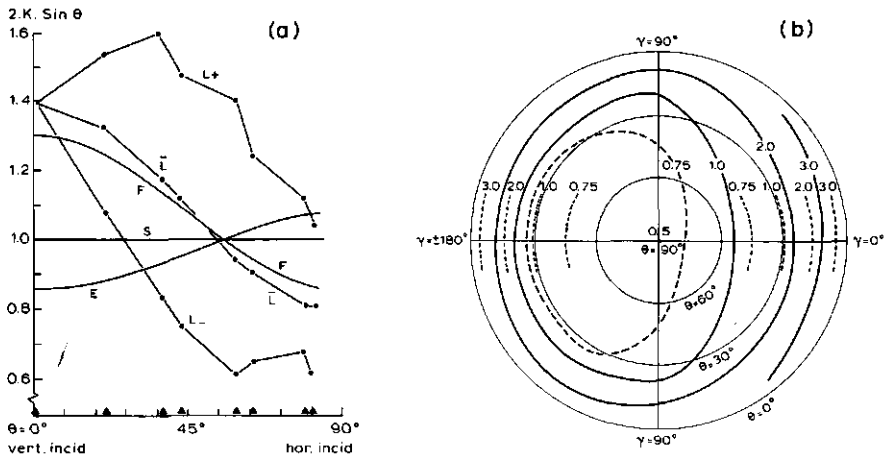


Figure 4.4: Penetration of direct light in crops.

a): Interception coefficient K for the penetration of primary radiation. Horizontal axis: inclination of the incoming direction. Vertical axis: $2.K \sin \theta$, S : spherical, E : erectophile, F : planophile distribution. For the distribution according to Lang (1973), the highest (L_+), the lowest (L_-) and the mean value (\bar{L}) are given. Marks on the x-axis indicate inclinations of model directions. b): K -values for penetration of primary radiation for the canopy according to Lang (1973) (solid and broken lines) and for the spherical distribution (dotted lines, only partly drawn). Azimuth and inclination of the incoming radiation are indicated by γ and θ , respectively.

to Lang (1973) is a planophile one, but it must be noted that the interception coefficient strongly depends on the azimuth of the incoming direction. It is striking that the curve that depicts the mean value of K for the Lang distribution crosses the common point of intersection of the other curves. This point coincides with the value of 32.5° found by Warren Wilson (1965) with a point-quadrat method. At this inclination, the penetration depth for primary radiation is independent of the actual leaf angle distribution for natural vegetations. A comparable result is found by Oliver & Smith (1974). The distribution as given by Lang shows a striking difference between the minimum and maximum interception coefficients for observation directions with equal inclination. In Figure 4.5 this is expressed in another way. The fraction of visible soil is computed as a function of observation direction and leaf area index. If the difference between the reflection of crop elements and the soil is large, as in the case of red radiation, this will directly influence the directionally dependent radiation.

4.1.2 Leaf reflection and transmission

If a beam of light that enters a layer is intercepted by a leaf within that layer, a fraction of the intercepted radiation is reflected by the leaf, a fraction is absorbed and a fraction is transmitted through the leaf. The optical behaviour of the leaves, and with that the optical behaviour of the layer, mainly depends on the mutual ratios of these quantities. Gausman & Allen (1973) presented a review of some optical parameters of the leaves of 30 crops, Gausman *et al* (1981) did the same for 7 weeds. They reported their results

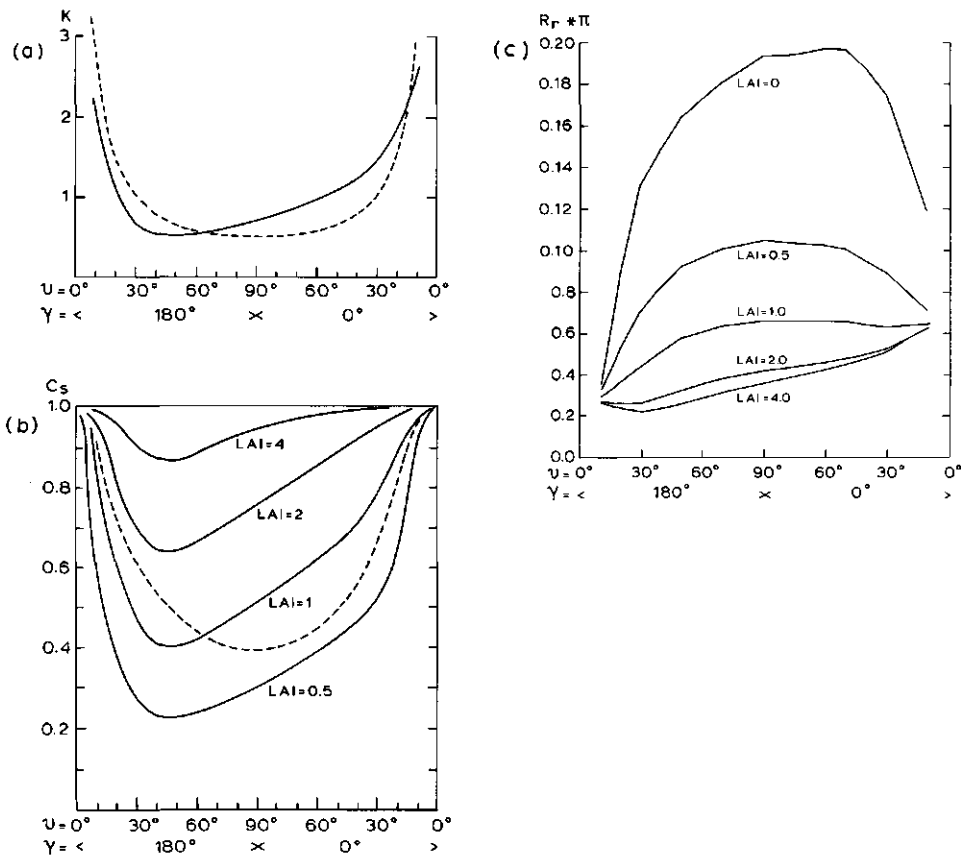


Figure 4.5: Interception in relation to observation direction for crop with azimuthal preference (Lang, 1973).

a): Interception coefficient K as a function of the observation direction (γ, ν) . Broken line: spherical leaf angle distribution.

b): Invisible fraction of the soil C_s for different LAI values as a function of the observation direction (γ, ν) . Broken line: spherical leaf angle distribution with $LAI=1$.

c): Observed radiance R_r for crops with different LAI values. Inclination of the sun = 60° . γ indicates the azimuth of the observer, the azimuth of the sun is 0° .

Optical parameters are $\rho = 0.08$, $\tau = 0.03$ and $\omega = 0.21$.

in the form of the KM-parameters (Kubelka & Munk, 1931), R_∞ for the reflection of a stack of leaves of infinite depth, the absorption coefficient k and the scattering coefficient s . These parameters were used to calculate the Stokes parameters a and b (Stokes, 1862); in their turn, these were used to compute the values of the leaf reflection coefficient ρ and the leaf transmission coefficient τ , by means of the following equations:

$$a = \frac{1}{R_\infty} \quad (4.6)$$

Table 4.2: Values for the reflection coefficient ρ and the transmission coefficient τ of a single leaf as used in the model-computations.

spectral band	leaf type		
	bright	mean	dark
green ($\lambda = 550$ nm)	$\rho = 0.13$ $\tau = 0.17$	$\rho = 0.13$ $\tau = 0.12$	$\rho = 0.13$ $\tau = 0.07$
red ($\lambda = 670$ nm)	$\rho = 0.08$ $\tau = 0.06$	$\rho = 0.08$ $\tau = 0.03$	$\rho = 0.08$ $\tau = 0.$
infrared ($\lambda = 870$ nm)	$\rho = 0.50$ $\tau = 0.40$	$\rho = 0.45$ $\tau = 0.45$	$\rho = 0.40$ $\tau = 0.50$

and

$$b = e^{\{k \cdot (a+1)/(a-1)\}} \quad (4.7)$$

or

$$b = e^{\{s \cdot (a^2-1)/(2a)\}} \quad (4.8)$$

ρ and τ were computed according to:

$$\frac{\rho}{b - b^{-1}} = \frac{\tau}{a - a^{-1}} = \frac{1}{a \cdot b - (a \cdot b)^{-1}} \quad (4.9)$$

With Equation (4.9) ρ and τ can be obtained by:

$$\rho = \frac{b - b^{-1}}{a \cdot b - a^{-1} \cdot b^{-1}} \quad (4.10)$$

$$\tau = \frac{a - a^{-1}}{a \cdot b - a^{-1} \cdot b^{-1}} \quad (4.11)$$

It will be clear that there is a redundancy in the combination of R_∞ , k and s . Any two of these can be used to calculate the third one. This property was used to check the consistency of each given combination. All but one of the 37 crops and weeds show a good correspondence of R_∞ , k and s . For one crop (lettuce) the values for these parameters are conflicting. Because this crop was found to be 'out of range' in other aspects too, it was omitted from further considerations. Figures 4.6 to 4.8 show the calculated values for ρ and τ in the three wavelength bands under consideration. From these figures, three combinations of ρ and τ in these bands were selected for further calculations. These values are indicated in the figures and also in Table 4.2. In Figure 4.9, ρ and τ for a healthy maize leaf are presented for the whole spectral range from blue to near infrared.

As can be seen in Figures 4.6 and 4.7, the reference values used in the remaining calculations represent the central and extreme values of ρ and τ in the green and red bands. In the infrared band (values used seem to be fairly extreme, because the reported values correspond to a wavelength of 880 nm and the calculations were carried out for 870 nm.

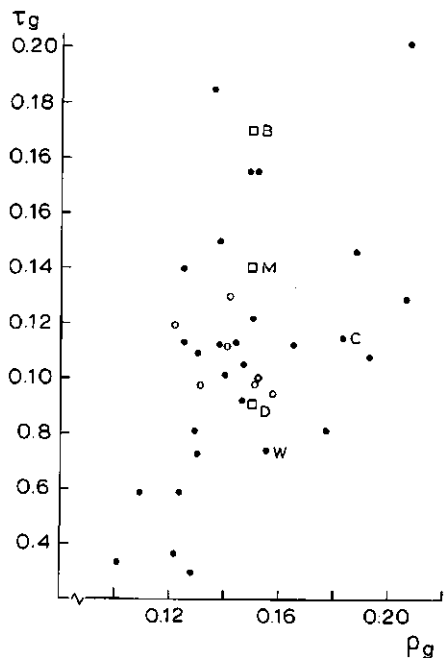


Figure 4.6: Scattergram of the combined leaf reflection ρ_g (horizontal axis) and leaf transmission τ_g (vertical axis) for 29 crops (●) and 7 weeds (○). Wavelength is 550 nm (green). W : wheat. C : maize. Values as used in the model calculations are given as □. D : dark, M : medium, B : bright leaves.

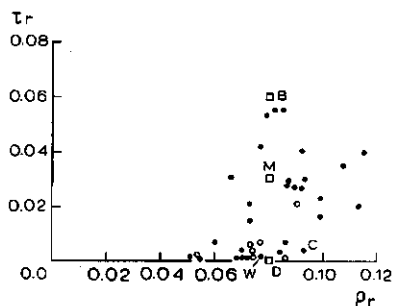


Figure 4.7: Scattergram of the combined leaf reflection ρ_r (horizontal axis) and leaf transmission τ_r (vertical axis) for 36 crops and weeds. Wavelength is 670 nm (red). Symbols are explained Figure 4.6.

4.1.3 Leaf surface

The optical properties of a leaf do not only include the values of ρ and τ , but also the spatial distribution of the remitted radiation. As a first approximation, it was assumed that leaves are Lambertian remitters, so the remitted radiation is distributed isotropically. This means that ρ and τ are independent of the angle of incidence, and that the radiance of a leaf does not depend on the angle of observation. A more comprehensive explanation of the leaf-light interaction was presented in Subsection 3.1.3. In the calculations in Sections 4.3 and 4.4 three types of reflection are used, one of them being Lambertian reflection. This one was used as a reference; other surface properties were compared with the crop with Lambertian remittance. The assumption of Lambertian remittance is in accordance with the assumptions of Allen *et al.* (1969) and Suits (1972) in their respective models.

Leaves show specular reflection as well as diffuse reflection. This means that a fraction of the intercepted radiation is reflected directly at the surface of the intercepted leaf. The extent of this fraction is a function of the angle of incidence and of the refraction

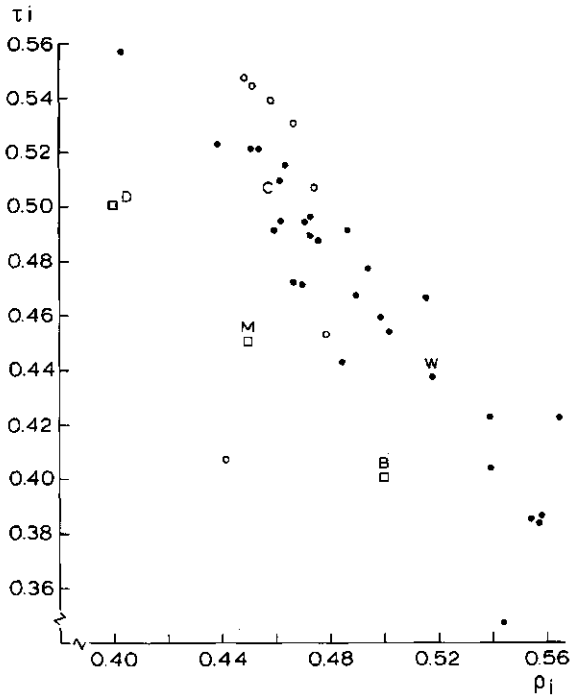


Figure 4.8: Scattergram of the combined leaf reflection ρ_i (horizontal axis) and leaf transmission τ_i (vertical axis) for 36 crops and weeds. Wavelength is 870 nm (near infrared). Symbols are explained in Figure 4.6.

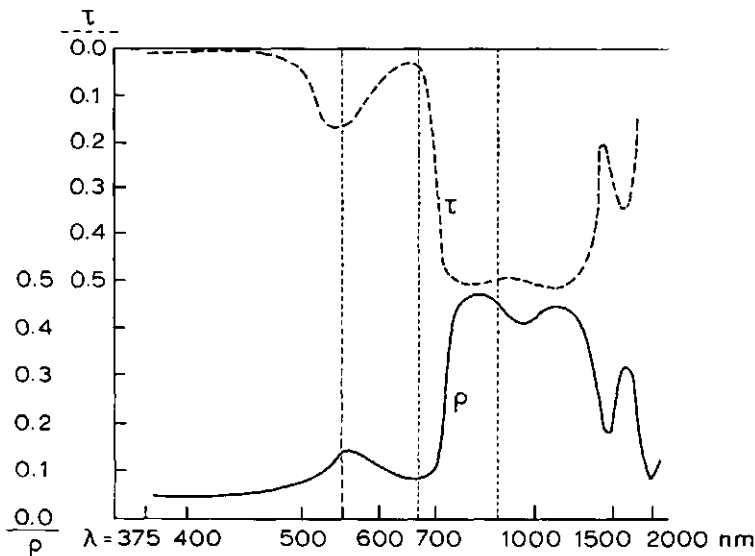


Figure 4.9: Reflection (solid line, left ordinate) and transmission (broken line, right ordinate) for a healthy maize leaf. Transmission is drawn upside down, so between the curves the leaf absorption can be read. Vertical dotted lines indicate wavelengths as used in the model computations. (based on Goudriaan, 1977.)

Table 4.3: Values for the optical parameters for the interaction between leaves and light for non Lambertian behaviour of leaves as used in the model computations.

spectral band	refraction index	fractions of the not specular reflected radiation	
		diffusely reflected	diffusely transmitted
green ($\lambda = 550$ nm)	$n = 1.45$	$\rho_d = 0.0997$	$\tau_d = 0.1243$
red ($\lambda = 670$ nm)	$n = 1.40$	$\rho_d = 0.0540$	$\tau_d = 0.0310$
infrared ($\lambda = 870$ nm)	$n = 1.40$	$\rho_d = 0.4341$	$\tau_d = 0.4629$

index. The equations that describe this process quantitatively are given in Subsection 3.1.4. The two consequences of specular reflection are:

- The total reflection coefficient ρ increases with increasing angle of incidence, that is with a more oblique incidence.
- The spatial distribution of the reflected radiation is not only isotropic, but also shows a uni-directional component. The direction of this component depends on the orientations of the leaf's normal and the direction of incidence.

For the index of refraction of a maize leaf n Allen *et al.* (1969) reported values of 1.45 for $\lambda = 550$ nm (green) and of 1.40 for $\lambda = 600 - 1000$ nm (red and infrared). Application of these values in Fresnel's formula (Equation (3.6)) explains the observations of Sheehy (1975) very well. The measurements presented by Breece & Holmes (1971) for leaves of maize and soyabean also confirm the occurrence of a surface reflection component that depends on the angle of incidence.

In the third model applied for the optical behaviour of the leaf surface a surface reflection component is assumed which size is calculated in the same way as in the case of specular reflection. In this model, however, the leaf surface itself is assumed to be so rough that only the quantitative aspect of the specular reflection is present, but that the radiation that is reflected at the leaf's surface is distributed isotropically. So, in this model, ρ depends on the angle of incidence, but the distribution of the reflected radiation is assumed to be Lambertian (Equation (3.20)). The influence of the internal scattering in the leaves is generally such, that only isotropical distribution can be assumed. Only in the case of very thin leaves, it could be meaningful to take account of a fraction of the intercepted radiation that passes through the leaf unaffectedly. Although the models provide for this, it is not applied in the model calculations presented in the following sections.

Table 4.3 gives a review of the parameter values that are used if leaves are assumed to show surface reflection, Figures 4.10 to 4.12 show the consequences of these parameters for the different fractions of the remitted radiation as a function of the angle of incidence.

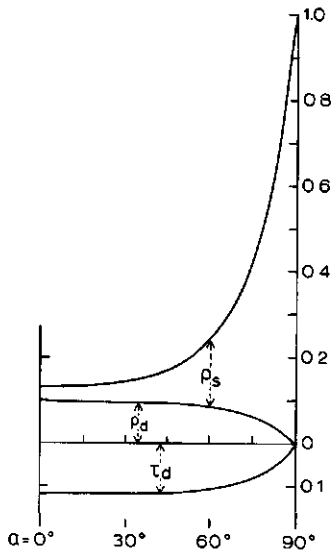


Figure 4.10: Remitted radiation as a function of the angle of incidence α for non Lambertian reflecting leaves for green radiation ($\lambda = 550 \text{ nm}$). α is the angle between the direction of incidence and the leaf's normal. Reflection is given above, transmission below x-axis. ρ_s : surface reflection, ρ_d : diffuse reflection, τ_d : diffuse transmission.

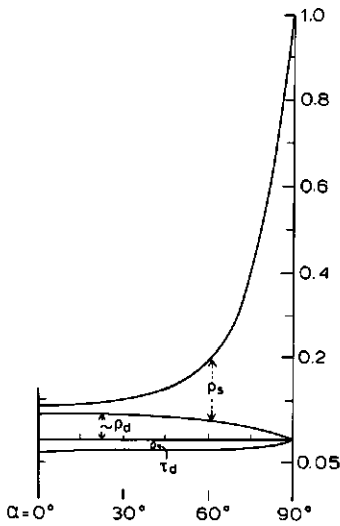


Figure 4.11: As Figure 4.10 for red radiation ($\lambda = 670 \text{ nm}$).

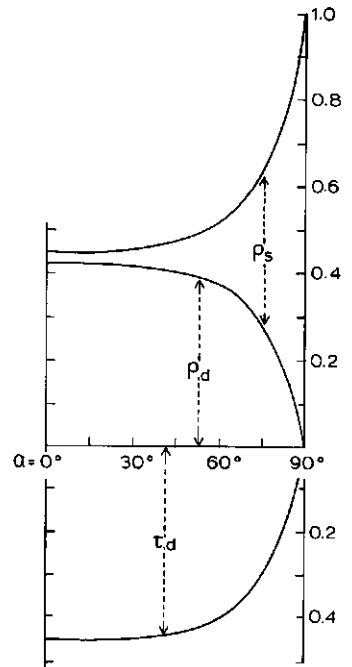


Figure 4.12: As Figure 4.10 for near infrared radiation ($\lambda = 870 \text{ nm}$).

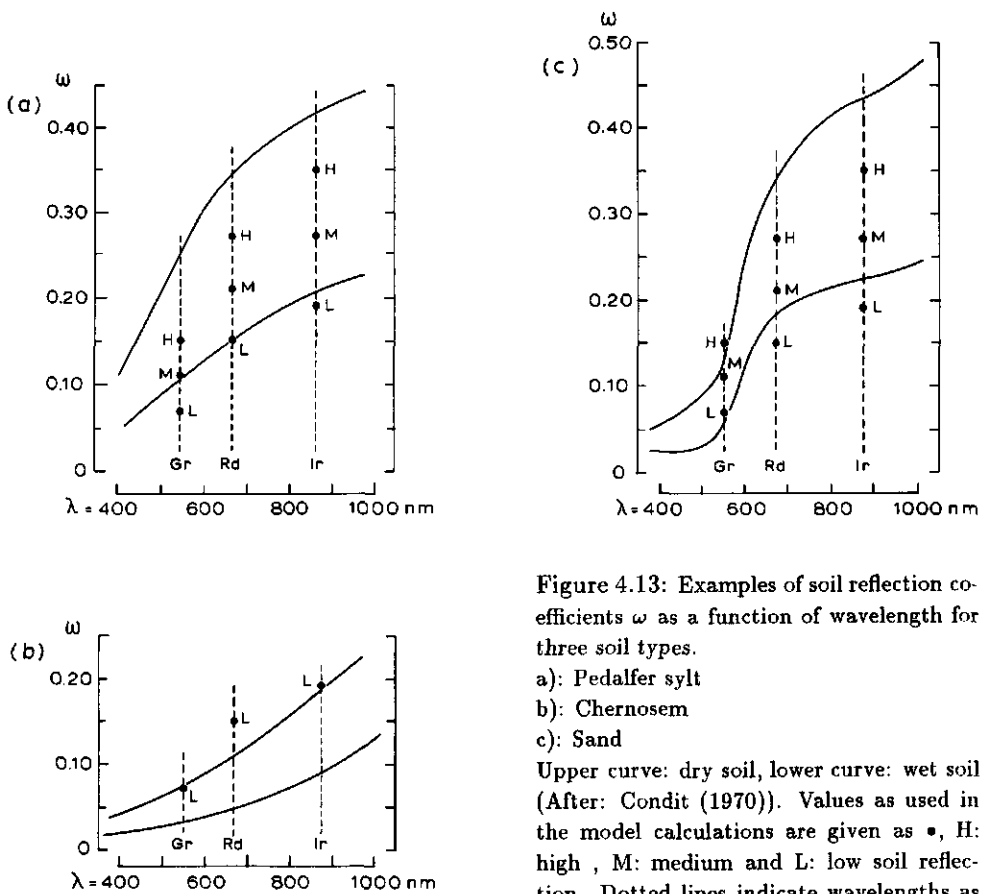


Figure 4.13: Examples of soil reflection coefficients ω as a function of wavelength for three soil types.

- a): Pedalfer silt
- b): Chernosem
- c): Sand

Upper curve: dry soil, lower curve: wet soil (After: Condit (1970)). Values as used in the model calculations are given as •, H: high, M: medium and L: low soil reflection. Dotted lines indicate wavelengths as used in the calculations ($\lambda_{\text{green}} = 550 \text{ nm}$, $\lambda_{\text{red}} = 670 \text{ nm}$, $\lambda_{\text{infrared}} = 870 \text{ nm}$).

4.1.4 Soil reflection coefficient

The relation between the wavelength and the soil reflection coefficient is completely different from the relation between the wavelength and the leaf reflection. In the case of leaf reflection we can very clearly distinguish the regions of the spectrum that are related to photochemical properties (mainly of the chlorophyll). In contrast, a soil shows a smoother relation between wavelength and reflection coefficient within the wavelength bands 400-1000 nm. Depending on the type of soil, the moisture content and the content of organic matter, the reflection of soils increases more or less regularly with increasing wavelength. Only at wavelengths of 1450 nm and 1950 nm dips are found in this relation, caused by water absorption at these values of λ .

Condit (1970) presents a great number of data about soils in the USA. Depending on the soil type, he finds curves for the relation between wavelength and reflection under dry and wet circumstances, as presented in Figure 4.13. For Newtonian silt loam Bowers & Hanks (1965) demonstrate the relation between soil reflection and moisture and humous

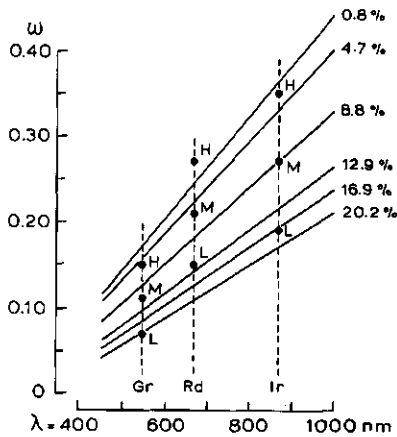


Figure 4.14: Reflection of Newtonian silt loam as a function of wavelength for different moisture conditions (After Bowers & Hanks (1965), simplified). For explanation of the symbols see Figure 4.13.

contents, respectively (see Figure 4.14).

From these data three reflection levels were derived. These are presented in Table 4.4. Because in the wavelength bands under consideration the radiation hardly penetrates the soil, only a thin upper layer of a few mm takes part in the reflection process, and with a cloudless sky this layer is generally dry; therefore the values for the soil reflection that were used as mean values were taken on the 'dry' side of the mean value. In the calculation where soil reflection itself was not studied, the mean value is applied. In all calculations, the spatial distribution of the radiation that is reflected by the soil, was modelled with the SOIL model as presented in Section 3.3.

4.1.5 Incoming radiation, sky irradiance

The radiation that is remitted by a crop in upward direction is the result of a process in which the crop, including the underlying soil, influences the downward incoming radiation. Only under the totally hypothetical circumstance of a crop with horizontal leaves only and a horizontal soil, where both show perfect isotropic reflection, does the spatial distribution of the reflected radiation not depend on the distribution of the incoming radiation. So it is necessary to define the distribution of the incoming radiation over the 46 directions in this model. This distribution depends on several factors such as sun's inclination and azimuth and the optical properties of the atmosphere. In this

Table 4.4: Values for the reflection coefficient of the soil ω as used in the model computations.

spectral band	soil reflection type		
	low	medium	high
green ($\lambda = 550 \text{ nm}$)	$\omega = 0.07$	$\omega = 0.15$	$\omega = 0.19$
red ($\lambda = 670 \text{ nm}$)	$\omega = 0.11$	$\omega = 0.21$	$\omega = 0.27$
infrared ($\lambda = 870 \text{ nm}$)	$\omega = 0.15$	$\omega = 0.27$	$\omega = 0.35$

Table 4.5: Review of the composition of the incident radiation as used in the model computations. For symbols see text.

crop geometry model	incident radiation				
	diffuse part		direct part		
	fraction	distrib.	fraction	direction (ϕ, θ)	
spherical	20 %	SOC	80 %	$\phi = 0^\circ$	$\theta = 60^\circ$
erectophile	40 %	SOC	60 %	$\phi = 0^\circ$	$\theta = 45^\circ$
planophile					
Lang (1973)	20 %	SOC	80 %	$\phi = 0^\circ$	$\theta = 60^\circ$
	20 %	SOC	80 %	$\phi = 45^\circ$	$\theta = 60^\circ$
	20 %	SOC	80 %	$\phi = 90^\circ$	$\theta = 60^\circ$

study, relatively little attention was paid to these aspects of the reflection measurements and calculations. Only three aspects were taken into account: the fraction of the total incoming flux that comes directly from the sun, the direction of the sun and, the inclinational distribution of the diffuse component of the incoming radiation. The path of the radiation through the atmosphere from the crop to the sensor was assumed to be completely transparent.

There are several theories for the ratio between the direct and the diffuse component and for the spatial distribution of the diffuse component. In practice, two distribution models are distinguished for the distribution of the diffuse component. One assumes an equal radiance of the entire sky. This distribution is called the 'Uniform Overcast Sky' or UOC. Under this assumption, the flux that hits the earth's surface from a direction with inclination θ is proportional to $\sin \theta$. The second model is based on an empirical relation proposed by Moon & Spencer (1942). This relation was later verified by Grace (1971). In this model the sky radiance increases with an increasing value of θ . The relation itself is given by $1 + 2 \sin \theta$, so a threefold increase between sky radiance on the horizon and in the zenith is assumed. In this so-called 'Standard Overcast Sky' or SOC, the flux from a direction with inclination θ is proportional to $\sin \theta + 2 \sin^2 \theta$. The calculations in this chapter were all carried out with the second model. Two values were applied for the inclination of the sun: $\theta = 60^\circ$ and $\theta = 45^\circ$, with related values for the ratio direct-diffuse 80 : 20 for $\theta = 60^\circ$ and 60 : 40 for $\theta = 45^\circ$. The calculations for crops without azimuthal preference were carried out with both inclinations of the sun. The calculations with a crop with a leaf orientation according to Lang (1973) were only carried out with a sun's inclination of 60° , but with three different azimuthal directions of the sun (0° , 45° and 90°) with respect to the direction of the normal vector of the mass centre of the leaf distribution. A review of the sky radiance distributions as used in the model studies is given in Table 4.5.

In all calculations the concept 'crop reflection' is principally defined as the ratio of reflected flux to incoming flux, both measured in a horizontal plane above the crop. Therefore, it is not necessary to account for the absolute values of the 46 elements in the vector that depicts the incoming radiation. In the models, the calculation of these elements is performed in such way that they sum to 1, representing the total downward flux. The total upward flux, summed over the 46 model directions, automatically yields the hemispherical reflection of the crop, in terms of reflected radiative energy.

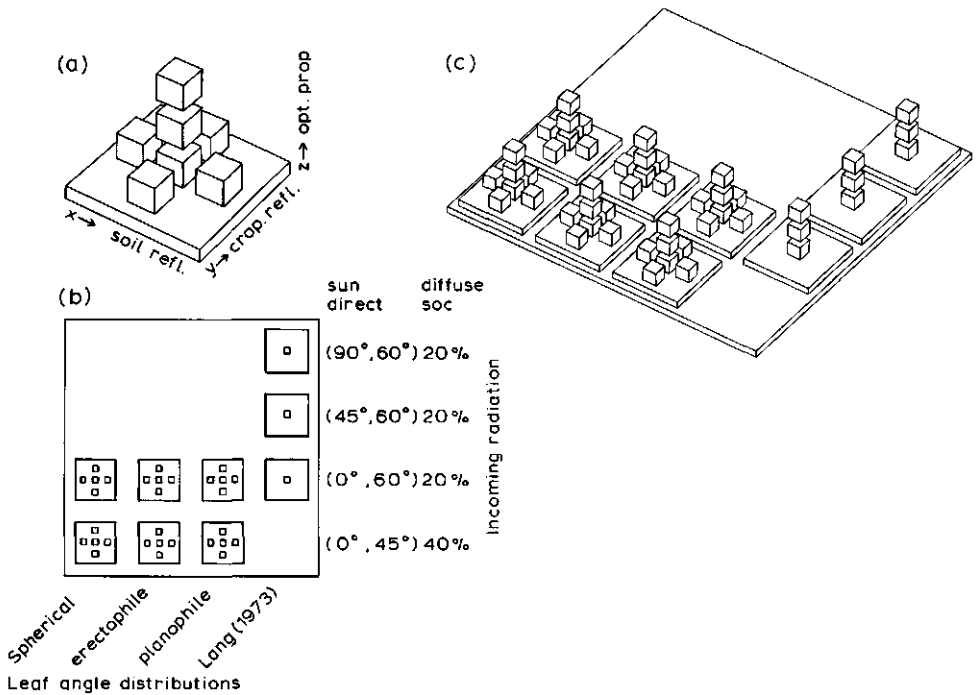


Figure 4.15: Scheme of all computations used in Sections 4.4 and 4.5.

a): The little tablets indicate combinations of crop geometry and the distribution of the incoming radiation.

b): The cubes above each tablet indicate:

x-direction: low, medium and high soil reflection;

y-direction: dark, medium and bright leaves;

z-direction: lower cube Lambertian reflection, medium cube specular reflection and upper cube rough surface.

c): A total view on all combinations for which the calculations are carried out.

4.1.6 Summary

The graphical presentation in Figure 4.15 gives a complete review of all calculations on which the figures in the Sections 4.2 and 4.3 are based.

4.2 Presentation of the calculation results

All calculation results with the model crops from Section 4.1 are presented as graphs. On the vertical axis of these, a quantity related to the radiation is presented, whereas on the horizontal axis a crop property (LAI, coverage) is given. Some general remarks about the radiative quantities are made in Subsection 4.2.1, some remarks on the crop properties are made in Subsection 4.2.2.

4.2.1 Radiative properties

All the calculations with the TURTLE and HARE models concern ratios between upward and downward fluxes, measured with respect to a horizontal plane just above the crop. The way observations are collected from a plane or satellite or any platform, however, never permits the total upward flux to be measured. The usual practice is to measure the radiation that hits a sensor from a small solid opening angle, where the major axis of the sensor is pointed in a certain direction. To take account of that difference, a transformation was applied. This transformation was calculated as follows. Notice that, because in all situations, the calculations are related to ratio's, no dimensions are included in the formulas.

With the models the upward flux is calculated as a fraction of the downward flux with respect to a horizontal plane. Each element of the flux vectors represents a solid angle of $2\pi/46 = \pi/23$ sr. The radiance R_j perpendicular to a direction with v_j as the inclination of the central axis of the solid angle under consideration can be computed from the flux in that direction F_j as:

$$R_j = F_j \cdot \frac{46}{2\pi} \cdot \frac{1}{\sin v_j} \quad (4.12)$$

For the zenith radiance R_z , it now holds (because $v_j = \pi/2$):

$$R_z = F_z \cdot 23/\pi \quad (4.13)$$

To make the numerical values of the radiance comparable with the numerical values that are computed in the flux calculations, in all cases where the radiance is considered, the calculated values are multiplied with π . So, the presented values R_j^* are calculated as:

$$R_j^* = \pi \cdot R_j \quad (4.14)$$

$$= \pi \cdot F_j \cdot \frac{23}{\pi} \cdot \frac{1}{\sin v_j}$$

$$R_j^* = 23 \cdot F_j / \sin v_j \quad (4.15)$$

The advantage of this transformation is that the values can be compared directly with the total hemispherical reflection of the crop, expressed as the ratio of total reflected flux to total downward flux. For a crop that should be an ideal Lambertian reflector with reflection coefficient ρ_c , R_j^* can be computed as follows:

For the flux in direction j , F_j , it holds that (compare Equation (3.39) for a Lambertian reflecting soil):

$$F_j = \rho_c \cdot \frac{\sin v_j}{\sum_{m=1}^{46} \sin v_m} \quad (4.16)$$

Substitution of Equation (4.16) in (4.12) gives:

$$R_j^* = \frac{23 \cdot F_j}{\sin v_j} \quad (4.17)$$

Calculation of R_j^* with Equation (4.14) gives:

$$R_j^* = \frac{23\rho_c}{\sum_{m=1}^{46} \sin v_m} \quad (4.18)$$

The average value of $\sin v$ is 0.5, ignoring an error of 1.5%, caused by the discretization process. Therefore, for R_j^* it holds that:

$$R_j^* = \frac{23 \cdot \rho_c}{46 \cdot 0.5} = \rho_c \quad (4.19)$$

The transformation described can thus be used to compare total fluxes and radiances directly.

4.2.2 Crop properties

For most crops, during the vegetative growing phase there is a high correlation between biomass and LAI, because during the growth of a crop the specific leaf weight (= the leaf weight per leaf surface unit) hardly changes. Therefore, instead of the biomass itself, LAI is a suitable quantity to use in the graphics that show the relation between biomass and reflectional data. A second quantity that can be applied instead of the LAI is the vertically measured soil coverage. Using this quantity instead of the LAI has the advantage that crops with different leaf angle distributions can be compared without taking account of different soil influences. Another advantage of using the coverage is that there is a generally better relation between growth rate and coverage than between growth rate and LAI. For these reasons, in most graphs, the coverage is linearly drawn on the horizontal axis. The relation between LAI and coverage C_z is given by the expression:

$$C_z = 1 - e^{-K \cdot LAI} \quad (4.20)$$

In this equation K depends on the leaf angle distribution $d(\gamma, \kappa)$. K is equal to the integral over all possible directions of the product of the relative density in direction (γ, κ) and the sine of the inclination of the leaf normal κ . This factor takes account of the coverage of leaves with an inclination of the normal direction κ compared to their actual surface. Because the integrations are applied to a hemispherical surface, a factor $\cos \kappa$ must also be included. So, for K it holds that:

$$K = \int_0^{2\pi} \int_0^{\pi/2} d(\gamma, \kappa) \sin \kappa \cdot \cos \kappa \cdot d\kappa \cdot d\gamma \quad (4.21)$$

It is obvious that in this equation $d(\gamma, \kappa)$ must fulfil the criterion:

$$\int_0^{2\pi} \int_0^{\pi/2} d(\gamma, \kappa) \cdot \cos \kappa \cdot d\kappa \cdot d\gamma = 1 \quad (4.22)$$

The use of the discrete equivalent of this integral in the models, gives the following equation for K :

$$K = \sum_{k=1}^{46} d_k \cdot \sin \kappa_k \quad (4.23)$$

(κ_k is the inclination of the leaf normal direction with index k). In this equation, d_k must fulfil the discrete equivalent of Equation (4.22), which is:

$$\sum_{k=1}^{46} d_k = 1 \quad (4.24)$$

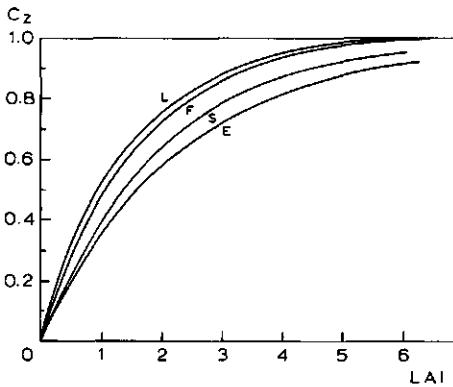


Figure 4.16: Relation between LAI and vertical coverage C_z for the four model crop types: spherical (S), erectophile (E), planophile (F) and Lang (L).

The relation between LAI and coverage C_z is presented for the four model crops in Figure 4.16.

When using aeroplanes to collect remote sensing data, the relatively low flight altitude, combined with the need to collect a large number of data in a given time, means that the scanning is not limited to a small strip below the plane. Instead, a wide strip on either side of the flightline is observed. This strip may be twice as wide as the flight altitude, so instead of only nadir observations, observations with an inclination of 45° are also done. The newest generation of satellites allows the earth's surface to be scanned with a deviation of up to 27° from the nadir direction. This complicates the interpretation of the observations, because the radiance of a crop depends on the observation direction. Even if the crop itself does not show azimuthal preference in its leaf angle distribution, an azimuthal component in the reflected radiation is introduced by the direction of the sun. Figure 4.17 shows some examples of this phenomenon. The results agree very well with the results found by Verhoef (1984). For a crop with a leaf angle distribution according to Lang (1973), the directional radiance for several LAI-values was already given in Figure 4.5c.

4.3 Calculations on the reflection in single spectral bands

Figure 4.18 shows the ratio between the upward and downward fluxes as a function of the LAI for a crop with a spherical leaf angle distribution, isotropically scattering leaves and a soil with an average reflection coefficient. In the same figure the zenith radiance is also drawn. The latter has been transformed according to Equation (4.13). If the crop was an isotropical reflector, the curves should coincide. The figure shows that this is not the case. In the green band it appears that for low LAI values ($LAI < 2$) the corrected zenith radiance is higher than the upward flux caused by the same crop, but for higher LAI values the opposite is true. In the red band, the corrected zenith radiance for a crop that is not closed is higher than the flux, whereas for a closed crop, these become equal. Because of the relatively low values of the reflection and transmission coefficients in this band, it may be expected that these values do not change considerably for a crop with an LAI even higher than 5. Finally, for the infrared band it appears that, except

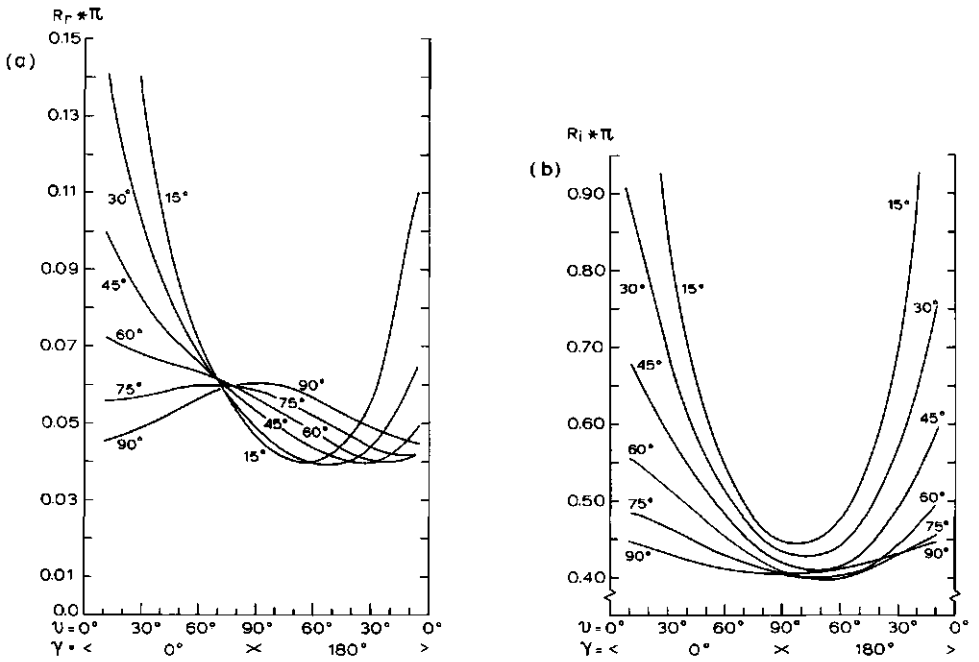


Figure 4.17: Directional radiance R as a function of the observation direction (γ, ν) for a crop with $LAI=2.5$ and a spherical leaf angle distribution. Curves are given for different inclinations of the sun. Values for the optical parameters are taken from Verhoef (1984). ν : inclination of the observation, γ : azimuthal difference between the sun and the observer.

a): For red radiation (R_r).

b): For infrared radiation (R_i)

for a bare soil, the zenith radiance is lower than the average radiance. From this it can be concluded that the total upward flux and the zenith radiance corrected according to Equation (4.13) may not be interchanged freely. This was already proved by the calculations in Subsections 2.1.2 and 4.2.2. In this section, unless explicitly stated, all calculations concern the zenith radiance.

4.3.1 Crop geometry

In addition to the LAI, the leaf angle distribution is another important crop property that influences reflection and light interception and, with that, the photosynthetic activity of a plant. The leaf angle distribution also determines the visibility of the soil. Figure 4.19 presents the reflection as a function of the LAI, for three different leaf angle distributions. It appears that for high LAI values the reflection increases in all bands if the leaf angle distribution becomes a more planophile one. For low LAI values this is only true in the visible part of the spectrum. This is caused by the relatively high soil reflection. This can also be seen in Figure 4.20 where the zenith radiance is given as a function of vertically measured coverage C_z . This figure shows that a more planophile

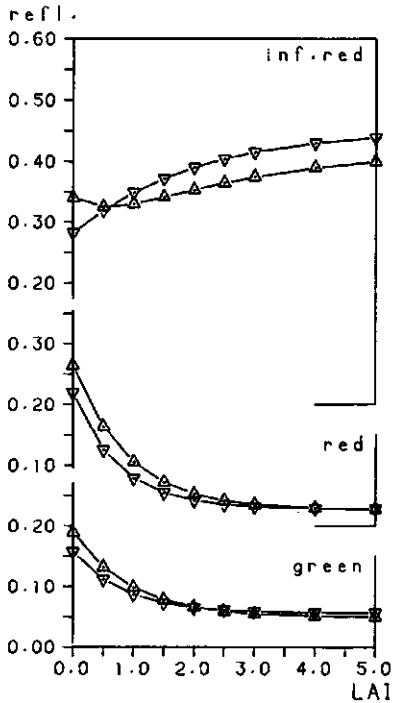


Figure 4.18: Reflection as a function of the LAI for a crop with a spherical leaf angle distribution. Drawn are the total upward flux (∇) and the zenith radiance (\triangle) of the same crop. Incoming radiation is 80% direct (sun's inclination: 60°) and 20% diffuse with a SOC distribution. This crop is also used as the reference crop in Tables 4.7 and 4.8.

leaf angle distribution causes a higher zenith radiance at equal coverage values. This phenomenon results from the fact that an increase in the relative fraction of horizontal leaves also increases the interception of the direct and diffuse incoming radiation, so the reflection process is more concentrated in the upper layers of the crop. The result is that a larger fraction of the reflected radiation can escape from the crop, rather than being reflected by the underside of leaves in the layers above the reflective one. Also the fact that horizontal leaves show a more extended projection perpendicular to the observation direction, and hence give a larger reflected flux in that direction, intensifies the mentioned differences.

4.3.2 Optical properties of the leaves

In the previous sections only crops with isotropically reflecting leaves were considered. Figure 4.21 shows the influence of the optical properties of leaves. The curves concern isotropically (Lambertian) reflecting leaves, leaves that show specular reflection according to Fresnel (Equation (3.6)) and rough leaves as described in Subsection 4.1.3. This figure also shows that the optical behaviour of the leaf surface influences the zenith radiance. Calculations with the other model crop showed similar differences. The reason for the calculated differences is not completely clear. Of course, the average reflection of a leaf that shows specular reflection is higher than the reflection of a leaf without specular reflection, because the model parameters are adjusted in such way that the total reflections are equal for perpendicular incidence. For specularly reflecting and rough leaves, the reflection increases with a decreasing angle of incidence. In the case

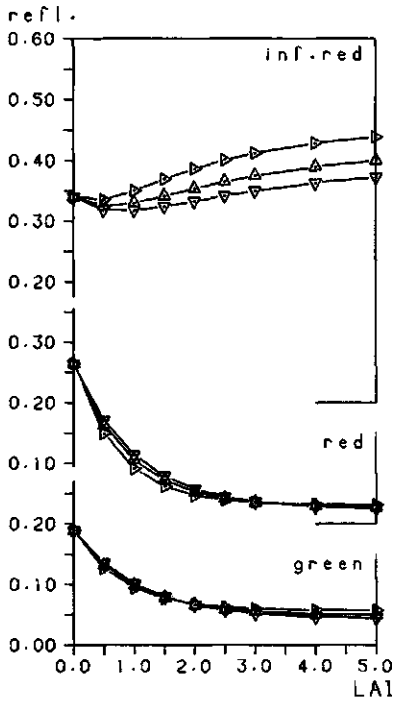


Figure 4.19: Zenith radiance as a function of LAI for three different crops with leaf angle distributions: spherical (Δ), erectophile (∇) and planophile (\triangleright). The incoming radiation is as in Figure 4.18.

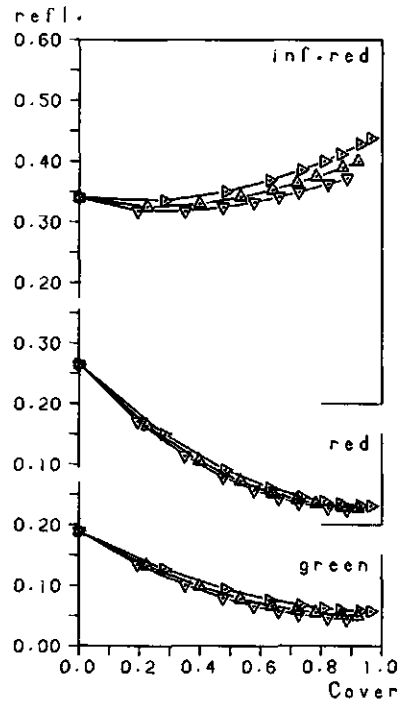


Figure 4.20: Zenith radiance as a function of the vertical coverage instead of LAI. Incoming radiation is as in Figure 4.18.

of specular reflection the direction of remittance is determined by the direction of incidence and the direction of the normal on the leaf plane. The reflection increases as the angle between the direction of incidence and the normal on the leaf plane increases. But, because the incoming radiation comes from above, the exitant direction is pointed downwards, so the result is layer transmission rather than layer reflection. The relatively higher reflection of the leaves therefore does not contribute importantly to the reflection of the crop, but to the transmission of the layers, which has only a limited effect on the crop reflection. This is probably why the higher average reflection of specularly reflecting leaves hardly influences the zenith radiance. Rough leaves also show the same higher reflection as specularly reflecting leaves, but the isotropic character of the reflected radiation is not changed, so the increased leaf reflection will result in an increase of both the layer reflection and the layer transmission, giving a higher overall crop reflection.

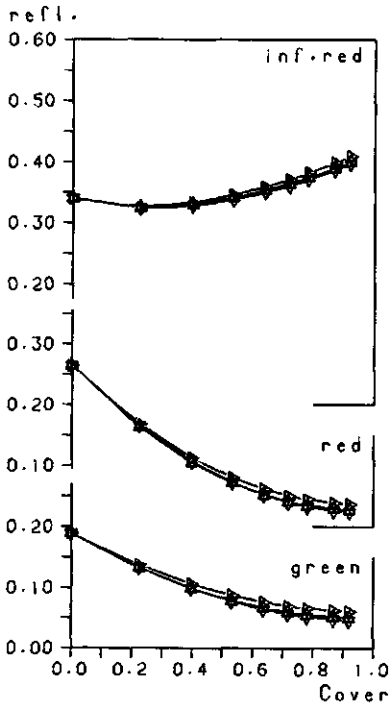


Figure 4.21: Zenith radiance as a function of coverage for a crop with a spherical leaf angle distribution for three types of leaf reflection: Lambertian reflecting leaves (Δ), leaves with a specular component (∇) and rough leaves with increasing reflection for more oblique incidence (\triangleright). Incoming radiation is as in Figure 4.18.

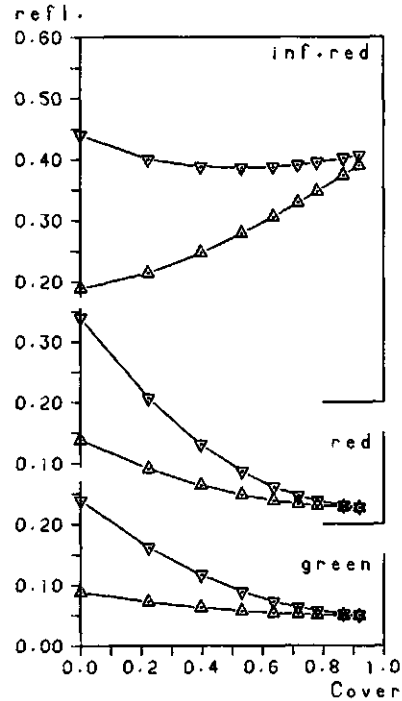


Figure 4.22: Zenith radiance of a crop with a spherical leaf angle distribution as a function of the coverage for two levels of the soil reflection coefficient: low (Δ) and high (∇). Incoming radiation is 40% diffuse (SOC), 60% direct, sun's inclination is 45° .

4.3.3 Soil reflection

If a crop is not closed, the soil reflection coefficient ω plays a role in the total reflection of the crop and soil system, regardless of the spectral band. Because of the low absorption of the leaves in the infrared band, in this band this influence is also noticeable for crops with a high LAI (LAI=5, coverage > 90%), although less than 1% of the soil is both directly irradiated and observed. In Table 4.6 this is presented for the whole LAI range. As well, for the three wavelength bands, the crop reflection was compared with the reflection of the same crop with an optically black soil underneath. It appears that for all three crops (spherical, erectophile and planophile) the total soil contribution to the reflection hardly exceeds the contribution of the directly irradiated and observed soil, whereas this influence in the infrared band is much more important. Apparently, the soil reflection plays an important role in the infrared band because of the transmissivity of the leaves. Figure 4.22 shows the influence of the soil reflection coefficient to the crop

Table 4.6: Influence of the soil reflection level on the total reflection in three wavelength bands for three different crops, five LAI values and two values of the inclination of the sun. See Subsection 4.3.3 for further explanation.

LAI	Visible directly irradiated soil	Difference between crop reflection with and without a soil divided by the reflection of a bare soil (cols. 3,5,7) and the quotient of this value and column 2 (cols. 4,6,8)					
		green		red		inf.red	
(1)	(2)	(3)	(4)	(5)	(6)	(7)	(8)
Spherical, Sky: 80% direct, sun's inclination 60°, 20% diffuse (SOC)							
1	.3160	.3561	1.13	.3323	1.05	.5601	1.77
2	.1019	.1251	1.23	.1101	1.08	.3259	3.20
3	.0331	.0437	1.32	.0367	1.11	.1913	5.78
4	.0108	.0152	1.4	.0124	1.15	.1123	10.4
5	.0036	.0053	1.5	.0040	1.1	.0663	18.
Spherical, Sky: 60% direct, sun's inclination 45°, 40% diffuse (SOC)							
1	.2778	.3252	1.17	.3002	1.08	.5456	1.96
2	.0814	.1063	1.31	.0920	1.13	.3128	3.84
3	.0245	.0350	1.43	.0289	1.18	.1823	7.44
4	.0075	.0121	1.6	.0091	1.2	.1065	14.2
5	.0024	.0043	1.8	.0027	1.1	.0625	26.
Erectophile, Sky: 80% direct, sun's inclination 60°, 20% diffuse (SOC)							
1	.3605	.3997	1.11	.3775	1.05	.5963	1.65
2	.1331	.1588	1.19	.1429	1.07	.3648	2.74
3	.0496	.0629	1.27	.0541	1.09	.2235	4.51
4	.0186	.0245	1.32	.0208	1.12	.1366	7.34
5	.0070	.0099	1.4	.0079	1.1	.0834	12.
Erectophile, Sky: 60% direct, sun's inclination 45°, 40% diffuse (SOC)							
1	.3108	.3588	1.15	.3360	1.08	.7180	2.31
2	.1031	.1312	1.27	.1161	1.13	.4296	4.17
3	.0354	.0492	1.39	.0407	1.15	.2600	7.34
4	.0125	.0178	1.42	.0144	1.15	.1573	12.6
5	.0045	.0073	1.6	.0054	1.2	.0952	21.2
Planophile, Sky: 80% direct, sun's inclination 60°, 20% diffuse (SOC)							
1	.2442	.2883	1.16	.2579	1.06	.4962	2.03
2	.0605	.0794	1.31	.0665	1.10	.2644	4.37
3	.0150	.0218	1.45	.0169	1.13	.1449	9.7
4	.0038	.0060	1.6	.0045	1.2	.0802	21.
5	.0009	.0013	1.4	.0010	1.1	.0445	49.
Planophile, Sky: 60% direct, sun's inclination 45°, 40% diffuse (SOC)							
1	.2238	.2682	1.20	.2418	1.08	.4951	2.21
2	.0518	.0713	1.38	.0584	1.14	.2632	5.08
3	.0122	.0193	1.58	.0144	1.18	.1438	11.8
4	.0029	.0050	1.7	.0037	1.3	.0790	27.2
5	.0007	.0014	2.	.0005	1.	.0445	64.

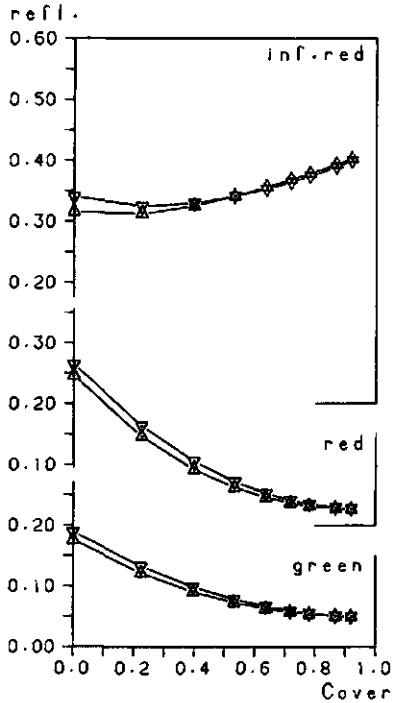


Figure 4.23: Zenith radiance of a crop with a spherical leaf angle distribution as a function of coverage for two distributions of the incoming radiation: (Δ): low sun inclination ($\theta = 45^\circ$, 40% diffuse (SOC)), (∇): high sun inclination ($\theta = 60^\circ$, 20% diffuse (SOC)).

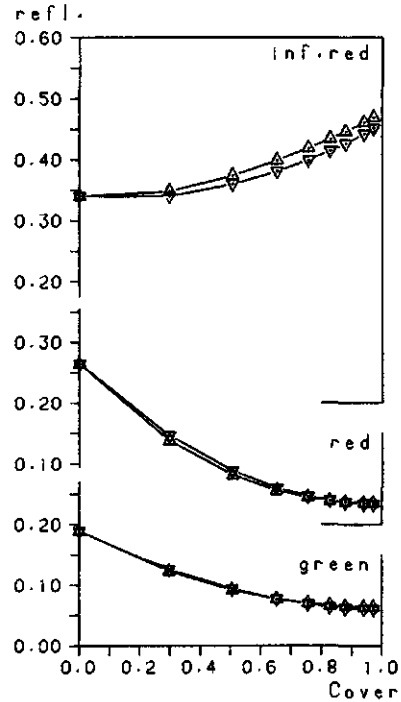


Figure 4.24: Zenith radiance as a function of coverage for a crop according to Lang (1973) for two values of the azimuth of the sun; Δ : direction with the greatest interception; ∇ : azimuth perpendicular to this one. Sun's inclination is 60° , diffuse radiation is 20% with an SOC distribution.

reflection for a spherical crop. Similar results were found for the other model crops.

4.3.4 Incoming radiation

The next phenomenon studied was the influence of the sun's inclination and, with that, the ratio direct/diffuse incoming radiation. Figure 4.23 shows this influence for the spherical crop. From this figure it appears that a higher sun's inclination causes a lower zenith radiance for lower LAI values. For higher LAI values, the differences may be ignored. Figure 4.24 shows the influence of the azimuthal rotation of the sun with respect to the crop, according to Lang (1973). Here too, the differences appear to be relatively small, but the differences in the red and in the infrared band show an opposite effect: in the red band the zenith radiance decreases with an increasing angle between the azimuth of the sun and the azimuth of the predominant normal direction of the leaves, whereas in the infrared band, the zenith radiance increases slightly with the same change in circumstances.

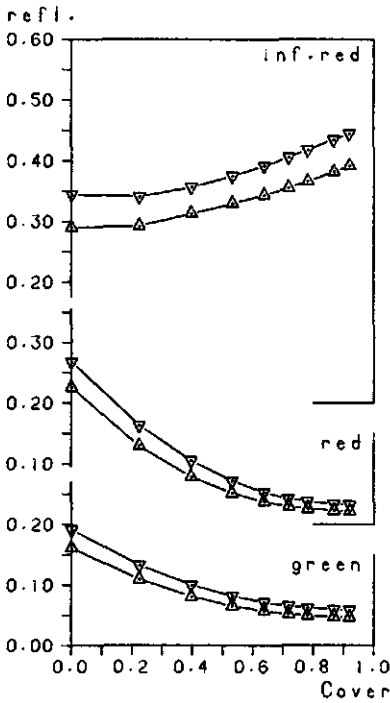


Figure 4.25: Maximum and minimum radiance caused by the observation direction as function of coverage. Drawn are for a spherical crop the lowest (Δ) and the highest (∇) value of the radiance within a cone around the nadir direction with a half top-angle of 45° . Incoming radiation as in Figure 4.18.

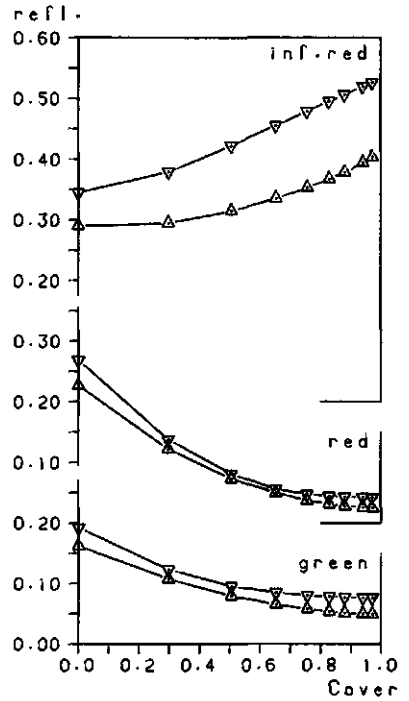


Figure 4.26: As Figure 4.25 for a crop according to Lang (1973). The azimuth of the sun is the direction with the greatest interception, its inclination is 60° .

4.3.5 Observation direction

Crops are not Lambertian reflectors. This means that the measured radiance depends on the direction in which the sensor is pointed. For a spherical crop the minimum and maximum values as computed within a cone with a half topangle of 45° around the nadir direction are presented in Figure 4.25. It appears that within this cone, differences of up to 20% can be seen in the visible bands, and up to 15% in the infrared band. For Lang's crop (Figure 4.26) these differences become to 50% and 30%, respectively. From the calculations in Subsection 2.1.2 it may be concluded that the major differences are found in the directions that are in the vertical plane through the sun's azimuth. To check this, Figure 4.27 was drawn. For the same crop as in Figure 4.25, this figure shows the radiance in the spectral bands for three directions: the zenith and two directions with an inclination of 60° ; one with the sun behind the observer, and one with the sun in front. It can be concluded that differences of up to 10% from the nadir observations occur for lower LAI values and observations towards the sun, and for higher LAI values

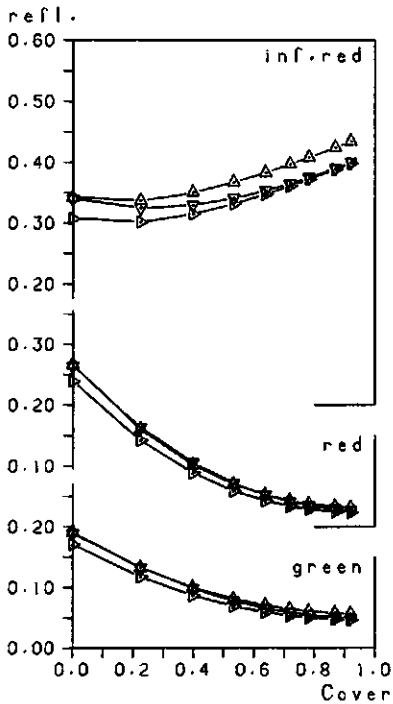


Figure 4.27: Radiance as a function of coverage for a spherical crop for three observation directions: towards the sun (hot-spot effects are neglected) (Δ), zenith (∇), direction with an azimuth opposite to the sun's direction (\triangleright). Incoming radiation as in Figure 4.18.

and observations with the sun behind.

4.3.6 Conclusions

The calculations in Section 4.3 were carried out to determine the relation between the measured reflected radiance and the phenomenon or the phenomena that influenced this radiance. These influences can be divided in three groups

- The crop properties that are of agricultural relevance.
- The properties of crop and soil that do not have this relevance.
- The properties of the incoming radiation and of the observation direction.

The most important of the first group is the vertical coverage C_z , or, in close relation to C_z , the leaf area index. The second group includes phenomena like the soil reflection coefficient, the instantaneous leaf angle distribution at the moment of observation and the optical properties of the leaves (glossy or rough). The most important representants of the third group are the direction of the sun and the direction in which the observer's equipment is pointed. For a crop that shows no azimuthal preference from these directions only the azimuthal difference is relevant, for a crop that does show this property, their absolute values are relevant. Table 4.7 can be considered as a summary of the calculations that are described in Section 4.3. In this table, the deviations in radiance for the three considered wavelength bands are listed for 17 cases and for three values of

Table 4.7: Effects of several parameters on reflected radiation and on interpretation of measured radiance R_{obs} . The relation between the zenith radiance R_{ref} and the vertical coverage of the reference crop (Figure 4.18) is used. Values are given for three values of coverage (C_z) and LAI for three wavelength bands. Parameters are only indicated as far as they differ from the reference crop. Values for other crops are given as percentual differences or ratios compared to the reference crop. In all cases, 'measured' radiation (R_{obs}) and estimated coverage (\widetilde{C}_z) and LAI (\widetilde{LAI}) are given.

Crop- and observation properties		$C_z=0.25$			$C_z=0.50$			$C_z=0.75$		
band	R_{ref}	C_z	LAI	R_{ref}	C_z	LAI	R_{ref}	C_z	LAI	
Grn:	.127	.250	.569	.083	.500	1.37	.057	.750	2.74	
Red:	.155	.250	.569	.080	.500	1.37	.038	.750	2.74	
Inf:	.326	.250	.569	.339	.500	1.37	.370	.750	2.74	
		R_{obs}	\widetilde{C}_z	\widetilde{LAI}	R_{obs}	\widetilde{C}_z	\widetilde{LAI}	R_{obs}	\widetilde{C}_z	\widetilde{LAI}
Leaf properties										
Bright leaves										
Grn:	2%+	6%-	7%-	5%+	6%-	8%-	8%+	8%-	15%-	
Red:	1%+	2%-	3%-	3%+	2%-	3%-	5%+	2%-	5%-	
Inf	1%+	40%+	43%-	2%+	15%+	24%+	3%+	9%+	22%+	
		53%+	68%+							
Dark leaves										
Grn:	2%-	6%+	7%+	5%-	5%+	8%+	7%-	9%+	24%+	
Red:	1%-	2%+	3%+	3%-	2%+	3%+	4%-	2%+	5%+	
Inf	1%-	\widetilde{C}_z too low		2%-	73%-	79%-	3%-	10%-	19%-	
					19%-	25%-				
Specularly reflecting leaves										
Grn:	0%+	1%-	1%-	1%-	1%+	2%+	5%-	7%+	17%+	
Red:	1%+	3%-	3%-	1%+	1%-	1%-	5%-	3%+	6%+	
Inf	0%-	\widetilde{C}_z too low		1%-	89%-	92%-	1%-	3%-	6%-	
					6%-	9%-				
Rough leaves										
Grn:	4%+	10%-	12%-	10%+	12%-	16%-	18%+	17%-	29%-	
Red:	4%+	7%-	7%-	11%+	7%-	9%-	25%+	11%-	20%-	
Inf	1%+	27%-	30%-	1%+	10%+	14%+	2%+	6%+	15%+	
		25%+	30%+							
Leaf angle Distribution										
Erectophile crop										
Grn:	3%-	9%+	6%-	8%-	10%+	2%-	11%-	18%+	34%-	
Red:	3%-	5%+	10%-	8%-	5%+	9%-	12%-	7%+	1%-	
Inf	2%-	\widetilde{C}_z too low		4%-	61%-	73%-	4%-	15%-	38%-	
					43%-	59%-				
Planophile crop										
Grn:	5%+	13%-	11%+	11%+	12%-	9%+	16%+	15%-	5%-	
Red:	5%+	9%-	17%+	10%+	6%-	19%+	17%+	7%-	11%+	
Inf	3%+	76%-	72%-	4%+	26%+	87%+	5%+	16%+	90%+	
		86%+	*2.8							
Lang (1973)										
Grn:	5%+	12%-	21%+	11%+	12%-	16%+	23%+	20%-	7%-	
Red:	2%+	4%-	33%+	4%+	2%-	35%+	17%+	8%-	19%+	
Inf:	6%+	*2.3	*4.2	10%+	54%+	*3.0	13%+	\widetilde{C}_z too high		

[To be continued]

Table 4.7: [Continued]

Crop and observation properties		$C_z=0.25$			$C_z=0.50$			$C_z=0.75$		
band	R_{ref}	C_z	LAI	R_{ref}	C_z	LAI	R_{ref}	C_z	LAI	
Grn:	.127	.250	.569	.083	.500	1.37	.057	.750	2.74	
Red:	.155	.250	.569	.080	.500	1.37	.038	.750	2.74	
Inf:	.326	.250	.569	.339	.500	1.37	.370	.750	2.74	
		R_{obs}	\widetilde{C}_z	LAI	R_{obs}	\widetilde{C}_z	LAI	R_{obs}	\widetilde{C}_z	LAI
Soil properties										
Dark Soil	Grn:	44%-	*2.4	*3.2	30%-	46%+	90%+	10%-	15%+	45%+
	Red:	44%-	89%+	*2.2	35%-	29%+	49%+	16%-	10%+	27%+
	Inf:	33%-	\widetilde{C}_z too low		20%-	\widetilde{C}_z too low		9%-	96%-	98%-
									35%-	52%-
Bright soil	Grn:	22%+	47%-	51%-	15%+	17%-	22%-	5%+	6%-	11%-
	Red:	26%+	39%-	42%-	21%+	14%-	19%-	10%+	5%-	10%-
	Inf:	22%+	*3.7	*8.5	14%+	70%+	*2.7	6%+	18%+	56%+
Observation conditions										
Sun's inclin. 45°	Grn:	8%-	22%+	26%+	7%-	9%+	13%+	3%-	4%+	8%+
	Red:	11%-	20%+	24%+	13%-	9%+	14%+	10%-	5%+	12%+
	Inf:	3%-	\widetilde{C}_z too low		0%-	94%-	96%-	1%+	4%+	8%+
									2%-	3%-
Minimum observed value	Grn:	17%-	45%+	56%+	17%-	22%+	36%+	11%-	16%+	48%+
	Red:	21%-	39%+	49%+	27%-	21%+	35%+	27%-	20%+	68%+
	Inf:	9%-	\widetilde{C}_z too low		4%-	59%-	67%-	2%-	8%-	15%-
									47%-	56%-
Maximum observed value	Grn:	1%+	2%-	2%-	4%+	4%-	6%-	13%+	12%-	22%-
	Red:	0%	0%	0%	0%	0%	0%	6%+	3%-	6%-
	Inf:	6%+	*2.2	*2.8	9%+	51%+	*2.0	12%+	32%+	>5.0
Combinations of phenomena										
Erectophile, rough leaves	Grn:	1%+	3%-	17%-	3%+	3%-	19%-	8%+	8%-	28%-
	Red:	1%+	2%-	17%-	4%+	2%-	18%-	15%+	7%-	26%-
	Inf:	2%-	\widetilde{C}_z too low		2%-	76%-	84%-	2%-	7%-	27%-
									17%-	34%-
Planophile, rough leaves	Grn:	9%+	20%-	1%+	20%+	22%-	7%-	34%+	27%-	25%-
	Red:	8%+	14%-	10%+	20%+	13%-	8%+	41%+	16%-	7%-
	Inf:	4%+	86%-	84%-	5%+	32%+	*2.0	7%+	20%+	>5.0
			95%+	*3.0						
Lang (1973), min. obs. value	Grn:	9%-	23%+	78%+	3%-	4%+	47%+	1%+	1%-	36%+
	Red:	10%-	19%+	71%+	7%-	4%+	49%+	2%-	1%+	42%+
	Inf:	10%-	\widetilde{C}_z too low		7%-	\widetilde{C}_z too low		5%-	17%-	2%-
Lang (1973), max. obs. value	Grn:	5%+	13%-	19%+	16%+	18%-	7%+	40%+	31%-	26%-
	Red:	2%+	4%-	32%+	4%+	2%-	35%+	24%+	10%-	12%+
	Inf:	15%+	*3.1	*7.2	24%+	\widetilde{C}_z too high		29%+	\widetilde{C}_z too high	
Lang (1973), sun's azim. 90°	Grn:	7%+	16%-	14%+	14%+	15%-	11%+	21%+	18%-	5%-
	Red:	7%+	12%-	21%+	13%+	8%-	24%+	22%+	10%-	14%+
	Inf:	5%+	*2.1	*3.6	6%+	35%+	*2.3	8%+	22%+	>5.0

C_z . These figures are presented in conjunction with the 'calculated' estimated values for \widetilde{C}_z and \widetilde{LAI} . These values are calculated with the curves for the reference crop. This reference crop is the crop that is presented in Figure 4.18, and with a sun's inclination of 60° . For instance, the value that is found for $C_z = 0.25$ for a crop with bright leaves for green radiation is presented as '2%+' (see the first line in Table 4.7). This means that the calculated zenith radiance $R_{g,crop}$ for this crop was 1.02 times the corresponding value for the reference crop $R_{g,ref}$. Interpretation of the calculated value with the curve for the reference crop resulted in an underestimation of 6% of the coverage (0.235 instead of 0.250) and of 7% of the LAI (0.530 instead of 0.569).

Before Table 4.7 is discussed in more detail, it makes sense to give some general remarks on the calculations on infrared radiation.

- The minimum value of $R_{i,ref}$ is found for $C_z = 0.224$. This is very close to $C_z = 0.25$, so for about half of the crops that are presented in Table 4.7, the calculated value of $R_{i,crop}$ for this value of C_z cannot be interpreted, because the calculated value of $R_{i,crop}$ is lower than the lowest value that is found for $R_{i,ref}$. This means also that no values for \widetilde{C}_z and \widetilde{LAI} could be computed.
- As can be seen in Figure 4.18, the curve for the infrared radiation for the reference crop $R_{i,ref}$ is very flat. This means that even small differences between the values of $R_{i,crop}$ of the crop under consideration and of $R_{i,ref}$ will cause serious differences between the actual and the estimated values of \widetilde{C}_z and LAI . And, even worse, that it happened several times that $R_{i,crop}$ was beyond the range for $R_{i,ref}$. This did not only happen for $C_z = 0.25$ at the low side of the curve, but also, although less frequently, for other values of C_z . If this happened, then this is reported in Table 4.7 as ' \widetilde{C}_z too low' or ' \widetilde{C}_z too high'. All calculations were carried out with values for LAI in the range [0...5] so if a value for \widetilde{C}_z was computed that exceeded 0.92, this is indicated with '>5.0'.
- In the contrary to $R_{g,ref}$ and $R_{r,ref}$, $R_{r,ref}$ is not a monotonically in- or decreasing function of C_z . Therefore it is possible that the calculated value of $R_{i,crop}$ cannot be interpreted unambiguously, but that two values for \widetilde{C}_z and \widetilde{LAI} are found. These are both listed in Table 4.7.

Because of these reasons it may be concluded that, especially for low values of C_z , the use of $R_{i,crop}$ as a single value gives extremely inaccurate results, because its value is determined by other properties rather than by C_z or LAI .

The interpretation of $R_{g,crop}$ and $R_{r,crop}$ gives better results, although also with these values the interpretation may lead sometimes to wrong conclusions.

Most crop properties have only little influence on the measured radiation in the visible bands. Exceptions must be made for the crop with rough leaves and for the crop with dark leaves for the high values of C_z . Differences of over 20% are found in the calculated value of \widetilde{LAI} in these cases. Differences in the leaf angle distribution cause larger differences in the green than in the red band, but for the two crops without azimuthal preference these are, with three exceptions, limited to 11% in the value of \widetilde{LAI} . For the crop with azimuthal preference, the calculated differences are larger. The calculated values of \widetilde{C}_z are not too bad, but the \widetilde{LAI} is overestimated up to 35%.

A much more serious source of interpretation deviations appears to be the soil reflection coefficient. For the lowest value of C_z , differences to 50% underestimation in \bar{LAI} for a bright dry soil and to 2-3 times the actual value for \bar{LAI} for a dark (wet) soil.

Another source of misinterpretation is the sun's inclination. A lower sun's direction appears to cause differences in the interpreted values of \bar{C}_z and \bar{LAI} of 10-25%. Also the direction of the observation may cause differences. Especially if the lowest value is measured (and this happens if the observation is done in the direction opposite to the sun and with an inclination of 45°), then \bar{C}_z may be an overestimation of 40% for the low value of C_z and of 20% for $C_z = 0.75$. The consequences for \bar{LAI} are an overestimation of 35-65%.

In the last section of the table, some combinations of phenomena are listed. As may be expected, the differences found here are comparable to the sum of the differences of the sole phenomena. This means sometimes that these influences neutralize each other to some extent, but it is also possible that they intensify each others effect.

A general conclusion of the calculations in Section 4.3, is that the interpretation of single wavelength band values will not yield reliable results.

A second conclusion can be made by only looking to the figures on the differences between R_{crop} and R_{ref} for one arbitrary case in the three wavelength bands. In almost all cases, these differences have an equal sign. In other words, if some property causes a lower reflection in the red band, than it causes also a lower reflection in the infrared band. This means that it will make sense to use the ratio between two bands for the interpretation rather than the radiance in one single band. This is done in the next section.

4.4 Combination of the reflection in different spectral bands

The final conclusion of Section 4.3 was that the use of a ratio between two spectral bands (one in the visible region and the near infrared band) can diminish the uncertainties in the deviation of the coverage of a crop from the measured reflection of that crop, because most non relevant crop properties give similar deviations in the three considered wavelength bands. Because the band that shows the most marked relation with the coverage is the red spectral band, the quotient Q of the infrared reflection R_i and the red reflection R_r seems to be the best choice for this ratio. The discriminating properties of Q can be derived from Figure 4.20. The curves for the three crops in this figure show an increasing zenith radiance in the infrared band for the coverage range $0.50 < C_z < 1.00$, whereas the reflection in the red band decreases over the whole range between a bare and a completely covered soil. In practice, in addition to Q , the normalized difference of R_i and R_r is also used. This quantity is called the vegetation index VI . The advantage of using VI rather than Q is that the relation between C_z and VI is more linear than the relation between C_z and Q . Apart from that, VI does not give more information than Q : they can be expressed in each other according to the

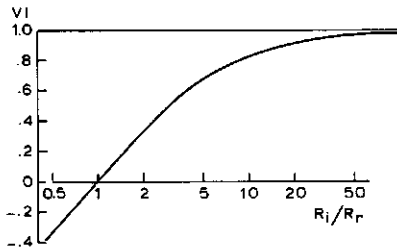


Figure 4.28: Relation between the quotient Q (=infrared reflection/red reflection) (horizontal axis, logarithmic scale) and vegetation index VI (vertical axis, linear scale).

equations:

$$VI = \frac{R_i - R_r}{R_i + R_r} = \frac{R_i/R_r - 1}{R_i/R_r + 1} = \frac{Q - 1}{Q + 1} \quad (4.25)$$

or vice versa:

$$Q = \frac{1 + VI}{1 - VI} \quad (4.26)$$

Figure 4.28 shows this relation between Q and VI . Figure 4.29 shows Q as a function of C_z , for three crops with different leaf angle distribution; Figure 4.30 does the same for the relation between C_z and VI . Comparison of the two sets of curves shows that Q is especially sensitive if $C_z > 0.50$, whereas VI varies mostly if $C_z < 0.70$. Because the growth rate of a not closed crop depends greatly on the coverage, it is preferable to use VI instead of Q .

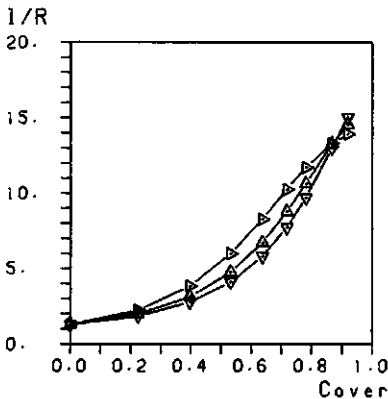


Figure 4.29: Ratio red reflection/infrared reflection Q as a function of the vertical coverage C_z for three different leaf angle distributions (∇ = spherical, \blacklozenge = planophile, \triangle = erectophile) as calculated for the zenith direction. Sun's inclination is 60° , 20% diffuse incoming radiation (SOC).

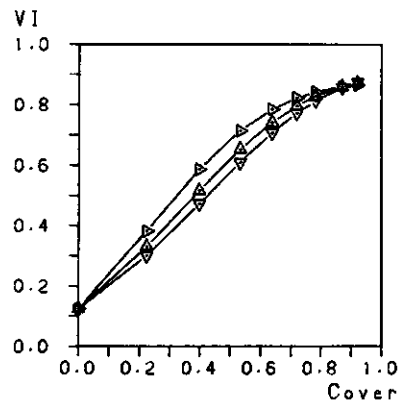


Figure 4.30: As Figure 4.29, vertical axis gives the vegetation index VI instead of Q .

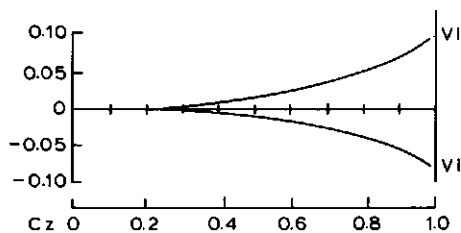


Figure 4.31: Errors in the estimation of the coverage C_z from the vegetation index VI as a function of C_z . Errors are caused by a lack of knowledge on the leaf angle distribution of the observed crop. Vertical axis: differences between this coverage and the coverage of crops with arbitrary leaf angle distributions with equal values for VI .

4.4.1 Crop geometry

Figure 4.20 shows that in all bands the zenith radiance increases if the leaf angle distribution tends to be more planophile. Because the leaf angle distribution has relatively larger effect on the reflection in the red and the green bands than on the reflection in the infrared band, VI decreases slightly with an increasing planophile nature of crops with equal coverage, as can be seen in Figure 4.30. In Figure 4.31 the uncertainties in the estimation of C_z from VI are presented, under the assumption that the leaf angle distribution is the only unknown crop property. This uncertainty is defined as the horizontal distance between the curves for the planophile and erectophile crop as found in Figure 4.30.

4.4.2 Optical properties of the leaves

An important factor in the crop reflection is the reflective behaviour of the individual leaves. To show this, the relations between C_z and VI for three crops with different optical behaviour and spherical leaf angle distributions are presented in Figure 4.32. Similar calculations were performed for the crop with azimuthal preference, and the azimuth direction of the sun chosen so that the interception is at its maximum. The same effects as in Figure 4.32 were found, although less marked than in the case of a spherical crop. The explanation for the smaller effect is as follows:

- The average angle between the direction of incidence and the leaf's normal is larger for the spherical crop than for the crop with azimuthal preference.
- The reflection of a rough leaf increases concomitantly with the angle of incidence; for a Lambertian reflecting leaf the reflection coefficient is independent of this angle.
- The increase of the reflection correlates with the refraction index. This refraction index hardly changes in the spectral range under consideration (500-900 nm), so the absolute values of the increases are almost independent of the spectral band considered.

- The isotropic nature of the reflected radiation means that an increasing reflection coefficient influences both layer reflection and layer transmission
- The crop reflection in the infrared band is much higher than in the red band, so the influence of the surface reflection is more important in the red band than in the infrared band.
- If crop reflection coefficients in both bands increase by the same amount, their quotient decreases. The greater the increase of the numerator and the denominator, the greater the decrease of the quotient Q .
- The vegetation index is a monotonously increasing function of Q .

Combining these statements leads to the conclusion that the decrease in Q and VI becomes less if the average interception increases. Because the interception of the spherical crop is less than the interception of the crop with azimuthal preference, larger differences can be expected for the spherical crop. The errors in the estimation of C_z arising from lack of knowledge about the leaf reflection type are between 5% and 10% for a spherical crop, and between 3% and 5% for a crop with azimuthal preference.

A calculation with the crop with azimuthal preference and another azimuth of the sun confirms the previous explanation. The larger average angle of incidence in this case resulted in larger differences between corresponding values of VI for the three types of leaf surface reflection.

In Figure 4.32 the VI -curve for a crop with specularly reflecting leaves is presented. These curves hardly deviate from the curves for crops with Lambertian reflecting leaves. This is because an increased leaf reflection that is caused by a larger angle of incidence leads to layer transmission rather than to layer reflection in many combinations of leaf orientation and incident radiation. Because layer transmission only contributes to crop reflection indirectly, the differences between the reflection of crops with specularly reflecting leaves and the reflection of crops with isotropically reflecting leaves is smaller than the differences between crops with rough leaves and crops with isotropically reflecting leaves.

4.4.3 Reflection and transmission coefficients of the leaves

Different crops, or the same crop at different stages of development, show differences in the reflection and transmission coefficients in the same spectral bands (see Figures 4.6 to 4.8). These differences are related to leaf thickness (especially concerning the transmission coefficient) and the presence of active chlorophyll (concerning both reflection and transmission). For that reason, besides the standard or 'mean' crop, two other crops were also defined, one with a lower scattering coefficient and one with a scattering coefficient higher than the values that were chosen for the standard crop. (In the infrared band, higher reflection is related to lower transmission because as it can be seen from Figure 4.8 that the general characteristic of the combined values for ρ and τ is that they are highly negatively correlated). The other properties used were a medium soil reflection coefficient and a spherical leaf angle distribution. Figure 4.33 shows the relation between coverage and VI for the four combinations that can be derived from

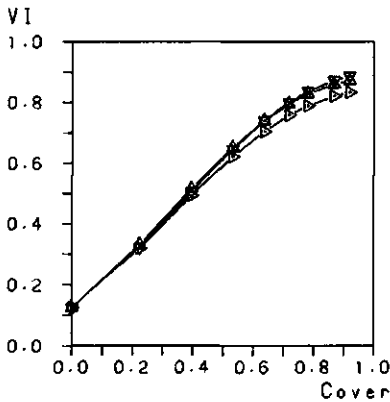


Figure 4.32: Vegetation index VI as a function of C_z for three crops with different type of surface reflection: Lambertian (\triangle), glossy (∇) and rough (\triangleright). Leaf angle distribution is spherical, sun's inclination is 60° , medium levels of leaf reflection, leaf transmission and soil reflection. Curves are based on zenith radiance.

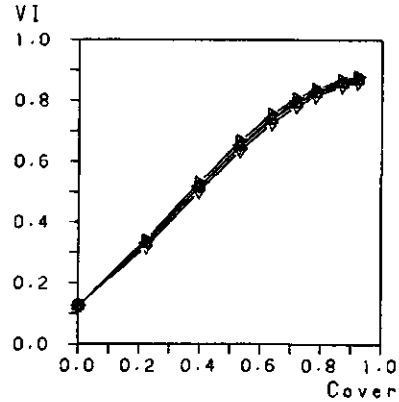


Figure 4.33: Vegetation index VI for four different crops with different leaf reflection coefficients as a function of coverage. Crop types are:
 \triangleleft : infrared dark, red dark
 \triangleright : infrared bright, red dark
 ∇ : infrared dark, red bright
 \triangle : infrared bright, red bright
 Other crop and radiation parameters are as in Figure 4.32.

Figure 4.10. It appears that even for the extreme combinations (infrared highly reflective and red low reflective, and vice versa), the values for VI show only little differences for the same values of C_z . Only if the coverage exceeds a value of 0.8, errors over 5% can occur in the estimation of the coverage from the vegetation index, caused by differences in ρ and τ .

4.4.4 Soil reflection

In Subsection 4.3.3 attention was paid to the effect of the soil reflection coefficient on the zenith radiance in individual spectral bands. It appears that the soil reflection coefficient is also a major factor for the value of VI for an incompletely closed crop. As shown in Figure 4.34, for crops with a coverage in the range 0.3 to 0.7, the interpretation error may rise to 10%. If, as shown in Figure 4.35, the observation direction is also taken into account, the error in the estimation of C_z caused by these effects can increase up to 15%. This is a remarkable effect, because a more oblique angle of observation leads to a decreasing visibility of the soil. No direct explanation for this effect is found, except that, as will be shown in Table 4.8, a more oblique angle generally causes an increasing value of VI .

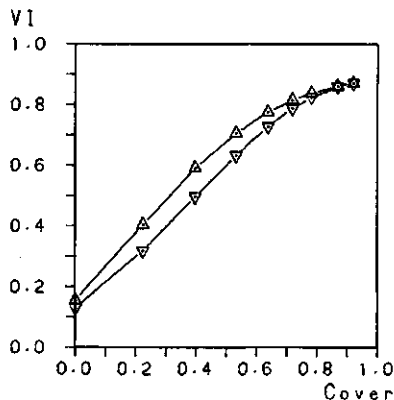


Figure 4.34: Differences in the relation between coverage and the vegetation index VI , based on the reflection coefficient of the soil. ∇ : bright soil; \triangle : dark soil. Other parameters are as in Figure 4.32.

4.4.5 Incident radiation and observation direction

Figure 4.27 showed that the measured crop radiance depends on the geometrical aspects of the incident radiation and the observation: observation direction and inclination and azimuth of the sun. Therefore, for the crop with azimuthal preference, the influence of the sun's azimuth on the estimation of the coverage is presented in Figure 4.36. For two azimuth directions of the sun two VI curves are drawn. These represent the highest and lowest value that are found in a cone with a half top angle of 45° and a vertical axis. This figure suggests that the influence of the sun's direction is still present and it may cause an estimation error of about 5%. The observation direction itself can cause an error of up to 10% in the estimation of the coverage.

4.4.6 Conclusions

Similar to Subsection 4.3.6, also here a table is used to present a summary of all results that are obtained in the calculations in Section 4.4 (Table 4.8). The symbols used in this table have the same meaning as in Table 4.7, in Subsection 4.3.6, so they are not explained here. If Table 4.8 is compared to Table 4.7 it can be seen that the use of

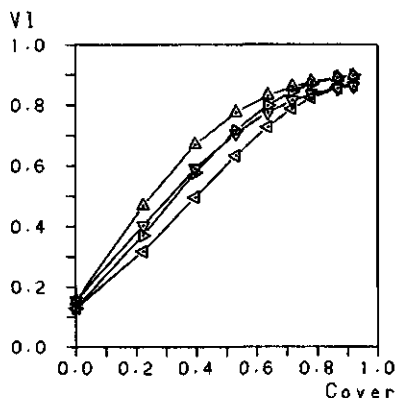


Figure 4.35: Minimum and maximum values of the vegetation index VI as a function of coverage for crop with a bright and with a dark soil below. \triangleright : bright soil, upper value of VI ; \triangleleft : bright soil, lower value of VI ; \triangle : dark soil, upper value of VI ; ∇ : dark soil, lower value of VI . Other parameters are as in Figure 4.32. Crops have medium reflection and transmission coefficients, sun's inclination is 60° .

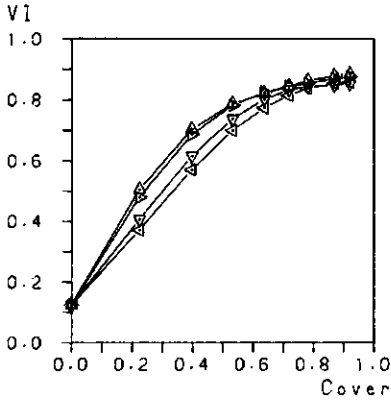


Figure 4.36: Differences in the relation between the vegetation index VI and the coverage for the crop with azimuthal preference caused by differences in sun direction:

- \triangle : maximal interception, upper value of VI
- ∇ : maximal interception, lower value of VI
- \triangleright : medium interception, upper value of VI
- \triangleleft : medium interception, lower value of VI

Table 4.8: Effects of several parameters on the measured vegetation index and on the interpretation of this VI_{obs} . The relation between VI_{ref} measured in zenith direction and the vertical coverage of the reference crop (Figure 4.18) is used. Values are given for three values of the coverage (C_z) and LAI. Parameters are only indicated as far as they differ from the reference crop. Values for other crops are given as percentual differences with the reference crop. In all cases, the vegetation index that is calculated from the 'measured' radiation (VI_{obs}) and estimated coverage (\tilde{C}_z) and LAI (\tilde{LAI}) are given.

Crop- and observation properties	$C_z=0.25$			$C_z=0.50$			$C_z=0.75$		
	VI_{ref}	C_z	LAI	VI_{ref}	C_z	LAI	VI_{ref}	C_z	LAI
	.359	.250	.569	.620	.500	1.37	.813	.750	2.74
	VI_{obs}	\tilde{C}_z	\tilde{LAI}	VI_{obs}	\tilde{C}_z	\tilde{LAI}	VI_{obs}	\tilde{C}_z	\tilde{LAI}
Leaf properties									
Bright leaves	0%	0%	0%-	0%-	0%-	1%-	0%-	1%-	1%-
Dark leaves	0%	0%	0%	0%+	0%+	0%+	0%+	0%+	1%+
Specularly refl. leaves	2%-	3%-	3%-	1%-	1%-	2%-	1%+	2%+	4%+
Rough leaves	4%-	5%-	6%-	5%-	6%-	8%-	5%-	8%-	16%-
Leaf angle distribution									
Erectophile crop	1%+	2%+	13%-	2%+	3%+	12%-	2%+	3%+	9%-
Planophile crop	1%-	1%-	28%+	3%-	4%-	24%+	2%-	5%-	18%+
Lang (1973)	7%+	10%+	55%+	3%+	3%+	46%+	1%-	2%-	34%+
Soil properties									
Dark soil	20%+	27%+	33%+	10%+	13%+	20%+	2%+	4%+	8%+
Bright soil	4%-	5%-	6%-	3%-	4%-	5%-	1%-	1%-	3%-
Observation conditions									
Sun's inclination 45°	10%+	13%+	15%+	7%+	8%+	13%+	2%+	5%+	11%+
Minimum observed value	0%	0%	0%	0%	0%	0%	0%	0%	0%
Maximum observed value	17%+	23%+	28%+	13%+	18%+	28%+	6%+	16%+	47%+
Combinations of phenomena									
Erectophile, rough leaves	3%-	4%-	19%-	3%-	4%-	20%-	4%-	7%-	27%-
Planophile, rough leaves	4%-	6%-	22%+	7%-	8%-	15%+	6%-	11%-	3%+
Lang (1973), min. value	1%+	1%+	42%+	2%-	2%-	35%+	2%-	3%-	29%+
Lang (1973), max. value	24%+	32%+	94%+	13%+	17%+	77%+	1%+	2%+	45%+
Lang (1973), sun's az. 90°	1%-	1%-	38%+	3%-	4%-	32%+	3%-	5%-	24%+

VI instead of single band values gives a real enhancement of the possibilities and the accuracy of the estimated C_z and LAI values. No cases were found where the value of VI_{crop} was beyond the range of VI_{ref} , and especially for higher values of VI_{crop} the interpretation gives fairly accurate results in the estimated values of \bar{C}_z and \bar{LAI} . Also for different optical properties of the leaves (dark or bright, reflective properties), the estimated values of \bar{C}_z and \bar{LAI} are with one exception always reasonable close to the actual values. The influence of the soil reflection, one of the major problems found in Table 4.7, is decreased from a factor 2 to 3 to at most about 30% for low and 8% for high C_z values. For the different leaf angle distributions, the quality of the estimations of \bar{C}_z is much better (differences are limited to 5%), but the estimation of \bar{LAI} is not improved: the differences found are of the same order of magnitude as found for the single visible bands in Table 4.7: 10 - 50%.

The direction of the sun gives the same problems if VI is used for the interpretation rather than the single visible bands, and this also holds for the observation direction.

The general conclusion that can be drawn from the calculations in Sections 4.3 and 4.4 is that the use of the vegetation index VI gives generally better results if the measured reflection in two bands are used to estimate the coverage or the LAI of a crop than the use of single spectral bands, even if only the ratio between the reflected fraction in both bands is used. The infrared band acts rather as a 'reference level adjustor' than as an information-source on its own. The actual information comes from the large differences in the visible bands between a (nearly) bare soil and an (almost) completely closed crop.

4.5 Improvement of the estimation of the crop parameters by a correction on the measured radiation

In Figure 4.17 it was shown clearly that a relation exists between the observation direction and the measured or calculated radiance. It also showed two properties of this relation:

- The curve that depicts this relation is, regardless of the wavelength bands and sun's inclination, shaped as a parabola.
- These parabolas are completely differently shaped in the visible and in the infrared bands of the spectrum.

The conclusion of this is that if the measured radiances are used to calculate the vegetation index, differences in the calculation results will occur, depending on the observation direction. If it is assumed that the relation between vegetation index VI and for instance the coverage is known for the nadir direction, a correction on the measured radiations to all off-nadir observations could be applied before these radiances are applied in the calculation of VI . Because the relation between the radiation and the position in the observed strip is of a parabolic nature, all measured radiances can be corrected by subtracting a suitable parabola, resulting in corrected radiances that will be independent of the observed viewing direction. To check this for other LAI values,

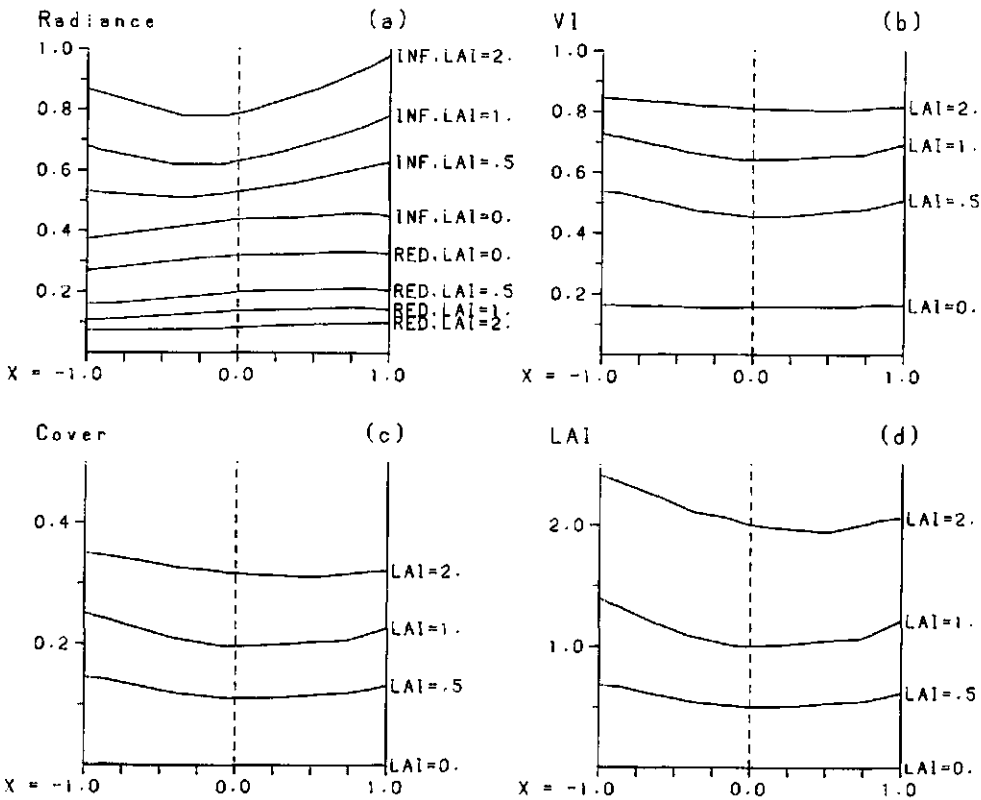


Figure 4.37: Directional radiance for four LAI levels and related quantities.

- a): Radiance as a function of observation direction for four LAI levels in two spectral bands.
- b): VI computed from corresponding radiances in Figure a.
- c): C_z computed from uncorrected VI values.
- d): LAI computed from C_z values from Figure c.

Figure 4.37a is drawn. This figure shows that a parabolic relation exists for all LAI values. The upper four curves in Figure 4.37a show the relation in the infrared band, the lower four in the red band. Figure 4.37b is derived from the data in Figure 4.37a. It gives the VI for the four LAI values as computed with the uncorrected radiances. If these are used to calculate the vertical coverage Figure 4.37c is obtained. Finally, these coverages are translated into LAI values. These are presented in Figure 4.37d. The equations for the relations between VI, C_z and LAI for the nadir direction are:

$$C_z = 1.692 VI^3 - 1.776 VI^2 + 1.324 VI - 0.171 \quad (4.27)$$

$$LAI = 2 \cdot \ln(1 - C_z) \quad (4.28)$$

The range for VI is [0.158 ... 0.956], for C_z [0 ... 0.95] and for LAI [0 ... 6]. Values that are calculated outside these ranges are set to the appropriate boundary value. Equation (4.27) is completely empirical and obtained by fitting the simulated results, Equation (4.28) is based on an ideal spherical leaf angle distribution. These relations are shown together in Figure 4.38.

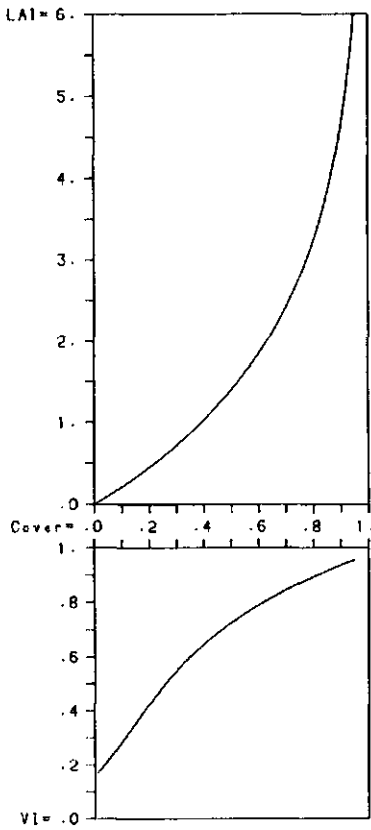


Figure 4.38: The relations between vegetation index VI (vertical axis, lower half), coverage (horizontal axis, both figures) and LAI (vertical axis, upper half) as used in the calculations in Section 4.5. The curves are based on zenith radiances as computed with the HARE model.

4.5.1 LAI=1 for the whole area

At first, the described method is applied to a situation for a crop with $LAI=1$. The correction calculations are carried out as follows:

For both spectral bands the 'measured' radiances are written as $R_{1.0}(x)$, with $-1 < x < 1$. The index 1.0 on R denotes the 'real' LAI , x denotes the position in the flight strip (see Figure 4.39). For 40 positions x_i , uniformly distributed over $[-1 \dots 1]$, $R(x_i)$

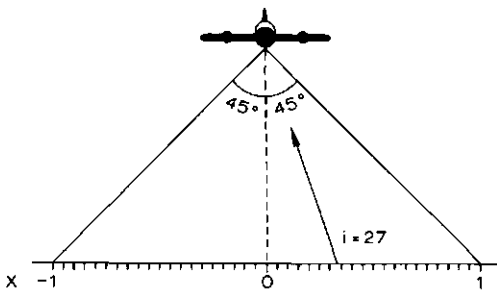


Figure 4.39: Geometry of the observations as used in Section 4.5.

is used to calculate the regression parabola $P(x_i)$ in such a way that

$$\sum_{i=1}^{40} \{P(x_i) - R_{1,0}(x_i)\} \quad (4.29)$$

is minimized. $P(x)$ can be written as

$$P(x) = a_2x^2 + a_1x + a_0 \quad (4.30)$$

The coefficients a_0 , a_1 and a_2 can be calculated by solving the regression equation (R_i is an abbreviation of $R_{1,0}(x_i)$):

$$\begin{pmatrix} \sum(x_i^4) & \sum(x_i^3) & \sum(x_i^2) \\ \sum(x_i^3) & \sum(x_i^2) & \sum(x_i) \\ \sum(x_i^2) & \sum(x_i) & n \end{pmatrix} \begin{pmatrix} a_2 \\ a_1 \\ a_0 \end{pmatrix} = \begin{pmatrix} \sum(R_i x_i^2) \\ \sum(R_i x_i) \\ \sum R_i \end{pmatrix} \quad (4.31)$$

Because the x -values are positioned symmetrically on both sides of $x = 0$, the values of $\sum(x_i^3)$ and $\sum(x_i)$ are 0. This permits a simplification of the equations to

$$\begin{pmatrix} \sum(x_i^4) & \sum(x_i^2) \\ \sum(x_i^2) & n \end{pmatrix} \begin{pmatrix} a_2 \\ a_0 \end{pmatrix} = \begin{pmatrix} \sum(R_i x_i^2) \\ \sum R_i \end{pmatrix} \quad (4.32)$$

and

$$\sum(x_i^2) a_1 = \sum(R_i x_i) \quad (4.33)$$

From Equations (4.32) and (4.33) the following equations can be derived:

$$a_0 = \frac{\sum(x_i^4) \cdot \sum R_i - \sum(x_i^2) \cdot \sum(R_i x_i^2)}{n \cdot \sum(x_i^4) - (\sum x_i^2)^2} \quad (4.34)$$

$$a_1 = \frac{\sum(R_i x_i)}{\sum(x_i^2)} \quad (4.35)$$

$$a_2 = \frac{n \cdot \sum(R_i x_i^2) - \sum(x_i^2) \cdot \sum R_i}{n \cdot \sum(x_i^4) - (\sum x_i^2)^2} \quad (4.36)$$

Of the parabola $P(x)$, the part $a_2x^2 + a_1x$ is used for the correction, so the corrected values $R_{1,0}^*(x)$ are

$$R_{1,0}^*(x_i) = R_{1,0}(x_i) - P(x_i) + a_0 \quad (4.37)$$

The correction for the nadir direction ($x = 0$) is 0 because $P(0) = a_0$. Figure 4.40 shows the calculated estimations. It can be seen in this figure that for LAI=1 the correction gives very good results. The curves for the other LAI values show some deviations (especially the curve with LAI=2), but it must be remembered that no pixels with LAI=2 were in the calculation, so the meaning of that curve is only of theoretical importance. In fact, it says that if the whole observed area is covered with a crop with LAI=1, and one spot near the left margin of the strip should have an LAI of 2, the LAI calculated for that spot is 1.8 instead of 2.

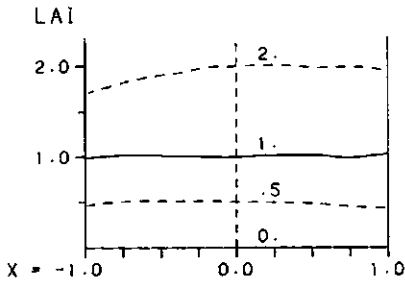


Figure 4.40: Estimated values of LAI if the complete observed area is covered with a crop with LAI=1 (see Subsection 4.5.1). Horizontal axis: position in the observed strip; vertical axis: LAI values calculated with the corrected radiances. Numbers with the curves indicate the 'real' LAI values. The solid line indicates actual, the dotted lines indicate potential estimations.

4.5.2 A uniform LAI distribution

The situation of a uniform LAI over the whole area is not very common, so the same calculations were repeated for more complex compositions of crop types in the observed area. The first of these studied situations was one in which four crop types (with LAI=0, 0.5, 1 and 2) were uniformly distributed over the complete flight strip. In other words, no relation existed between the distribution of the crop types across the flight strip and the position in the strip. For reasons of uniformity, the following fractions were used:

- crop type 1 $LAI_1 = 0$ $d_1 = 20\%$
- crop type 2 $LAI_2 = 0.5$ $d_2 = 20\%$
- crop type 3 $LAI_3 = 1.0$ $d_3 = 30\%$
- crop type 4 $LAI_4 = 2.0$ $d_4 = 30\%$

The result is an average LAI of 1.0. The calculation of the correction is now slightly more complex and goes as follows:

For each value of x , the average reflection radiance $\overline{R(x)}$ in both bands is computed as a weighted mean over the four crop types c :

$$\overline{R(x_i)} = \sum_{c=1}^4 d_c \cdot R_{LAI_c}(x_i) \tag{4.38}$$

The two so-computed values of $\overline{R(x_i)}$ are used to calculate two regression-parabolas $P(x)$ (one for the red and one for the infrared reflection). This is done by minimizing the equation:

$$\sum_{i=1}^{40} \{P(x_i) - \overline{R(x_i)}\} \tag{4.39}$$

in the two bands. The corrected radiances are computed with

$$R_{LAI_c}^*(x_i) = R_{LAI_c}(x_i) - P(x_i) + a_0 \tag{4.40}$$

The results of the calculations are presented in Figure 4.41. Also here it can be seen that the applied correction improves the accuracy of the estimation of the LAI from the radiation considerably.

4.5.3 Non-uniform LAI distributions

For the third case we will consider a completely different situation: it will be assumed that the four crop types from Subsection 4.5.2 are not uniformly distributed over the

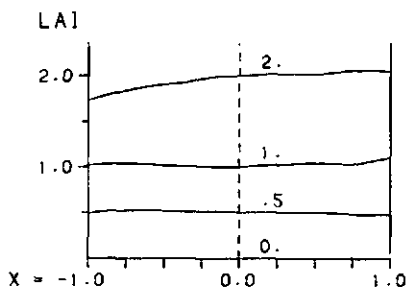


Figure 4.41: Estimated values of LAI if the LAI values are uniformly distributed over the flight strip. See text of Figure 4.40 for further explanation. Figure is related to the case described in Subsection 4.5.2.

flight strip, but starting on the left side, first all pixels with LAI=0 are found, then all pixels with LAI=0.5 and so on. The fractions are like in the previous calculation (so LAI=0: 20%, LAI=0.5: 20%, LAI=1: 30% and LAI=2: 30%). If the same correction formulas are applied in this situation, the result is completely different. In Figure 4.42 it can be seen that the course of the LAI as computed with the corrected radiances is a sawtooth-like function around LAI=1, rather than the stepfunction that should represent the actual LAI values. In the part of the strip with low actual LAI values, these are overestimated, in the part of the strip with high LAI values, these are underestimated, where, regardless of the actual LAI, the corrected LAI values are all in the range [0.5 ... 1.5]. Single pixels with a deviant value may result in extreme values: a pixel with LAI=0.5 near the left margin of the strip would have been computed after correction as LAI=6, a single pixel with LAI=0.5 near the right margin as LAI=0. Similar results were found if the distribution of the crop types over the flight strip was set at a continuous gradient in LAI from left to right or vice versa.

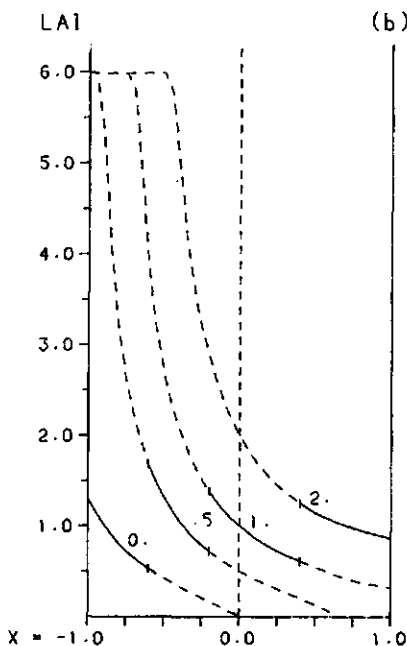
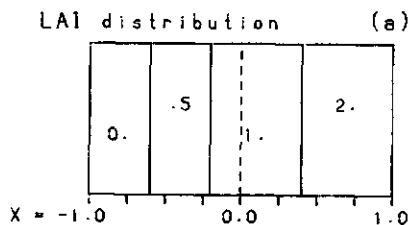


Figure 4.42: Estimated values of LAI if the LAI values are distributed with the low values near the left margin and the high values near the right margin of the flight strip. See Figure 4.40 and Subsection 4.5.3 for further explanation. Figure is related to the third case.

- a): LAI distribution (input).
- b): Estimated LAI values.

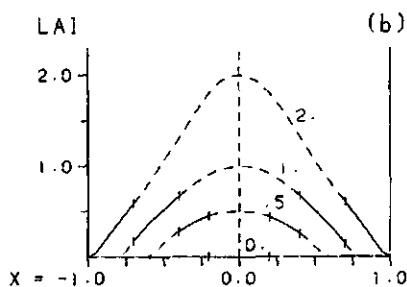
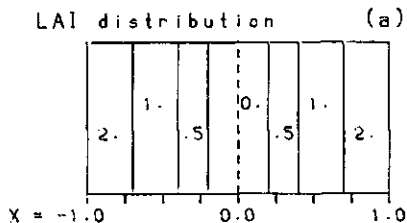


Figure 4.43: Estimated values of LAI if the LAI values are distributed with the low values near the centre of the flight strip. See Figure 4.40 and Subsection 4.5.3 for further explanation. Figure is related to the fourth case.

- a): LAI distribution (input).
- b): Estimated LAI values.

The fourth case was a strip with high LAI values at the margins of the flight strip and low LAI values in its centre. The results of these calculations are presented in Figure 4.43. The calculated LAI is less than 0.7 over the whole area. At both margins of the strip, even an LAI of 2 in the input resulted in a calculated LAI after correction of 0.

The opposite of the fourth case, the fifth case, is shown in Figure 4.44, where the distribution of high and low LAI values has been interchanged. Now we see that over the whole strip LAI values are overestimated. They are calculated as being in the range [1.5 ... 3.5].

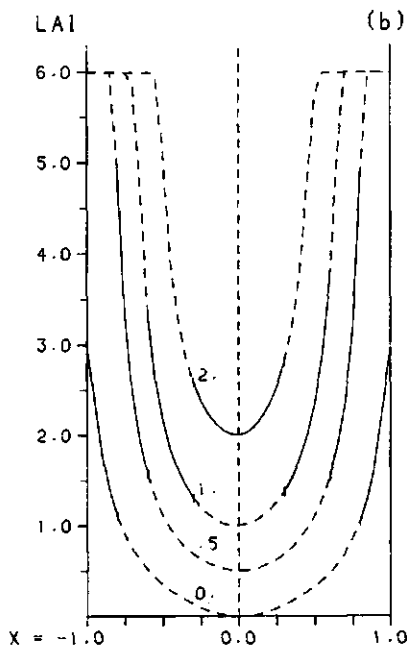
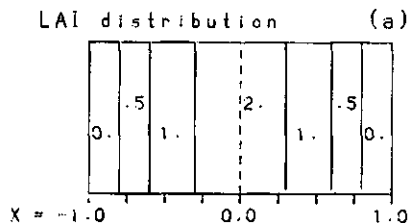


Figure 4.44: Estimated values of LAI if the LAI values are distributed with the high values near the centre of the flight strip. See Figure 4.40 and Subsection 4.5.3 for further explanation. Figure is related to the fifth case.

- a): LAI distribution (input).
- b): Estimated LAI values.

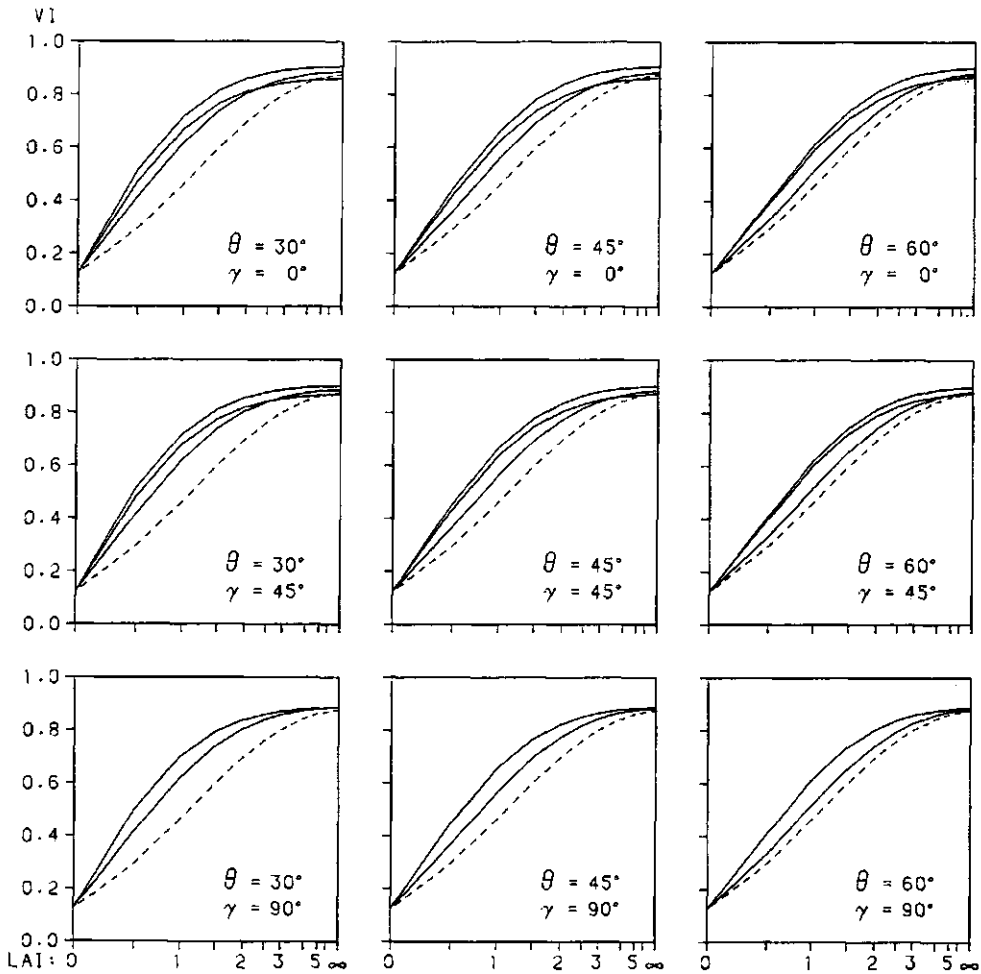


Figure 4.45: Some examples of the relation between vertical coverage C_z or LAI and the vegetation index VI for 24 combinations of sun's inclination θ , observer's inclination ν and sun's azimuth γ . θ and γ are given in the figures. $\gamma=0^\circ$ is perpendicular to the flight direction. Each subfigure gives (reading downward) $\nu=45^\circ$ with the sun in the back, $\nu=45^\circ$ opposite to the sun and $\nu=90^\circ$ (nadir). For the figure in the lower line with $\gamma=90^\circ$ the two curves for $\nu=45^\circ$ coincide. The dotted lines are the same in all figures. They represent the relation for $\theta=90^\circ$ and $\nu=90^\circ$.

4.5.4 Conclusions

From Subsections 4.5.1 to 4.5.3 it may be concluded that a correction with a parabola of which the coefficients are only determined by the measured radiances only gives satisfactory results if the different crop types are uniformly distributed over the complete observed flight strip. If this is not true, the calculations correct for differences in crop types rather than for differences in observation direction.

If differences in radiative intensity are small caused by LAI and observation direction, a set of calibration curves can be calculated to relate the measured radiations in any direction to the LAI. This set will be rather large, because (see also Subsection 2.1.2) not only the inclination of the observation direction is a source of variation, but also the direction (inclination and azimuth) of the sun. These curves were produced by the HARE model for a set with the following properties:

- Sun's azimuth γ with respect to the scan direction: $0^\circ, 15^\circ, 30^\circ, 45^\circ, 60^\circ, 75^\circ, 90^\circ$.
- Inclination of the observation v : $90^\circ, 75^\circ, 60^\circ, 45^\circ$ (the latter three for both sides of the flight strip).
- Inclination of the sun θ : $30^\circ, 45^\circ, 60^\circ$.

resulting in 138 different curves (if the sun's azimuth γ is 90° , not all curves need to be calculated). In a particular case, these curves can be used as a kind of grid in which the actual values of θ , v and γ can be interpolated. Some of these curves are presented in Figure 4.45. The algorithm to calculate a full set of curves (with any arbitrary set of combinations of γ , θ and v) is available on request.

4.6 List of symbols used in Chapter 4

		Eqn.	Fig.
a	Stokes parameter	4.6	
a_0, a_1, a_2	coefficients in $P(x)$ (calculation of correction function)	4.30	
b	Stokes parameter	4.7	
B_κ	relative leaf density for leaves with inclination κ	4.1	T. 4.1
C_z	horizontal coverage	4.20	
\tilde{C}_z	estimated horizontal coverage		T. 4.7
d	depth in LAI units	4.4	
d_k	relative density for leaves with orientation k	4.23	
$d(\gamma, \kappa)$	leaf angle distribution	4.21	
D_d	penetration fraction of incident radiation at depth d	4.4	
F_j	upward flux in direction j	4.12	
F_κ	integral of B_κ over $0 \leq k \leq \kappa$	4.2	T. 4.1
k	KM-parameter	4.7	
K	interception coefficient for vertical incidence	4.3	T. 4.1
\tilde{LAI}	estimated leaf area index		T. 4.7
n	refraction index		T. 4.3
$P(x)$	regression parabola (calculation of correction function)	4.29	
P_κ	relative leaf density for leaves with orientation (γ, κ)	4.1	T. 4.1
Q	ratio infrared reflection/red reflection	4.26	4.28
$R_i(x)$	radiance for pixel x for LAI=1 (calculation of correction function)	4.29	
$\overline{R(x)}$	average radiance from pixel x for LAI=1 (calculation of correction function)	4.38	
$R_i^*(x)$	corrected radiance for pixel x (calculation of correction function)	4.37	
R_j^*	scaled upward radiance in direction j	4.14.	
R_i	upward radiance for infrared radiation		4.17
R_j	upward radiance in direction j	4.12	
R_r	upward radiance for red radiation		4.17
R_z	zenith radiance	4.13	
R_∞	KM-parameter	4.6	
s	KM-parameter	4.8	
VI	vegetation index	4.25	4.28
x_i	position of pixel i (calculation of correction function)	4.31	
α	angle of incidence		4.10
γ	azimuthal orientation		
θ	inclination of the incoming radiation	4.5	
κ	inclination of leaf's normal	4.1	T. 4.1

		Eqn.	Fig.
κ_k	inclination of direction k	4.23	
ρ	leaf reflection coefficient	4.9	
ρ_c	reflection coefficient of a crop	4.16	
ρ_d	diffuse reflection coefficient	T. 4.3	4.10
ρ_s	surface reflection coefficient		4.10
τ	leaf transmission coefficient	4.9	
τ_d	diffuse leaf transmission coefficient	T. 4.3	4.10
v	observation inclination		4.17
v_j	inclination of direction j	4.12	
ϕ	azimuth of the incoming radiation		T. 4.5
ω	soil reflection coefficient	T. 4.4	4.14

Chapter 5

Calculations with actual crop data

The calculations in the previous chapters were primarily based on estimated, strongly simplified crop properties and environmental factors. These simplifications were needed so that the influence of changes in individual factors on the reflection observations and derived figures could be analysed without interference from other crop and environmental factors that might be related to those under study. In contrast, the data used in this chapter are, as far as possible, derived from a crop of which detailed field measurements are available. These data are used to determine the parameters for the HARE model. By varying these parameters, the relation between their changes and the measured reflection is used to estimate the accuracy that may be expected if the process is reversed, that is, if the reflection measurements are used to determine the crop properties. In Section 5.1 some calculations on winter wheat are described; the last section of this chapter deals with sugarbeet, and how to use remote sensing to detect drooping of leaves by this crop.

5.1 Winter wheat

Wheat is one of the most important crops on earth. In The Netherlands, the crop is mostly grown as a winter crop. It is sown in October, after which the seeds undergo a vernalization in the soil. The date of emergence is somewhere around November 15th, but during winter the growth rate is very low. Depending on the temperature in the winter the real starting date of the vegetative growth period is usually somewhere around March 1st. This period lasts until the end of May. As in most crops, this growing period starts with exponential growth which gradually changes to linear growth. During these phases the growth consists of stem and leaf development, combined with stem elongation. The leaf growth decreases rapidly after flowering (medium June). Subsequent dry matter production is mainly located in the kernels. Total leaf area decreases as leaves die, and some yellowing of the leaves occurs. The rate of this process not only depends on the age of the leaves, but also on water and nutrient supply and occurrence of pests and diseases.

The calculations in this section are based on the results of field experiments with winter wheat (*Triticum aestivum* cv. *Arminda*) in 1980 (experiment CABO¹ 315) and in 1983

¹CABO: Centre for Agrobiological Research, Wageningen, The Netherlands.

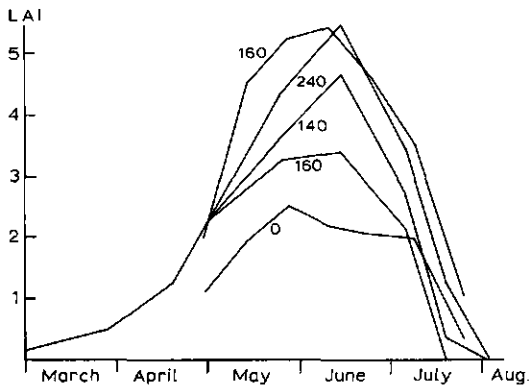


Figure 5.1: The LAI development of a wheat crop as measured in several field experiments in The Netherlands in 1980 and 1983. The figures with the curves indicate the total amount of N fertilizer before and during the growing season (in $\text{kg}\cdot\text{ha}^{-1}$). Vertical axis: LAI; horizontal axis: time.

(CABO 628 = PAGV² 945). Both experiments were carried out near Lelystad, The Netherlands. The LAI development of the wheat crops in the experiments that were used as the inputs for this section is shown in Figure 5.1. The curves in this figure were used to define an average development of a wheat crop. This crop is presented in Figure 5.2. The reflection and transmission values that are used in the calculations were measured in Wageningen (The Netherlands) in 1983 with a Carl-Zeiss RA3 apparatus for measuring spectral remission. The results of the previously mentioned field experiments were used to estimate the dry matter of different crop components such as the leaves, stems and ears of the average crop as a basis for the further calculations. From these data, the LAI of all components was calculated for April 15th, May 15th, June 15th, July 1st and 15th. To do this, the stem was modelled as a vertical cylinder with a diameter of 6 mm, the ears as square prisms with a base of 1 cm^2 . Three crops were constructed for the dates mentioned: one with the computed LAI values for all components; one with an LAI for all components of 0.61 times the computed values; and one with an LAI of 1.61 times the computed values. The values 0.61, 1 and 1.61 relate to each other as the golden ratio; this ratio was chosen to decrease the calculation time needed. Starting on May 15th, strongly yellowing variants of these crops were

²PAGV: Research Station for Arable Farming and Field Production of Vegetables, Lelystad, The Netherlands

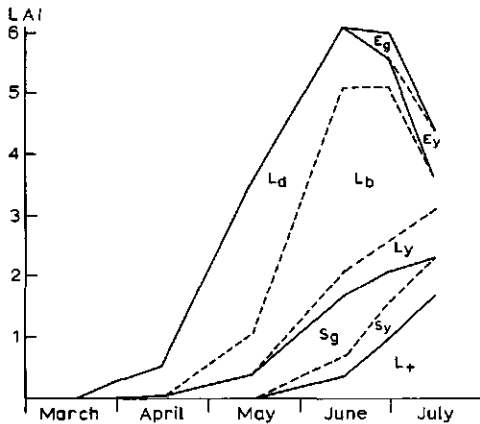


Figure 5.2: Generalized wheat crop as used in the calculations in Section 5.1. Horizontal axis: time; vertical axis: cumulative LAI units for the crop organs distinguished; E_g , E_y : green, yellow ears; L_d , L_b , L_y , L_+ : dark green, bright green, yellow, dead leaves; S_g , S_y : green, yellow stems.

Table 5.1: Wheat: optical parameters used in Section 5.1.

wavelength band:	green		red		infrared	
	refl.	transm.	refl.	transm.	refl.	transm.
ears, green	0.15	0.00	0.06	0.00	0.48	0.00
ears, yellow	0.35	0.00	0.20	0.00	0.55	0.00
leaves, dark green	0.12	0.10	0.06	0.01	0.45	0.53
leaves bright green	0.15	0.15	0.06	0.02	0.48	0.50
leaves, yellow	0.35	0.15	0.30	0.10	0.50	0.48
stems, green	0.15	0.00	0.06	0.00	0.48	0.00
stems, yellow	0.35	0.00	0.20	0.00	0.55	0.00
soil, moist	0.08	-	0.11	-	0.14	-
soil, dry	0.18	-	0.23	-	0.30	-
soil, medium	0.13	-	0.17	-	0.21	-

also constructed and used in the calculations. All crops used in the models, including their 'construction' in crop layers and components are presented in Figure 5.3. Table 5.1 reviews the optical properties of all crop layers and crop components and Table 5.2 gives an equivalent review of the geometrical properties. The soil reflection depends strongly on the moisture content of the top layer; therefore, some calculations were done with three different values for the soil reflection coefficient. One of the conclusions of the previous chapter was that the distribution of the incoming radiation influences the reflection. Therefore, three different types of incoming radiation were compared: no direct radiation, sun's elevation = 30° (with 40% diffuse radiation) and sun's elevation = 60° (with 20% diffuse radiation). After the emergence of the ears (e.g. after June 15th), the influence of the wind is taken into account. To do so, the calculations were repeated with a different geometry for the ear layer. Without wind, ears are assumed to be vertical on July 1st and horizontal, but randomly oriented on July 15th. With the influence of wind, ears are assumed to be horizontal, with parallel central axes for the ears and stems in this layer. The leaves are assumed to keep their spherical distribution, because in a closed crop the wind only influences the top layer. Storms that also influence the leaf layers are rare during the summer period. If direct radiation is present, four different angles between the wind direction and the sun's azimuth are used (0°, 30°, 60°, 90°).

The aim of all calculations was to ascertain the possibility of estimating the LAI of a crop from the measured reflections, and also to ascertain how side-effects such as wind, soil moisture and sun's elevation influence these estimations.

The HARE model was used for all calculations. To carry out the calculations, the crop was divided into layers. Each layer is assumed to be a homogeneous mixture of different components. Each crop layer is again divided into identical model layers, each with an LAI value between 0.06 and 0.10. All model layers contain two or more crop components, and all components have their own optical and geometrical properties. For this purpose, an extension of the HARE model was developed. This extension allows an arbitrary number of sets of two matrices (one for the reflection and one for the transmission) to be combined to the two matrices that represent the combined model layer. This process goes as follows:

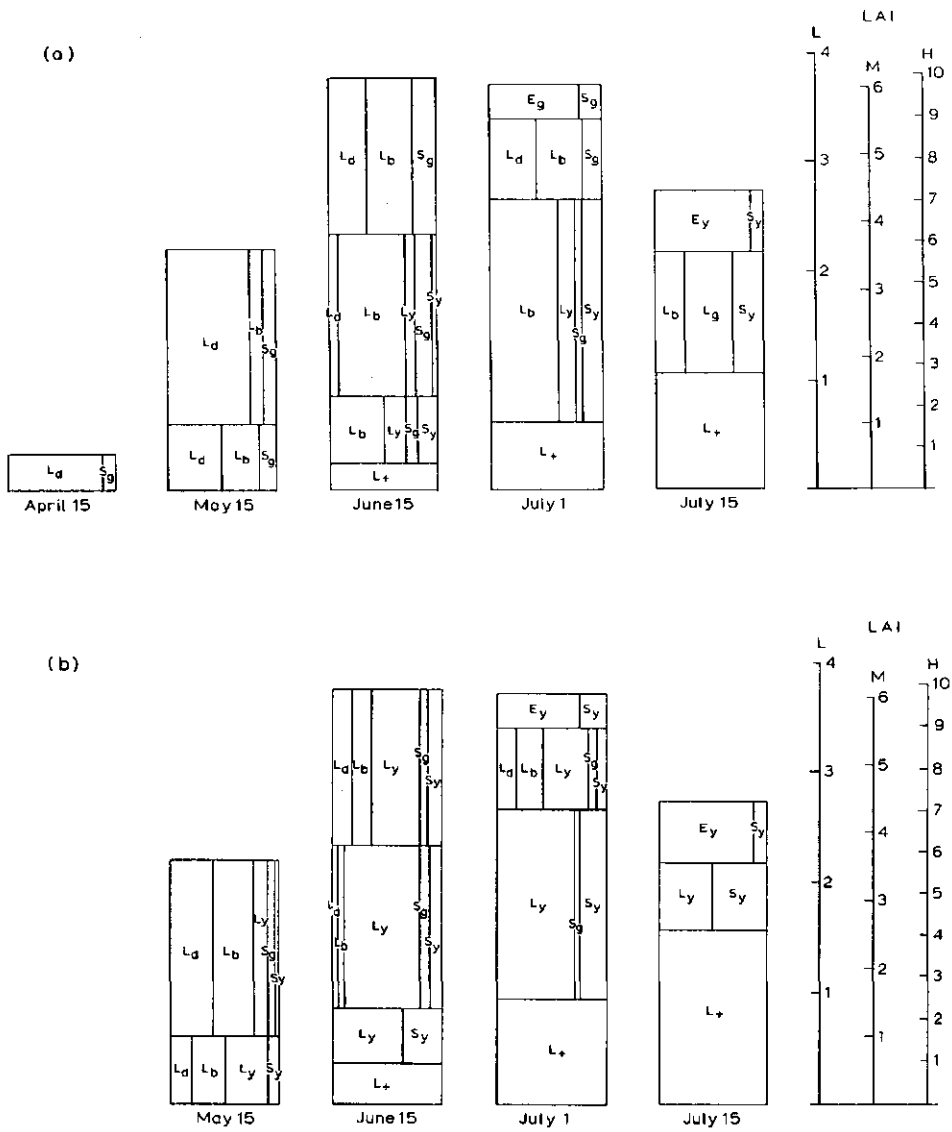


Figure 5.3: Detailed view of the model crops.

Symbols are similar to those used in Figure 5.2. Horizontal lines separate crop layers, vertical lines separate different organs that are mixed in one layer. Vertical axis: LAI units. Each of the three ordinates gives the units for one of the three LAI levels: high (H), medium (M) and low (L).

a): Green crop.

b): Yellow crop.

Table 5.2: Wheat, crop composition used in Section 5.1.

For each date, the layers are numbered downwards									
Figures in the table indicate LAI, capitals indicate leaf angle distribution:									
	S	:	spherical	U	:	cylindrical, without azimuthal preference			
	V	:	vertical	C	:	cylindrical, with azimuthal preference			
	H	:	horizontal	LAI is given for the crop with medium LAI					
green crop:									
date,	layer	green cars	yellow cars	d.green leaves	b.green leaves	yellow leaves	green stems	yellow stems	total LAI per layer
15/4-1		-	-	S 0.5	-	-	V 0.05	-	0.55
15/5-1		-	-	S 2.0	S 0.3	-	V 0.3	-	2.6
	-2	-	-	S 0.5	S 0.4	-	V 0.1	-	1.0
	Σ LAI	-	-	2.5	0.7	-	0.4	-	3.6
15/6-1		-	-	S 0.8	S 1.0	-	V 0.5	-	2.3
	-2	-	-	S 0.2	S 1.5	S 0.2	V 0.4	V 0.1	2.4
	-3	-	-	-	S 0.5	S 0.2	V 0.1	V 0.2	1.0
	-4	-	-	-	-	H 0.4	-	-	0.4
	Σ LAI	-	-	1.0	3.0	0.8	1.0	0.3	6.1
1/7-1a		V 0.4	-	-	-	-	V 0.1	-	0.5
	-1b	C 0.4	-	-	-	-	V 0.1	-	0.5
	-2	-	-	S 0.5	S 0.5	-	V 0.2	-	1.2
	-3	-	-	-	S 2.0	S 0.5	V 0.2	V 0.6	3.3
	-4	-	-	-	-	H 1.0	-	-	1.0
	Σ LAI	0.4	-	0.5	2.5	1.5	0.5	0.6	6.0
15/7-1a		-	U 0.8	-	-	-	-	U 0.1	0.9
	-1b	-	C 0.8	-	-	-	-	C 0.1	0.9
	-2	-	-	-	S 0.5	S 0.8	-	V 0.5	1.8
	-3	-	-	-	-	H 1.7	-	-	1.7
	Σ LAI	-	0.8	-	0.5	2.5	-	0.6	4.4
yellow crop:									
date,	layer	green cars	yellow cars	d.green leaves	b.green leaves	yellow leaves	green stems	yellow stems	total LAI per layer
15/5-1		-	-	S 1.0	S 1.0	S 0.3	V 0.2	V 0.1	2.6
	-2	-	-	S 0.2	S 0.3	S 0.4	-	V 0.1	1.0
	Σ LAI	-	-	1.2	1.3	0.7	0.2	0.2	3.6
15/6-1		-	-	S 0.4	S 0.4	S 1.0	V 0.2	V 0.3	2.3
	-2	-	-	S 0.1	S 0.1	S 1.7	V 0.2	V 0.3	2.4
	-3	-	-	-	-	S 0.5	-	V 0.3	0.8
	-4	-	-	-	-	H 0.6	-	-	0.6
	Σ LAI	-	-	0.5	0.5	3.8	0.4	0.9	6.1
1/7-1a		-	V 0.4	-	-	-	-	V 0.1	0.5
	-1b	-	C 0.4	-	-	-	-	V 0.1	0.5
	-2	-	-	S 0.2	S 0.3	S 0.5	V 0.1	V 0.1	1.2
	-3	-	-	-	-	S 2.0	V 0.1	V 0.7	2.8
	-4	-	-	-	-	H 1.5	-	-	1.5
	Σ LAI	-	0.4	0.2	0.3	4.0	0.2	0.9	6.0
15/7-1a		-	U 0.8	-	-	-	-	U 0.1	0.9
	-1b	-	C 0.8	-	-	-	-	C 0.1	0.9
	-2	-	-	-	-	S 0.5	-	V 0.5	1.0
	-3	-	-	-	-	H 2.5	-	-	2.5
	Σ LAI	-	0.8	-	-	3.0	-	0.6	4.4

N.B. Layers 1/7-1a and b resp. 15/7-1a and b describe the crop without (a) or with (b) wind influence.

Assume n components have to be combined in one layer. The sets of matrices $\{R_1, T_1\}$, $\{R_2, T_2\}$, ..., $\{R_n, T_n\}$ have already been computed. These matrices are the reflection and transmission matrices of components 1, 2, ..., n , all for a model layer with a LAI = 0.1. The result should be the set of the two matrices $\{R, T\}$ for a mixed layer with LAI = L , where L_1, L_2, \dots, L_n are the LAI values for the components in this layer ($L_1 + L_2 + \dots + L_n = L$).

For the reflection matrix it holds that components j ($1 \leq j \leq n$) must be taken into account with a coefficient $L_j/0.1$, so R can be computed as follows:

$$R = \sum_{j=1}^n \begin{pmatrix} L_j \\ 0.1 \end{pmatrix} \cdot R_j \quad (5.1)$$

A similar equation can be applied to the transmission matrices, with one difference in the calculation. The reason for this difference is that the transmission matrix is, in fact, the sum of three matrices:

- A matrix that denotes the transmission caused by the reflection and transmission of the crop components (with non-negative elements only).
- A diagonal matrix, representing the interception caused by all components (all diagonal elements of this matrix are negative or 0).
- A unitary matrix for the non-intercepted radiation.

If we change the components of a layer, then only the first two of these matrices must be changed. Therefore, we must apply an equivalent to Equation (5.1) not to the matrices T_1, T_2, \dots, T_n , but to T'_1, T'_2, \dots, T'_n , where $T'_j = T_j - E$. Finally, a unitary matrix must be added again, to obtain the complete transmission matrix T :

$$T = E + \sum_{j=1}^n \begin{pmatrix} L_j \\ 0.1 \end{pmatrix} \cdot (T_j - E) \quad (5.2)$$

If the LAI of the combined layer is equal to 0.1, it suffices to compute T by weighted addition of the T_j matrices, but Equation (5.2) allows also other values for the LAI of the combined layer. For reasons of uniformity, Equation (5.2) is applied in all calculations in this section.

5.1.1 Individual spectral bands

First, the zenith radiance in the individual spectral bands will be presented and discussed. Some results of the calculations are presented in Figure 5.4 (green), Figure 5.5 (red) and Figure 5.6 (infrared spectral band). The calculations ascertained the influence of some properties with minor agricultural relevance to the relation between the crop colour or the LAI and the zenith radiance. The conclusions based on these calculations are:

For calculated observations in the visible bands (green, Figure 5.4 and red, Figure 5.5):

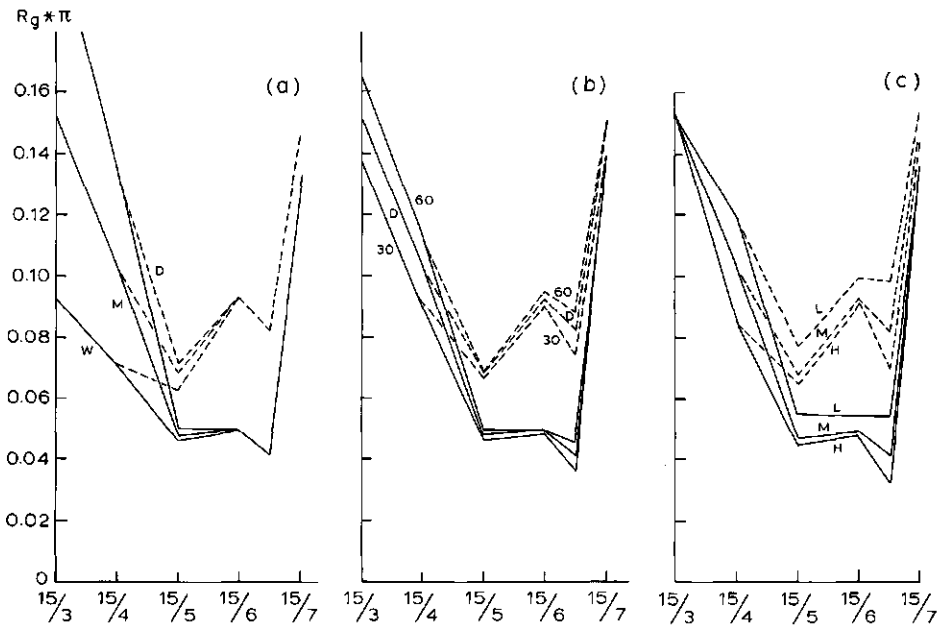


Figure 5.4: Influences of crop parameters on the zenith radiance of the crop for green radiation ($\lambda=550\text{nm}$).

a): Soil reflection coefficient. W: wet, low reflective soil; M: medium soil; D: dry, high reflective soil.

b): Incoming radiation. 30, 60: sun's inclination in degrees; D: only diffuse radiation.

c): LAI-level. L: low; M: medium; H: high.

Curves are presented for the green crop (solid lines) and for the yellow crop (broken lines).

Horizontal axis: time; vertical axis: zenith radiance, scaled with Equation (4.13).

- The influence of the soil reflection coefficient ω is large in the first phase of the growing season, but, because the crop closes after May 15th, the influence of ω disappears after this date.
- Throughout the entire growing season there is a large difference between a green crop and a yellow crop. The magnitude of this difference exceeds the differences caused by different LAI values. Only at the end of the growing season, when the ears dominate in the reflection process, these differences decrease, because the ears themselves grow yellow in this phase.
- The influence of the inclination of the sun is small during the complete growing season.
- An increasing LAI leads to a decreasing reflection for LAI values <6 . This means that the curves for the crop with the medium and the high LAI are very close to each other and that the curve for the crop with the lower LAI is somewhat above the others. This holds for the green crop and for the yellow crop in both the green band and the red band.

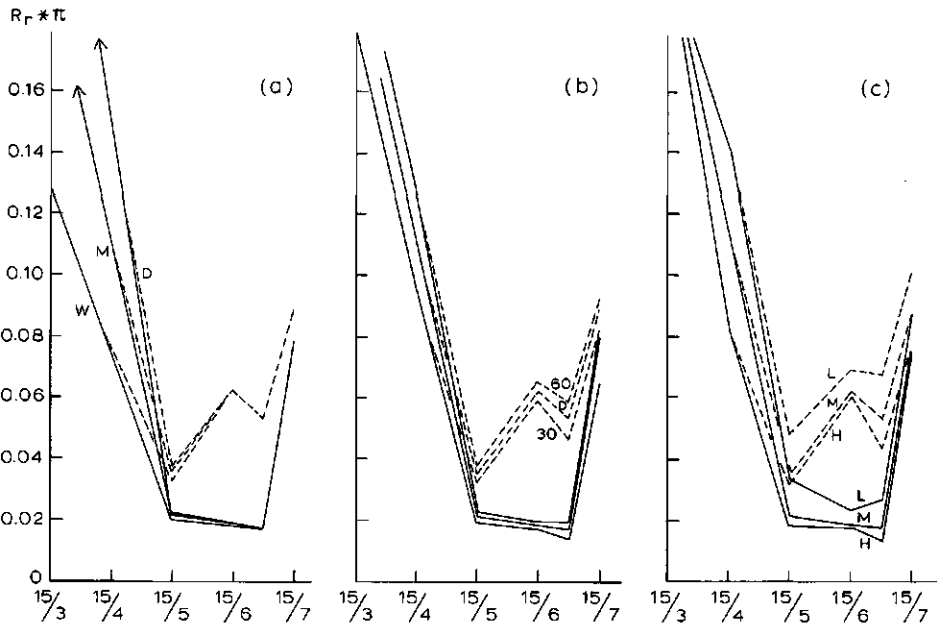


Figure 5.5: As figure 5.4 for red radiation ($\lambda = 670\text{nm}$).

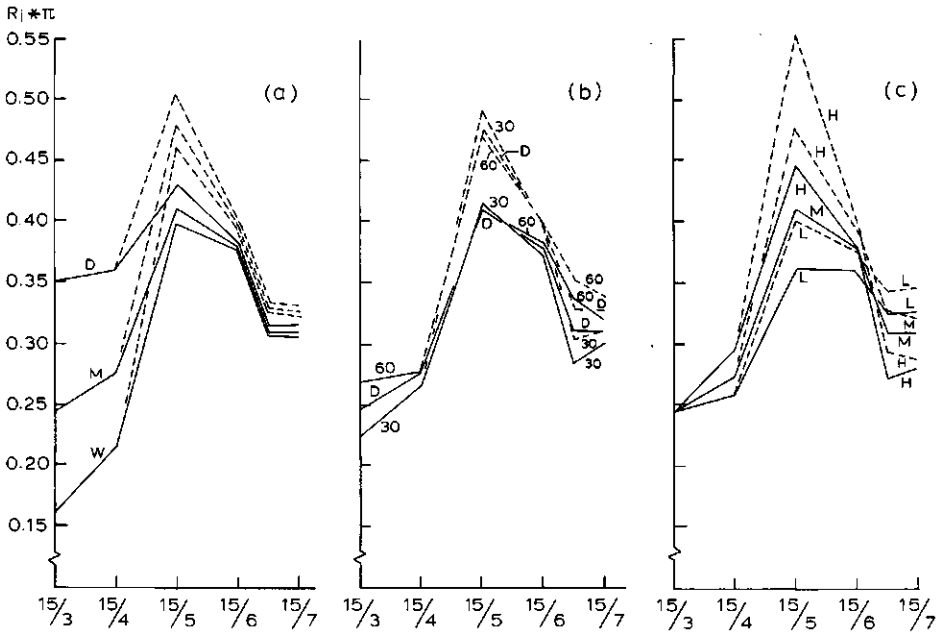


Figure 5.6: As figure 5.4 for infrared radiation ($\lambda = 870\text{nm}$).

- The vertical ears that are assumed to be present on July 1st, cause another decrease in the crop reflection which is superimposed on the course of the reflection level determined by the leaf area index. The total effect of the combination of these effects depends on the LAI: for low LAI values, the effects level each other out, for high LAI levels, the occurrence of vertical yellow ears causes the total reflection of the crop to decrease.
- As soon as the stems bend by the weight of the ears (as is assumed for July 15th) the crop reflection increases rapidly.

In the infrared band (Figure 5.6):

- The influence of the soil reflection coefficient is large at the beginning of the growing season, but, in contrast to the visible bands, this influence remains present throughout the growing season, although it decreases to only 1% after June 15th. Somewhat surprisingly, there is a major difference between a green and a yellow crop, because both green and yellow leaves show an absorption coefficient of 0.02. This difference is probably caused by the horizontal dead leaves that are assumed to be present in the yellow crop, and which cause a higher layer reflection than a layer with a spherical leaf angle distribution. The ratio of leaf reflection to leaf transmission also contributes to this effect (compare Figure 3.11).
- Because the effect of multiple scattering is more important in the infrared band than in the visible bands, the angular distribution of the incoming radiation is less important. As can be seen in Figure 5.6b, during the growing phases in which leaves are the major reflecting organs, differences between the three distributions of the incoming radiation distinguished give very similar reflection curves. Only at the beginning of the season, when the direct soil reflection is of importance, and near the end when ears are present, some differences are found. It must be noted that in these cases an increasing inclination of the sun is accompanied by an increasing crop reflection, whereas in the middle of the growing season, the opposite effect occurs.
- The influence of the differences in LAI is much more pronounced than in the visible bands, and overlaps the differences caused by the two crop types (green and yellow).
- As soon as ears occur, the relation between LAI level and reflection level is reversed: the crop with the highest LAI causes the lowest reflection and vice versa.

5.1.2 Combinations of two bands

The interpretation of the observation of the reflected radiation in the individual wavelength bands is difficult: in Subsection 5.1.1 it was shown that several phenomena cause differences in the crop reflection, at least when only one single band is observed. Therefore, it may be useful to combine the measured reflection in the individual bands to try to eliminate or reduce the inaccuracies in the interpretation of the observations. Based on the calculations in Chapter 4, the vegetation index was chosen as one of these

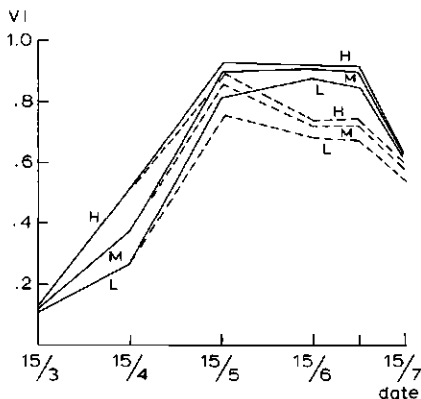


Figure 5.7: Vegetation index VI versus time for three LAI levels (L: low; M: medium; H: high) of the green crop (solid lines) and the yellow crop (broken lines).

possible combinations. Another combination was found in the ratio red reflection/green reflection.

Considering the vegetation index, the following conclusions can be drawn (see Figures 5.7 and 5.8):

From Figure 5.7 (vegetation index VI , versus time) it can be seen that:

- The vegetation index increases from 0.15 to 0.8–0.9 on May 15th, with only small differences between the crop types. The VI varies with the total LAI, and the differences between the green and the yellow crop are small until this date.
- Between May 15th and July 1st, the VI of the yellow crop decreases to 0.7–0.75, depending on the LAI, for the green crop the VI remains fairly constant.
- After July 1st, VI decreases to 0.6–0.65 for all crops, with only small differences between the green and the yellow crop.

Figure 5.8 shows the relation between total reflective LAI and VI .

- For the green crop, there is a fairly unambiguous relation between the total LAI and VI . This relation is not influenced by the growth rate. This relation increases from 0.13 (for LAI=0.0) to 0.9 (for LAI >3.5). This means that as long as no ears or only vertical ears are present, VI can be a good indicator of the LAI values <3.5. LAI values higher than 3.5 cannot be distinguished by examination of the value of VI . As soon as horizontal yellow ears occur, the value of VI decreases to 0.55 for all crops, regardless of the LAI.
- The curves for the yellow crop in Figure 5.8 resemble those for the green crop until May 15th, but because these curves decrease as soon as a substantial amount of yellow leaves is present in the top layer, a decrease in the value of VI is observed. This means that for a yellow crop, the determination of the LAI from VI is very difficult, even for low values of the LAI.

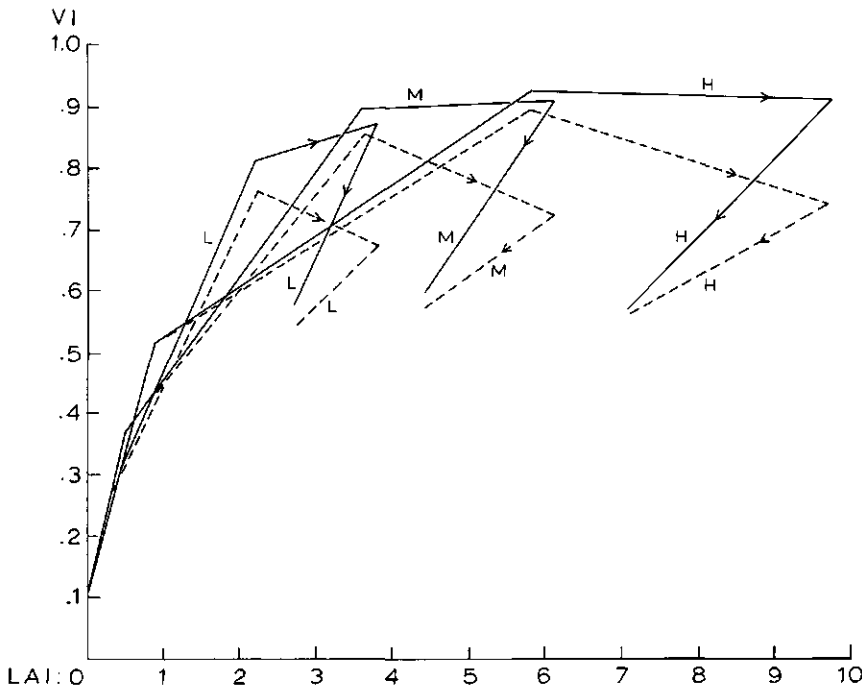


Figure 5.8: Vegetation index VI versus total interceptive LAI for three LAI levels of the green and the yellow crops. See Figure 5.7 for meaning of symbols.

The general conclusion is that as long as it may be expected that a crop has green leaves only and an LAI < 3.5 , VI can be used very well to determinate this LAI. But for high values of the LAI, or if the crop is yellowing, there is a serious risk of misinterpretation.

A second ratio that could be used in combination with VI is the ratio of red reflection to green reflection or R_r/R_g . Because (Table 5.1) the reflection coefficients in these bands are much lower than in the infrared band, more information about the top layer of the crop may be expected. Figures similar to Figures 5.7 and 5.8 are presented for the ratio R_r/R_g (Figures 5.9 and 5.10). These figures appear to give little extra information than Figures 5.7 and 5.8, with only a few exceptions. These exceptions are:

- R_r/R_g decreases from 1.3 to 0.4 if LAI increases from 0 to 6. This means that the range in which the ratio varies with LAI is extended from $[0 \dots 3.5]$ to $[0 \dots 6]$ if R_r/R_g is used instead of VI . The discrimination between the green and the yellow crop is hardly better than when VI is used.
- A second difference with the VI curves is that for the yellow crop after June 15th, the slope of the R_r/R_g curves is opposite to the slope before the period May 15th to June 15th. This leads to the conclusion that only repeated observations will give enough information to enable the status of the crop to be determined by interpreting R_r/R_g .

Combination of these facts leads to the following final conclusions.

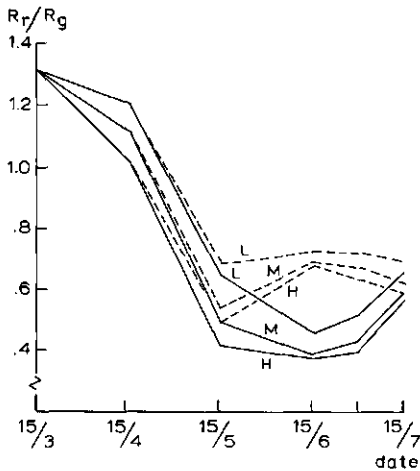


Figure 5.9: Red/Green ratio R_r/R_g versus time for three LAI levels of the green and the yellow crops. See Figure 5.7 for for meaning of symbols.

- For a green crop, LAI can be determined best by VI calculations until $LAI=3.5$. Between $LAI=3.5$ and $LAI=6$, R_r/R_g gives some additional information, but for a green crop with LAI values over 6 no further differentiation can be made.
- After the emergence of the ears, the VI value decreases after a period of fairly

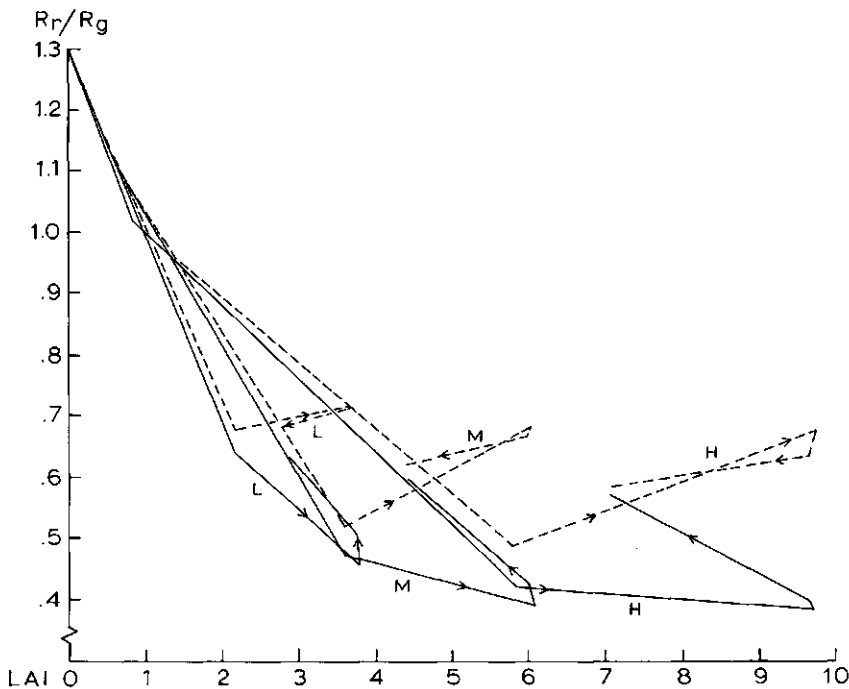


Figure 5.10: Red/Green ratio R_r/R_g versus total interceptive LAI for three LAI levels of the green and the yellow crops. See Figure 5.7 for for meaning of symbols.

constant VI (for the green crop) or decreasing VI (for the yellow crop). If the value of R_r/R_g in the same period increases, the crop is green, but if this value decreases after an increase in the same period that VI decreased, the crop became yellow in an early stage of the growing season.

- Near the end of the growing season the only differences that can be seen are a weak relation between the total LAI and R_r/R_g in that sense that a higher value for R_r/R_g coincides with a higher value for the LAI.

An examination of the results of the calculations revealed that the use of VI or R_r/R_g deleted or reduced most deviations caused by soil colour and sun's direction. Also, differences caused by wind (the ears pointing in one horizontal direction) were almost completely neglectable, where they could be found very clearly in the individual spectral bands.

5.2 Drooping of leaves by sugarbeet

The leaf angle distribution of a healthy sugarbeet crop is close to spherical, with some tendency to a more planophile distribution in the lower layers and a more erectophile distribution in the top layers (Hodáňová, 1972). In the calculations in this section the leaf angle distribution of a healthy crop is assumed to be spherical. During the growth of a sugarbeet crop the phenomenon of leaf drooping frequently occurs. The leaves become flaccid because of a shortage in water supply, and their erect orientation turns to a more horizontal one. This leaf drooping causes a serious decrease in the growth rate of the shoot, and therefore also in the growth of the root system, including the beets themselves. It is extremely useful to be able to detect when drooping of leaves occurs, especially in experimental fields. The HARE model was used to ascertain the optimal conditions for detecting the areas in a beet crop where the plants droop their leaves. Drooped leaves differ from normal leaves in two aspects. Both their leaf angle distribution and, in a later phase, their colour, differ from normal leaves. Leaves of plants that are dehydrating, will turn yellow faster than leaves on healthy plants, resulting in an increase of the reflection in the visible bands. In this section only geometrical changes are taken into account, because the geometrical changes precede the optical changes. Of course, to prevent changes in the optical properties from obscuring the effect of leaf drooping, the measuring conditions must be limited to those in which the expected optical difference causes a change in the reflection similar to that caused by the geometrical differences. Therefore we must use measuring conditions in which the reflection in the visible bands of the crop that droops its leaves is higher than the reflection of the healthy crop. Table 5.3 gives a review of the optical and geometrical data used.

The calculations are based on the principle that only the comparison of ratios makes sense. Absolute reflection values are strongly influenced by small differences in reflection and transmission coefficients of crop and soil. The calculations are based on two bands: red and infrared. For both crop types (dehydrating (D) and normal (N)) the same optical properties of the leaves are assumed. Therefore it may be expected that the ratio $\{(R_i/R_r)_D / (R_i/R_r)_N\}$ can be a good discriminator for patches where the leaves are

Table 5.3: Optical and geometrical parameters of a sugarbeet crop and definitions of incoming radiation used in the calculations in Section 5.2.

Crop: Sugarbeet

Optical properties of leaves and soil:			
optical band	leaf reflection	leaf transmission	soil reflection
red	0.09	0.045	0.15
infrared	0.50	0.40	0.20
type:	Lambertian	Lambertian	rough

Leaf angle distributions and LAI:		
leaf-inclination (0°: horiz.)	healthy crop (=spherical)	dehydrated crop
0°-12°	2%	30%
12°-30°	11%	70%
30°-45°	16%	-
45°-60°	21%	-
60°-75°	24%	-
75°-90°	26%	-
LAI	5	5

Incoming radiation		
type	sun's inclination	diffuse radiation
1	60°	20% (SOC)
2	30°	40% (SOC)
3	-	100% (SOC)

drooped. In practice, the crop that droops its leaves may show an increased yellowing, resulting in a higher reflection in the visible bands, and in a lower value for these ratios. To prevent the effect of leaf drooping being compensated for yellowing, only those conditions in which these ratios are less than one can be used to identify areas where the crop droops its leaves.

Figure 5.11 shows the directional radiance for a sun's inclination of 60° for both a dehydrated crop and a normal crop in the infrared and the red spectral bands. This figure was the basis for Figure 5.12, in which the ratio R_i/R_r is given for both crop types. The differences between the two crop types are large: a dehydrated crop gives hardly any directional effect to the ratio R_i/R_r , whereas the normal crop shows directional differences up to a factor of 1.5. It may thus be concluded that the final ratio to be calculated will depend on the direction of the observation. In Figure 5.11 it can be seen that the directional differences between a dehydrated and a normal crop are primarily caused by the directional differences in the reflection in the red band for the normal crop (Figure 5.11b). Finally, the ratio $\{(R_i/R_r)_D / (R_i/R_r)_N\}$ is given as a function of the observation direction in Figure 5.13. This figure shows that the best discrimination is based on observations inclined at about 50° and facing the sun. The azimuthal difference between the sun's azimuth and the azimuth of the observation direction must be in the range of $180 \pm 60^\circ$. To investigate the importance of the inclination of the sun, a similar figure is presented for a sun's inclination of 30° (Figure 5.14). The conclusion based on this figure is that with a lower sun the same discrimination can also be made, but it is best for the observer to be approximately 65°. For these directions,

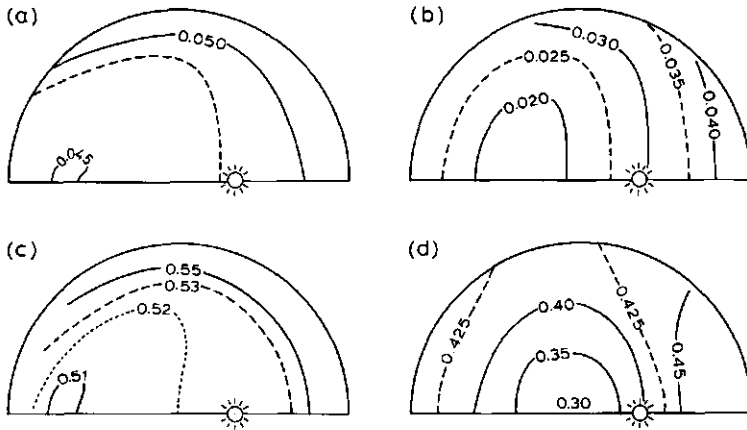


Figure 5.11: Reflection of a sugarbeet crop as a function of the observation direction.

a): Dehydrated crop, red radiation: $(R_r)_D$

b): Normal crop, red radiation: $(R_r)_N$

c): Dehydrated crop, infrared radiation: $(R_i)_D$

d): Normal crop, infrared radiation: $(R_i)_N$

Sun's inclination is 60° , diagrams show isoreflexion lines for $R \cdot \pi$ over a half hemisphere. For more explanation see text of Subsection 5.2.

$\{(R_i/R_r)_D / (R_i/R_r)_N\}$ ratios of 0.6 were calculated. The difference between this value and 1 is large enough to be detected. Even if the pixel size exceeds the size of these areas, then for mixed pixels with 50% leaf drooping plants and 50% normal plants, the ratio (R_i/R_r) is 20% below the value for the surrounding pixels. The influence of the diffuse fraction of the incoming radiation can be derived from Figure 5.15, where the ratio $\{(R_i/R_r)_D / (R_i/R_r)_N\}$ is given for three types of incoming radiation. Because the detection of areas of leaf drooping must be done sometimes on a relatively small-scale basis, the use of microlight airplanes can be preferable. This type of plane has a flight altitude between 50 and 150 metres, and therefore it can be used successfully in cloudy conditions. For this reason, Figure 5.15 also includes a sky irradiance of

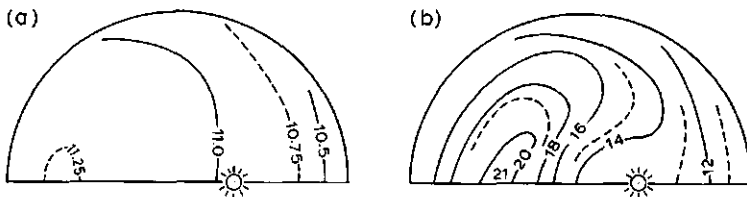


Figure 5.12: Ratio infrared reflection/red reflection as a function of the observation direction for two types of leaf angle distribution as used in Subsection 5.2. Sun's inclination is 60° .

a): Dehydrated crop $(R_i/R_r)_D$.

b): Normal crop $(R_i/R_r)_N$.

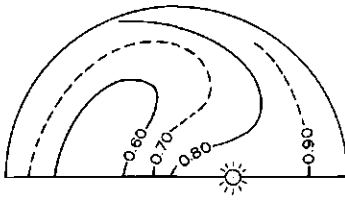


Figure 5.13: $\{(R_i/R_r)_D / (R_i/R_r)_N\}$ as a function of the observation direction. Sun's inclination is 60° . See text of Subsection 5.2 for further explanation.

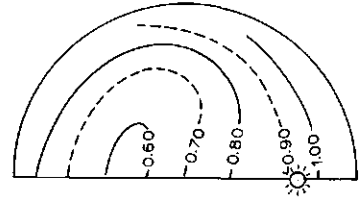


Figure 5.14: As Figure 5.13, sun's inclination is 30° .

SOC type without any direct influence of the sun. This figure shows that even under complete cloud cover, these observations are still possible, though with a less pronounced difference between a dehydrated and a normal crop. The calculations were repeated with an estimation of the visible band instead of the red band. The advantage of using the total visible band is that because of the relatively lower reflection coefficients in the visible bands and especially in the red band, the increase in the total amount of radiation measured may enhance the accuracy of the estimation of R_{vis} compared with R_r . Because the results based on R_i/R_{vis} ratios were very similar to the results based on R_i/R_r ratios, only Figure 5.16 is presented. As can be seen, it corresponds very well with Figure 5.15. Therefore, the intermediate results of the calculations have been not presented in graphical or tabular form.

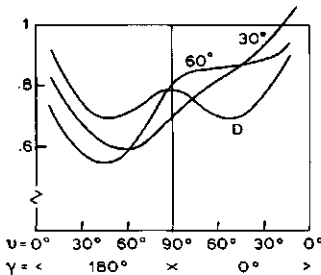


Figure 5.15: Comparison of $\{(R_i/R_r)_D / (R_i/R_r)_N\}$ for three types of incoming radiation: sun's inclination 60° , sun's inclination 30° and only diffuse incoming radiation (D).

Horizontal axis gives the observation direction. v : inclination; γ : azimuthal difference between observation and sun (for diffuse radiation the figure is cyclo-symmetric).

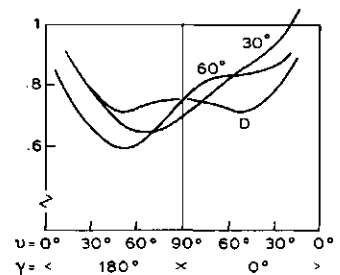


Figure 5.16: As Figure 5.15 for the ratio $\{(R_i/R_{vis})_D / (R_i/R_{vis})_N\}$.

Appendix A

Kubelka-Munk equations

Kubelka-Munk equations, applied to crop reflection.

In 1931, Kubelka & Munk published the solution of a set of two differential equations that describe the reflective behaviour of a layer of paint. These so-called KM-equations give the relation between the depth in a semi-transparent medium and the flux in two directions: one inwards the medium and one in the opposite direction. The equations are based on the following principles:

- In a layer with thickness dd at depth d (d is measured starting at the outside of the layer) a certain fraction of the incident flux is intercepted by the medium. The intercepted part of the flux is linearly proportional to the total flux in that direction at depth d and with the thickness dd of the layer.
- Of all intercepted flux, a fixed fraction τ is scattered in forward direction and a fixed fraction ρ is scattered backward.

For a crop with horizontal leaves, this set of equations can be applied as follows:

$$\begin{pmatrix} dD/dd \\ dU/dd \end{pmatrix} = \begin{pmatrix} \tau - 1 & \rho \\ -\rho & -(\tau - 1) \end{pmatrix} \begin{pmatrix} D \\ U \end{pmatrix} \quad (\text{A.1})$$

In these equations, D depicts the downward flux, U the upward flux, d is the depth, measured from above and expressed in LAI units. ρ and τ are the reflection- and transmission coefficient of the leaves, respectively. The minus-signs in the second equation express the opposite direction of the upward flux.

Assume that the set in Equation (A.1) has the following solution:

$$\begin{pmatrix} D \\ U \end{pmatrix} = \begin{pmatrix} e^{s \cdot d} \\ a \cdot e^{s \cdot d} \end{pmatrix} \quad (\text{A.2})$$

then (expand and divide by $e^{s \cdot d}$):

$$\begin{pmatrix} s \\ a \cdot s \end{pmatrix} = \begin{pmatrix} \tau - 1 & \rho \\ -\rho & -(\tau - 1) \end{pmatrix} \begin{pmatrix} 1 \\ a \end{pmatrix} \quad (\text{A.3})$$

This is solved if following equality holds:

$$\begin{vmatrix} \tau - 1 - s & \rho \cdot a \\ -\rho & (1 - \tau - s) \cdot a \end{vmatrix} = 0 \quad (\text{A.4})$$

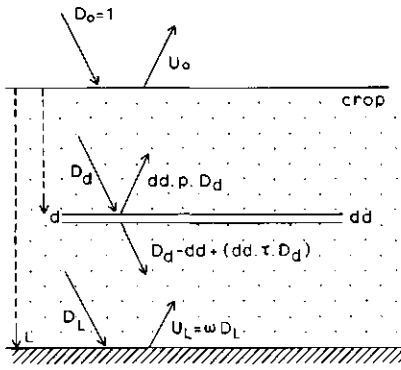


Figure A.1: Schematic view of some quantities involved in the KM-equations. The situation at the top of the crop (D_0 and U_0) and at the soil (D_L and U_L) are drawn. In the middle of the figure the scattering process on the downward flux at depth d is also shown.

Solving yields:

$$s = \pm \sqrt{(1 - \tau)^2 - \rho^2} = \pm W \quad (\text{A.5})$$

Substitution of Equation (A.5) in (A.4) gives:

$$s = W \quad a = (W - (\tau - 1)) / \rho \quad (\text{A.6})$$

$$s = -W \quad a = (-W - (\tau - 1)) / \rho \quad (\text{A.7})$$

Substitution of two independent solutions in Equation (A.2) yields:

$$\begin{pmatrix} D \\ U \end{pmatrix} = \lambda \cdot \begin{pmatrix} 1 \\ (W - (\tau - 1)) / \rho \end{pmatrix} \cdot e^{W \cdot d} + \mu \cdot \begin{pmatrix} 1 \\ (-W - (\tau - 1)) / \rho \end{pmatrix} \cdot e^{-W \cdot d} \quad (\text{A.8})$$

Assume the downward flux at the surface D is equal to 1, the total crop depth is L and the soil reflection coefficient is ω , then the boundary conditions are:

$$\text{I} : D_0 = 1 \quad (\text{A.9})$$

$$\text{II} : U_L = \omega \cdot D_L \quad (\text{A.10})$$

For a crop of infinite depth the second boundary condition must be replaced by:

$$\text{III} : U_d / D_d \text{ is constant} \\ \text{and independent of } d \quad (\text{A.11})$$

$$\text{IV} : U_\infty \rightarrow 0 \text{ and } D_\infty \rightarrow 0 \quad (\text{A.12})$$

Substitution of boundary condition I in Equation (A.8) gives:

$$D_0 = 1 = \lambda \cdot e^{W \cdot 0} + \mu \cdot e^{-W \cdot 0} = \lambda + \mu \quad (\text{A.13})$$

This results in:

$$\mu = 1 - \lambda \quad (\text{A.14})$$

From II follows:

$$\lambda \cdot (1 - \tau + W) / \rho \cdot e^{W \cdot L} + (1 - \lambda) \cdot (1 - \tau - W) / \rho \cdot e^{-W \cdot L} = \dots \\ \dots \omega \cdot (\lambda \cdot e^{W \cdot L} + (1 - \lambda) \cdot e^{-W \cdot L}) \quad (\text{A.15})$$

Expansion of Equation (A.15) gives:

$$\lambda = \frac{(\rho\omega - 1 + \tau + W) \cdot e^{-W.L}}{(1 - \tau + W - \rho\omega) \cdot e^{W.L} - (1 - \tau - W - \rho\omega) \cdot e^{-W.L}} \quad (\text{A.16})$$

and

$$\mu = \frac{(1 - \tau - \rho\omega + W) \cdot e^{W.L}}{(1 - \tau + W - \rho\omega) \cdot e^{W.L} - (1 - \tau - W - \rho\omega) \cdot e^{-W.L}} \quad (\text{A.17})$$

Assume

$$V = 1 - \tau - \rho\omega \quad (\text{A.18})$$

and substitute Equation (A.18) in (A.16) and (A.17):

$$\lambda = \frac{(W - V) \cdot e^{-W.L}}{(W + V) \cdot e^{W.L} + (W - V) \cdot e^{-W.L}} \quad (\text{A.19})$$

and

$$\mu = \frac{(W + V) \cdot e^{W.L}}{(W + V) \cdot e^{W.L} + (W - V) \cdot e^{-W.L}} \quad (\text{A.20})$$

At last, substitution of Equations (A.19) and (A.20) in (A.8) gives for D_d :

$$D_d = \frac{(W + V) \cdot e^{W(L-1)} + (W - V) \cdot e^{-W(L-1)}}{(W + V) \cdot e^{W.L} + (W - V) \cdot e^{-W.L}} \quad (\text{A.21})$$

Assume:

$$X = \omega - \tau\omega - \rho \quad (\text{A.22})$$

Now U_d may be written as:

$$U_d = \frac{(W\omega - X) \cdot e^{W(L-d)} + (W\omega + X) \cdot e^{-W(L-d)}}{(W + V) \cdot e^{W.L} + (W - V) \cdot e^{-W.L}} \quad (\text{A.23})$$

For the upward flux at the top of the crop U_0 holds:

$$U_0 = \frac{(W\omega - X) \cdot e^{W.L} + (W\omega + X) \cdot e^{-W.L}}{(W + V) \cdot e^{W.L} + (W - V) \cdot e^{-W.L}} \quad (\text{A.24})$$

To define a crop with infinite depth, boundary conditions I, III and IV must be applied:

From I follows (Equation (A.14)) $\mu = 1 - \lambda$; substitution of III yields:

(define $p = (1 - \tau + W) / \rho$ and $q = (1 - \tau - W) / \rho$):

$$\frac{U_d}{D_d} = \frac{\lambda \cdot p \cdot e^{W.L} + (1 - \lambda) \cdot q \cdot e^{-W.L}}{\lambda \cdot e^{W.L} + (1 - \lambda) \cdot e^{-W.L}} \quad (\text{A.25})$$

This fraction is independent of d if and only if the first or the second term can be deleted from numerator and denominator, so if $\lambda = 0$ or $\lambda = 1$.

For $\lambda = 0$:

$$\left(\frac{D}{U} \right) = \left(\frac{1}{(1 - \tau - W) / \rho} \right) \cdot e^{-W.d} \quad (\text{A.26})$$

For $\lambda = 1$:

$$\left(\frac{D}{U} \right) = \left(\frac{1}{(1 - \tau + W) / \rho} \right) \cdot e^{W.d} \quad (\text{A.27})$$

Equation (A.26) violates boundary condition IV, whereas Equation (A.27) does not. For a crop of infinite depth it holds therefore:

$$D_d = e^{-W.d} \quad (\text{A.28})$$

$$U_d = (1 - \tau - W) / \rho . e^{-W.d} \quad (\text{A.29})$$

$$U_0 = (1 - \tau - W) / \rho \quad (\text{A.30})$$

The set of differential equations from Equation (A.1) may degenerate in two ways:

1. If $\rho = 0$ then D and U are only coupled by means of the soil reflection.
2. If $\rho \neq 0$ and $\rho + \tau = 1$ (so if absorption is 0), then $dD/dd = dU/dd$.

In these cases the solution cannot be found by means of Equations (A.2) to (A.8), because the solution of the problem with boundary conditions does not fit to Equations (A.21) to (A.24) or (A.28) to (A.30).

For these two special cases the solution is calculated separately.

First case ($\rho = 0$)

$$dD/dd = (\tau - 1) . D \quad (\text{A.31})$$

$$dU/dd = -(\tau - 1) . U \quad (\text{A.32})$$

Separation of variables, integration and exponentiation gives:

$$D_d = \lambda . e^{(\tau-1).d} \quad (\text{A.33})$$

$$U_d = \mu . e^{-(\tau-1).d} \quad (\text{A.34})$$

Boundary condition I ($D_0 = 1$) gives:

$$\lambda = 1 \quad (\text{A.35})$$

Which yields for D_d :

$$D_d = e^{(\tau-1).d} \quad (\text{A.36})$$

Boundary condition II ($U_L = \omega . D_L$) gives:

$$\mu . e^{-(\tau-1).L} = \omega . e^{(\tau-1).L} \quad (\text{A.37})$$

$$\mu = \omega . e^{2(\tau-1).L} \quad (\text{A.38})$$

Which yields for U_d and U_0 :

$$U_d = \omega . e^{(\tau-1).(2L-d)} \quad (\text{A.39})$$

$$U_0 = \omega . e^{2(\tau-1).L} \quad (\text{A.40})$$

For a crop of infinite depth no reflection occurs anywhere. So without further calculations it may be concluded that:

$$U_d = 0 \quad \text{for each crop depth } d \quad (\text{A.41})$$

(The same result can also be obtained by application of Equations (A.33), (A.34) and (A.11).)

So there is no upward flux, neither in the crop, nor above it.

Second case (no absorption, $\rho + \tau = 1$).

Although this is a very rare situation in real world situations, it is given here for reasons of completeness and because the TURTLE model is tested with this rather pathological situation.

If $\rho + \tau = 1$, the two differential equations of Equation (A.1) transforms to:

$$\begin{pmatrix} dD/dd \\ dU/dd \end{pmatrix} = \begin{pmatrix} -\rho & \rho \\ -\rho & \rho \end{pmatrix} \begin{pmatrix} D \\ U \end{pmatrix} \quad (\text{A.42})$$

Which yields:

$$dD/dd = -\rho.(D - U) \quad (\text{A.43})$$

$$dU/dd = -\rho.(D - U) \quad (\text{A.44})$$

Assume $\delta = D - U$. Now from Equations (A.43) and (A.44) we may conclude:

$$dD/dd = -\rho.\delta \quad (\text{A.45})$$

$$dU/dd = -\rho.\delta \quad (\text{A.46})$$

Integration yields:

$$D_d = -\rho.\delta.d + \lambda \quad (\text{A.47})$$

$$U_d = -\rho.\delta.d + \mu \quad (\text{A.48})$$

so:

$$\delta = \lambda - \mu \quad (\text{A.49})$$

boundary condition I ($D_0 = 1$) gives:

$$\lambda = 1 \quad (\text{A.50})$$

$$U_0 = 1 - \delta \quad (\text{A.51})$$

$$U_d = 1 - \delta - \rho.\delta.d \quad (\text{A.52})$$

$$D_d = 1 - \rho.\delta.d \quad (\text{A.53})$$

From boundary condition II ($U_d = \omega.D_L$) it may be concluded that:

$$1 - \delta - \rho.\delta.L = \omega.(1 - \rho.\delta.L) \quad (\text{A.54})$$

Transformation yields:

$$\delta = \frac{1 - \omega}{1 + \rho.(1 - \omega).L} \quad (\text{A.55})$$

This gives for D_d , U_0 and U_d :

$$D_d = \frac{1 + \rho.(1 - \omega).(L - 1)}{1 + \rho.(1 - \omega).L} \quad (\text{A.56})$$

$$U_0 = \frac{\omega + \rho.(1 - \omega).L}{1 + \rho.(1 - \omega).L} \quad (\text{A.57})$$

$$U_d = \frac{\omega + \rho.(1 - \omega).(L - 1)}{1 + \rho.(1 - \omega).L} \quad (\text{A.58})$$

We can see that in this situation both $D - U$ and dD/dd do not depend on d .
Boundary condition III yields (quotient of Equations (A.52) and (A.53)):

$$\frac{U_d}{D_d} = \frac{1 - \delta - \rho \cdot \delta \cdot d}{1 - \rho \cdot \delta \cdot d} \quad (\text{A.59})$$

This quotient is only independent of d if $\delta = 0$. In that case holds:

$$D_d = 1 \quad (\text{A.60})$$

$$U_d = 1 \quad (\text{A.61})$$

$$U_0 = 1 \quad (\text{A.62})$$

Appendix B

Orientations of Model Directions

Model directions as used in the TURTLE and HARE model. The table gives for the 46 directions the azimuth (ϕ) and the inclination (θ), both in radians and degrees.

NR	ϕ (in radians)	θ	ϕ (in degrees)	θ
1	$(\pi/2)$	$\pi/2$	(90.)	90.
2	-1.885	1.207	-108.	69.16
3	-0.628	„	-36.	„
4	0.628	„	36.	„
5	1.885	„	108.	„
6	π	„	180.	„
7	-2.513	0.918	-144.	52.62
8	-1.257	„	-72.	„
9	0.	„	0.	„
10	1.257	„	72.	„
11	2.513	„	144.	„
12	-1.885	0.827	-108.	47.41
13	-0.628	„	-36.	„
14	0.628	„	36.	„
15	1.885	„	108.	„
16	π	„	180.	„
17	-2.735	0.543	-156.73	31.08
18	-2.291	„	-131.27	„
19	-1.479	„	-84.73	„
20	-1.035	„	-59.27	„
21	-0.222	„	-12.73	„
22	0.222	„	12.73	„
23	1.035	„	59.27	„
24	1.479	0.543	84.73	31.08
25	2.291	„	131.27	„
26	2.735	„	156.73	„
27	-1.885	0.464	-108.	26.57
28	-0.628	„	-36.	„
29	0.628	„	36.	„
30	1.885	„	108.	„
31	π	„	180.	„
32	-2.513	0.189	-144.	10.81
33	-1.257	„	-72.	„
34	0.	„	0.	„
35	1.257	„	72.	„
36	2.513	„	144.	„
37	-2.928	0.161	-167.77	9.23
38	-2.098	„	-120.23	„
39	-1.672	„	-95.77	„
40	-0.842	„	-48.23	„
41	-0.415	„	-23.77	„
42	0.415	„	23.77	„
43	0.842	„	48.23	„
44	1.672	„	95.77	„
45	2.098	„	120.23	„
46	2.928	„	167.77	„

Appendix C

Arbitrary directions

In two cases there is a need in the TURTLE and the HARE model to define an arbitrary direction in terms of the 46 predefined reference directions. This happens:

- When a leaf density in an arbitrary direction must be estimated to calculate the specular reflection; and
- When an arbitrary sun's or observation direction must be defined.

For these situations an algorithm is developed with which it is possible to define any direction d as the weighted mean of three surrounding reference directions j_1 , j_2 and j_3 . This algorithm is described in this appendix in four succeeding steps. All calculations are described with respect to a sphere. D , J_1 , J_2 and J_3 are the intersections of this sphere with vectors d , j_1 , j_2 and j_3 , respectively.

1. Define the tangent plane to the sphere in D .
2. Determine in which spherical triangle the point D is positioned. The vertices of this triangle are J_1 , J_2 and J_3 .
3. Use the point D' on the sphere opposite to D as the projection centre to construct the central projection of the points J_1 , J_2 and J_3 on the plane. Call the respective projections J'_1 , J'_2 and J'_3 (see Figure C.1). The choice of D' as the projection centre is a compromise between the centre of the sphere and a point at distance twice the radius of the sphere in the same direction as D . The centre of the sphere should project spherical triangles to flat triangles, but with possibly fairly large differences between the spherical distances $D : J_i$ and their respective projections $d : J'_i$.

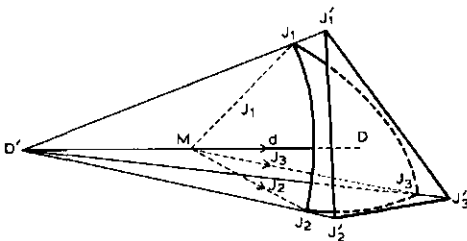


Figure C.1: Nomenclature as used in Appendix C. The spheric triangle (J_1 , J_2 , J_3) is replaced by its projection (J'_1 , J'_2 , J'_3). M is the centre of the sphere, D' is the projection centre opposite to D , which is the tangent point of the plane and the sphere.

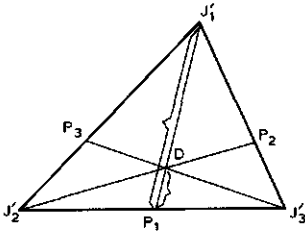


Figure C.2: Relative ratios in the distribution of a quantity in D over the fractions f_1 , f_2 and f_3 related to vectors j_1 , j_2 and j_3 , respectively.

The other mentioned alternative should give a good correspondence between the spherical distances and their projections, but should influence the shape of the projected triangle $D : J'_1, D : J'_2, D : J'_3$ too much.

4. Draw the three lines through D and respectively J'_1, J'_2 and J'_3 , according to Figure C.2. Now the ratios

$$f_1 = \frac{DP_1}{J'_1P_1}, f_2 = \frac{DP_2}{J'_2P_2} \text{ and } f_3 = \frac{DP_3}{J'_3P_3}$$

can be computed. From geometry is known that $f_1 + f_2 + f_3 = 1$.

If the flux in direction d must be distributed over the three surrounding directions, the fractions f_i of this flux are assigned to the directions j_i . If the outcoming flux in direction d is desired, it is calculated as the weighted mean of the values in directions j_i with f_i as weight factors. If on the other hand the leaf density in direction d is needed, it is estimated by the weighted mean density in directions j_i with f_i as weight factors.

Appendix D

The associative property of the adding algorithm

In this appendix the proof is given that the extended adding algorithm as applied in the HARE model (Section 3.3) obeys the associative law. This means that, if the algorithm is applied repeatedly to calculate the reflection and transmission matrices for a stack that consists of more than two layers, the result of the calculations is not influenced by the order in which the layers are combined (of course, as long as the order of the layers in the stack is not altered). The proof is carried out in two steps:

- In Section D.1, a complete proof is given that the associative property holds for a stack of three layers. It does not matter whether is calculated first, the combination of the top layer and and the central layer, or the combination of the central layer and the lower layer.
- In Section D.2, a method of symbol-manipulation is applied to proof the general case for a number of layers N ($N > 3$). This step makes use of the proof for a stack of three layers.

Combining of these results leads to the conclusion that, regardless of the number of layers N , the order of the calculations does not influence the final results of the calculations.

D.1 The proof for three layers

A stack of three layers can be computed in two orders:

1. Combine the top layer (with T_{a1} , R_{a1} , T_{b1} and R_{b1}) and the central layer (with T_{a2} , R_{a2} , T_{b2} and R_{b2}) to layer (1,2). This leads to the calculation of the matrices T_{a12} , R_{a12} , T_{b21} and R_{b21} . These can be combined with the matrices of the lower layer (T_{a3} and R_{a3}) to the matrices that define the optical properties of the stack $T_{a123}^{(1)}$ and $R_{a123}^{(1)}$.
2. Starting with the central and lower layer (with T_{a2} , R_{a2} , T_{b2} , R_{b2} and T_{a3} , R_{a3} respectively). These are combined to T_{a23} and R_{a23} . In the second step the

matrices for the top layer T_{a1} , R_{a1} , T_{b1} and R_{b1} can be combined with these, resulting in $T_{a123}^{(2)}$ and $R_{a123}^{(2)}$.

It will be clear that if it holds that $T_{a123}^{(1)} = T_{a123}^{(2)}$ and $R_{a123}^{(1)} = R_{a123}^{(2)}$, then the associative property holds for the extended adding algorithm for three layers.

Before the proof is given two remarks must be made to the proof method.

- The proof is based on repeated substitution and simplification. In this process several matrix inversions are applied, which could lead to problems if such matrix is singular. Except for the case where a layer without transmission (e.g. a soil) is included in the model, no matrices with this property are involved. If some layer is or includes a soil, the determinant of the transmission matrix of that layer is equal to 0 (this may occur for matrices T_{a3} , T_{a23} , $T_{a123}^{(1)}$ and $T_{a123}^{(2)}$). In that case, the proof for transmission may be bypassed, because the calculation of the combined transmission matrix of two layers is a product of three factors, of which the transmission matrix for the lower layer (the layer with the soil) is the first one. The result will be a zero matrix for the combined transmission matrix, so if $T_{a3}=0$, then $T_{a23}=0$ (Equation D.7) and also $T_{a123}^{(2)}=0$ (Equation D.9). But in that case it also holds that, regardless of the matrices for layer (1,2), $T_{a123}^{(1)}=0$ (Equation D.5).
- A second remark is that only the proofs for downward incident radiation are given. By exchanging the indices 1 and 3 and a and b respectively, the proof also holds for the incoming radiation from below, so the proof for this need not to be given explicitly.

First the matrices for the combination of the top layer and the central layer T_{a12} , R_{a12} , T_{b21} and R_{b21} are computed (E denotes the unitary matrix):

$$T_{a12} = T_{a2} \cdot (E - R_{b1} \cdot R_{a2})^{-1} \cdot T_{a1} \quad (D.1)$$

$$R_{a12} = R_{a1} + T_{b1} \cdot R_{a2} \cdot (E - R_{b1} \cdot R_{a2})^{-1} \cdot T_{a1} \quad (D.2)$$

$$T_{b21} = T_{b1} \cdot (E - R_{a2} \cdot R_{b1})^{-1} \cdot T_{b2} \quad (D.3)$$

$$R_{b21} = R_{b2} + T_{a2} \cdot R_{b1} \cdot (E - R_{a2} \cdot R_{b1})^{-1} \cdot T_{b2} \quad (D.4)$$

These are combined with the matrices of the lower layer to T_{a3} and R_{a3} $T_{a123}^{(1)}$ and $R_{a123}^{(1)}$:

$$T_{a123}^{(1)} = T_{a3} \cdot (E - R_{b21} \cdot R_{a3})^{-1} \cdot T_{a12} \quad (D.5)$$

$$R_{a123}^{(1)} = R_{a12} + T_{b21} \cdot R_{a3} \cdot (E - R_{b21} \cdot R_{a3})^{-1} \cdot T_{a12} \quad (D.6)$$

Starting with the middle and the lower layers gives for T_{a23} and R_{a23} :

$$T_{a23} = T_{a3} \cdot (E - R_{b2} \cdot R_{a3})^{-1} \cdot T_{a2} \quad (D.7)$$

$$R_{a23} = R_{a2} + T_{b2} \cdot R_{a3} \cdot (E - R_{b2} \cdot R_{a3})^{-1} \cdot T_{a2} \quad (D.8)$$

These are in their turn used to calculate $T_{a123}^{(2)}$ and $R_{a123}^{(2)}$:

$$T_{a123}^{(2)} = T_{a23} \cdot (E - R_{b1} \cdot R_{a23})^{-1} \cdot T_{a1} \quad (D.9)$$

$$R_{a123}^{(2)} = R_{a1} + T_{b1} \cdot R_{a23} \cdot (E - R_{b1} \cdot R_{a23})^{-1} \cdot T_{a1} \quad (D.10)$$

The proofs for transmission ($T_{a123}^{(1)} = T_{a123}^{(2)}$) and for reflection ($R_{a123}^{(1)} = R_{a123}^{(2)}$) are given separately. First $T_{a123}^{(1)}$, $T_{a123}^{(2)}$ and $R_{a123}^{(1)}$ are expressed in the matrices for the individual layers, by means of substitution of Equations (D.1) to (D.4), (D.7) and (D.8) in Equations (D.5), (D.6) and (D.10). For $R_{a123}^{(2)}$ it will appear that such substitution is not needed.

$$T_{a123}^{(1)} = T_{a3} \cdot \left[E - \left\{ R_{b2} + T_{a2} \cdot R_{b1} \cdot (E - R_{a2} \cdot R_{b1})^{-1} \cdot T_{b2} \right\} \cdot R_{a3} \right]^{-1} \cdot \dots \cdot T_{a2} \cdot (E - R_{b1} \cdot R_{a2})^{-1} \cdot T_{a1} \quad (D.11)$$

$$T_{a123}^{(2)} = T_{a3} \cdot (E - R_{b2} \cdot R_{a3})^{-1} \cdot T_{a2} \cdot \dots \cdot \left[E - R_{b1} \cdot \left\{ R_{a2} + T_{b2} \cdot R_{a3} \cdot (E - R_{b2} \cdot R_{a3})^{-1} \cdot T_{a2} \right\} \right]^{-1} \cdot \dots \cdot T_{a1} \quad (D.12)$$

$$R_{a123}^{(1)} = R_{a1} + T_{b1} \cdot R_{a2} \cdot (E - R_{b1} \cdot R_{a2})^{-1} \cdot T_{a1} + \dots \cdot T_{b1} \cdot (E - R_{a2} \cdot R_{b1})^{-1} \cdot T_{b2} \cdot R_{a3} \cdot \left\{ E - R_{b2} + T_{a2} \cdot R_{b1} \cdot \dots \cdot (E - R_{a2} \cdot R_{b1})^{-1} \cdot T_{b2} \cdot R_{a3} \right\}^{-1} \cdot T_{a2} \cdot (E - R_{b1} \cdot R_{a2})^{-1} \cdot T_{a1} \quad (D.13)$$

Transmission, proof that $T_{a123}^{(1)} = T_{a123}^{(2)}$

$$T_{a123}^{(1)} = \left[T_{a1}^{-1} \cdot (E - R_{b1} \cdot R_{a2}) \cdot T_{a2}^{-1} \cdot \dots \cdot \left\{ E - R_{b2} \cdot R_{a3} - T_{a2} \cdot R_{b1} \cdot (E - R_{a2} \cdot R_{b1})^{-1} \cdot T_{b2} \cdot R_{a3} \right\} \cdot \dots \cdot T_{a3}^{-1} \right]^{-1} \quad (D.14)$$

$$T_{a123}^{(2)} = \left[T_{a1}^{-1} \cdot \left\{ (E - R_{b1} \cdot R_{a2}) \cdot T_{a2}^{-1} \cdot (E - R_{b2} \cdot R_{a3}) - \dots \cdot (E - R_{b1} \cdot R_{a2}) \cdot T_{a2}^{-1} \cdot T_{a2} \cdot R_{b1} \cdot (E - R_{a2} \cdot R_{b1})^{-1} \cdot \dots \cdot T_{b2} \cdot R_{a3} \right\} \cdot T_{a3}^{-1} \right]^{-1} \quad (D.15)$$

$$T_{a123}^{(1)} = \left[T_{a1}^{-1} \cdot \left\{ (E - R_{b1} \cdot R_{a2}) \cdot T_{a2}^{-1} \cdot (E - R_{b2} \cdot R_{a3}) - \dots \cdot (E - R_{b1} \cdot R_{a2}) \cdot (E - R_{b1} \cdot R_{a2})^{-1} \cdot R_{b1} \cdot T_{b2} \cdot R_{a3} \right\} \cdot T_{a3}^{-1} \right]^{-1} \quad (D.16)$$

$$T_{a123}^{(2)} = \left[T_{a1}^{-1} \cdot \left\{ (E - R_{b1} \cdot R_{a2}) \cdot T_{a2}^{-1} \cdot \dots \cdot (E - R_{b2} \cdot R_{a3}) - R_{b1} \cdot T_{b2} \cdot R_{a3} \right\} \cdot T_{a3}^{-1} \right]^{-1} \quad (D.17)$$

$$T_{a123}^{(1)} = T_{a3} \cdot \left\{ (E - R_{b1} \cdot R_{a2}) \cdot T_{a2}^{-1} \cdot \dots \cdot (E - R_{b2} \cdot R_{a3}) - R_{b1} \cdot T_{b2} \cdot R_{a3} \right\}^{-1} \cdot T_{a1} \quad (D.18)$$

$$T_{a123}^{(2)} = \left[T_{a1}^{-1} \cdot \left\{ E - R_{b1} \cdot \left(R_{a2} + T_{b2} \cdot R_{a3} \cdot (E - R_{b2} \cdot R_{a3})^{-1} \cdot T_{a2} \right) \right\} \cdot \dots \cdot T_{a2}^{-1} \cdot (E - R_{b2} \cdot R_{a3}) \cdot T_{a3}^{-1} \right]^{-1} \quad (D.19)$$

$$T_{a123}^{(2)} = \left[T_{a1}^{-1} \cdot \left\{ E - R_{b1} \cdot R_{a2} - R_{b1} \cdot T_{b2} \cdot R_{a3} \cdot (E - R_{b2} \cdot R_{a3})^{-1} \cdot T_{a2} \right\} \cdot \dots \cdot T_{a2}^{-1} \cdot (E - R_{b2} \cdot R_{a3}) \cdot T_{a3}^{-1} \right]^{-1} \quad (D.20)$$

$$T_{a123}^{(2)} = \left[T_{a1}^{-1} \cdot \left\{ (E - R_{b1} \cdot R_{a2}) \cdot T_{a2}^{-1} \cdot (E - R_{b2} \cdot R_{a3}) - \dots \right\} \right]^{-1}$$

$$\begin{aligned} & \cdots R_{b_1} \cdot T_{b_2} \cdot R_{a_3} \cdot (E - R_{b_2} \cdot R_{a_3})^{-1} \cdot T_{a_2} \cdot T_{a_2}^{-1} \cdot \cdots \\ & \qquad \qquad \qquad \cdots (E - R_{b_2} \cdot R_{a_3}) \cdot T_{a_3}^{-1} \Big]^{-1} \end{aligned} \quad (D.21)$$

$$\begin{aligned} T_{a_{123}}^{(2)} &= \left[T_{a_1}^{-1} \cdot \left\{ (E - R_{b_1} \cdot R_{a_2}) \cdot T_{a_2}^{-1} \cdot \cdots \right. \right. \\ & \qquad \qquad \qquad \left. \left. \cdots (E - R_{b_2} \cdot R_{a_3}) - R_{b_1} \cdot T_{b_2} \cdot R_{a_3} \right\} \cdot T_{a_3}^{-1} \right]^{-1} \end{aligned} \quad (D.22)$$

$$\begin{aligned} T_{a_{123}}^{(2)} &= T_{a_3} \cdot \left\{ (E - R_{b_1} \cdot R_{a_2}) \cdot T_{a_2}^{-1} \cdot \cdots \right. \\ & \qquad \qquad \qquad \left. \cdots (E - R_{b_2} \cdot R_{a_3}) - R_{b_1} \cdot T_{b_2} \cdot R_{a_3} \right\}^{-1} \cdot T_{a_1} \end{aligned} \quad (D.23)$$

Because the expressions for $T_{a_{123}}^{(1)}$ and $T_{a_{123}}^{(2)}$ are identical, the equality of these matrices may be considered to be proved.

Reflection, proof that $R_{a_{123}}^{(1)} = R_{a_{123}}^{(2)}$

For the proof that $R_{a_{123}}^{(1)} = R_{a_{123}}^{(2)}$ an auxiliary matrix C for which it holds:

$$\begin{aligned} C &= \left[R_{a_2} + (E - R_{a_2} \cdot R_{b_1})^{-1} \cdot T_{b_2} \cdot R_{a_3} \cdot \cdots \right. \\ & \qquad \qquad \qquad \left. \cdots \left\{ E - (R_{b_2} + T_{a_2} \cdot R_{b_1} \cdot (E - R_{a_2} \cdot R_{b_1})^{-1} \cdot T_{b_2}) \cdot R_{a_3} \right\}^{-1} \cdot T_{a_2} \right] \cdot \cdots \\ & \qquad \qquad \qquad \cdots (E - R_{b_1} \cdot R_{a_2})^{-1} \end{aligned} \quad (D.24)$$

will be applied. $R_{a_{123}}^{(1)}$ can now be rewritten as:

$$R_{a_{123}}^{(1)} = R_{a_1} + T_{b_1} \cdot C \cdot T_{a_1} \quad (D.25)$$

C can be simplified as follows:

$$\begin{aligned} C &= \left[R_{a_2} + \left\{ T_{a_2}^{-1} \cdot (E - R_{b_2} \cdot R_{a_3} - T_{a_2} \cdot R_{b_1} \cdot (E - R_{a_2} \cdot R_{b_1})^{-1} \cdot T_{b_2} \cdot R_{a_3}) \cdot \cdots \right. \right. \\ & \qquad \qquad \qquad \left. \left. \cdots R_{a_3}^{-1} \cdot T_{b_2}^{-1} \cdot (E - R_{a_2} \cdot R_{b_1}) \right\}^{-1} \right] \cdot (E - R_{b_1} \cdot R_{a_2})^{-1} \end{aligned} \quad (D.26)$$

$$\begin{aligned} &= \left[R_{a_2} + \left\{ T_{a_2}^{-1} (E - R_{b_2} \cdot T_{a_2}) \cdot R_{a_3}^{-1} \cdot T_{b_2}^{-1} \cdot (E - R_{a_2} \cdot R_{b_1}) - \cdots \right. \right. \\ & \qquad \qquad \qquad \left. \left. \cdots T_{a_2}^{-1} \cdot T_{a_2} \cdot R_{b_1} \cdot (E - R_{a_2} \cdot R_{b_1})^{-1} \cdot T_{b_2} \cdot R_{a_3} \cdot R_{a_3}^{-1} \cdot T_{b_2}^{-1} \cdot \cdots \right. \right. \\ & \qquad \qquad \qquad \left. \left. \cdots (E - R_{a_2} \cdot R_{b_1}) \right\}^{-1} \right] \cdot (E - R_{b_1} \cdot R_{a_2})^{-1} \end{aligned} \quad (D.27)$$

$$\begin{aligned} &= \left[R_{a_2} + \left\{ T_{a_2}^{-1} (E - R_{b_2} \cdot T_{a_2}) \cdot R_{a_3}^{-1} \cdot T_{b_2}^{-1} \cdot (E - R_{a_2} \cdot R_{b_1}) - R_{b_1} \right\}^{-1} \right] \cdot \cdots \\ & \qquad \qquad \qquad \cdots (E - R_{b_1} \cdot R_{a_2})^{-1} \end{aligned} \quad (D.28)$$

A second auxiliary matrix D is introduced:

$$D = R_{a_{23}} - R_{a_2} \quad (D.29)$$

$$= T_{b_2} \cdot R_{a_3} \cdot (E - R_{b_2} \cdot R_{a_3})^{-1} \cdot T_{a_2} \quad (D.30)$$

By substitution of Equation (D.30), Equation (D.24) can be written as:

$$C = \left[R_{a_2} + \left\{ D^{-1} \cdot (E - R_{a_2} \cdot R_{b_1}) - R_{b_1} \right\}^{-1} \right] \cdot (E - R_{b_1} \cdot R_{a_2})^{-1} \quad (D.31)$$

$$= \left[R_{a_2} + \left\{ D^{-1} \cdot (E - R_{a_2} \cdot R_{b_1} - D \cdot R_{b_1}) \right\}^{-1} \right] \cdot (E - R_{b_1} \cdot R_{a_2})^{-1} \quad (D.32)$$

$$= [R_{a2} + (E - R_{a2} \cdot R_{b1} - D \cdot R_{b1})^{-1} \cdot D] \cdot (E - R_{b1} \cdot R_{a2})^{-1} \quad (D.33)$$

$$= (E - R_{a2} \cdot R_{b1} - D \cdot R_{b1})^{-1} \cdot \dots \cdot [(E - R_{a2} \cdot R_{b1} - D \cdot R_{b1}) \cdot R_{a2} + D] \cdot (E - R_{b1} \cdot R_{a2})^{-1} \quad (D.34)$$

$$= (E - R_{a2} \cdot R_{b1} - D \cdot R_{b1})^{-1} \cdot \dots \cdot [R_{a2} - R_{a2} \cdot R_{b1} \cdot R_{a2} - D \cdot R_{b1} \cdot R_{a2} + D] \cdot (E - R_{b1} \cdot R_{a2})^{-1} \quad (D.35)$$

$$= (E - R_{a2} \cdot R_{b1} - D \cdot R_{b1})^{-1} \cdot \dots \cdot [R_{a2} \cdot (E - R_{b1} \cdot R_{a2}) + D \cdot (E - R_{b1} \cdot R_{a2})] \cdot (E - R_{b1} \cdot R_{a2})^{-1} \quad (D.36)$$

$$= (E - R_{a2} \cdot R_{b1} - D \cdot R_{b1})^{-1} \cdot \dots \cdot [(R_{a2} + D) \cdot (E - R_{b1} \cdot R_{a2})] \cdot (E - R_{b1} \cdot R_{a2})^{-1} \quad (D.37)$$

$$= (E - R_{a2} \cdot R_{b1} - D \cdot R_{b1})^{-1} \cdot (R_{a2} + D) \quad (D.38)$$

$$= [(R_{a2} + D)^{-1} \cdot (E - R_{a2} \cdot R_{b1} - D \cdot R_{b1})]^{-1} \quad (D.39)$$

$$= [(R_{a2} + D)^{-1} - R_{b1}]^{-1} \quad (D.40)$$

Substitution of Equation (D.29) in (D.40) gives:

$$C = [R_{a23}^{-1} - R_{b1}]^{-1} \quad (D.41)$$

$$= [(E - R_{b1} \cdot R_{a23}) \cdot R_{a23}^{-1}]^{-1} \quad (D.42)$$

$$= R_{a23} \cdot (E - R_{b1} \cdot R_{a23})^{-1} \quad (D.43)$$

Substitution of Equation (D.43) in (D.25) gives:

$$R_{a123}^{(1)} = R_{a1} + T_{b1} \cdot R_{a23} \cdot (E - R_{b1} \cdot R_{a23})^{-1} \cdot T_{a1} \quad (D.44)$$

The righthand side of this expression is exactly the same as the righthand side of Equation (D.9) for $R_{a123}^{(2)}$. This means that $R_{a123}^{(1)}$ and $R_{a123}^{(2)}$ are identical.

With this result, both identities $R_{a123}^{(1)} = R_{a123}^{(2)}$ and $T_{a123}^{(1)} = T_{a123}^{(2)}$ have been proved, so the extended adding algorithm for three layers may be considered to obey the associative law.

D.2 The proof for an arbitrary number of layers

To prove that the associative property also holds for a stack of N layers (with $N > 3$), a much simpler notation is used. The complete extended adding algorithm for two layers is expressed in the following notation (p and q are arbitrary layer numbers, the other symbols have the same meaning as in Section D.1):

$$\{T_{a,p}, R_{a,p}, T_{b,p}, R_{b,p}\} \equiv p \quad (D.45)$$

$$\{T_{a,pq}, R_{a,pq}, T_{b,qp}, R_{b,qp}\} \equiv (p \star q) \quad (D.46)$$

So the complete set of four matrices for one layer is indicated with one symbol, representing the index of that layer. A complete adding-step on two layers is represented by one operator-symbol ' \star ' between the two layer symbols. If needed, parentheses are

used to indicate the order of the operations: $((p \star q) \star r)$ means that first layers p and q are combined to one layer, and that this layer is combined with layer r . With this notation, the property that is proved in Section D.1 can be expressed as:

$$((1 \star 2) \star 3) \simeq (1 \star (2 \star 3)) \quad (\text{D.47})$$

This notation will be called the star-notation, strings like the left- and righthand side of Equation (D.47) are called star-strings.

Besides the notation in star-strings, a second notation is introduced. This notation is based on the successive operations that are carried out. To do so, all \star -operators are numbered from left to right, regardless of the parentheses in the star-string. If the number of layers is N , the number of \star -operators is $N-1$, so:

$$\left(\left(\dots \left(\left(\left(\left(1 \overset{1}{\star} 2 \right) \overset{2}{\star} \left(3 \overset{3}{\star} 4 \right) \right) \overset{4}{\star} 5 \right) \right) \overset{5}{\star} 6 \right) \dots \right) \overset{N-1}{\star} N \right) \quad (\text{D.48})$$

By use of the operator-indices, the ordering of the calculations can be expressed as a series of the $N-1$ indices. A possible ordering of the example in Formula (D.48) is:

$$1 \cdot 3 \cdot 2 \cdot 4 \cdot 5 \cdot \dots \cdot N-1 \quad (\text{D.49})$$

This is called the dot-notation, a string like Formula (D.49) is called a dot-string. Because in Formula (D.48), the operations $\left(1 \overset{1}{\star} 2 \right)$ and $\left(3 \overset{3}{\star} 4 \right)$ are mutually independent, another dot-string that corresponds with this formula is

$$3 \cdot 1 \cdot 2 \cdot 4 \cdot 5 \cdot \dots \cdot N-1 \quad (\text{D.50})$$

It will be clear that each of the possible $(N-1)!$ dot-strings, related to a stack of N layers, is equivalent to exactly one star-string, and that vice-versa each possible star-string can be expressed as at least one dot-string (sometimes in more than one way, if mutually independent operations are present). Orderings are indicated with the symbol \mathcal{F} . For reasons of simplicity, a standard ordering \mathcal{F}_S is defined. This is the ordering for which holds:

$$\mathcal{F}_S = 1 \cdot 2 \cdot \dots \cdot N-2 \cdot N-1 \simeq \left(\left(\dots \left(\left(\left(1 \overset{1}{\star} 2 \right) \overset{2}{\star} 3 \right) \overset{3}{\star} \dots \right) \right) \overset{N-1}{\star} N \right) \quad (\text{D.51})$$

The actual proof is that by means of repeated permitted transformations in an arbitrary string \mathcal{F} , the standard string \mathcal{F}_S can be obtained. The transformation that will be used for this is a very simple one: it encloses only the exchange of two adjacent operator-numbers in the dot-string. Any arbitrary string \mathcal{F}_0 can be transformed to \mathcal{F}_S in at most $(N-1) \cdot (N-2)/2$ transformations using a sorting algorithm called "bubble sort" (Knuth, 1973). Of course, these steps need not to be carried out in practice, it suffices to know that they could be carried out with the desired result.

The only part of the proof that still remains to be done is the proof that it is permitted to exchange two adjacent numbers in the dot-string. In the related star-string it can be seen that two different situations can occur with respect to the operands of two adjacent operator-numbers in the dot-string:

1. The operands involved in the two operations are mutually exclusive, like:

$$\mathcal{F}_j = \dots \cdot p \cdot q \cdot \dots \simeq (\dots (a \overset{p}{\star} b) \dots (c \overset{q}{\star} d) \dots) \quad (\text{D.52})$$

a , b , c and d are the operands of operations p and q . They may represent single layers or the result of previous \star -operations. In this case it is clear that the dot-string $\mathcal{F}_j = \dots \cdot p \cdot q \cdot \dots$ may be changed freely to the dot-string $\mathcal{F}_{j+1} = \dots \cdot q \cdot p \cdot \dots$, because they both are equivalent to the righthand side of Equation (D.52).

2. The other situation that can occur is that the result of the first operation is one of the operands of the second operation, e.g.:

$$\mathcal{F}_j = \dots \cdot p \cdot q \cdot \dots \simeq (\dots ((a \overset{p}{\star} b) \overset{q}{\star} c) \dots) \quad (\text{D.53})$$

In this case, exchanging p and q gives:

$$\mathcal{F}_{j+1} = \dots \cdot q \cdot p \cdot \dots \simeq (\dots (a \overset{p}{\star} (b \overset{q}{\star} c)) \dots) \quad (\text{D.54})$$

In Section D.1 it is proved that the righthand sides of Equations (D.53) and (D.54) are equivalent with respect to their computational result, so also in this case exchanging p with its neighbour q in the dot-strings is a permitted operation.

Now it has been proved that in all possible situations, two adjacent numbers in a dot-string may be exchanged freely, without influencing the result of the calculations that are represented by such string.

With this it has been proved that all possible dot-strings \mathcal{F} with $N-1$ elements are equivalent with dot-string \mathcal{F}_S , so it may be concluded that all dot-strings \mathcal{F} with $N-1$ elements are representants of series of operations that should have, if they actually were performed, equal results. And because each possible order of calculations on N layers can be written as a dot-string with $N-1$ elements, all possible orders of calculations are equivalent with respect to the result of their calculations.

Summary

This thesis describes research done to ascertain the possibilities and limitations of the use of remote sensing observations for agriculture. The topic is defined in Chapter 1. In Chapter 2 the possible applicability of certain existing models for this study is examined. Three models are developed further in Chapter 3. Two of them describe the relation between properties of a crop and its reflective behaviour; the third is a model for soil reflection. Chapter 4 presents calculations on hypothetical crops; in Chapter 5 some calculations based on actual crop data are described.

In the early years of the use of remote sensing, the agricultural applications of this technique were almost exclusively qualitative. However, the quantitative applications have been steadily increasing. These applications always require measured electromagnetic radiative energy to be translated into parameters of agricultural interest, such as coverage, leaf area index, biomass, development stage or health conditions of a crop, and in most situations the qualitative information which crop is being grown must also be determined from the observed radiation.

The problem is defined in Chapter 1. The conclusion is that the optical behaviour of a crop is determined by a number of more or less independent parameters. This number generally exceeds the number of data measured. Consequently, in many situations it is very difficult to reliably estimate the quantities that cause this behaviour, if these estimations are only based on the observations. Two additional complicating factors are that the relations between the optical and the agricultural properties of a crop are surely not unequivocal, and that the reflection of a crop also depends on the spatial distribution of the incident radiation. This justifies the conclusion that it is useful to study the relations between the agricultural properties of a crop and the upward radiation, measured under different irradiance conditions.

In Chapter 2, it is investigated if, and under which conditions, existing models could be used as reflection models. To determine the requirements of reflection models, an existing analytical model (Kubelka & Munk, 1931) is used to calculate the ratio of reflected radiation to absorbed radiation, and a new analytical model is used to ascertain the spatial distribution of the reflected radiation. From the calculations with the Kubelka-Munk model it is concluded that for the calculation of the absorption of incident radiation by a crop the modelling of the spatial distribution of the intercepted and remitted radiation can be strongly simplified, without compromising the quality of the absorption calculations. This justifies that in the models used by plant physiologists for calculating the absorption of photosynthetically active radiation, the spatial distribution of this secondary radiation is strongly simplified. Calculations with the distribution model show that both the crop properties and the spatial distribution of the incoming radiation may strongly influence the reflected radiation in one direction.

Four existing models are examined to ascertain their applicability in the situation under consideration. As might be expected, the two absorption models (De Wit, 1965; Goudriaan, 1977) lack the level of detail that is required for the modelling of the reflected radiation. Of the two models that have primarily been developed as reflection models (Suits, 1972; Chen, 1984), the first is a very theoretical model, so if it is applied to a real crop it only permits qualitative statements. The second model should, in principle, be applicable, but its intensive use of computer resources means that a prohibitive number of calculations is required. The conclusion is that it makes sense to develop a new reflection model, incorporating several aspects of the existing models both in its theoretical basis and in its implementation.

Chapter 3 is devoted to the three models that are developed in this study: the TURTLE, HARE and SOIL models. TURTLE and HARE describe a crop and SOIL describes a non-flat soil. Both TURTLE and HARE are based on the description of a crop as a stack of thin crop layers. For this description, 46 directions are defined in a semispace. These directions, which are used as representatives of all possible directions, are distributed in such way that each represents an equal solid angle (0.14 sr). The mutual angle between adjacent directions is 0.42 rad. Because each model direction represents all directions within a fairly regular pentagonal or hexagonal conic sector of the space, the angle between a representative and a represented direction never exceeds 0.24 rad. These model directions are used both to represent radiation patterns and to define leaf angle distributions. In the latter case, the directions are used as vectors perpendicular to possible leaf orientations.

The optical properties of a single crop layer are derived from the optical properties of the crop components and of the leaf angle distribution of this layer. The optical properties of a crop layer are described in the form of a set of four 46*46 matrices: one for the upperside reflection of the layer, one for the underside reflection, one for the upward transmission and one for the downward transmission through the layer. In the models as described, upperside and underside are assumed to be identical, so only two matrices have to be computed: one for the layer reflection and one for the layer transmission. From these matrices, and in combination with another 46*46 matrix for the soil reflection, one matrix is calculated. This matrix describes the optical behaviour of the total crop. The TURTLE and HARE models differ in the aspect that the TURTLE model allows the radiation pattern and the radiation intensity throughout the complete crop to be calculated. To enable this, in the calculations the layers are stacked one by one, in an upward direction, starting with the soil matrix. In the HARE model, the matrices for stacks of identical model layers are calculated by means of a doubling method. This way of combining layer matrices prohibits the calculation of a radiation pattern throughout the crop, but this limitation is not very drastic in remote sensing applications. The advantage of this method is that it reduces the computer time required by a factor of 5 to 10, compared with the TURTLE model. Also, the incoming radiation is described as a vector that comprises in the 46 previously mentioned directions. Multiplying this vector by the crop reflection matrix yields the radiation remitted by the crop. The TURTLE model allows the radiation regime within the crop to be calculated in a similar way.

The SOIL model is developed to investigate if the influence of a non-flat soil to the reflected radiation is so large that it would be unrealistic to model the soil as a flat reflecting surface. The calculations show that only if the coverage of the crop is very low (< 0.25), the spatial distribution of the radiation reflected by the soil is of importance

in case individual wavelength bands are considered, but that this influence vanishes if instead of single spectral bands, the ratio between two bands (or a function of such a ratio) is used as a basis for the interpretation of remote sensing observations.

In Chapter 4, a large number of calculations with the HARE model are presented. For these calculations, test values based on values that are found in literature are chosen for the parameters that can be varied in the model. These parameters concern the leaf angle distribution, the leaf reflection and the leaf transmission coefficient, the reflective behaviour of the leaves, the soil reflection coefficient, the spatial distribution of the incoming radiation and the direction of observation. The calculations always concern the relation between the upward radiation and the primary crop property, namely the vertically measured coverage. It is investigated how this relation is influenced by variations in the values of the given parameters. Based on these calculations it can be concluded that these variations can be large, but that it may be expected that the relation between the vertical coverage and the ratio between the reflection in the infrared and the red bands (or a derived function such as the normalized difference between these two, the vegetation index), will be much less sensitive to the mentioned variations. For this reason a second series of calculations is done. In these calculations, the sensitivity of the relation between coverage and vegetation index for the same parameter variations is examined. It appears that this relation is indeed much less sensitive, except for changes in the observation direction. The latter phenomenon is investigated separately. The conclusion of the latter investigation is that the commonly used method to reduce the directional dependency that is based on a quadratic regression, only enhances the quality of the interpretation under special conditions, but that in some cases, this correction yields an even worse result than the result that would have been found if the correction had not been applied at all. It is indicated how, by means of the HARE model, the calculations may be improved.

Finally, Chapter 5 discusses the interpretation of remote sensing observations applied to winter wheat and sugarbeet. The aim of the wheat calculation is to investigate which variation in the crop can be determined and at which moments. For the calculations, a normal developing wheat crop was constructed, based on literature data. Some variants with a higher and a lower LAI and also three variants with strongly yellowing leaves were derived from this crop. The calculation indicates that the vegetation index only gives information about the LAI as long as the crop is green and the LAI does not exceed 3.5. Higher LAI-values cannot be distinguished, and if the crop turns yellow, it cannot be distinguished from a crop with a much lower LAI. If, besides the vegetation index the ratio red/green is also applied, the interpretation possibilities increase somewhat. The red/green ratio decreases until the crop reaches an LAI of 6, higher LAI-values cannot be determined. It is also possible, if repeated observations are carried out, to distinguish yellowing in a late growth phase from a decreasing LAI-value. The use of the vegetation index or the red/green ratio causes a drastic decrease in the influence of factors that are of no agricultural interest, but which were present in the reflection in the individual bands.

The aim of the calculations with sugarbeet was to ascertain which conditions are most applicable for the detection of places where the crop droops its leaves. For this purpose the spatial pattern of the reflected radiation by a beet crop in different wavelength bands is calculated. These calculations are done both for a healthy crop and for a

dehydrated crop. For both crop types the infrared/red ratio is calculated for all possible observation directions, and then the quotient of these ratios is calculated. It appears that the areas where leaf drooping has occurred can easily be identified, providing that the observation direction is chosen well (e.g. facing the sun, and with an inclination that is approximately the complement of the sun's inclination). These areas can be distinguished, even if the observations are carried out under full cloud cover. The latter conclusion is especially important if the observations are done on a small scale by using a micro-light airplane.

Samenvatting

Dit proefschrift beschrijft een onderzoek naar mogelijkheden en beperkingen van het gebruik van teledetectie waarnemingen ten behoeve van landbouwkundige toepassingen. Na de probleemstelling waarop in Hoofdstuk 1 wordt ingegaan, worden in Hoofdstuk 2 enkele bestaande modellen voor de interactie tussen een gewas en de erop vallende elektromagnetische straling onderzocht op hun toepasbaarheid in deze studie. In Hoofdstuk 3 worden drie modellen ontwikkeld. Twee ervan beschrijven de relatie tussen de eigenschappen van een gewas en het reflectiegedrag ervan, het derde is een model voor de bodemreflectie. In Hoofdstuk 4 volgen dan een aantal berekeningen aan geconstrueerde gewassen, waarna in Hoofdstuk 5 enkele berekeningen beschreven worden die gebaseerd zijn op echte gewassen.

In de beginjaren van de teledetectie waren de landbouwkundige toepassingen ervan nagenoeg alleen kwalitatief van aard, maar in de loop van de tijd zijn daar steeds meer kwantitatieve toepassingen aan toegevoegd. Deze laatste vragen altijd een vertaling van gemeten elektromagnetische stralingsenergie naar landbouwkundig relevante grootheden als bedekking, LAI, biomassa, ontwikkelingsstadium of gezondheidstoestand van een gewas, waarbij in veel gevallen het kwalitatieve gegeven om welk gewas het gaat ook bepaald moet worden uit de waargenomen straling.

In Hoofdstuk 1 wordt ingegaan op de probleemstelling. De conclusie is dat het aantal min of meer onafhankelijke grootheden die het optische gedrag van een gewas bepalen in het algemeen groter is dan het aantal gemeten grootheden. Het gevolg hiervan is dat het in veel gevallen bijzonder moeilijk is een betrouwbare schatting te doen van de grootheden die dit gedrag veroorzaken alleen op grond van de waarnemingen. Twee extra complicerende factoren zijn dat de relatie tussen de optische en de landbouwkundige eigenschappen van een gewas ook zeker niet eenduidig is en dat de reflectie van een gewas ook samenhangt met de ruimtelijke verdeling van de invallende straling. Dit rechtvaardigt de conclusie dat een studie naar de relatie tussen de landbouwkundige eigenschappen van een gewas en de onder verschillende belichtingscondities gemeten opwaartse straling op zijn plaats is.

In Hoofdstuk 2 is nagegaan in hoeverre bestaande modellen gebruikt zouden kunnen worden als reflectiemodel. Voor het bepalen aan welke eisen reflectiemodellen moeten voldoen is gebruik gemaakt van een bestaand analytisch model (Kubelka & Munk, 1931) voor het berekenen van de verhouding tussen de gereflecteerde straling en de geabsorbeerde straling en een zelf ontwikkeld analytisch model voor de ruimtelijke verdeling van de gereflecteerde straling. Op grond van berekeningen met het Kubelka-Munk model blijkt dat voor het berekenen van de absorptie van invallend licht door een gewas een sterk vereenvoudigde modellering van de ruimtelijke verdeling van de onderschepte en daarna geremitteerde straling mogelijk is zonder dat dit afbreuk doet aan de kwaliteit

van de absorptie-berekeningen of -schattingen. In modellen die in plantenfysiologische omgeving gebruikt worden voor het berekenen van de absorptie van fotosynthetisch actieve straling is de richtingsafhankelijkheid van deze secundaire straling dan ook terecht sterk vereenvoudigd. Berekeningen met het verdelingsmodel tonen aan dat zowel de gewaseigenschappen als de ruimtelijke verdeling van de inkomende straling een belangrijke invloed kunnen hebben op de in een enkele richting door het gewas gereflecteerde straling.

Vier bestaande modellen zijn onderzocht op hun toepasbaarheid in de onderhavige situatie. De twee absorptie modellen (De Wit, 1965; Goudriaan, 1977) missen zoals verwacht de voor dit onderzoek noodzakelijke gedetailleerdheid waarmee de gereflecteerde straling gemodelleerd is. Van de twee modellen die primair ontwikkeld zijn als reflectie model (Suits, 1972; Chen, 1984), is het eerste een zeer theoretisch model, dat slechts kwalitatieve uitspraken toelaat als het wordt toegepast op een reëel gewas. Het tweede model zou in principe bruikbaar zijn in het onderhavige onderzoek, ware het niet dat het model zodanig rekenintensief is, dat het daarom niet in aanmerking komt voor het doen van een groot aantal berekeningen. De conclusie is dat het daarom zinvol is zelf een model te ontwikkelen, waarbij de verschillende aspecten van de bestaande modellen een rol spelen in de theorievorming omtrent en in de implementatie van dat nieuwe model.

Hoofdstuk 3 handelt geheel over de drie in het kader van deze studie ontwikkelde modellen: TURTLE, HARE en SOIL. TURTLE en HARE zijn modellen voor de beschrijving van een gewas en SOIL is een model voor de beschrijving van een niet vlakke bodem. TURTLE en HARE zijn beide gebaseerd op de beschrijving van een gewas als een stapel dunne gewaslagen. Hiertoe zijn in de halve ruimte 46 richtingen gedefinieerd. Deze worden gebruikt als representanten van alle mogelijke richtingen. De verdeling van deze 46 richtingen is zodanig dat elke richting een even grote ruimtehoek ($0,14$ sr) representeert. De onderlinge hoek tussen naburige richtingen is $0,42$ rad. Aangezien elke modelrichting alle richtingen binnen een betrekkelijk regelmatig 5- of 6-hoekige conische sector van de ruimte representeert, is de hoek tussen de representerende en de gerepresenteerde richting in geen enkel geval groter dan $0,24$ rad. Deze modelrichtingen worden zowel gebruikt voor het representeren van stralingspatronen als voor het definiëren van bladhoekverdelingen. In het laatste geval worden de richtingen gebruikt als vectoren loodrecht op de mogelijke blad-oriëntaties.

De optische eigenschappen van een enkele gewaslaag worden afgeleid uit de optische eigenschappen van de gewascomponenten en uit de bladhoekverdeling in deze laag. De optische eigenschappen in een gewaslaag worden beschreven in de vorm van een verzameling van vier 46×46 matrices: een voor de reflectie aan de bovenzijde van de laag, een voor de reflectie aan de onderzijde, een voor de naar boven gerichte en een voor de naar beneden gerichte transmissie door de laag heen. In de modellen zoals deze beschreven zijn worden boven- en onderzijde van een laag identiek verondersteld, zodat slechts twee matrices uitgerekend hoeven te worden: een voor de reflectie en een voor de transmissie van een laag. Uit deze laag-matrices wordt dan, tesamen met een 46×46 matrix waarin de bodemreflectie is vastgelegd, een matrix berekenend waarin het optische gedrag van het gehele gewas is vastgelegd. Het TURTLE en het HARE model verschillende daarin dat het TURTLE model de mogelijkheid biedt het stralingspatroon en de stralingsintensiteit door het gehele gewas heen te berekenen. Daartoe worden in de berekening de lagen van beneden af één voor één op elkaar gestapeld, te beginnen

bij de bodemmatrix. In het HARE model worden de matrices voor dikkere pakketten identieke modellagen met een verdubbelingsmechanisme berekend. Deze wijze van het combineren van de laag-matrices maakt het onmogelijk om het stralingspatroon door het hele gewas heen te berekenen, maar deze beperking is in teledetectie-toepassingen niet bezwaarlijk. Het voordeel van deze berekeningsmethode is dat een reductie van de rekentijd met een factor 5 tot 10 bereikt wordt, vergeleken met het TURTLE model. Ook de inkomende straling wordt beschreven als een vector waarin de eerder genoemde 46 richtingen voorkomen. Door deze vector te vermenigvuldigen met de gewas-reflectie matrix wordt dan de door het gewas geremitterde straling berekend. Met het TURTLE model is het op vergelijkbare wijze mogelijk het stralingsregime binnen het gewas te berekenen.

Het SOIL model is ontwikkeld om na te gaan of de invloed van een niet vlakke bodem op de gereflecteerde straling zodanig groot is dat de bodem niet voorgesteld mag worden als een vlakke reflector. Berekeningen tonen aan dat alleen bij een gewas met een zeer lage bedekking ($<0,25$) de ruimtelijke verdeling van de door de bodem gereflecteerde straling een rol speelt in de individuele golflengte banden, maar dat deze invloed verdwijnt als in plaats van enkele banden, de verhouding tussen twee banden (of een functie van zo'n verhouding) gebruikt wordt als basis voor de interpretatie van de teledetectie-waarnemingen.

In Hoofdstuk 4 worden een groot aantal berekeningen met het HARE model gepresenteerd. Hiertoe zijn voor de parameters die in het model gevarieerd kunnen worden een aantal testwaarden gekozen. Deze zijn gebaseerd op waarden die in de literatuur zijn gevonden. Deze parameters betreffen de bladhoekverdeling, de bladreflectie- en transmissie-coëfficiënt, de wijze waarop de bladeren het opvallende licht reflecteren, de reflectie-coëfficiënt van de bodem, de ruimtelijke verdeling van het inkomende licht en de waarnemingsrichting. In de berekeningen is steeds een relatie gelegd tussen de opwaartse straling en de meest primaire gewaseigenschap, namelijk de vertikaal gemeten bedekking. Onderzocht is hoe deze relatie beïnvloed wordt door variaties in waarden van de genoemde parameters. De conclusie die op grond van deze berekeningen getrokken kan worden is dat deze variaties vrij groot kunnen zijn, maar dat de relatie tussen de verticale bedekking en de verhouding tussen de reflectie in de infrarode en de rode band (of een daarvan afgeleide functie zoals het genormaliseerde verschil tussen de reflectie in deze twee banden, de vegetatie index) veel minder gevoelig zal zijn voor de bedoelde variaties. Om deze reden is een tweede serie berekeningen uitgevoerd waarin de gevoeligheid voor dezelfde parameter-varianties van de relatie tussen de bedekking en de vegetatie index is onderzocht. Het blijkt dat deze relatie inderdaad veel minder gevoelig is, behalve voor veranderingen in de waarnemingsrichting. Dit laatste fenomeen is apart onderzocht. De conclusie van dat laatste onderzoek is dat de gebruikelijke, op kwadratische regressie gebaseerde, methode om de richtingsafhankelijkheid te verminderen slechts onder speciale omstandigheden een verbetering van de interpretatie oplevert, maar dat in andere gevallen zelfs slechtere resultaten waargenomen worden dan in het geval geen correcties worden toegepast. Aangegeven is hoe, met behulp van het HARE model, waarschijnlijk een aanmerkelijke verbetering te bereiken is.

In Hoofdstuk 5 tenslotte wordt aandacht besteed aan de interpretatie van teledetectie-waarnemingen toegepast op wintertarwe en suikerbieten. Voor deze berekeningen is, uitgaande van literatuurgegevens, een zich normaal ontwikkelend tarwegewas ontwikkeld. Van dit gewas zijn twee varianten afgeleid met hogere c.q. lagere LAI en ook

drie varianten met sterk vergelende bladeren. Uit de berekening blijkt dat de vegetatie-index slechts informatie over de LAI geeft zolang het een groen gewas betreft met een $LAI < 3,5$. Hogere LAI waarden zijn niet te onderscheiden, en als het gewas vergeeld is, is het niet te onderscheiden van een gewas met een veel lagere LAI. Als naast de vegetatie-index ook de rood/groen verhouding gebruikt wordt, zijn de mogelijkheden wat groter. De rood/groen verhouding blijft afnemen tot het gewas een LAI bereikt van 6. Een nog hogere LAI kan niet onderscheiden worden. Ook kan, indien herhaalde waarnemingen gedaan worden, vergeling in een later stadium van het groeiseizoen onderscheiden worden van een lagere LAI. Het gebruik van de vegetatie-index of de rood/groen verhouding heeft in ieder geval tot gevolg dat een aanzienlijk deel van de invloeden van niet-landbouwkundige factoren, die wel in de individuele banden te zien zijn, verdwijnen.

Het doel van de berekeningen aan bieten was te onderzoeken welke omstandigheden het meest geschikt zijn voor het detecteren van legeringsplekken. Voor dit onderzoek is het ruimtelijke patroon van de door een bietengewas gereflecteerde straling berekend in verschillende golflengte banden voor zowel een gezond gewas als voor een legerend gewas. Voor beide gewastypen is voor alle mogelijke waarnemingsrichtingen de infrarood/rood verhouding uitgerekend, waarna het quotiënt van deze twee verhoudingen onderzocht is. Het blijkt dat, mits de waarnemingen in de goede richting gedaan worden (tegen de zon in, en met een inclinatie die ongeveer het complement is van de zonshoogte), de legeringsplekken goed te bepalen zijn. Zelfs als gemeten wordt onder volledig bewolkte condities, zijn deze plekken te onderscheiden. Deze laatste conclusie is vooral van belang als kleinschalige waarnemingen gedaan worden met behulp van ultra-lichte vliegtuigen.

References

- Allen, W.A., H.W. Gausman, A.J. Richardson & J.R. Thomas, 1969. Interaction of isotropic light with a compact plant leaf. *Journal of the Optical Society of America* 59(10): 1376-1379.
- Allen, W.A., H.W. Gausman & A.J. Richardson, 1970. Mean effective optical constants of cotton leaves. *Journal of the Optical Society of America* 60(4): 542-547.
- Bowers, S.A. & R.J. Hanks, 1965. Reflection of radiant energy from soils. *Soil Science* 100(2): 130-138.
- Breece, H.T. & R.A. Holmes, 1971. Bidirectional scattering characteristics of healthy green soybean and corn leaves in vivo. *Applied Optics* 10(1): 119-127.
- Bunnik, N.J.J., 1978. The multispectral reflectance of shortwave radiation by agricultural crops in relation with their morphological and optical properties. Mededelingen Landbouwhogeschool Wageningen, The Netherlands 78-1. 175 p.
- Chen, J., 1984. Mathematical analysis and simulation of crop meteorology. Department of Theoretical Production Ecology, Agricultural University Wageningen, The Netherlands. 116 p.
- Clevers, J.G.P.W., 1986. Application of remote sensing to agricultural field trials. Agricultural University Wageningen Papers 86-4. 227 p.
- Condit, H.R., 1970. The spectral reflectance of American soils. *Photogrammetric Engineering* 36: 955-966.
- Cooper, K., J.A. Smith & D. Pitts, 1982. Reflectance of a vegetation canopy using the Adding method. *Applied Optics* 21(22): 4112-4118.
- Duntley, S.Q., 1942. The optical properties of diffusing materials. *Journal of the Optical Society of America* 32(2): 61-70.
- Gausman, H.W. & W.A. Allen, 1973. Optical parameters of leaves of 30 plant species. *Plant Physiology* 52: 57-62.
- Gausman, H.W., R.M. Menges, A.J. Richardson, H. Walter & S. Tamez, 1981. Optical parameters of leaves of seven weed species. *Weed Science* 29: 24-26.
- Grace, J., 1971. The directional distribution of light in natural and controlled environment conditions. *Journal for Applied Ecology* 8: 155-165.
- Goudriaan, J., 1977. Crop meteorology: a simulation study. Simulation Monograph Series, Pudoc, Wageningen. 249 p.
- Hodáňová, D., 1972. Structure and development of sugar beet canopy. Part I, Leaf area - leaf angle relations. *Photosynthetica* 6(4): 401-409.

- Hulst, H.C. van de, 1980. Multiple light scattering, tables, formulas and applications. Vol.1, Academic Press, London. 299 p.
- Knuth, D.E., 1969. The art of computer programming. Vol.2, Seminumerical Algorithms. Addison-Westley Publishing Company, Reading, Massachusetts, USA. 624 p.
- Knuth, D.E., 1973. The art of computer programming. Vol.3, Sorting and Searching. Addison-Westley Publishing Company, Reading, Massachusetts, USA. 723 p.
- Kubelka, P. & F. Munk, 1931. Ein Beitrag zur Optik der Farbanstriche. A. Techn. Physik, 11: 593-601.
- Lang, A.R.G., 1973. Leaf orientation of a cotton plant. Agricultural Meteorology 11: 37-51.
- Moon P. & D.E. Spencer, 1942. Illumination from a non-uniform sky. Trans. Illumination Engineering Society, New York 37: 707-712.
- Nichiporovich, A.A., 1961. On properties of plants as an optical system. Soviet Plant Physiology 8(5): 536-546 (in Russian).
- Nichiporovich, A.A., 1963. On ways of raising productivity of photosynthesis of plants in crops. In: Photosynthesis and Problems of Plant Production. USSR Academy of Science Press, M. (in Russian).
- Oliver, R.E. & J.A. Smith, 1974. A stochastic canopy model of diurnal reflectance. Final report, U.S. Army Research Office-Durham. DAH-C04-74-G0001. Colorado State University, Fort Collins, Colorado 80521, USA.
- Ranson, K.J., L.L. Biehl & C.S.T. Daughtry, 1984. Soybean canopy reflectance modeling data sets. Laboratory for Application of Remote Sensing, Purdue University, West Lafayette, Indiana 47906, U.S.A. LARS Technical Report 071584.
- Ross, J., 1981. The radiation regime and architecture of plant stands. Dr W. Junk Publishers, The Hague, The Netherlands. 391 p.
- Ross, J. & T. Nilson, 1967a. The vertical distribution of biomass in crop stands. In: Photosynthesis of Productive Systems. Ed. A.A. Nichiporovich. Israel Program for Science Transl., Jerusalem, p. 75-85.
- Ross, J. & T. Nilson, 1967b. The spatial orientation of leaves in crop stands and its determination. In: Photosynthesis of Productive Systems. Ed. A.A. Nichiporovich. Israel Program for Science Transl., Jerusalem, p. 86-99.
- Ross, J. & M.P. Vlasova, 1967. Biometric characteristics of maize stand and the dynamics of its development. In: Photosynthesis of productive systems. Ed. A.A. Nichiporovich. Israel Program for Science Transl., Jerusalem, p. 60-74.
- Ross, V. & J. Ross, 1969. Biometric measurements in agricultural crops. In: Methodological Instructions for Determinating and Checking Basic Indices of Photosynthetic Activity of Plants in Crops. Ed. M. Vashnil, p. 25-34. (in Russian).
- Sheehy, J.E., 1975. Some optical properties of leaves of eight temperate forage grasses. Annals of Botany 39: 377-386.
- Stokes, G.G., 1862. Proceedings of the Royal Society (London) 11: 545.
- Suits, G.H., 1972. The calculation of the directional reflectance of a vegetative canopy.

Remote Sensing of Environment 2: 117-125.

Verhoef, W., 1984. Light scattering by leaf layers with application to canopy reflectance modeling: the SAIL model. Remote Sensing of Environment 16: 125-141.

Warren Wilson, J., 1965. Stand structure and light penetration. I. Analysis by point quadrats. Journal of Applied Ecology 2(2): 383-390.

Williams, R., 1972. The geometrical foundation of natural structure. A source book of design. Dover Publications, Inc. New York, USA. 265 p.

Wit, C.T. de, 1965. Photosynthesis of leaf canopies. Agricultural Research Reports 663, Pudoc, Wageningen. 57 p.

Curriculum Vitae

Jan Arie den Dulk werd geboren op 20 April 1948 te 's-Gravenhage. Na de lagere school in Wageningen, volgde hij de middelbare school te Wageningen (Wageningsch Lyceum) en te 's-Gravenhage (Grotius Lyceum), en behaalde het diploma HBS-B in 1968. Na zijn militaire diensttijd (november 1968 - januari 1970) studeerde hij enkele jaren aan de Technische Hogeschool te Delft (studierichting Geodesie), waarna hij in 1972 zijn studie voortzette aan de Landbouwhogeschool te Wageningen. Hij behaalde in 1978 het ingenieursdiploma met lof in de studierichting Cultuurtechniek-B met als afstudeervakken Cultuurtechniek, Theoretische Teeltkunde en Informatica. Aansluitend aan zijn studie kwam hij in 1978 in dienst bij het Rekencentrum van de Landbouwhogeschool als hoofd van de groep Toepassingen. In 1981 kreeg hij de gelegenheid over te stappen naar de vakgroep Theoretische Teeltkunde (nu: Theoretische Productie-Ecologie) om daar het in dit proefschrift beschreven onderzoek te doen. Hiertoe was hij gedetacheerd bij het Centrum voor Agrobiologisch Onderzoek te Wageningen. Vanaf 1985 is hij verbonden aan de vakgroep Informatica van de Landbouwhogeschool (inmiddels: Landbouwuniversiteit), eerst als toegevoegd docent, sinds 1987 als universitair docent.